Ice Supersaturated Regions: Validation of ERA5 Reanalysis with IAGOS In-Situ Measurements and Effect on Contrail Formation Potential of Flights

Master Thesis Aerospace Engineering

Katarina Grubbe Hildebrandt

Delft University of Technology

Cover image: SevenStorm JUHASZIMRUS [35]

TU Delft

Ice Supersaturated Regions: Validation of ERA5 Reanalysis with IAGOS In-Situ Measurements and Effect on Contrail Formation Potential of Flights

by

Katarina Grubbe Hildebrandt
Student number: 4784995

to obtain the degree of
Master of Science

at the Delft University of Technology,
to be defended publicly on Thursday, October 17, 2024 at 10:45.

Supervisor:	Dr. F. Yin	
Thesis committee:	Dr. F. Yin,	TU Delft, Supervisor
	Prof. Dr. Ir. M. Snellen,	TU Delft, Chair
	Prof. Dr. V. Grewe,	TU Delft, Examiner
	Dr. Ir. T. Sinnige,	TU Delft, Examiner

An electronic version of this thesis is available at http://repository.tudelft.nl/.

TU Delft

Preface

My thesis on '*Ice Supersaturated Regions: Validation of ERA5 Reanalysis with IAGOS In-Situ Measurements and Effect on Contrail Formation Potential of Flights*' marks the end of my academic journey at TU Delft, after six years. It has been an exciting and fulfilling journey, but not without a few bumps in the way.

I would like to express my sincere gratitude to my supervisor, Dr. F. Yin, for letting me take on this project and progressing the research for better contrail mitigation. I hope I was able to make a meaningful contribution and provide new insights for improvements needed in numerical weather prediction model.

Moreover, a large thank you to my boyfriend for being by my side for these last five years, and through all the ups and downs of my academic journey. I know it was not always easy. He also deserves special praise for always listening to me talk about airplanes or getting distracted by them during a conversation, or more recently, going on and on about contrails. Not only that, but he has always pushed me to be the better version of myself and has given me lots of confidence in my abilities, especially when I needed it the most. He has also helped me improve my coding skills and learn new techniques to become an even better engineer. I would not be the person or aerospace engineer I am today without him.

A massive thank you goes out to my parents as well. Thank you for making the decision to move our family to Argentina all those years ago. Those nine years in South America have given me so much; they taught me to venture out of my comfort zone, they taught me new languages, they gave me lifelong friends, and they let me live through new cultures and experiences. Though, more importantly, I don't know if I would have found my passion for aerospace or been this fueled by climate change or moved to Delft if I had grown up in Denmark. Also, thank you for all you've taught me in the last 25 years and the support over the last six years. I will be forever grateful.

A shout-out to my brother as well. We may not always see eye to eye, but that has always made for interesting discussions. These have let me see things from new perspectives and have pushed me to improve my work. Thank you for that.

To my friends: a special thank you goes out to Cami, Ben and Sofi. We may live in completely different countries and not see each other often, but I know you are always there to support me. Also thank you to Juliet, who has been my friend since the first day of the masters. A shoutout also goes out to the people in the old NB1.09 (Juliet, Farouk and Najib) for being supportive throughout the thesis. Last but not least, thank you to Daniel, JT, Matti, Rahiq, and Wouter for being my friends since the first year of my bachelor's. And to newer friends, Chiara, Malina and Trayana.

Katarina Grubbe Hildebrandt
Delft, October 2024

Abstract

Minimisation of the climate impact of flights in the short term may be achieved by contrail avoidance. This involves avoiding ice supersaturated regions (ISSRs), which cause contrails to persist. ISSRs occur when the relative humidity over ice is above 1, but numerical weather prediction (NWP) models struggle to predict such regions. Below 235.15 K, solely ice supersaturation can be considered. This study validates the prediction of ISSRs in the ERA5 reanalysis using IAGOS in-situ measurements from a pressure level (350 to 175 hPa), seasonal, yearly (2011 to 2022) and regional perspective. Validation of ERA5's temperature showed a cold bias in all extratropic regions and at low altitudes in the tropics, which can result in ERA5 predicting ISSRs when none are observed. Increasing temperature deviations between IAGOS and ERA5 were observed between the years 2020 and 2022. In terms of relative humidity over ice, ERA5 and IAGOS showed good agreement below ice supersaturation, but ERA5 struggled in simulating values close to or above a value of 1. For the latter conditions, ERA5 showed a dry bias in the extratropics below the tropopause. A moist bias was found in some regions and seasons, including South Asia, in June, July, and August. This may be due to inconsistencies in the modelling of the atmospheric ice content in ERA5. Years 2013 and 2014 also showed a possibility of a moist bias in ERA5 in some regions, but this was most likely the result of regional changes in sampling by IAGOS. The moist bias caused false detection of ISSRs in ERA5. Meanwhile, the dry bias led to an underestimation of the occurrence of ISSRs, with 25 to 50% remaining undetected. This causes an overestimation of no persistent contrail regions and an underestimation of persistent contrail and reservoir regions. When ERA5 overestimates the ISSR occurrence, it leads to an overestimation of persistent contrail and reservoir regions but an underestimation of no persistent contrail regions. Hence, improvements are necessary to successfully avoid or ensure unnecessary avoidance of ISSRs, where the latter could cause an increase in the climate impact of flights. Improvements should be done before implementation in contrail avoidance strategies, otherwise the benefit of such strategies may be defeated.

Contents

Nomenclature

Abbreviations

Abbreviation	Definition
AIRS	Atmospheric Infrared Sounder
CARIBIC	Civil Aircraft for the Regular Investigation of the Atmosphere Based on an Instrument Container
CDS	Climate Data Store
CO_2	Carbon dioxide
DJF	Season: December, January, February
ECMWF	European Centre for Medium Range Forecasts
IFS	Integrated Forecast System
IAGOS	In-Service Aircraft for a Global Observing system
IPCC	Intergovernmental Panel on Climate Change
ISSR	Ice supersaturated region
JJA	Season: June, July, August
MAM	Season: March, April, May
MD	Mean difference
MLS	Microwave Limb Sounder
MOZAIC	Measurement of Ozone and Water Vapour on Airbus in-service Aircraft
NC	No contrail
NO_x	Nitrogen oxide
NPC	Non-persistent contrail
NWP	Numerical weather prediction
PC	Persistent contrail
PDF	Probability density function
R	Reservoir
RHI	Relative humidity over ice
RMSE	Root mean square error
SAC	Schmidt-Appleman criterion
SON	Season: September, October, November

Symbols

Abbreviation	Definition
c_p	Isobaric heat capacity of air [$Jkg^{-1}K^{-1}$]
EI_{H_2O}	Emission index of water vapour of kerosene [$kgkg^{-1}$]
$e_{sat}^{(L)}$	Saturation water vapour pressure over liquid water [hPa]
$e_{sat}^{(i)}$	Saturation water vapour pressure over ice [hPa]
G	Mixing line slope [PaK^{-1}]

Abbreviation	Definition
N_iN_e	Contingency: No IAGOS, No ERA5
N_iY_e	Contingency: No IAGOS, Yes ERA5
p	Ambient pressure [Pa]
Q	Specific combustion heat of kerosene [Jkg^{-1}]
RH_{contrail}	Critical relative humidity for contrail formation [-]
T	Ambient temperature [K]
T_{contrail}	Critical temperature for contrail formation [K]
Y_iN_e	Contingency: Yes IAGOS, No ERA5
Y_iY_e	Contingency: Yes IAGOS, Yes ERA5
ϵ	Ratio of molecular masses of water vapour and dry air [-]
η	Aircraft engine propulsion efficiency [-]

1. Introduction

Climate change is affecting Earth at an ever-increasing pace. The average global temperature is expected to increase by 5°or more in the next decades if no intervention is done [84]. Human activities, including those due to aviation, are one of the reasons for this. In 2018, the aviation industry accounted for 2.5% of Earth's anthropogenic CO_2 emissions [82] and 5% of the world's anthropogenic radiative forcing [72]. The largest contributor to the radiative forcing is persistent contrails and contrail cirrus, though it comes with large uncertainties [72]. These phenomena occur when flying through ice supersaturated regions. Minimisation of the climate impact due to persistent contrails and contrails cirrus may be possible through flight re-routing, in which ice supersaturated regions are avoided. However, it is known that numerical weather prediction models are not accurate in the detection of such regions. A better understanding of the limitations of current numerical weather prediction models in the prediction of ice supersaturated regions is required. This is to deduce how these models need to be improved for contrail mitigation strategies to ensure the benefit of such policies.

Currently, there is some research on the validation of ice supersaturated regions in numerical weather prediction models, such as the European Centre for Medium Range Forecasts (ECMWF) reanalysis products, ERA-interim and ERA5. These products are most commonly compared to the in-situ measurements from MOZAIC/IAGOS. Studies validating ERA-interim and ERA5 using MOZAIC/IAGOS are generally limited to the midlatitude regions and focus on pressure level variations, with some attempts at validation from a seasonal and yearly perspective. Thus, the aim of this thesis is to build upon previous research validating ice supersaturated regions in numerical weather prediction models from a pressure level, seasonal, yearly and regional perspective. The regional analysis will include North Asia and tropical regions, which have not previously been validated in the ECMWF reanalysis products. Furthermore, since ice supersaturated regions are directly responsible for the persistence of contrails, the effect of deviations in the identification of ice supersaturated regions on the contrail formation potential will also be investigated. Based on these findings, recommendations for contrail mitigation will be formulated.

All in all, the current research aims to answer the following research question: "To what extent are numerical weather prediction models accurate in estimating the occurrence of ice supersaturated regions?". This has been divided into three subquestions, as shown below:

1. "How accurate is the prediction of ice supersaturated regions simulated with ERA5 reanalysis in comparison to those detected with IAGOS in-situ measurements from a yearly, seasonal, regional and altitude perspective?"
2. "What is the effect of the accuracy of the prediction of ice supersaturated regions on the contrail formation potential?"
3. "What recommendations can be made for contrail mitigation based on the findings related to the accuracy of the prediction of ice supersaturated regions?"

To answer these research questions, the thesis report is structured as follows. First, the reader is provided with background information on the topic in Chapter 2. Here, the importance of studying ice supersaturated regions is highlighted, along with the research done so far on the topic. This allows for identifying the research gap, which leads to the definition of the project and research questions in Chapter 3. Thereafter, information on the IAGOS measurements and ERA5 reanalysis model are provided and the methodology needed to answer these questions is explained in Chapter 4. After that, results and analysis are presented. Given that ice supersaturated regions are identified using the temperature and relative humidity over ice, the temperature is first compared in Chapter 5. Then, deviations in relative humidity over ice are identified in Chapter 6. With the biases in temperature and relative humidity over ice identified, the validation of ice supersaturated regions in the ERA5 reanalysis is presented in Chapter 7. This sums up the work to answer the first subquestion. Regarding the second subquestion, the contrail formation potential is a function of ice supersaturated regions and the Schmidt-Appleman criterion. Therefore, the differences in the Schmidt-Appleman criterion when

using IAGOS and the ERA5 reanalysis are analysed in Chapter 8. Hereafter, Chapter 9 examines the effect of deviations in ice supersaturated regions and the Schmidt-Appleman criterion on the contrail formation potential is examined. Lastly, based on all of these findings, recommendations for contrail mitigation are given in Chapter 10.

2. Background Information (Literature Study AE4020)

In this chapter, the importance of studying ice supersaturated regions and the research done on the topic thus far are highlighted and discussed. Section 2.1 explains the reasons behind studying ice supersaturated regions and their relationship to climate change. Then, Section 2.2 describes the different methodologies that can be used to assess these regions and outlines the advantages and disadvantages associated with these methods. One important methodology is numerical weather prediction models, though they are known to have issues in simulating ice supersaturated regions. These issues are highlighted in Section 2.3. Hence, several studies have attempted to validate ice supersaturated regions in numerical weather prediction models. The results of these studies are detailed in Section 2.4.

2.1. Why Study Ice Supersaturated Regions?

Earth's climate is changing faster than ever due to human activities. At the end of the century, the average global temperature is expected to increase by 5° or more if there are no major reductions in emissions [84]. One of the main reasons for climate change is human activities, in which the aviation industry plays a major role. In 2018, aviation CO_2 accounted for 2.5% of the world's CO_2 emissions [82]. If considering anthropogenic radiative forcing, the aviation industry's contribution accounts for 5%, including CO_2 and non-CO_2 emissions [72].

Focus is increasing on reducing non-CO_2 effects, which include those of NO_x emissions, soot, persistent contrails and contrail cirrus. The latter occurs when persistent contrails disperse. The effective radiative forcing and uncertainty of CO_2 and non-CO_2 effects can be found in Figure 2.1. As can be seen, the non-CO_2 terms have a higher forcing than the CO_2 terms. In 2018, the non-CO_2 terms resulted in a net positive effective radiative forcing that accounted for 66% of the net aviation effective radiative forcing, as a best estimate [73]. Furthermore, the uncertainty of non-CO_2 forcing terms was 8 times higher than that of CO_2 [73].

From Figure 2.1, it is seen that contrail cirrus has the largest net positive effective radiative forcing, followed by CO_2 and then NO_x. The contrail cirrus effective radiative forcing is almost twice as large as that of CO_2, but also subject to much larger uncertainties. Contrail cirrus also has a far higher uncertainty compared to other non-CO_2 terms. This is due to a number of uncertainty sources in the evaluation of contrail cirrus [80]. The uncertainty sources include those from radiative transfer calculation and simplifications made in these estimations, such as the modelling of contrail dynamics, as well as the variability of weather conditions [80, 42]

One solution to lowering the climate impact of aviation is to minimise the radiative forcing due to persistent contrails and contrail cirrus. Persistent contrails form when the Schmidt-Appleman criterion (SAC) is met and the ambient air is supersaturated with respect to ice [83]. The Schmidt-Appleman criterion determines the critical temperature and relative humidity for contrail formation. It states that a contrail can only form when the mixture of aircraft exhaust gases with the ambient air reaches a supersaturated state with respect to the liquid phase [80]. Persistence of the contrail occurs if the ambient air is supersaturated with respect to ice. A region where this occurs is called an ice supersaturated region (ISSR). It is characterised by having a relative humidity over ice that is greater than 100% [57].

Minimising the radiative forcing due to persistent contrails and contrail cirrus may be achieved with flight re-routing. In this case, flights would be re-routed to avoid ice supersaturated regions to minimise the formation persistent of contrails. However, a lot of research is still required to consider contrail avoidance through flight re-routing. One of the reasons for this is due to the challenges in the prediction of ice supersaturation, which is also one of the reasons for the large uncertainties in the contrail cirrus climate impact. In fact, the prediction of ice supersaturated regions is considered a bottleneck to better contrail mitigation [67]. The issues in the prediction of ISSRs are due to ice supersaturation not being accounted for or underestimated in most climate and numerical weather prediction (NWP) models [56,

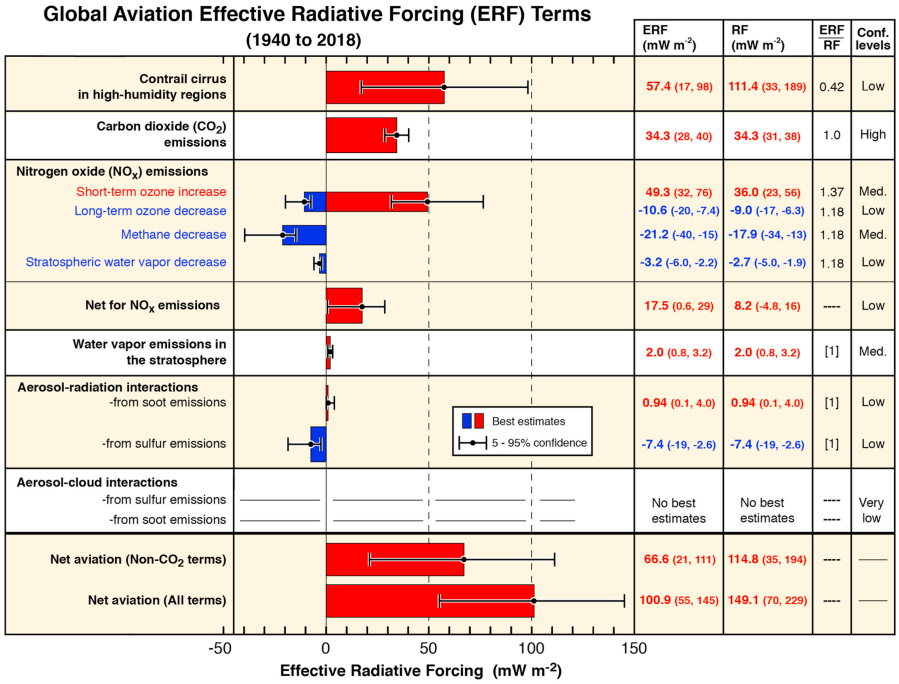

Figure 2.1: Effective radiative forcing of different aircraft emission types [73]

79, 82]. Hence, improvements in the detection of ice supersaturation in such models is required before flight re-routing to avoid ice supersaturated regions can be considered.

2.2. Assessment of Ice Supersaturated Regions

This section explores the different methods for assessing ice supersaturated regions. It will help provide an insight into what has been done on the topic and how such regions can be validated. This is particularly important given the need for improvement in the detection of ice supersaturation for flight re-routing to mitigate climate impact due to contrails. The assessment methods have been identified through literature. First, a description of the different methodologies will be presented. Thereafter, the advantages and disadvantages of each method will be discussed.

Five different methods have been identified for assessing ice supersaturated regions. These are as follows:

1. **Ground-based observations**: Since contrails are often visible to ground observers, it is possible to make observations with cameras on the ground. Wide-angle digital cameras, such as whole-sky imagers using a fish eye lens and narrow wide-angle cameras, have been utilised [41, 64, 40].
2. **Satellite-based observations**: This type of measurement uses satellites to obtain observations, such as of aerosols and clouds, on Earth. Some satellite-based observations can also provide atmospheric profiles of different measurements, such as temperature and specific humidity. For example, the Microwave Limb Sounder (MLS) and Atmospheric Infrared Sounder (AIRS) have been used for mapping ice supersaturated regions and cirrus cloud coverage [53].
3. **Numerical weather prediction models**: These are numerical models that use current weather observations to forecast future weather [47]. Weather observations come from various sources, such as satellites, weather stations and radiosondes [71]. Data assimilation techniques are used to incorporate these observations [47]. Furthermore, these models also include an atmospheric model since the dynamics of the atmosphere and physical processes, such as cloud formation, influence the weather [16].
4. **In-situ measurements:** These types of measurements use instrumentation to directly probe the properties of ice supersaturated regions [83]. In-situ measurements can be gathered using ra-

diosondes or measurement campaigns with aircraft, for example. For the latter method, aircraft are equipped to record the properties of ice supersaturated regions. Several measurement campaigns already exist, such as IAGOS, MOZAIC and CARIBIC.

5. **Lidar measurements:** Lidar stands for light detection and ranging [49]. It is a remote sensing technique that can be used to examine the surface of the Earth [49] and can also measure atmospheric properties, such as water vapour [46]. Lidars can be airborne or ground-based [18].

Each of the methodologies mentioned comes with advantages and disadvantages when used for assessing ice supersaturated regions. An overview of these can be found in Table 2.1.

Table 2.1: Advantages and Disadvantages of Assessment Methods for Ice Supersaturated Regions

Assessment method	Advantages	Disadvantages
Ground-based observations	- Can allow for continuous observations if using cameras for longer periods of time [64] - Allows for some insight into vertical variation of relative humidity and temperature at location of camera [64] - May have high temporal and spatial resolution [41]	- Limited in terms of locations and spatial coverage [83] - ISSR only visible if persistent contrail has formed [23] - Can be compromised due to cloud layers between camera and contrails [83] - Need several cameras to determine distance of observable object [64] - Images can be distorted [64, 41]
Satellite-based observations	- Allows for continuous observations - Allows for global observations [59] - Some satellites, such as Aqua, have onboard instruments, i.e. AIRS, which provide high resolution measurements of Earth [37]	- Some limited vertical resolution [53, 37] - Some limited temporal resolution [83] - Some limited spatial resolution [83] - Can be compromised due to high cloudiness [83, 37] - Integration of relative humidity with coarse vertical resolution leads to frequency of ice supersaturation being underestimated [37]
Numerical weather prediction models	- Some models allow for high spatial resolution, i.e. HRRR [48] - High vertical resolution - Allow for full global analysis [37]	- Require accurate representation of humidity fields [83] - Challenging to get accurate representation of relative humidity due to high temporal and spatial variability of water vapour [79, 83, 67] - Require accurate representation of temperature fields [83] - Some models cannot model small fluctuations due to coarse model resolution, i.e. ERA-interim [57]
In-situ measurements	- High vertical resolution, especially for radiosonde measurements [82] - Radiosonde measurements not limited to flight-levels of current aircraft fleet [82] - Directly probe ice supersaturated region properties [83] - Appropriate correction of radiosonde measurements allow for prediction of ISSRs [82, 56]	- Lack of global observations [53, 38] - Lack of continuous observations [38] - In-situ measurements from aircraft measurement campaigns limited to cruise flight levels - Radiosonde measurements are subject to environmental conditions [82] - Radiosonde measurements are subject to biases [82, 56] - Not many flight dedicated measurement campaigns [83]
Lidar measurements	- High spatial and temporal resolution [18] - Provides continuous measurements [10] - High vertical resolution [10] - Can be ground-based, airborne or satellite bound [12] - Airborne lidars are highly versatile and accurate [12]	- Peak RHI values may not always be captured, leading to underestimation of frequency and magnitude of ice supersaturation [18] - Ground-based lidars lack versatility. For example, they can only measure what passes over their location [12] - Satellite lidars lack accuracy [12] - Airborne lidars need to reach high altitudes, which few research aircraft are capable of reaching [12]

Overall, every assessment method comes with several advantages and disadvantages. It is only satellite-based observations which allow for continuous and global observations. However, such observations are limited in vertical, temporal and spatial resolution, which may cause issues in the integration of relative humidity. Lidar measurements can provide high spatial, temporal and vertical resolution. However, peak relative humidity over ice may not be captured, causing an underestimation of the frequency and magnitude of ice supersaturation. Some lidars may also lack accuracy. On the other hand, in-situ measurements would allow for directly analysing the value of the relative humidity since they can

directly probe the ambient air. If the numerical weather prediction models had an accurate representation of the humidity field and other parameters, it would solve such issues. Moreover, the latter method is the only one suitable for forecasting ice supersaturation. A further discussion of the limitations of numerical weather prediction models in forecasting such regions is given in Section 2.3. Hence, there is a need for validation of this method, which can be done using the other methods presented.

2.3. Issues with Numerical Weather Prediction Models for Detecting Ice Supersaturated Regions

For proper contrail avoidance, it is necessary to have an accurate prediction of ice supersaturated regions in numerical weather prediction (NWP) models. However, ice supersaturation is often not accounted for in NWP models [56]. Though, it is included in some models, such as in the integrated forecast system (IFS) from the European Centre for Medium Range Forecast (ECMWF). In the latter case, ice supersaturation may not be properly accounted for. Ignoring the state of ice supersaturation or not properly accounting for it can lead to inaccuracies in the frequency of ice supersaturation occurrence. This further leads to uncertainties in the prediction of persistent contrails and, thus, the climate impact due to contrails and contrail cirrus.

The state of ice supersaturation was first reported in 1906, by A. Wegener [21]. It was not incorporated into NWP models until somewhere between the end of the 1900s and the start of the 2000s [25, 56]. According to K. Gierens et al., the state of ice supersaturation was first introduced in the UK Meteorological Office United Model in the 1990s [67]. Thereafter, ECWMF incorporated ice supersaturation in its Integrated Forecast System in 2006 [25, 67]. The inclusion of ice supersaturation in the IFS increased the predicted humidity in the upper troposphere, decreased high-level cloud cover, and decreased the amount of ice in clouds [39]. ECMWF later evolved to also include ice supersaturation in their reanalysis products, including ERA-interim and ERA5 [25], with ERA5 being the newest reanalysis product from ECMWF.

The incorporation of ice supersaturation in numerical weather prediction models does not mean that ice supersaturated regions are perfectly predicted. There is often good agreements in the temperature between NWP models and in-situ measurements, as has been shown with ERA-interim and ERA5 when compared to in-situ measurements [14, 57, 83]. However, the same cannot be said for humidity. P. Reutter et al. showed that ERA-interim struggled to properly estimate the relative humidity over ice when greater than 100% [57]. However, good agreement in relative humidity over ice between ERA-interim and the MOZAIC in-situ measurements was found when relative humidity over ice was below 100% [57]. K. Wolf et al. found that ERA5, a newer renalysis model compared to ERA-interim, also had low accuracy in the estimation of relative humidity over ice [83]. In this study, ERA5 also agreed well with observed measurements for relative humidity over ice below ice supersaturation. It is again above a relative humidity over ice of 100% that ERA5 struggled to predict the observed value of relative humidity over ice [83]. However, these are not the only studies attempting to validate the humidity in numerical weather prediction models. Table 2.2 provides a larger overview of the humidity biases identified in NWP models from literature.

Table 2.2: Humidity biases in numerical weather prediction models identified in literature

Study	Observation	Numerical weather prediction model	NWP Humidity bias
P. Reutter et al. [57]	MOZAIC	ERA-interim	Good agreement of relative humidity over ice below ice supersaturation. However, relative humidity over ice above 100% is underestimated by ERA-interim, causing less occurrences of ice supersaturation
K. Wolf et al. [83]	IAGOS	ERA5	Dry bias in upper troposphere of ERA5
C. Dyroff et al. [14]	CARIBIC	ECMWF-IFS	IFS showed a moist bias in lowermost stratosphere
G. Rädel et al. [56]	Radiosonde measurements over England	ECMWF-IFS	IFS 1 day forecast showed good correlation of relative humidity over ice below ice supersaturation, but has large peak at a value of 100% and large fall-off
K. Gierens et al. [20]	IAGOS	ERA5	Underestimation of frequency of ice supersaturation and underestimation of relative humidity over ice in ERA5
J. Bland et al. [7]	Radiosondes over North Atlantic	ECMWF-IFS, MetUM	Mean moist bias in the lower stratosphere
A. Kunz et al. [36]	FISH	ERA-Interim, ECMWF operational analysis	High water vapour mixing ratios are underestimated by both models in the upper troposphere and low mixing ratios are overestimated in lower stratosphere
U. Schumann et al. [63]	MOZAIC	ECMWF IFS forecast, ERA5	Underestimation of occurrence of high ice supersaturation
L. V. Thien et al. [74]	Aura MLS	GFS, NAM	Overall moist bias in GFS and NAM
E.K. Oikonomou and A. O'Neill [50]	MOZAIC	ERA-40	Wet bias in ERA-40 at tropopause and in upper troposphere
D.G. Feist et al. [17]	AMSOS	ERA-40	Moist bias in ERA-40 in lower stratosphere
W. Woiwode et al. [81]	GLORIA	ECMWF operational analysis	Moist bias in lower stratosphere in polar regions
R. Teoh et al. [72]	IAGOS	ERA5	Underestimation of relative humidity over ice above ice supersaturation and weakly supersaturated ISSRs
G. Thompson et al. [75]	IAGOS, radiosondes	SATAVIA-WRF NOAA-GFS, ECMWF-IFS	GFS and IFS show underestimation of relative humidity over ice above ice supersaturation, with large peak at 100%. SATAVIA-WRF has deficiency at 100%, but better estimation of RHI values above 100%, albeit slightly underestimated
A. Agarwal et al. [2]	IGRA V2 (radiosonde)	ERA5, MERRA-2	ERA5 and MERRA-2 generally overestimate ice supersaturation occurrence at aircraft cruise altitudes

Several studies have also attempted to answer why numerical weather prediction models have humidity biases. According to K. Wolf et al. issues in the prediction of relative humidity over ice in the state of ice supersaturation may be due to a saturation adjustment that often exists in numerical weather prediction models [83]. The saturation adjustment can be explained as when supersaturation occurs in a grid cell of the NWP model, the relative humidity is adjusted back to 100% in the next time

step [67, 70]. This causes an overall lack of ice supersaturation, leading to a lower frequency of ice supersaturated regions in NWP models compared to observations.

Issues due to the saturation adjustment in numerical weather prediction models mainly arise in cloudy conditions. For example, ERA5 showed a lack of ice supersaturation in cloudy conditions [83]. This is also particularly important because the upper troposphere can be in a state of ice supersaturation in clear air and within cirrus clouds [67, 61]. Furthermore, P. Reutter et al. detailed that in the study comparing ERA-interim and MOZAIC, the IFS model used for ERA-Interim only allowed for the existence of ice saturation in cloud-free conditions [57]. The model adjusts supersaturation in grid cells to RHI = 100% when clouds are present. Ignoring ice supersaturation in cirrus clouds may lead to the degree of ice supersaturation being underestimated, causing incorrect predictions of persistent contrails [67].

The main reason for these challenges in the prediction of ice supersaturation has to do with the humidity field itself; it has large temporal and spatial variability, with sharp gradients [79, 83, 67]. Furthermore, since there are few reliable humidity measurements available, it is not easy to improve this problem since this means that there is a lack of observations that could be used for data assimilation in these numerical weather prediction models [67]. Hence, using numerical weather prediction models for forecasting ice supersaturation still requires considerable amounts of improvements and cannot be used reliably given the humidity bias identified through literature.

2.4. Validation of Ice Supersaturated Regions in Numerical Weather Prediction Models

Several studies have attempted to examine and validate humidity biases in numerical weather prediction models, as seen in Table 2.2. However, only a handful of these studies focus on the validation of ice supersaturation, specifically. These include the studies from P. Reutter et al. [57], K. Wolf et al. [83], C. Dyroff et al. [14], G. Rädel et al. [56] and K. Gierens et al. [20]. Note that the study by U. Schumann et al. [63] is not considered because only results from P. Reutter et al. [57] were used to determine a humidity scaling for prediction of contrails. Likewise, R. Teoh et al. [72] is not taken into account either as IAGOS and ERA5 were compared to determine the necessary humidity scaling in ERA5.

Most studies in Table 2.2 use data from the MOZAIC/CARIBIC/IAGOS campaigns, as the reference observations. MOZAIC and IAGOS are often used interchangeably. However, for this study, a distinction will be made. Any MOZAIC/IAGOS data between 1994 and July 2011 (not inclusive) are termed MOZAIC. Data collected from July 2011 to the present are called IAGOS.

An overview of the studies that validate ice supersaturation in NWPs using in-situ measurements is shown in Table 2.3. The region, pressure altitudes and time frames used for the studies are also presented. Only five studies have been identified, where two use the newest ECMWF reanalysis, ERA5, and the newest set of in-situ measurements from MOZAIC/IAGOS. Furthermore, only one study uses radiosonde measurements for validation. The details of each study will be examined further below.

The occurrence and characteristics of ice supersaturated regions have been evaluated in several different ways in literature. One of the most common is to evaluate ISSRs from an altitude perspective. This is seen in the studies from P. Spichtinger et al. [69], K. Gierens et al. [23], A. Ruzmaikin et al. [59], K. Gierens et al. [22], K. Wolf et al. [83], A. Petzold et al. [53] and P. Reutter et al. [57].

Other studies have also attempted to characterise ISSR occurrence and characteristics from a regional point of view. For example, P. Spichtinger et al. [68] analysed ISSR path lengths by separating the analysed region into a tropic and an extratropic region, which is defined based on the latitude. A. Petzold et al. [53] analysed ISSRs from a regional perspective as well. However, in this case, the regions were divided in the longitudinal sense. The three regions defined were termed Eastern North America, North Atlantic and Europe. Other studies have only focused on the North Atlantic, including the study by R. Teoh et al. [72] and P. Reutter et al. [57].

Additionally, many studies have evaluated the seasonality of ice supersaturated region occurrence or the seasonality of ISSR characteristics. A. Petzold et al. [53] investigated the seasonality of ISSRs in the northern mid-latitudes. P. Reutter et al. [57] analysed the ISSR path length and distance between ISSRs from a seasonal perspective. The seasonality of the ISSR path length was also investigated by P. Spichtinger et al. [68]. The altitude distribution of the ice supersaturation layers was explored from a seasonal perspective in the study by P. Spichtinger et al. [69]. Lastly, K. Gierens et al. [20] also made

Table 2.3: Overview of Studies Comparing Ice Supersaturated Regions using In-Situ Measurements and Numerical Weather Prediction Models

Study	In-Situ Measurements	Numerical Weather Prediction Model	Region	Pressure Altitudes	Time Frame
P. Reutter et al. [57]	MOZAIC	ERA-interim	40N - 60N 65W - 5E	below 350 hPa	01/01/2000 - 31/12/2009
K. Wolf et al. [83]	IAGOS	ERA5	30N - 70N 110W - 30E	150 hPa - 325 hPa	2015 - 2021
C. Dyroff et al. [14]	CARIBIC	ECMWF-IFS	40N - 75N 140W - 140E	below 350 hPa	20/06/2005 - 13/12/3012
G. Rädel et al. [56]	Radiosonde measurements over England	ECMWF-IFS	51.20N, 1.79W 50.89N, 0.32E 52.95N, 1.15W 50.22N, 5.33W 55.02N, 1.88W	200 hPa - 1000 hPa	15/03/2009 - 30/06/2009
K. Gierens et al. [20]	IAGOS	ERA5	0N - 60N 180W - 180E	190 hPa - 310 hPa	01/2014, 04/2014, 07/2014, 10/2024

an attempt at identifying a seasonal variability in relative humidity over ice.

Attempts have also been made to analyse the yearly variability of temperature and relative humidity over ice, which allows for identifying ice supersaturated regions. Other ISSR characteristics have also been evaluated from a yearly point of view. A. Petzold et al. [53] and P. Reutter et al. [57] investigated the yearly variability of the ISSR fraction. Furthermore, the study by K. Wolf et al. [83] analysed the yearly variability of the monthly mean of temperature and relative humidity over ice.

As can be seen, there are several types of analysis to explore ISSR occurrence and characteristics, along with the variables that allow the identification of these regions. This includes yearly, seasonal, regional and altitude analysis. An overview of the types of analysis completed in studies validating ice supersaturated regions in numerical weather prediction models using in-situ measurements can be found in Table 2.4. This will be further evaluated in the subsequent subsections.

Table 2.4: Types of Analysis in Studies Comparing Ice Supersaturated Regions using In-Situ Measurements and Numerical Weather Prediction Models

Study number	Yearly Analysis	Seasonal Analysis	Regional Analysis	Altitude Analysis
P. Reutter et al. [57]	Only ISSR fraction	Only ISSR path length and distance between ISSRs	N	Y
K. Wolf et al. [83]	Y	N	No specific regions, but longitudinal and latitudinal analysis	Y
C. Dyroff et al. [14]	N	N	N	N
G. Rädel et al. [56]	N	N	N	N
K. Gierens et al. [20]	N	Y	N	N

2.4.1. Yearly Analysis

As seen in Table 2.4, two studies provided a yearly analysis. The study by P. Reutter et al. [57] provided a yearly analysis of the ice supersaturated region fraction. The other study providing a yearly analysis is the one by K. Wolf et al. [83].

The yearly analysis of the ISSR fraction in the study by P. Reutter et al. [57] counts the number of data points in a month where the relative humidity over ice is greater than or equal to 100% and divides it by the total number of data points for that month. This may allow for some idea of how the relative humidity over ice changes per year in ERA-interim and MOZAIC. For example, it was shown that ERA-interim had a lower overall occurrence of ISSRs in comparison to MOZAIC. This could point towards fewer data points above ice supersaturation in ERA-interim for most years compared to MOZAIC. This argument is further strengthened by the fact that ERA-interim shows a sudden increase to 1 in the

cumulative probability of relative humidity over ice above 100% [57]. However, it is hard to say how relative humidity over ice may deviate per year in ERA-interim and MOZAIC using the ISSR fraction. This is also because the ISSR fraction is highly affected by the number of data points. However, given a yearly analysis was possible on the ISSR fraction, this study could have further considered yearly variation in temperature and relative humidity over ice between MOZAIC and ERA-interim.

The study by K. Wolf et al. [83] examined the yearly variation of the monthly mean relative humidity over ice and the monthly mean temperature of ERA5 and IAGOS. Using the monthly mean could lead to somewhat false conclusions regarding how accurate ERA5 is in the prediction of temperature and relative humidity over ice. For example, if IAGOS shows a consistent relative humidity value throughout one month and ERA5 predicts very different relative humidity values, but the mean is close to IAGOS, it would inaccurately say that IAGOS and ERA5 have good agreement for that month. This could be mitigated by splitting the yearly analysis into altitudes and regions since the yearly analysis by K. Wolf et al. was combined for three pressure levels, namely 250, 225 and 200 hPa [83]. K. Wolf et al. showed a change in temperature and relative humidity over ice per pressure level, and per longitudinal and latitudinal points [83]. Therefore, different yearly trends in temperature and relative humidity over ice may be present at different altitudes and in different regions.

The studies by G. Rädel et al. [56] and K. Gierens et al. [20] do not allow for a yearly analysis given their time frames. The use of radiosondes in the study by G. Rädel et al. means it is difficult to obtain continuous observations for a yearly analysis. K. Gierens et al. could have increased the time frame, but seem to have been limited by their simulation results available for the Earth System model EMAC [20]. C. Dyroff et al. [14] has a seven-year time frame, but only 267 CARIBIC flights were completed between 2005 and 2012. Hence, the number of measurements collected by CARIBIC in this time period is not sufficient to obtain proper yearly estimates of differences to expect between in-situ measurements and an NWP model.

Thus, there are gaps present in the validation of ice supersaturated regions, using temperature and relative humidity over ice from a yearly perspective. The yearly trend of temperature and relative humidity over ice could be examined from an altitude and regional perspective to understand if some of the variations are purely due to the year or if they are also due to altitude or regional differences. However, it also requires sufficient measurements.

2.4.2. Seasonal Analysis

Two studies validate numerical weather prediction models with in-situ measurements from a seasonal perspective. K. Gierens et al. [20] attempt to identify a seasonal relationship in relative humidity over ice between ERA5 and IAGOS. P. Reutter et al. [57] only focuses on the difference in seasonal patterns of the ice supersaturated path length and the distance between ice supersaturated regions between MOZAIC and ERA-interim.

As seen in Table 2.3, K. Gierens et al. [20] only made use of four months, from one year. Each of these months represents a unique season. In other studies, use is made of three months to represent one specific season, i.e. December, January and February combined represent winter, and June, July, and August represent summer [53, 57]. Hence, it is questioned whether the use of one month to represent each season gives a clear overview of the seasonal variation of variables like relative humidity over ice. Moreover, it could be that there are slight seasonal variations every year, which would not be identifiable from 4 months of data from one specific year. Nevertheless, K. Gierens et al. identifies a low relative humidity over ice in the summer and the highest in the winter [20].

A. Petzold et al. [53] investigated the seasonal variation of relative humidity over ice using MOZAIC data from 1995 to 2010, though it was not compared to an NWP model. In this study, each season was represented by three months. The seasonal variation was assessed from a pressure level and regional perspective, unlike the study by K. Gierens et al., which made no distinction in altitude or region when looking at relative humidity over ice [20]. However, A. Petzold et al. [53] also identified summer (June, July, August) as the season with the lowest relative humidity over ice. However, the highest relative humidity over ice was sometimes found in winter (December, January, February) or in Spring (March, April, May). This depended on both the pressure altitude and the region [53]. Therefore, using only one month, without specifying altitude or region, might not guarantee an exact identification of the seasonal variation of relative humidity over ice.

P. Reutter et al. [57] analysed the ISSR path length and distance between ice supersaturated regions from a seasonal perspective. This study was an extension of the study by A. Petzold et al.

[53], which explored the seasonality of relative humidity over ice and temperature using the MOZAIC dataset. Given this, it would most likely have been possible to analyse seasonal deviations between ERA-interim and MOZAIC. However, it was out of the scope of the main aims of the study by P. Reutter et al. [57].

K. Wolf et al. [83] did have sufficient data for a seasonal analysis and given that K. Gierens et al. identified seasonal differences between IAGOS and ERA5, it is not entirely out of the scope to also examine corrections of ERA5 from a seasonal perspective. The study by C. Dyroff et al. [14] most likely did not have sufficient data for a seasonal analysis due to using only CARIBIC measurements and neither did G. Rädel et al. [56].

None of the studies attempt to validate temperature in numerical weather prediction models using in-situ measurements from a seasonal perspective. This could perhaps be due to the already good agreements found in temperature, as discussed in Section 2.3.

All in all, only small attempts have been made to validate the prediction of ice supersaturated regions in numerical weather prediction models, using temperature and relative humidity from a seasonal perspective. Hence, further analysis could be done to have a clearer understanding of how NWP models may deviate from in-situ measurements for each season.

2.4.3. Regional Analysis

As was seen in Table 2.3, several regions are covered by the different studies. However, only the study by K. Wolf et al. [83] attempted a regional analysis.

In the study by K. Wolf et al., the mean temperature and relative humidity difference between IAGOS and ERA5 were considered as a function of only longitude and as a function of only latitude [83]. Thus, for example, for the data analysed at a latitude of 30° N, the entire range of longitude is still included, which includes the regions of North America, North Atlantic and Europe. This means particular regions are not defined in this study, and thus, it is hard to consider this as a regional analysis of the difference between the prediction of ice supersaturated regions in IAGOS and ERA5.

P. Reutter et al. [57] would most likely not have been able to do a regional analysis with the chosen region (see Table 2.3), which only considers the North Atlantic corridor. However, it was also limited by the available MOZAIC data at the time of the study. C. Dyroff et al. [14] could have considered a regional analysis by splitting the data into regions encapsulating North America, North Atlantic, Europe and Asia due to the longitudinal range chosen in the study. Given the number of measurements available with CARIBIC, it would not have been possible to form proper conclusions. The same can be said for the study by K. Gierens et al. [20]. With the radiosondes in the study with G. Rädel et al. [56], it is very difficult to generate an extensive global coverage of measurements in order to consider a regional analysis.

None of the studies covers a large enough latitude range to consider extratropic and tropic regions, except for the study by K. Gierens et al. [20], given that a tropic region is defined by 30° S $\leq$ latitude $\leq$ 30° N and an extratropic region is defined by where latitude $\leq$ 30° S and latitude $\geq$ 30° N [68]. Yet, given only a year of data was collected, sufficient regional analysis would not be possible.

Therefore, the regional validation of ice supersaturated regions in numerical weather prediction models using in-situ measurements can be improved. Of course, this is also dependent on the in-situ measurements available and where these measurements are located. The global coverage map of the IAGOS data spanning from July 2011 to the most recent available date (December 2022 in this case) is shown in Figure 4.2. This shows that it is possible for regions such as North America, the North Atlantic and Europe, but also extratropic and tropic regions to be defined. In the analysis of the results, one would have to consider the difference in the density of measurements between the extratropic and tropic regions.

2.4.4. Altitude Analysis

From Table 2.3, it is clear that several pressure altitudes have been covered by the studies validating ice supersaturated regions in numerical weather prediction models using in-situ measurements. Yet, only two studies perform an altitude analysis on the variables allowing for determining ISSR occurrence and characteristics.

P. Reutter et al. [57] performs an altitude analysis by dividing the flight levels relative to the dynamical tropopause height. The vertical data is thereafter separated into three distinct layers: upper troposphere, tropopause layer, and lower stratosphere. The upper troposphere and lower stratosphere

and further subdivided into three layers, with a height of 30 hPa [57]. This is used to analyse the vertical profile of temperature and relative humidity over ice for the MOZAIC and ERA-interim datasets. The cumulative distribution of relative humidity over ice per layer for MOZAIC and ERA-interim is also investigated by P. Reutter et al., though the cumulative distribution of temperature is not [57].

P. Reutter et al. [57] also analysed the ISSR fraction as a function of pressure levels, along with the time evolution of the ISSR fraction per layer. However, in this case, the three tropospheric layers were combined into one layer, and so were the three stratospheric layers. However, some of the information on the time evolution of ISSR fraction on the individual layers may be lost by combining the layers in this case. For example, the difference in the ISSR fraction from the first lower stratospheric layer to the second lower stratospheric layer was around 8%, whereas barely any difference was detected between the second lower stratospheric layer and third lower stratospheric layer for the ERA-interim dataset as can be seen in Figure 2.2. However, when combining these three layers into one, the higher ISSR fraction on the first lower stratospheric layer in ERA-interim might be lost. In the MOZAIC dataset, this may not be as large an issue due to a much smaller variability in the ISSR fraction between the lower stratospheric layers. Furthermore, both the MOZAIC and ERA-interim datasets show a difference of approximately 10% in the ISSR fraction from the first to the third upper tropospheric layer, which again may also be lost when combining the three upper tropospheric layers. It should be kept in mind that the ISSR fraction may not say how much relative humidity over ice may deviate per year in the ERA-interim and MOZAIC datasets, as discussed in Section 2.4.1.

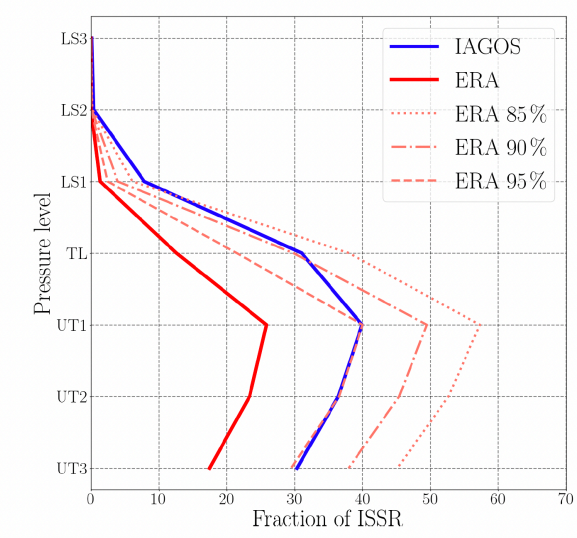

Figure 2.2: Vertical profile of the ice supersaturated region fraction for ERA-interim (ERA) and MOZAIC (IAGOS as the study refers to it as) in the study by P. Reutter er at. [57]

In the study by P. Reutter et al. [57], the altitude variation of temperature, relative humidity over ice and ISSR fraction were not further subdivided into regions. However, this study only focused on the Northern Atlantic region. Other studies also treat this as one region [53, 72], hence it is not deemed necessary to show the altitude variation per region.

The other study completing an altitude analysis on the ISSR occurrence and characteristics is the one by K. Wolf et al. [83]. In this study, the temperature and relative humidity over ice between ERA5 and IAGOS are compared using probability density functions at three pressure levels: 250, 225 and 200 hPa. The mean of the temperature and relative humidity over ice is also calculated for each of the pressure levels for the IAGOS and ERA5 datasets. Moreover, cumulative distribution functions are presented for pressure levels 350, 300, 250, 225 and 200 hPa. K. Wolf et al. analyse IAGOS and ERA5 on the most visited pressure levels by IAGOS flights [83] and provide further information on other pressure levels on which ice supersaturation regions can exist.

K. Wolf analyses these altitudes for the entire region included in this study [83], which combines a region in North America, the North Atlantic and Europe. In other studies, these regions have been separated [53] or there has only been a focus on the North Atlantic [72, 57]. However, K. Wolf et al. analysed the mean longitudinal and mean latitudinal difference per altitude in temperature and relative

humidity over ice between ERA5 and IAGOS. This showed that the mean difference between ERA5 and IAGOS changed per longitude and latitude. For example, a smaller difference in the relative humidity over ice was generally found for all pressure levels at a longitude of 100° W compared to at 20° E as shown in Figure 2.3. However, there was also a change per pressure level; at 20° E, the difference in relative humidity over ice at a pressure level of 225 hPa was approximately -7%, but approximately -18% at 250 hPa. For 100° W, the difference in relative humidity over ice at a pressure level of 225 hPa and 250 hPa was approximately 3% [83]. Hence, it is clear that altitude differences between ERA5 and IAGOS are not only just a function of altitude but also the region. Therefore, it would also be beneficial to analyse the difference between IAGOS and ERA5 per altitude, from a regional perspective.

Radiosondes typically allow for high vertical resolution, and G. Rädel et al. [56] show a pressure level range of 200 hPa to 1000 hPa. Moreover, vertical profiles of the relative humidity over ice measured by the radiosonde were presented. Hence, it could have been compared to the ECMWF-IFS. K. Gierens et al. [20] also did not perform an altitude analysis, but again, there may not have been sufficient points to do so given the time frame. C. Dyroff et al. [14] examined the difference in the vertical profile of water vapour between CARIBIC and ECMWF-IFS, and provided frequency distributions of temperature and relative humidity over ice. This shows that altitude deviations between CARIBIC and ECMWF-IFS could also have been done for temperature and relative humidity over ice.

Hence, improvements in the validation of ice supersaturated regions prediction can be done from an altitude perspective. This includes an altitude analysis that is further split by regions due to differences in the behaviour of temperature and relative humidity over ice per region. Moreover, care should be taken not to combine the data from several pressure levels into one, as this could cause variability of some of the data to be lost.

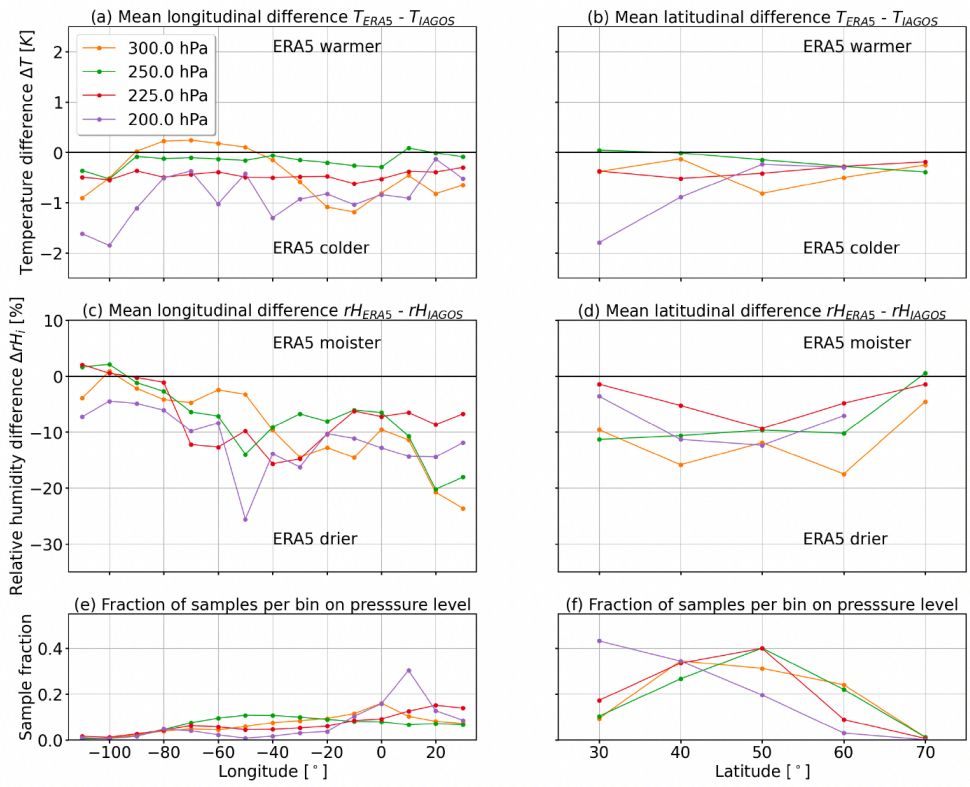

Figure 2.3: Longitudinal and latitudinal mean differences between IAGOS and ERA5 temperature and relative humidity over ice [83]

3. Project Description

There are minimal studies that attempt to validate numerical weather prediction models using in-situ measurements; a total of five were identified [57, 83, 14, 56, 20]. Of these five studies, only two studies used the newest ECWMF reanalysis, ERA5, and validated this numerical weather prediction model with the most recent in-situ measurements gathered from commercial flights, IAGOS [83, 20]. Most of these studies focused on the North American, North Atlantic and European regions, with no studies attempting to analyse ice supersaturated regions in the tropics or in the Far East. These studies mainly focused on validating ice supersaturated regions from a pressure level perspective, with some attempts at a yearly and seasonal analysis. However, all studies seem to be fairly limited. This study aims to expand the validation of ice supersaturated regions in the numerical weather prediction models, taking into account seasonal, regional and yearly variations. More specifically, the newest ECMWF reanalysis product, ERA5, will be validated using the IAGOS in-situ measurements.

3.1. Research Questions

This master thesis will attempt to answer the research question: ”To what extent are numerical weather prediction models accurate in predicting the occurrence of ice supersaturated regions?”. This is further divided into three sub-research questions, as shown below.

1. ”How accurate is the prediction of ice supersaturated regions simulated with ERA5 reanalysis in comparison to those measured with IAGOS in-situ measurements from a yearly, seasonal, regional and altitude perspective?”
2. “What is the effect of the accuracy of ice supersaturated regions on the contrail formation potential?”
3. ”What recommendations can be made for contrail avoidance based on the findings related to the accuracy of the prediction of ice supersaturated regions?”

4. Data and Methodology

In this chapter, a description of the IAGOS and ERA5 data is presented, along with the methodology that will be utilised for the study. First, Section 4.1 describes the selection of variables to be used, thereafter Section 4.2 details the IAGOS dataset, including the criteria used for selecting the measurements to use. Then, Section 4.3 describes the ERA5 dataset and how this will be used for validation with IAGOS. How IAGOS and ERA5 will be compared from a seasonal, regional, pressure level and yearly perspective is outlined in Section 4.4. Then, an explanation of the IAGOS-ERA5 contingency table, used for identifying undetected and false detected events in ERA5 is provided. Lastly, Section 4.6 describes how differences in contrail formation potential between IAGOS and ERA5 will be determined.

4.1. Selection of Variables

Ice supersaturated regions can be identified when the relative humidity over ice is greater than 100%. The temperature should be considered to avoid misidentifying air inside supercooled liquid or mixed phase clouds as ice supersaturated regions [24]. Below the threshold of homogeneous freezing, equal to 235.15 K, solely ice supersaturation can be considered given that this is the lowest temperature where supercooling of cloud droplets can occur [67, 24]. Hence, for the validation of ice supersaturated regions in numerical weather prediction models using in-situ measurements, two variables will be compared; relative humidity over ice and temperature.

4.2. IAGOS

The In-service Aircraft for a Global Observing System (IAGOS) provides atmospheric composition observations from commercial aircraft and was founded in July 2011 [31]. It is the successor of the Measurement of Ozone and Water Vapour on Airbus In-service Aircraft (MOZAIC) programme and Civil Aircraft for the Regular Investigation of the Atmosphere Based on an Instrument Container (CARIBIC), which began measurements in 1994. Meanwhile MOZAIC is no longer a project, CARIBIC continues within IAGOS and is a reference standard for the rest of the IAGOS fleet [52].

The IAGOS-CORE component is installed on long-range aircraft from internationally operated airlines [52], where 10 aircraft are currently active [29]. IAGOS-CORE contains several autonomous instruments for daily measurements of reactive and greenhouse gases, such as CO_2 and water vapour, as well as aerosol and cloud particles [52]. The main package installed on the entire IAGOS fleet is Package 1, which includes a humidity sensor (ICH), in charge of humidity measurements, and a backscatter cloud probe (BCP) that measures cloud particles [30].

The ICH consists of a capacitive relative humidity sensor [28], which is a modified Vaisala HUMICAP® of type H sensor [45]. Such a sensor is a small capacitor formed from a hygroscopic dielectric material placed between two electrodes [55]. The amount of moisture in this material, under equilibrium conditions, is dependent on ambient temperature and water vapour pressure. When moisture is absorbed by the dielectric material, it changes the capacitance [55, 19]. This can be used to estimate the relative humidity, as this variable is a function of temperature and water vapour pressure [55]. The ICH also has a platinum resistance sensor for temperature measurements at the surface of the humidity sensing element [28]. Hence, the ICH provides the temperature and relative humidity (with respect to (wrt) liquid) measurements. The relative humidity has a precision of $\pm$ 1% and an accuracy of $\pm$ 6%. Temperature measurements have a precision of $\pm$ 0.2 K and an accuracy of $\pm$ 0.5 K [28].

Given the start date of the IAGOS program and that the entire IAGOS fleet was equipped with the modified Vaisala HUMICAP® of type H sensor [45] in 2011, measurements will be collected between July 2011 and December 2022. The end date is set to December 2022 due to a lack of published flight measurements after this date (at the time of data collection). The frequency of altitudes visited by IAGOS flights can be found in Figure 4.1. The most frequently visited altitudes range from 10000 m to 12500 m. ISSRs can be present in an altitude range of 8000 m to 13000 m [78]. In the Arctic, ISSRs have been shown to be present between 4000 m and 14000 m [24], though the number of mea-

surements gathered by IAGOS flights between 4000 m and 8000 m, and above 12500 m is very small. Hence, the chosen pressure altitudes for this study range from 355 hPa to 150 hPa, corresponding to an altitude of 8000 m to 13600. The 150 hPa bound is based on ERA5's vertical resolution, as discussed in Section 4.3.

In selecting the IAGOS measurements, points with a relative humidity with respect to liquid (RHL) greater than 100% are rejected. Above this value, it implies that the aircraft is flying through a liquid cloud. At temperatures at which these types of clouds are present, contrails cannot form. Hence, there could never be a persistent contrail, meaning that these measurements are not of interest [78].

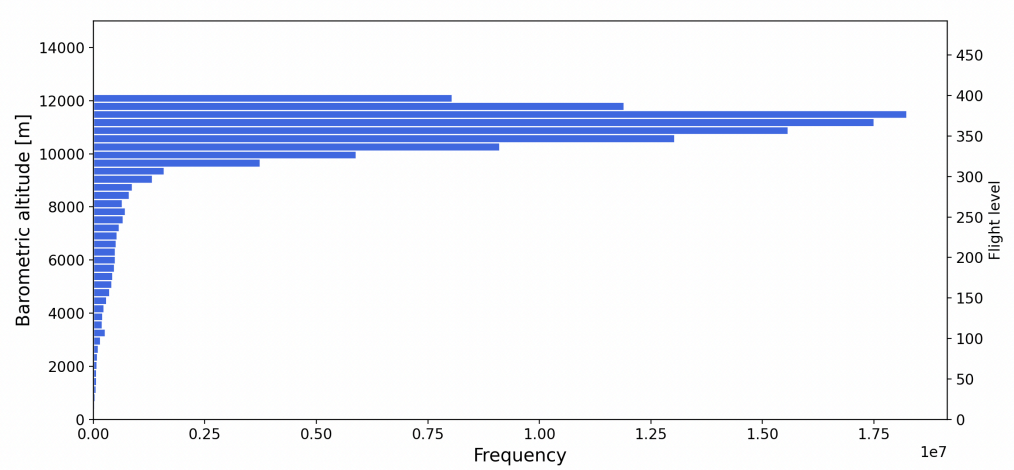

Figure 4.1: Frequency of altitudes visited by IAGOS flights, with respect to sea level, from July 2011 to December 2022

IAGOS also provides validity flags to indicate the quality of the measurements. In this case, only 'good' measurements are considered for temperature and relative humidity with respect to ice. Other types of validity flags can, for example, provide negative values of relative humidity with respect to ice, which is not accurate, or they may not be as reliable. However, for the relative humidity with respect to liquid, 'good' and 'limited' validity flags are considered sufficient since this variable is only used for determining the possibility of liquid clouds. Moreover, if restricting the validity flag of this variable to 'good', around half of the available data points disappear, not allowing for sufficient analysis.

Lastly, based on the global distribution of the number of IAGOS measurements during the considered time frame, only measurements located between 160°W and 150°E and between 30°S and 75°N will be considered. This is shown in Figure 4.2.

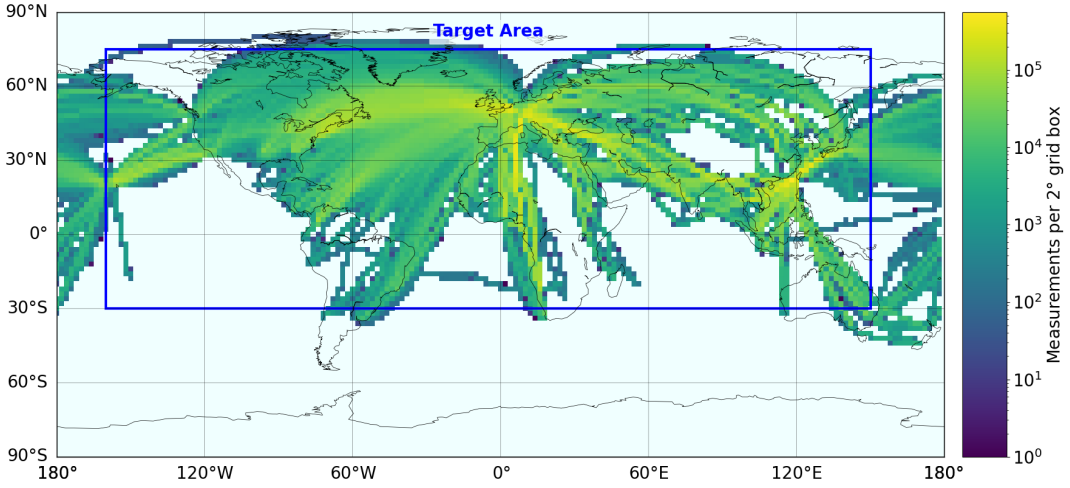

Figure 4.2: Target area for study based on IAGOS in-situ measurements from July 2011 to December 2022, with barometric altitude between 8000 and 13000 m, RHL between 0 and 100%, RHI and T 'good' validity flags, and RHL 'good' and 'limited' validity flags.

A summary of the criteria for the IAGOS measurements are provided below:

- Measurements are between 01/07/2011 and 31/12/2022.
- Pressure altitude is between 355 hPa and 150 hPa, which corresponds to an altitude range of 8000 m to 13600 m.
- Relative humidity with respect to liquid is between 0% and 100%
- The validity flag for temperature and relative humidity with respect to ice is equal to 0, which corresponds to 'good'.
- The validity flag for relative humidity with respect to liquid is equal to 0 or 2, corresponding to 'good' or 'limited'.
- Measurements are located between 160°W and 150°E, and between 30°S and 75°N

On an IAGOS flight, measurements are recorded every 4 seconds. It is normal for atmospheric measurements to exhibit autocorrelation [51], which describes the similarity between neighbouring measurements [43]. However, if ignoring autocorrelation, uncertainties of specific trends may be artificially reduced, which can cause the identification of insignificant trends [51]. To avoid autocorrelation, samples are taken approximately every minute, as also done by K. Gierens et al. [20] and R. Teoh et al. [72]. This means approximately 7% of the filtered IAGOS data, which has been filtered according to the above-mentioned conditions, is sampled, which is about 2.5% of all of the IAGOS measurements between 01/07/2011 and 31/12/22. To avoid systematic bias, the data points are randomly sampled without replacement, using a uniform random number generator with a range of 1 to the maximum number of rows.

4.3. ERA5 Reanalysis

For the numerical weather prediction model, the fifth generation reanalysis from European Centre for Medium-Range Forecasts (ECMWF), ERA5 reanalysis, is utilised. Such a model uses data assimilation, in which model data is combined with observations [11]. Renalyses are important for climate monitoring but also aid in assessing the impact of changes in the observing system in order to measure the progress in modelling and data assimilation abilities. This allows for developing the newest and most advanced climatologies to assess anomalies in forecast errors [26].

The ERA5 reanalysis is based on the model forecasts Cy41R2 of the Integrated Forecasting System (IFS) from ECMWF [26]. The IFS uses the saturation adjustment in its ice cloud micro-physical scheme [76, 83]. This means that the relative humidity over ice is forced back to 100% within one-time step when a cloud forms [83, 20, 76]. Usually, such a process can take several hours, though it is dependent on the crystal size number and ice concentration [20]. Issues related to this adjustment were highlighted in Section 2.3.

For this study, ERA5 hourly data on pressure levels is used and retrieved from the Copernicus Climate Data Store (CDS) [11]. K. Gierens et al. [20] and K. Wolf et al. [83] used the same dataset in their validation of ERA5. The reanalysis has a horizontal resolution of 0.25°x 0.25°, a temporal resolution of one hour, and a vertical resolution of 37 pressure levels, which covers a pressure altitude range of 1000 hPa to 1 hPa [11]. Between the pressure altitude of 350 hPa and 150 hPa, ERA5 has a vertical resolution of 25 hPa or 50 hPa [11]. This means that the selected pressure levels to retrieve the ERA5 data on are: 350 hPa, 300 hPa, 250 hPa, 225 hPa, 200 hPa, and 175 hPa.

ERA5 is projected onto IAGOS' flight tracks by quadrilinear interpolation using time, pressure level, longitude and latitude using the interpolation function from the xarray python library, which allows for multi-dimensional interpolation [85]. K. Gierens et al. [20] and R. Teoh et al. [72] also used quadrilinear interpolation to project ERA5 onto flight tracks. Due to the timely nature of interpolating the data volume associated with the ERA5 dataset and the amount of data points, the use of a supercomputer is necessary. The DelftBlue supercomputer is utilised [1].

The variables retrieved from ERA5 are temperature and relative humidity. It is important to note that ERA5 does not make a distinction between relative humidity with respect to liquid and relative humidity with respect to ice. It is only at ambient temperatures lower than 250.16 K at which relative humidity can be defined with respect to ice [83, 11]. Above this temperature, relative humidity is defined with respect to liquid. Thus, when retrieving the relative humidity from the interpolation result, the temperature has to be checked to identify if the relative humidity is defined with respect to liquid or with respect to ice.

4.4. Specification of Seasons, Regions, Pressure Altitudes and Years

This study will focus on validating ice supersaturated regions in the ERA5 reanalysis using the IAGOS in-situ measurements from a seasonal, regional, altitude and yearly perspective. In this section, the parameters for these perspectives are described.

Analysis with respect to seasons:
Four seasons will be considered. They are defined as follows, following the seasonal definitions by A. Petzold et al. [53] and P. Reutter et al [57]:

- DJF: December, January, February
- MAM: March, April, May
- JJA: June, July, August
- SON: September, October, November

Analysis with respect to regions:
Due to the distribution of the concentration of the measurements, several regions are defined. First, the selected region is split into four parts based on the longitude. This is partially based on previous study definitions [83, 57, 53]. Thereafter, each of these regions is separated latitudinally, based on the definition of a tropic (30°S $\leq$ latitude $\leq$ 30°N) and extratropic region (latitude $\leq$ 30°S and latitude $\geq$ 30°N) [68]. The longitude and latitude of each region, and whether it is a tropic or extratropic region, can be found in Table 4.1. These regions are shown on the IAGOS flight density map in Figure 4.3.

Table 4.1: Definition of regions for analysis

Region Name	Longitude & Latitude of Region	Extratropic/Tropic
North America	160°W to 65°W 30°N to 75°N	Extratropic
Central/South America	160°W to 65°W 30°S to 30°N	Tropic
North Atlantic	65°W to 5°W 30°N to 75°N	Extratropic
South Atlantic	65°W to 5°W 30°S to 30°N	Tropic
Europe	5°W to 30°E 30°N to 75°N	Extratropic
Africa	5°W to 30°E 30°S to 30°N	Tropic
North Asia	30°E to 150°E 30°N to 75°N	Extratropic
South Asia	30°E to 150°E 30°S to 30°N	Tropic

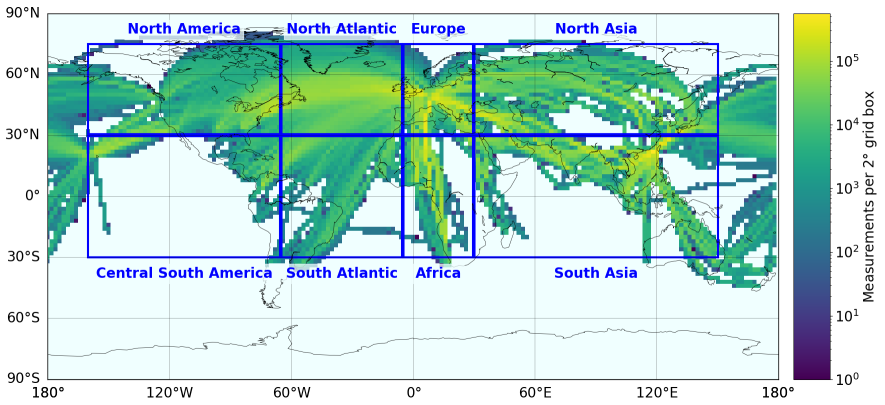

Figure 4.3: IAGOS flight density map per 2°grid box with regional division

Analysis with respect to pressure level:
This will be based on the selected ERA5 pressure levels, i.e. 350 hPa, 300 hPa, 250 hPa, 225 hPa, 200 hPa and 175 hPa. The corresponding pressure range in the IAGOS can be seen in Table 4.2.

Table 4.2: Pressure levels and pressure ranges used for ERA5 and IAGOS data

Pressure level (hPa)	Pressure range (hPa)
350	$325 \leq p \leq 356$
300	$275 \leq p < 325$
250	$237.5 \leq p < 275$
225	$212.5 \leq p < 237.5$
200	$187.5 \leq p < 212.5$
175	$150 \leq p < 187.5$

Figure 4.4 displays the fractions of samples per region and pressure level in the IAGOS dataset. There is a large difference in the fractions per region and pressure level. The three pressure altitudes with the highest fraction are 250 hPa, 225 hPa and 200 hPa. It should also be noted that in some regions, such as the North Atlantic and South Atlantic, there are no points at pressure level 350 hPa, corresponding to an altitude of approximately 8 km. Flights going through these two regions are transatlantic flights and thus tend to fly at higher altitudes. The regions with the highest number of points are the North Atlantic, Europe, North Asia and South Asia, with Central/South America and South Atlantic showcasing the least number of samples. This division of the samples should be considered for the validation of ice supersaturated regions.

Analysis with respect to years:
The yearly analysis is based on the timeline of the IAGOS measurements, that is, between 2011 and 2022, with analysis for every year in between.

4.5. Definition of Contingency Table

The aim of the contingency table is to investigate how often ERA5 is able to correctly identify certain criteria, such as the threshold of homogeneous freezing and the Schmidt-Appleman criterion (SAC). This is done through the contingency table defined in Table 4.3. It will determine how many events IAGOS and ERA5 both detect and how many events they both do not detect. It also considers if IAGOS detects an event while ERA5 does not and vice versa.

Table 4.3: Contingency table definition

IAGOS Detection	ERA5 Detection	
	Yes	No
Yes	Y_iY_e	Y_iN_e
No	N_iY_e	N_iN_e

The entries in the contingency table can be summarised using metrics, such as the hit rate, H, and the false alarm rate, F. The hit rate is calculated using Equation 4.1. It quantifies the probability of ERA5 detecting conditions such as the homogeneous freezing temperature or ice supersaturation, given that these conditions are also found in the IAGOS measurements. The false alarm rate quantifies the probability that a specific condition is observed in ERA5 but not in IAGOS. It can be determined using Equation 4.2.

$$H = \frac{Y_iY_e}{Y_iY_e + Y_iN_e} \tag{4.1}$$

$$F = \frac{N_iY_e}{N_iN_e + N_iY_e} \tag{4.2}$$

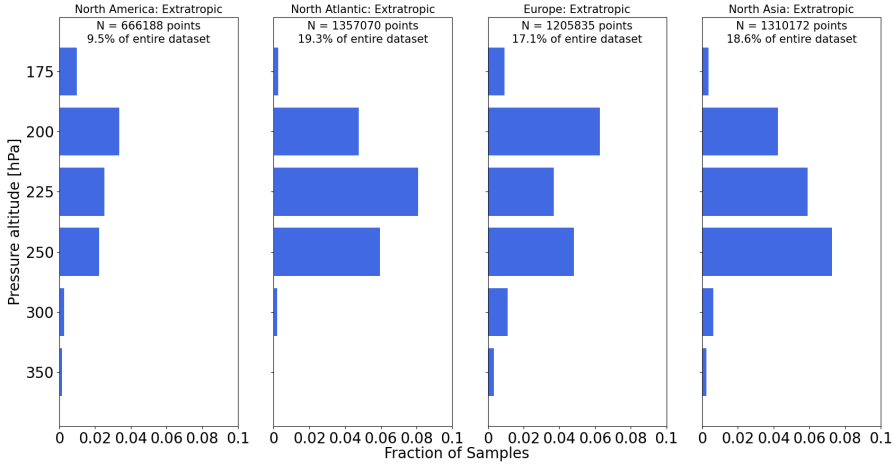

(a) Extratropic regions

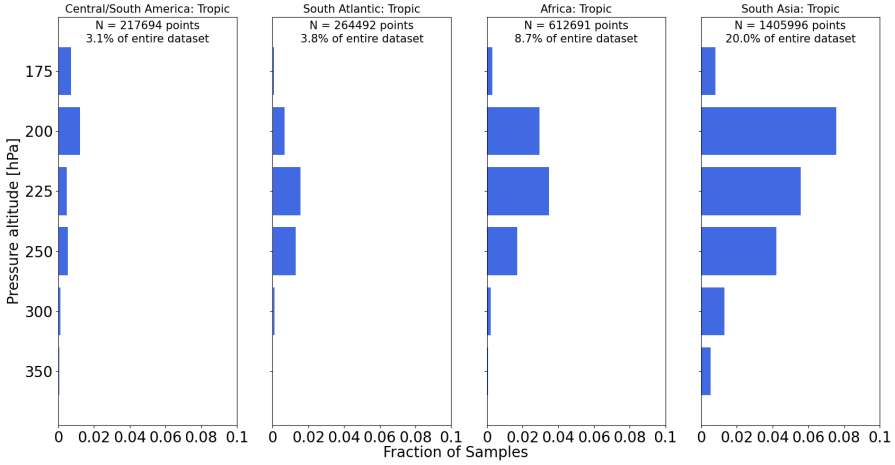

(b) Tropic regions

Figure 4.4: Fraction of sampled IAGOS observations per tropic region and pressure level

4.6. Evaluation of Contrail Formation Potential

This section explores the methodology for understanding how differences in the prediction of ice supersaturated regions affect the contrail formation potential. The contrail formation potential is a function of ice supersaturated regions and the Schmidt-Appleman criterion. First, how the Schmidt-Appleman criterion will be evaluated is described in detail. Then, the methodology for finding the contrail formation potential of the different flights is explained. This allows for identifying, for example, how many of the samples show the formation of a persistent contrail.

4.6.1. Schmidt-Appleman Criteria

In order to check if a contrail can occur given the ambient conditions, the Schmidt-Appleman criterion can be used, which determines the critical temperature and relative humidity (with respect to liquid) for contrail formation. A contrail forms when the ambient temperature is below the critical temperature and the relative humidity is greater than the critical humidity.

When kerosene is combusted in aircraft engines, hot and humid air is released and dilutes in the cold and dry atmosphere. This mixing process is modelled as isobaric, which leads to a straight line in the $p - T$ diagram (see [62]) [60]. The slope of this line termed the mixing line slope, can be calculated with Equation 4.3 [82]. Here, p is the ambient pressure at the flight altitude, and η is the aircraft engine propulsion efficiency. This study will also analyse the variation of the SAC with η. In 1999, the Intergovernmental Panel on Climate Change (IPCC) stated that modern engines had an overall engine efficiency between 30% and 37% at cruise [34]. Given the demand for increases in engine efficiency and the predicted trend in engine efficiency, the efficiency will be varied between 30% and 40% [66].

A baseline of 30% is considered given that the IAGOS fleet consists of A330CEO's and A340's [29], which were released in the 1990's [5]. The variables EI_{H_2O}, c_p, ε and Q are constants, and are defined in Table 4.4.

$$G = \frac{EI_{H_2O} \cdot c_p p}{\varepsilon Q(1-\eta)} \tag{4.3}$$

Table 4.4: Parameter definition of constant variables in mixing line slope

Parameter	Value
Emission index of water vapour of kerosene, EI_{H_2O}	1.25 KgKg^{-1} [82]
Isobaric heat capacity of air, c_p	1004 JKg^{-1} K^{-1} [82]
Ratio of molecular masses of water vapour and dry air, ε	0.622 [82]
Specific combustion heat of kerosene, Q	43.2 MJKg^{-1} [82]

The critical temperature for contrail formation can be approximated using Equation 4.4 [82].

$$T_{\text{contrail}} = 226.69 + 9.43\ln(G - 0.053) + 0.72[\ln(G - 0.053)]^2 \tag{4.4}$$

Given the ambient temperature at the altitude of the flight, T, the critical temperature, T_{contrail}, and the mixing line slope, the critical relative humidity, RH_{contrail}, for contrail formation can be determined. This is done using Equation 4.5 [82], where $e_{\text{sat}}^{(L)}$, the saturation water vapour pressure over liquid water, can be found with Equation 4.6 [8].

$$RH_{\text{contrail}}(T) = \frac{G \cdot (T - T_{\text{contrail}}) + e_{\text{sat}}^{(L)}(T_{\text{contrail}})}{e_{\text{sat}}^{(L)}(T)} \tag{4.5}$$

$$\ln(e_{\text{sat}}^{(L)}) = -\frac{6096.9385}{T} + 16.635794 - 0.02711193 \cdot T + 1.673952 \cdot 10^{-5} \cdot T^2 + 2.433502 \cdot \ln(T) \tag{4.6}$$

The SAC requires the ambient relative humidity with respect to liquid. If the temperature in ERA5 is below 250.16 K, the relative humidity with respect to liquid can be found with Equation 4.7 [82]. This formula utilises the relative humidity with respect to ice, the saturation water vapour pressure over liquid water and saturation water vapour pressure over ice, $e_{\text{sat}}^{(i)}$. $e_{\text{sat}}^{(i)}$ can be calculated using Equation 4.8 [8].

$$RH = RH_i \frac{e_{\text{sat}}^{(i)}}{e_{\text{sat}}^{(L)}} \tag{4.7}$$

$$\ln(e_{\text{sat}}^{(i)}) = -\frac{6024.5282}{T} + 24.7219 + 0.010613868 \cdot T - 1.3198825 \cdot 10^{-5} \cdot T^2 - 0.49382577 \cdot \ln(T) \tag{4.8}$$

4.6.2. Contrail Formation Potential

As discussed in Chapter 2, the Schmidt-Appleman criterion (SAC) must be met for a contrail to form. It is non-persistent if not formed in an ice supersaturated region (ISSR) and persistent if formed in an ice supersaturated region. However, if a contrail moves into a region that is an ISSR, the contrail can persist and spread. Such a region is called a reservoir. No contrail formation is possible if the SAC is not met and there is no ISSR. This means that there are four classifications for contrail formation potential. The points along flight paths can be flagged as non-persistent contrails (NPC), persistent contrails (PC), no contrail formation (NC) and reservoir conditions (R). They are summarised as follows:

- Non-persistent contrail (NPC): Point fulfils SAC, but it is not in an ISSR
- Persistent contrail (PC): Point fulfils SAC and is in an ISSR
- No contrail formation (NC): Point is not in an ISSR and does not fulfil SAC
- Reservoir (R): Point does not fulfil SAC, but it is in an ISSR

5. Validation of Temperature in ERA5 Reanalysis using IAGOS In-Situ Measurements

The following chapter focuses on validating temperature in the ERA5 reanalysis using the IAGOS in-situ measurements. First, a general comparison of the temperatures is done in Section 5.1 to get a general idea of the overall differences between the temperatures measured by IAGOS and the temperatures simulated by ERA5. Thereafter, Section 5.2 examines temperature deviations between IAGOS and ERA5 by considering the four seasons (DJF, MAM, JJA, SON), as well as the climates (extratropic, tropic). Section 5.3 then analyses differences between IAGOS and ERA5 considering regional, seasonal and pressure level variations. This is to understand if specific biases are introduced in ERA5 based on these three variables. A similar analysis is completed in Section 5.4, though in this case, deviations between IAGOS and ERA5 are examined from a pressure level, regional and yearly perspective to understand if the year also causes biases in ERA5. Lastly, based on the conclusions on the temperature differences between IAGOS and ERA5, it is explored how this may affect the selection of points that can be considered for ice supersaturation based on the threshold of homogeneous freezing. This can be found in Section 5.5.

5.1. General Comparison of Temperature Between ERA5 Reanalysis and IAGOS

This section gives a general comparison of the temperature found with IAGOS and the temperature simulated in the ERA5 reanalysis. This is to give an insight into the general behaviour of the temperature modelling in ERA5 compared to actual measured temperatures.

A scatter plot showing the temperature measured by IAGOS and the temperature simulated by ERA5 can be found in Figure 5.1. The vertical straight lines sometimes observed are due to the precision of IAGOS' temperature sensor, as described in Section 4.2. Good agreement in temperature between IAGOS and ERA5 is shown as most points are scattered along the y=x line. P. Reutter et al. also found good agreement between ERA-interim and MOZAIC [57].

The lowest temperatures measured or simulated lie around 205 to 210 K, and the highest measured temperatures are almost 260 K. A. Petzold et al. [53]. showed the MOZAIC fleet measured a low of 207 to 208 K and a high just above 230 K due to restriction of temperatures in the study. Similar observations were found by C. Dyroff et al. [14] found temperatures between 205 and 245 K in the midlatitudes using the CARIBIC measurements. F. Berkes et al. [6] measured temperatures between 200 and 245 K using MOZAIC/IAGOS over the North Atlantic. Thus, the highest measured temperatures in this study are most likely due to sampling in the tropic regions.

The general difference in temperature between IAGOS and ERA5 seems to lie between -5 K and 5 K. K. Wolf et al. [83] also found differences of -5 to 2.5 K at pressure level 250 hPa, though with low probability occurrence, and differences decreased with decreasing temperatures. However, K. Wolf et al. [83] used a far smaller region with fewer data points, which could affect observations. F. Berkes et al. [6] also saw a deviation of -5 to 5 K in the North Atlantic, though most points were concentrated between -2 and 2 K. As the measured temperature by IAGOS increases, deviations decrease, and more points are found below the y=x line, showing a cold bias in ERA5. C. Dyroff et al. [14] also detected a cold bias in ECMWF-IFS at higher measured temperatures by CARIBIC. This could be a seasonal, altitude or regional dependency, which will be investigated further in subsequent sections.

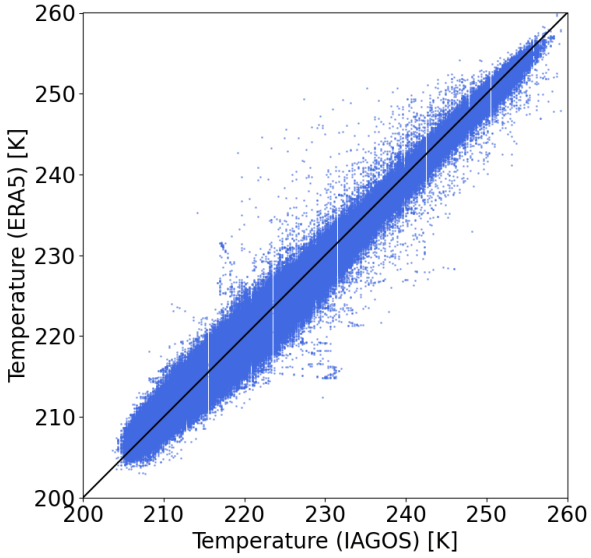

Figure 5.1: Comparison of temperature measured with IAGOS and temperature simulated in ERA5 reanalysis

5.2. Seasonal Comparison of Temperature Between ERA5 Reanalysis and IAGOS

This section will evaluate if the higher difference in temperature between IAGOS and ERA5 observed at lower temperatures is due to a potential seasonal bias in ERA5. In this seasonal comparison, the tropic and extratropics are also considered due to differences in these climates; the tropics are typically warm all year round, and their seasons can be broken into two: wet and dry [44]. Therefore, quantifying the seasonal influence on temperature without considering the climates may result in incorrect conclusions.

Figure 5.2 shows the temperature measured by IAGOS and the corresponding temperature simulated by ERA5 for seasons DJF, MAM, JJA and SON. All seasons appear to display a relatively equal difference between IAGOS and ERA5 and show higher differences at lower measured temperatures and lower differences at higher measured temperatures. The larger differences observed at lower temperatures occur in the extratropic regions, aligning with literature. P. Reutter et al. [57] showed that in the North Atlantic corridor, the largest differences between ERA-interim and MOZAIC were found around the tropopause and in the lowermost stratosphere, where some of the lowest temperatures were found. When K. Wolf et al. [83] examined latitudinal and longitudinal temperature differences in the midlatitudes, pressure level 200 hPa showed the largest cold bias in ERA5 compared to IAGOS, which is also where the lowest temperatures were found. However, when K. Wolf et al. [83] examined the overall mean difference, pressure levels 200 and 225 hPa showed the lowest differences between IAGOS and ERA5. Looking at Figure 5.2, this could occur due to similar scattering of points below and above the y=x line in the extratropics, as also seen in the North Atlantic by F. Berkes et al. [6]. K. Wolf et al. [83] also showed pressure level 250 hPa to have a larger cold bias compared to lower pressure levels; this was also the level with the highest measured temperatures by IAGOS.

The tropics have a lower temperature difference between IAGOS and ERA5 overall. Perhaps this is due to the tropics showing a much lower yearly variation in temperature compared to the extratropics, with yearly temperatures varying between 1°C and 4°C [77]. Hence, there are fewer fluctuations that ERA5 has to take into account.

Season DJF seems to have a few more data points scattered outside the highly dense area around the y=x line. Meanwhile, MAM (extratropic) has two small groups of points that are further from the y=x. One group is between an IAGOS temperature of 225 K to 230 K and around a temperature of 215 K simulated with ERA5. The other group is located around a measured temperature of 218 K with IAGOS where ERA5 simulates temperatures between approximately 220 K and 232 K. These are the most significant difference observed between ERA5 and IAGOS in terms of temperature.

Overall, there does not seem to be a seasonal bias that is causing the larger differences between ERA5 and IAGOS at lower temperatures or the smaller differences at higher temperatures. Whether there is a seasonal bias based on the pressure level or the exact region still has to be examined. How-

ever, there does seem to be a potential climate bias, with the extratropics showing larger differences between IAGOS and ERA5 at lower temperatures.

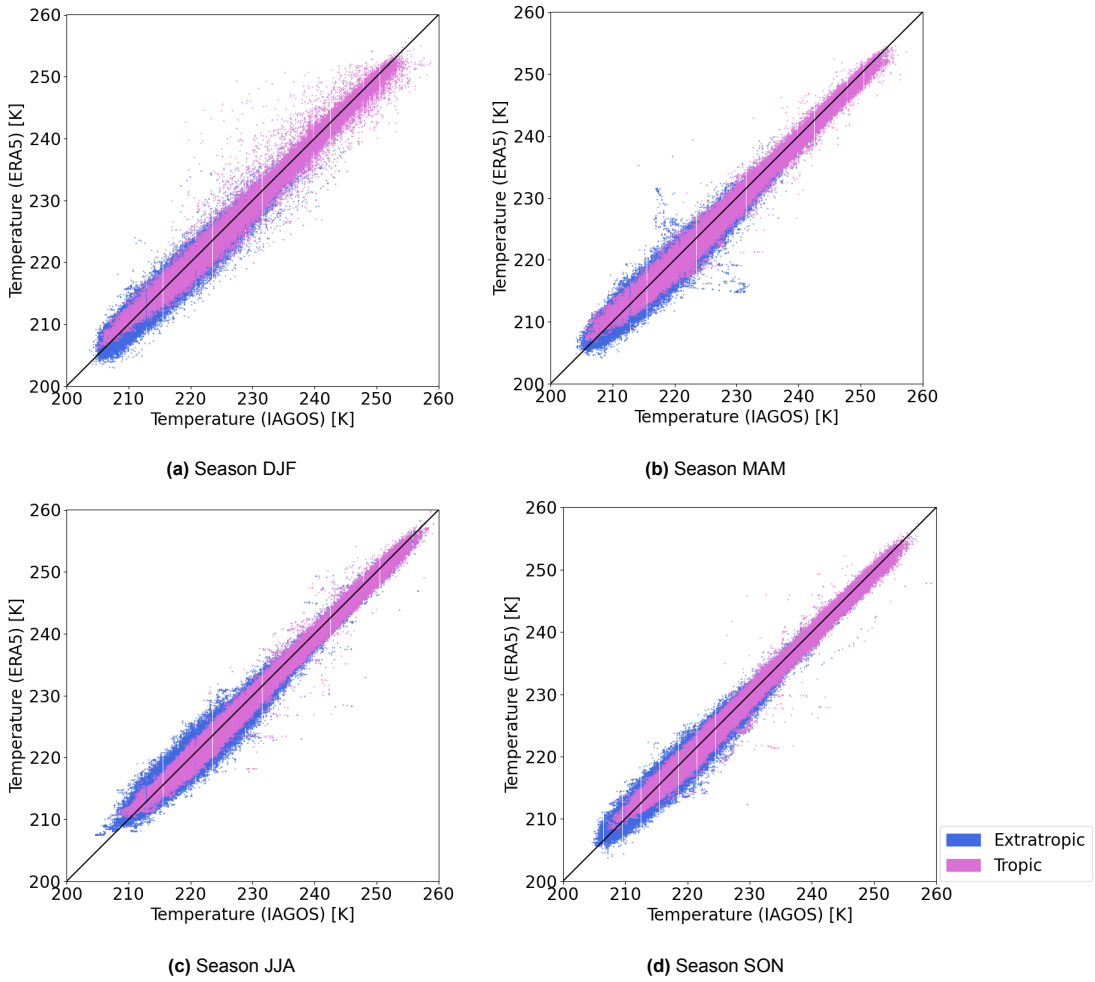

(a) Season DJF

(b) Season MAM

(c) Season JJA

(d) Season SON

Figure 5.2: Comparison of temperature measured with IAGOS and temperature simulated in ERA5 reanalysis per season

5.3. Comparison of Temperature from a Regional, Pressure Altitude and Seasonal Perspective

The following section looks into the temperature variation between IAGOS and ERA5 from a regional, pressure altitude and seasonal perspective. First, the vertical distribution of the IAGOS and ERA5 mean temperature per season and region is presented. Thereafter, the variation of the IAGOS and ERA5 temperature with respect to the mean are presented. This is followed by probability density functions to further classify the distribution of temperatures. Lastly, errors between the measured IAGOS temperature and simulated ERA5 temperature are presented.

The vertical distribution of the IAGOS and ERA5 mean temperature per season and per region is displayed in Figure 5.3. The tropopause height is also shown. It is calculated using the definition of the dynamic tropopause using potential vorticity (PV), where $PV = 2PVU$, $PVU = 10^{-6}$ $m^2Ks^{-1}kg^{-1}$. This was derived using one year of ERA5 potential vorticity data [53]. The overall difference in mean temperature between IAGOS and ERA5 is small. In the extratropic regions, ERA5 tends to predict slightly lower mean values of temperature in comparison to IAGOS, as also observed by K. Wolf et al. [83]. Generally, the mean difference in temperature per season and pressure level for the extratropics lies within the uncertainty of IAGOS' temperature sensor, though in some cases, it also lies outside as seen in Section A.1, pointing towards biases in ERA5. The lower ERA5 temperature could cause a false identification of ice supersaturation, which requires the temperature to be below the thresh-

old of homogeneous freezing (235.15 K). It would only be a false identification if ERA5 simulated a temperature below the threshold in combination with a relative humidity over ice above 1.

As the altitude increases, temperatures decrease until around the tropopause, consistent with literature [57, 53, 83]. Above the estimated tropopause, the difference in the mean temperature between IAGOS and ERA5 in the extratropics per season is less evident, where the change in mean temperature also slows down. This may be due to not defining the pressure levels with respect to the tropopause, such as done by A Petzold et al. [53], meaning the pressure levels close to the tropopause may contain both upper troposphere and lower stratosphere influences. Typically, temperatures increase again above the tropopause, as A. Petzold et al. show with the MOZAIC dataset [53]. Hence, the mean temperature is a function of higher and lower temperatures, where ERA5 shows more biases for the latter. The location at which the rate of the decrease in temperature begins does not exactly coincide with the calculation of the tropopause height. It could result from estimating the mean tropopause height per region and season, where certain fluctuations may not be visible. For example, the tropopause height varies greatly as a function of the latitude, particularly in the extratropics, from a height of 8 km at around 70°N to a height of 14 to 16 km at 30 °N [27].

In the tropics, larger differences between IAGOS and ERA5 are found at higher altitudes, with ERA5 becoming warmer than IAGOS. Here, the tropopause is below 175 hPa (generally less than 150 hPa). Hence, temperatures continue decreasing for the pressure levels considered in this study. As seen in Section 5.2, ERA5 may show a warm bias at sufficiently low temperatures in the tropics. Hence, pressure level biases may be related to the location of the tropopause.

Moreover, in the tropic regions, it is almost impossible to distinguish seasonal variations in the mean temperature of IAGOS and ERA5, which is in line with the observations in Section 5.2. South Asia shows some seasonal variation, though ERA5 is able to capture this behaviour in the mean temperature. In the extratropics, the highest temperatures always occur in JJA and the lowest in DJF, as also shown by A. Petzold et al. [53].

Overall, the analysis of the vertical distribution of IAGOS and ERA5 mean temperature does not show large deviations between the two datasets. There is a small influence of pressure levels related to the location of the tropopause and climates s seasons does not seem to play a large role.

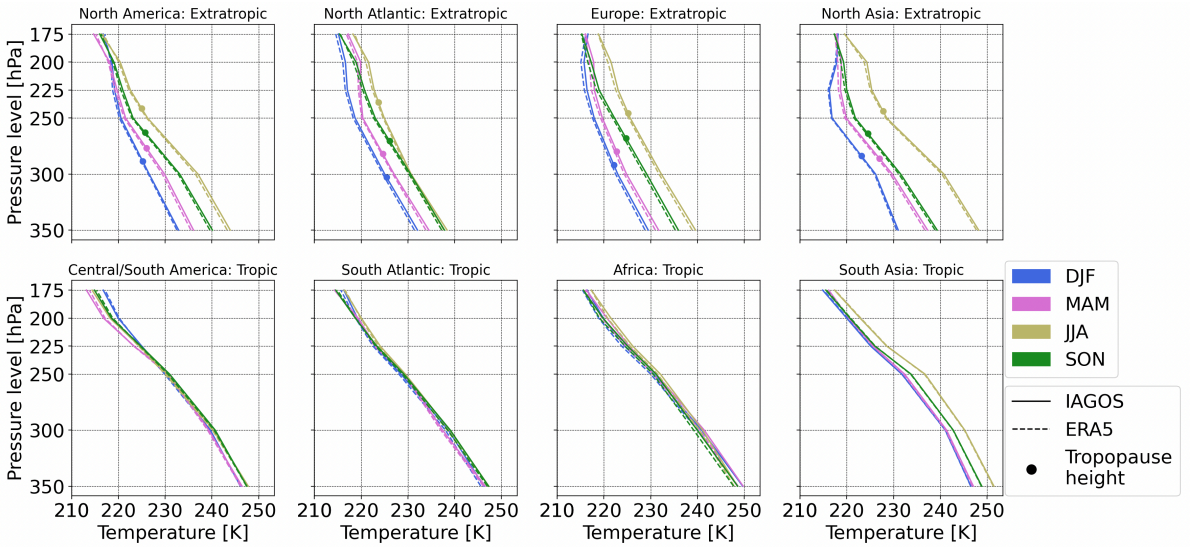

Figure 5.3: Vertical distribution of IAGOS and ERA5 mean temperature per season and per region

Figure 5.4 displays the mean plus or minus the standard deviation of the IAGOS and ERA5 temperature per season and pressure level for the extratropic regions. The standard deviations are found in Section A.2. ERA5 tends to have a slightly smaller interval in comparison to IAGOS, which is due to the smaller standard deviation in ERA5. P. Reutter et al. [57] also found a slightly smaller standard deviation for ERA-interim when compared to MOZAIC.

The lower bound is well estimated in most cases by ERA5, except for at pressure level 175 hPa where it tends to be higher than IAGOS. Upper tropospheric measurements may influence the lower

bound, which have lower temperatures than the lower stratosphere. As seen previously, ERA5 can show a warm bias at low measured temperatures. The variation of the temperature differences in Section A.1 also shows the lower bound being within IAGOS's accuracy range or close to, except at pressure level 175 hPa.

The upper bound tends to be underestimated by ERA5, and it is observed for almost all seasons, pressure levels and extratropic regions. This shows a cold bias in ERA5 and is in line with the observations in Section 5.2 and is a model bias in ERA5 as the differences lie outside the uncertainty of IAGOs' temperature sensor. At higher altitudes, particularly pressure levels 225, 200 and 175 hPa, the cold bias is expected; in the extratropics, studies generally observe a cold bias in the lower stratosphere using NWP models, such as the ECMWF-IFS, MetUM and ERA5 [7, 65]. It may be due to the sharp gradient of water vapour across the tropopause, which such models fail to maintain, causing a leakage of water vapour into the lower stratosphere [65]. However, the cold bias is not always observable, particularly at 175 hPa. This is due to a combination of a lower standard deviation in ERA5 and a higher mean compared to IAGOS. It is not assumed to be due to a lack of samples. Pressure level 175 hPa has more samples than 350 hPa in the extratropics, and as will be seen later, bootstrapping of probability density functions shows sufficient data points at 175 hPa.

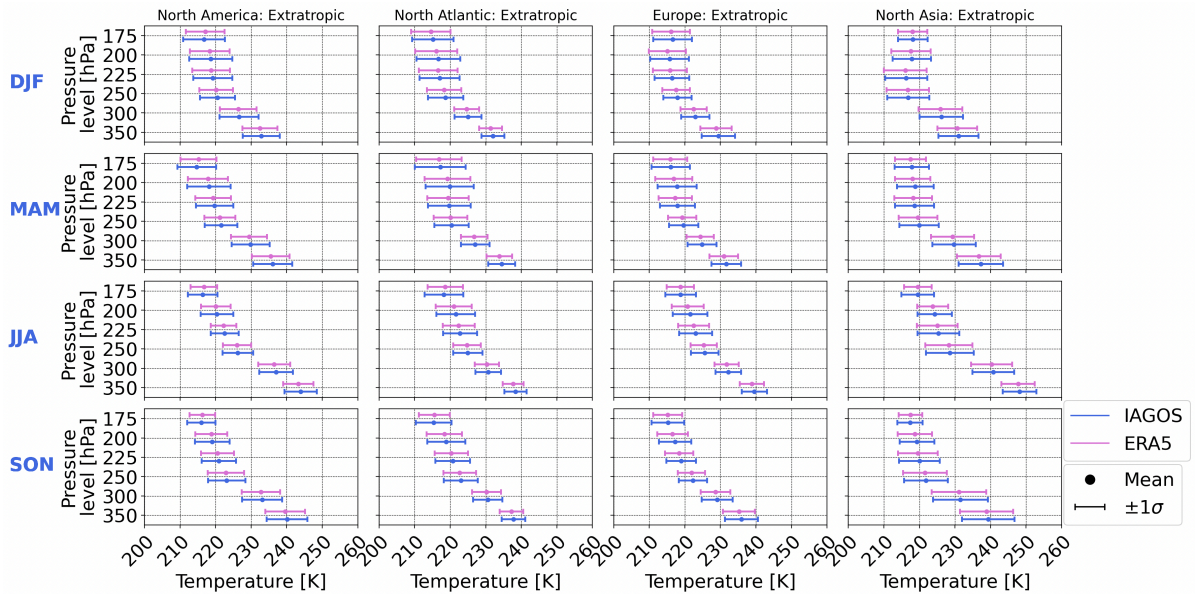

Figure 5.4: Mean $\pm 1\sigma$ of IAGOS and ERA5 temperature per pressure level and season for extratropic regions

The mean and the standard deviation of the IAGOS and ERA5 temperature per season and pressure level for the tropic regions are shown in Figure 5.5. For both ERA5 and IAGOS, the intervals have become smaller due to fewer temperature variations in the tropics. Given the lower number of measurements in Central/South America and South Atlantic compared to the other tropic regions, larger standard deviations for these two regions could occur. This is observable at pressure levels 175 hPa and 200 hPa. However, this may also be model biases, which will be examined further.

The upper bound is slightly lower for ERA5 than for IAGOS for most seasons, pressure levels and regions, showing a cold bias at higher temperatures in ERA5. It is also more prominent at lower altitudes. This is the cold bias seen at higher measured temperatures in Section 5.2. Examination of the standard deviation of the temperature differences in Section A.1, shows that this bias cannot be entirely attributed to the accuracy of IAGOS' temperature sensor.

The lower bound is also well estimated by ERA5 in the tropics, and differences are often within the uncertainty range of IAGOS' temperature. At pressure levels 175 hPa and 200 hPa, ERA5 has a higher lower bound than IAGOS. The cause of this is the warm bias in ERA5 at sufficiently low temperatures in the tropics and cannot be attributed to sensor uncertainty.

Figure 5.6 shows the probability density function (PDF) of the extratropic regions per pressure level for season DJF. The reader is referred to Section A.3 for all seasons. Bootstrapping was applied to examine if there were enough data points to make a PDF. The results are found in Section A.4

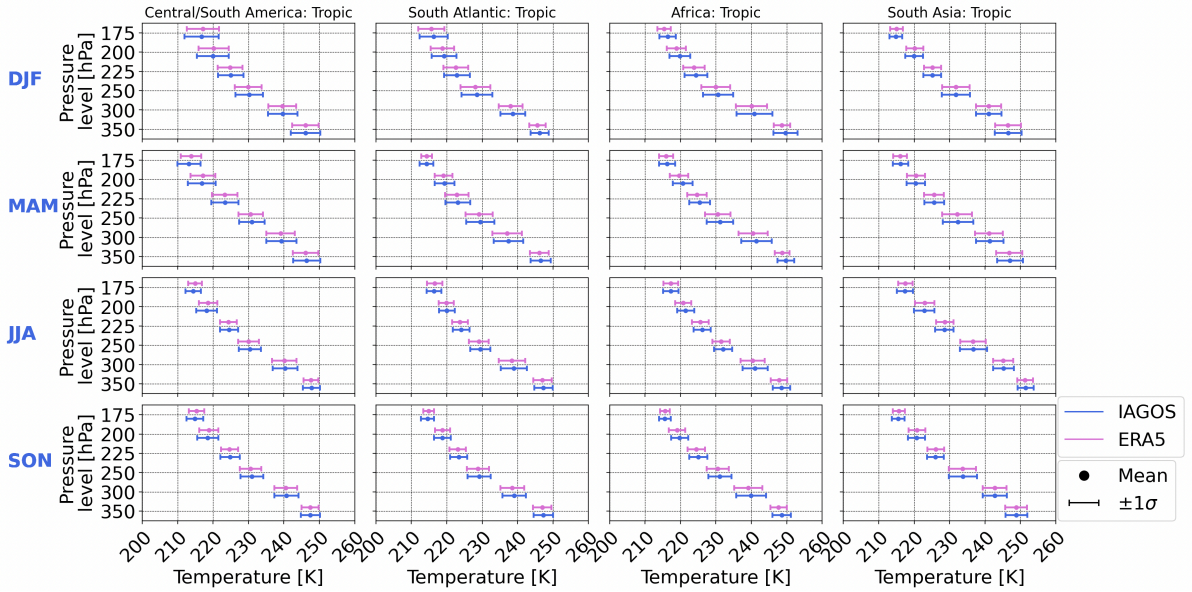

Figure 5.5: Mean $\pm 1\sigma$ of IAGOS and ERA5 temperature per pressure level and season for tropic regions

and showed that only North Atlantic at pressure level 350 hPa lacked measurements. Hence, the conclusions formed here come with more uncertainties.

The PDFS also show minor differences in temperature between IAGOS and ERA5 for the extratropics, and ERA5 is able to find the peak in the PDF. However, ERA5 seems to be shifted very slightly leftwards in comparison to IAGOS, showing the cold bias, as previously discussed. This is also observable on a PDF of the temperature differences, where the peak is located above +0.5 K and outside the sensor accuracy range. The slight leftwards shift was also observed by K. Wolf et al. [83] for a region covering the United States, North Atlantic and Continental Europe. The other three seasons (MAM, JJA, SON) all display the same behaviours observed in DJF, which can be seen in Section A.3. Hence, the cold bias is a model bias present in ERA5.

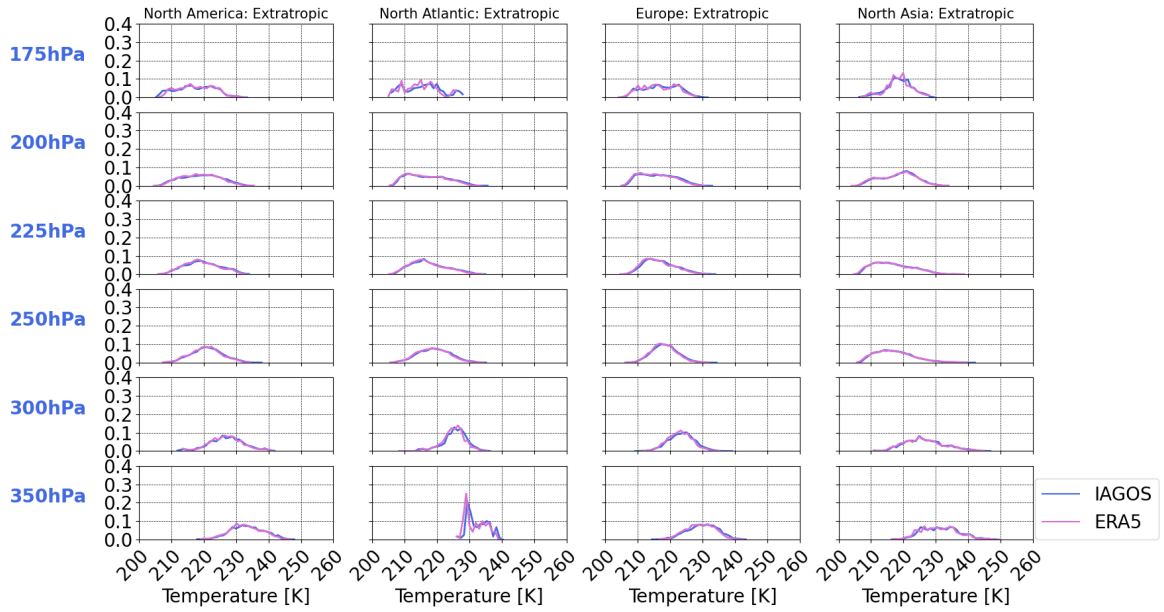

Figure 5.6: Probability density function of IAGOS and ERA5 temperature per pressure level for the extratropic regions and season DJF, with 1 K bin size

The probability density function as a function of pressure level for the tropic regions in DJF is displayed in Figure 5.7. The PDFs at pressure levels 175 and 350 hPa should not be used to establish differences between IAGOS and ERA5 due to the lack of samples, as shown by the bootstrapping of the PDFS. ERA5 struggles to find the temperature with the highest probability of occurrence in Africa compared to the other tropic regions. Africa also shows a more leftward shift of the ERA5 curve after the peak, showing the previously identified cold bias at higher temperatures. The other tropic regions show a much better agreement between ERA5 and IAGOS in the PDFs. Analysing the PDF of the relative difference in temperature for these three regions also shows the peak being located within IAGOS' temperature sensor accuracy range. The tropics also feature sharper peaks compared to the extratropics and the PDFs for all seasons in the tropics look relatively similar. Both observations are likely the result of low yearly variation in temperature for this climate. The PDFs for the other seasons can be found in Section A.3.

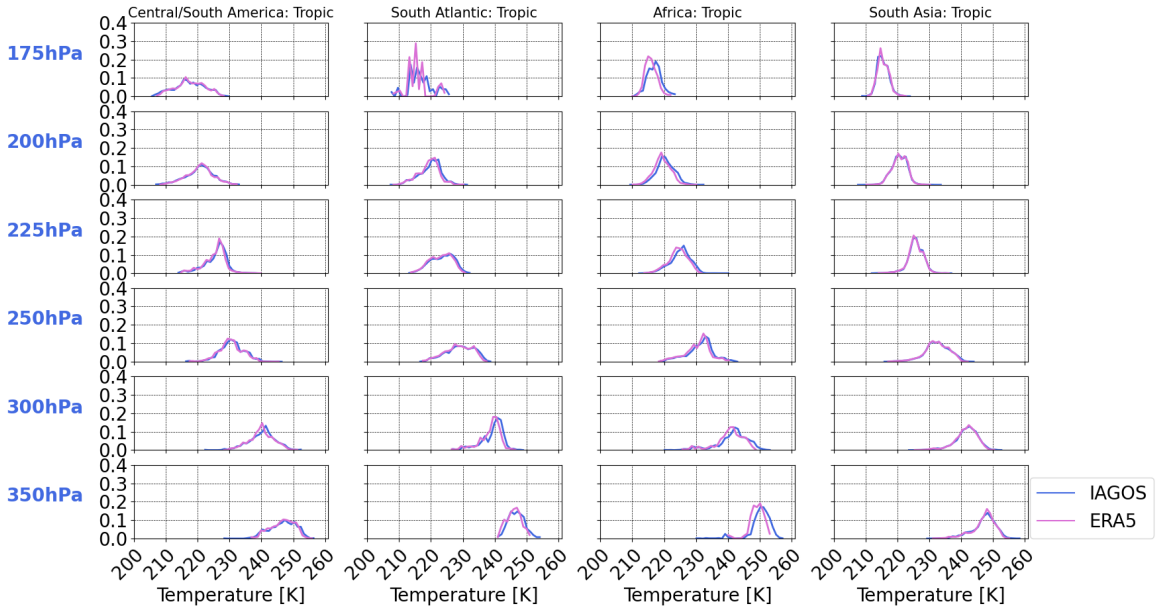

Figure 5.7: Probability density function of IAGOS and ERA5 temperature per pressure level for the tropic regions and season DJF, with 1 K bin size

Figure 5.8 shows the mean difference (MD) and the root mean square error (RMSE), with IAGOS taken as the baseline value per season and pressure level for the extratropics. The mean difference generally lies between 0.1 K and 0.5 K for the extratropics regions. K. Wolf et al. also determined a mean difference between 0.1 K and 0.5 K considering pressure levels 200 to 250 hPa [83]. This is within the uncertainty of IAGOS' temperature sensor. At pressure level 175 hPa, a negative mean difference between IAGOS and ERA5 is observed for all seasons in North America, JJA and SON in the North Atlantic and SON in North Asia. This means that ERA5 tends to be warmer than IAGOS, as seen in Figure 5.4. For all extratropic regions, the RMSE is between 1 K and 1.5 K, which is approximately equivalent to a range of 0.4 % to 0.7% of the measured and simulated temperatures by IAGOS and ERA5. K. Wolf et al. [83] found RMSE values between 1 K and 2 K.

Errors tend to decrease going from pressure level 350 hPa to either 300 or 250 hPa, after which they increase again until pressure level 200 hPa. In some instances, such as for seasons DJF and MAM in the North Atlantic, RMSE stays relatively constant between pressure levels 350 hPa and 250 hPa, after which the RMSE increases again. Overall, the smallest MD and RMSE generally occur at a pressure level of 250 hPa for all regions and seasons, and the largest occur at 175, 200 hPa or 350 hPa. K. Wolf et al. found the minimum temperature error to occur at 225 hPa and the largest at 250 hPa when using 'good' and 'limited' temperature validity flags. However, this was not considering the influence of the seasons, and it was found for a region covering 30°N to 70°N and 100°W to 30°E [83]. Moreover, the RMSE may also be influenced by how many data points are available; fewer measurements may lead to a larger RMSE.

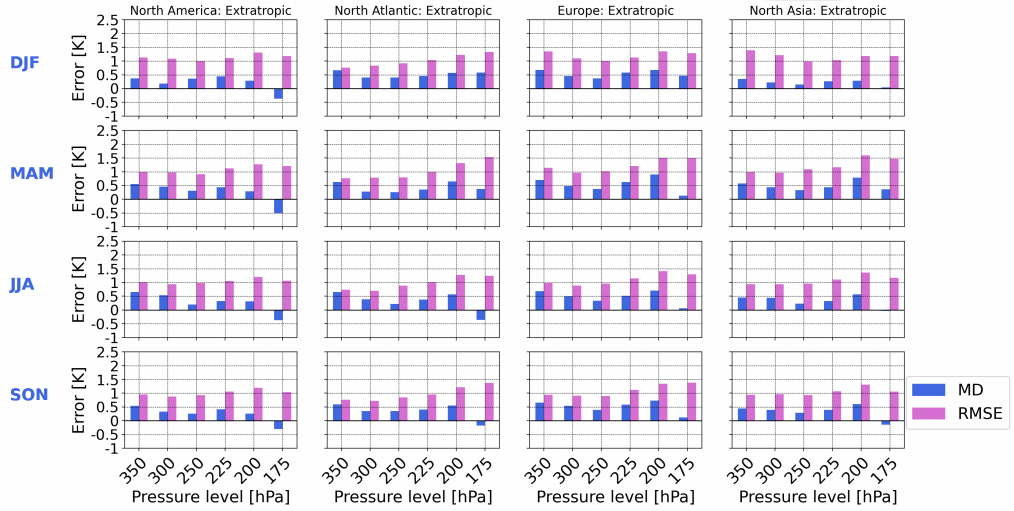

Figure 5.8: Mean difference (MD) and root mean square error (RMSE) between IAGOS and ERA5 temperature per season and pressure level for the extratropic regions

When analysing the mean difference and root mean square error in the tropics, in Figure 5.9, a regional bias can be seen for ERA5, with errors differing largely between the four regions considered. For example, South Asia shows the lowest mean difference, and Africa shows the highest mean difference. This is to be expected given the good approximation of the PDF in South Asia, but not in Africa, as seen in Figure 6.7. South Atlantic shows the second-highest mean difference values and Central/South America displays the second-lowest MD values. Overall, the mean difference values can range from 1 K to -0.5 K in the tropics, with a negative value showcasing a warm bias in ERA5, where the warm bias is typically observed at high altitudes.

More consistent values are found in the RMSE between the regions, though Africa displays a much larger RMSE for pressure levels 350 and 300 hPa compared to the other regions, which is more pronounced in DJF. Furthermore, the tropics generally show a decrease in RMSE from pressure level 350 hPa to around 250 hPa, in which it increases again until 200 hPa. However, in South Asia, seasons JJA and SON show almost equal RMSE values for all pressure levels, and DJF shows a decrease from 350 hPa to 175 hPa. Generally, the RMSE values lie between approximately 0.5 K and 1.5 K, which is still less than 1% of the measured and simulated temperatures. Hence, temperatures are still very well estimated in the tropics by ERA5, with the best-simulated values found in South Asia.

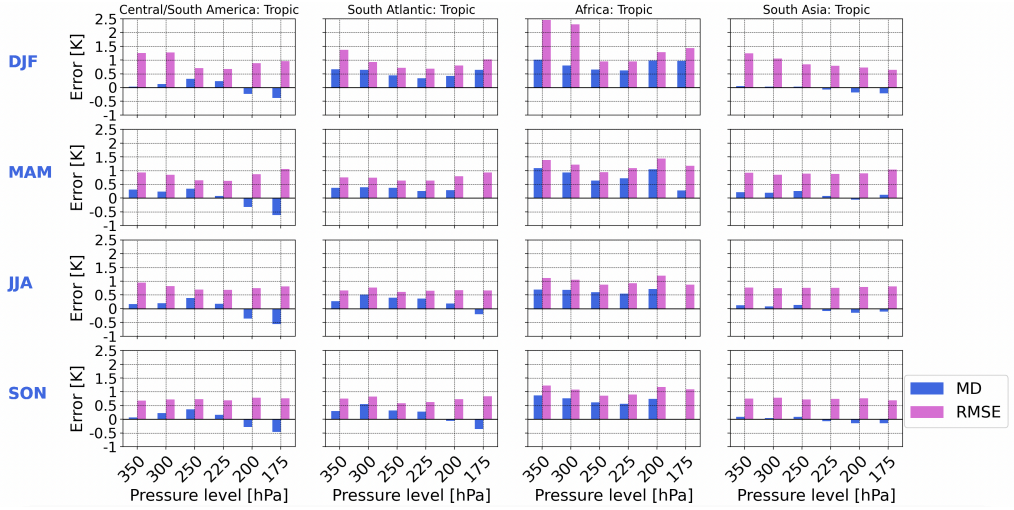

Figure 5.9: Mean difference (MD) and root mean square error (RMSE) between IAGOS and ERA5 temperature per season and pressure level for the tropic regions

In conclusion, this section focused on validating the temperature from the ERA5 reanalysis using

the IAGOS in-situ measurements from a regional, seasonal and pressure level perspective. ERA5 is highly accurate in simulating temperature but is subject to a cold bias, particularly at higher measured temperatures. The degree of the cold bias is dependent on the region and pressure level. Moreover, a warm bias appears at lower measured temperatures at high altitudes. In the tropics, this is due to colder observed temperatures in IAGOS, but in the extratropics it could be due to upper tropospheric influences. Lastly, differences in temperature between IAGOS and ERA5 did not seem to vary depending on the season, shown through similar errors and PDFs.

5.4. Comparison of Temperature from a Regional, Pressure Level and Yearly Perspective

As previously discussed, there seems to be an influence of region and pressure level on the temperature differences to expect between IAGOS and ERA5. However, yearly variations were not taken into account. Thus, the following section analyses differences in the temperature distribution between IAGOS and ERA5 from a regional, pressure level and yearly perspective.

The yearly variation of the mean temperature plus or minus one standard deviation measured by IAGOS and simulated by ERA5 per pressure level and region can be found in Figure 5.10 and Figure 5.11. The standard deviations are found in Section A.5. The means also takes into account seasons. For example, DJF in 2012 is shown on the vertical line at 2012 and JJA in 2012 is located at the halfway distance between 2012 and 2013. This is the same for all years. Hence, for the extratropics, the peaks generally represent JJA, given this is the season where the highest temperatures occur. Fewer peaks are apparent in the tropics due to low yearly temperature variation, as discussed in Section 5.3.

Examining Figure 5.10 shows that ERA5 is very good at approximating the yearly trend in temperature for all extra tropic regions. ERA5 is shifted slightly downwards compared to IAGOS, which is ERA5's cold bias discussed earlier. For the years 2018/2019 to 2022, an increasing deviation between IAGOS and ERA5 is observed, which is more evident at higher altitudes, starting at a pressure level of 225 hPa. ERA5 considers observations from across the world, which is combined with model data [11]. Hence, if the behaviour was, for example, due to global warming, one would expect such observations to already be included in the ERA5 product. This is also given that the latency of the final ERA5 product is 2-3 months [11]. Moreover, no data corruption in ERA5 has been observed for these years [15], and no studies seem to have validated ERA5 temperature for the pressure levels considered in this study beyond 2020. Furthermore, this is around when COVID-19 started impacting flights, though B. Ingleby et al. [33] showed that the ECMWF forecasts did not suffer due to COVID-19. It most likely stems from changes in sampling in IAGOS since 2020, as seen in Figure 5.12. This is also given that in 2022, for North Atlantic and Europe, where sampling levels have increased to the same levels as before COVID-19, deviations between IAGOS and ERA5 began to decrease again.

Figure 5.11 also displays ERA5's good ability to estimate the yearly temperature in the tropics. In Central/South America, South Atlantic and Africa, ERA5 underpredicts the temperature more often than in South Asia. Africa shows a consistent yearly underestimation. It may be due to ERA5 model errors in this particular region, as was shown previously, but also the number of data points. As seen in Figure 5.12, Central/South America, South Atlantic and Africa have fewer samples compared to South Asia. Africa shows more points sampled from 2011 to 2013, where fewer deviations are seen between IAGOS and ERA5. Fewer measurements are available from 2014 to 2016, and an increasing deviation can be seen. In South Asia, differences in IAGOS and ERA5 are also seen starting in 2020 and extending to 2022; measurements in IAGOS decreased drastically due to COVID-19 in 2020 and by 2022, the sampling in South Asia did not recover to levels before COVID-19. This shows that if there are not enough samples or inconsistencies in the yearly sampling, proper conclusions cannot be formed.

Overall, the yearly, pressure level and regional temperature validation showed that ERA5 is highly accurate in simulating temperature. The analysis showed a possible increase in the deviation between ERA5 and IAGOS after 2020. This was attributed to a decrease in measurements within IAGOS due to COVID-19. A general number of samples in Central/South America and the South Atlantic also led to more observable deviations between IAGOS and ERA5. Changes between a high and low number of measurements in Africa also led to ERA5 showing a larger colder bias for certain years. Therefore, the yearly analysis of temperature deviations between IAGOS and ERA5 in the tropics, excluding South Asia, and post-COVID-19 for most regions cannot be used as an accurate insight.

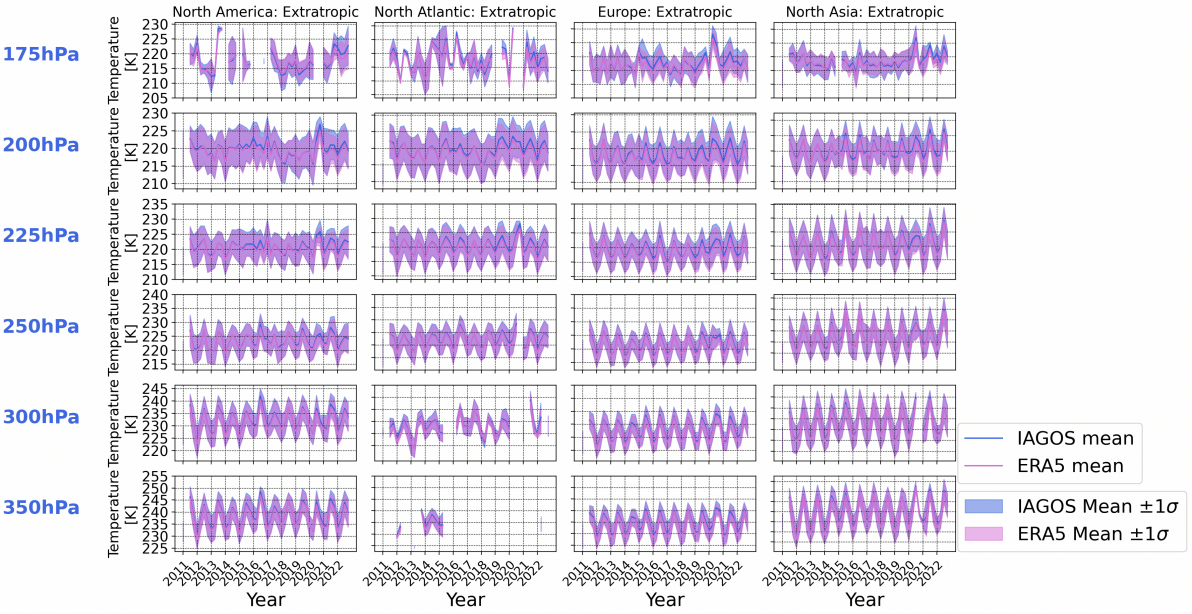

Figure 5.10: Yearly variation in IAGOS and ERA5 mean temperature per pressure level for extratropic regions, and variation due to one standard deviation $\pm 1\sigma$

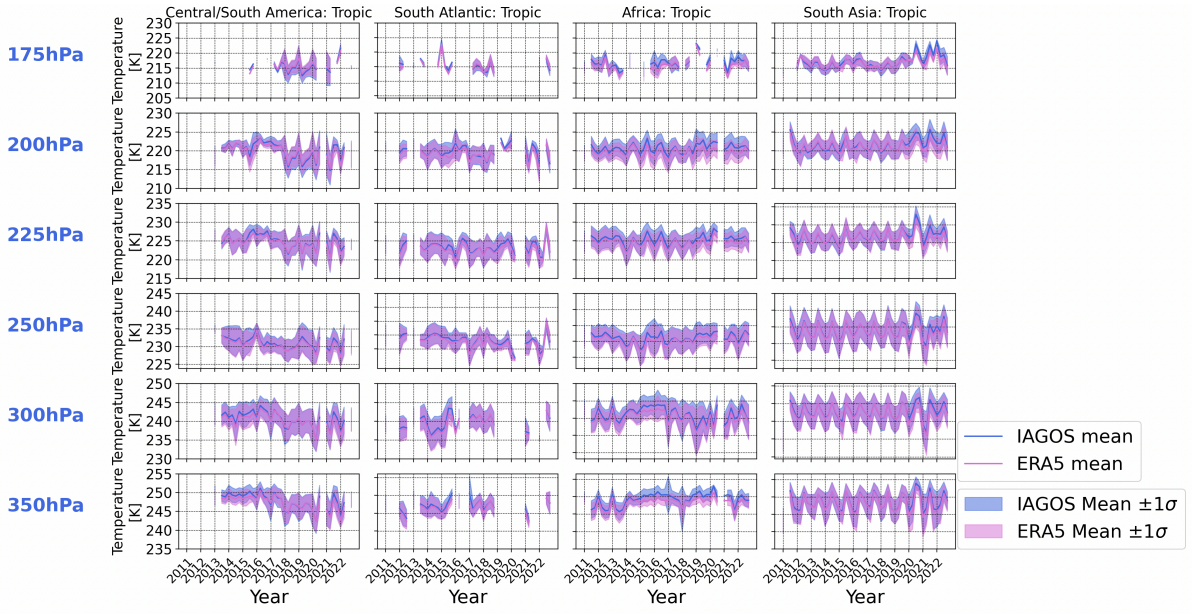

Figure 5.11: Yearly variation in IAGOS and ERA5 mean temperature per pressure level for tropic regions, and variation due to one standard deviation $\pm 1\sigma$

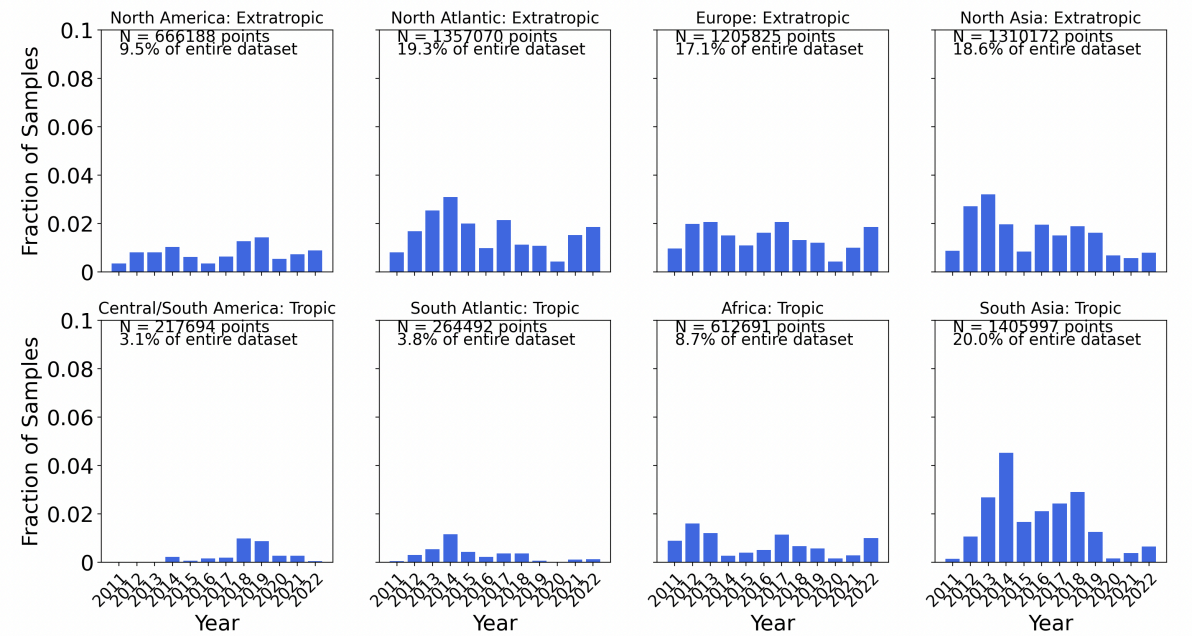

Figure 5.12: Fraction of measurements sampled per region and per year

5.5. Selection of Temperatures below Threshold of Homogeneous Freezing

The cold bias in ERA5 can potentially cause a false identification of ice supersaturated regions. This section quantifies the hit rate and false alarm rate for the selection of points below the threshold of homogeneous freezing, using the definitions in Section 4.5. While the temperature accuracy in ERA5 did not seem to be largely influenced by the seasons, this will still be considered to ensure no potential biases.

The hit and false alarm rate for the selection of points below the threshold of homogeneous freezing in the extratropic regions is shown in Figure 5.13. The hit rate is almost equal to 100% for all regions, seasons and pressure levels, meaning that, generally, ERA5 detects values below the threshold when IAGOS does as well. The false alarm rate shows ERA5's cold bias and it fluctuates between 0 and 100%. When it is equal to 100%, it means that there are no $N_i N_e$, but only $N_i Y_e$ combinations. This might be artificially higher in the case of a small number of $N_i Y_e$.

These high false alarm rates are more prominent in season MAM. This could be the group of outliers around the threshold of homogeneous freezing in the IAGOS measurements for the extratropic climate in season MAM, identified in Figure 5.2b. IAGOS and ERA5 temperatures show a temperature difference of around 10 to 15 K for these outliers, which is outside the accuracy of the IAGOS temperature sensor. Given that the high false alarm rate is generally found at pressure levels 225 to 175 hPa, where temperatures are below the threshold, it points to a possible issue in the IAGOS measurements, even though the IAGOS fleet is equipped with highly accurate temperature sensors. The high false alarm rate is also detected at pressure levels 225 to 175 hP in other regions and seasons, as well as at 250 hPa, equivalent to the regions and pressure levels where an increasing yearly temperature deviation was observed between IAGOS and ERA5. Hence, this may also cause the high false alarm rate.

The $N_i Y_e$ percentage lies between 1 to 5% per season, region and pressure level in the extratropics. Of each fraction, less than 15% of points show ERA5 simulating a relative humidity over ice greater than 1. This means that, overall, less than 1% of points in ERA5 would not be detected for ice supersaturation solely based on temperature. Therefore, the temperature does not greatly influence the selection of points for ice supersaturation in the extratropics.

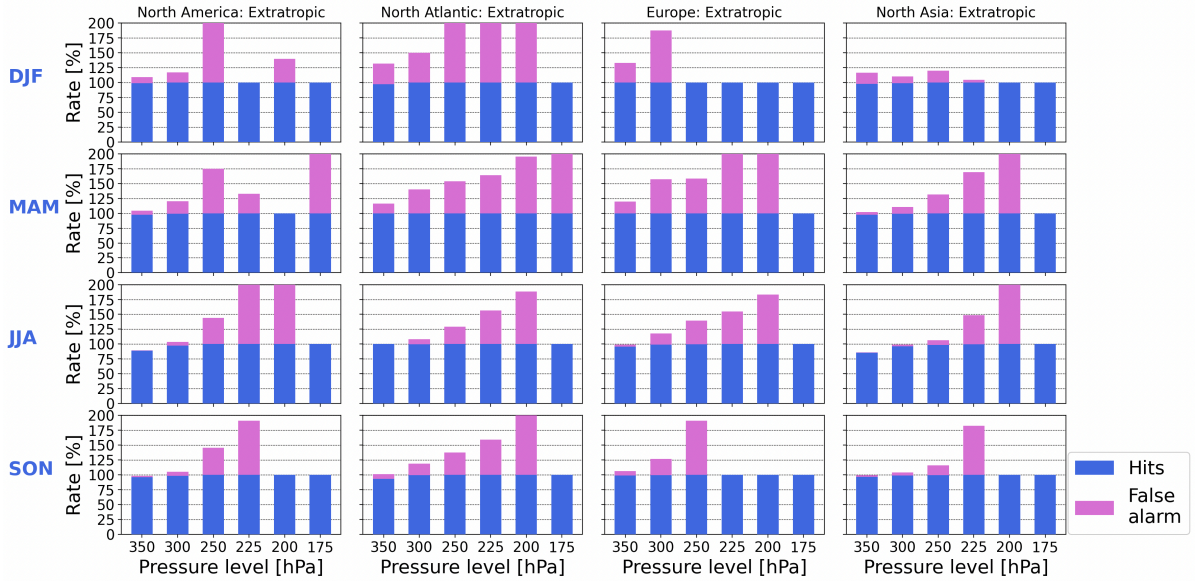

Figure 5.13: Hit rate and false alarm rate for threshold of homogeneous freezing per season and pressure level for extratropic regions

The hit and false alarm rate per season and pressure level for the tropic regions are shown in Figure 5.14. Again, the hit rate is mainly equal to 100%, showing ERA5's good ability in selecting points below the threshold. Though, at pressure level 350 hPa, most regions, except South Asia, have a hit rate equal to 0% due to the higher temperatures in this climate. This also results in a false alarm rate of 0%. At pressure level 300 hPa and at 350 hPa in South Asia (DJF and MMA), the hit rate is less than 100%, with a barely detectable false alarm rate. This shows that ERA5 is not detecting some points below the threshold, while IAGOS does. This is due to the slight warm bias present in ERA5 in the tropics.

At pressure level 225 hPa, Africa and South Asia show high false alarm rates across all seasons, as well as Central/South America in season SON. These may result from the increasing yearly temperature deviations between IAGOS and ERA5 but are also artificially high due to a low number of $N_i Y_e$ and no $N_i N_e$. Hence, the effect of this increasing deviation is almost negligible on the selection of points below the threshold of homogeneous freezing. Lastly, the false alarm rates are less prominent in the tropics than in the extratropics, which most likely stems from lower variations in temperature.

The percentage $N_i Y_e$ per season, region and pressure level in the tropics is approximately 1% at pressure level 250 and below. Though, in Africa, it can be up to 5%. It is negligible at 225 hPa and above for all tropic regions and seasons. Of the $N_i Y_e$ combinations, Africa has 25 to 60% of these points, with ERA5 having a relative humidity over ice above 1. In other tropic regions, the percentage is generally less than 5%. Hence, the cold bias might be more critical in Africa compared to any other region, albeit still small. Overall, the hit and false alarm rate for selecting points below the threshold of homogeneous freezing shows that temperature deviations between IAGOS and ERA5 almost have a negligible influence on the estimation of ice supersaturation.

5.6. Temperature Conclusion

The temperature simulated by ERA5 has been validated from a seasonal, yearly, pressure level and regional perspective using the IAGOS in-situ measurements. Overall, ERA5 is very accurate in the simulation of temperature. A cold bias in ERA5 is observed and is particularly evident at higher measured temperatures by IAGOS. However, warm biases have also been found in certain instances, which seem more significant in the tropics and at low measured temperatures by IAGOS.

Seasons do not greatly influence temperature deviations between IAGOS and ERA5. However, there is an influence of the region and pressure level. Pressure level influences seemed to be dependent on the location of the tropopause. Moreover, ERA5 shows better estimates in the tropics compared to the extratropics when not considering Africa, which has higher errors than any of the other regions considered in this study. The yearly temperature trend also showed good agreement

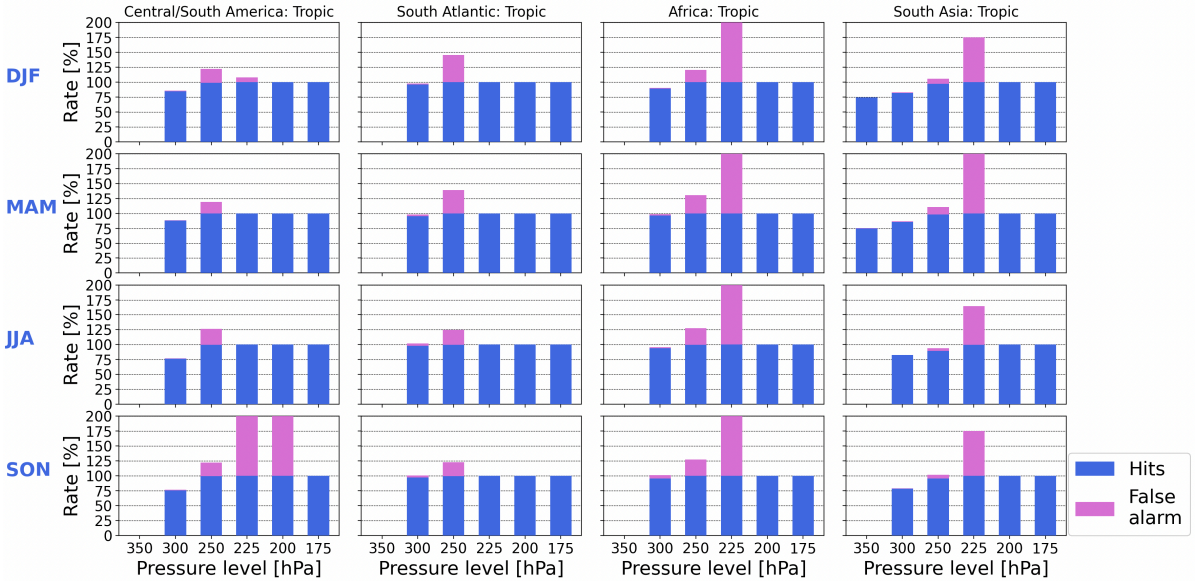

Figure 5.14: Hit rate and false alarm rate for threshold of homogeneous freezing per season and pressure level for tropic regions

between IAGOS and ERA5 but was influenced by the number of measurements. This was particularly evident in 2019/2020 due to COVID-19, which seemed to affect the IAGOS fleet until 2022.

The effect of these biases on the selection of points for ice supersaturation, based on the threshold of homogeneous freezing, was also investigated. This showed a good overall detection of values below the threshold. The cold bias led to instances of false alarms, which were sometimes artificially high due to a low number of data points. Nevertheless, the overall percentage of points being falsely selected for ice supersaturation solely based on the temperature was less than 1% for all regions except Africa and less than 3% in Africa. Hence, it can be concluded that the temperature is not a critical variable in detecting ice supersaturated regions in ERA5.

6. Validation of Relative Humidity over Ice in ERA5 Reanalysis using IAGOS In-Situ Measurements

The following chapter focuses on validating the relative humidity over ice simulated by ERA5 using the IAGOS in-situ measurements. First, a general comparison is done in Section 6.1, to get an overview of the overall deviations to expect between IAGOS and ERA5. This is followed by a seasonal comparison in Section 6.2. Thereafter, ERA5's relative humidity over ice is validated from a seasonal, regional and pressure level perspective in Section 6.3. However, this does not consider yearly variations. Hence, Section 6.5 compares ERA5 and IAGOS from a yearly, regional and pressure level perspective in order to separate any possible influences on the deviations to expect between the two datasets.

6.1. General Comparison of Relative Humidity over Ice Between ERA5 Reanalysis and IAGOS

In this section, the relative humidity over ice measured with IAGOS and the relative humidity over ice simulated in the ERA5 reanalysis are compared. The purpose of this comparison is to give an insight into the general differences to be expected in the relative humidity over ice between IAGOS and ERA5.

Figure 6.1a shows the relative humidity over ice measured by IAGOS and the corresponding relative humidity over ice (RHI) simulated by ERA5. Points scatter below the y=x line show a dry bias in ERA5, and when points are situated above this line, it means that ERA5 has a moist bias. The threshold for homogeneous freezing is considered in Figure 6.1b. Large differences cannot be observed between the two cases. Therefore, for further analysis of relative humidity, only cases with temperature below the threshold are considered, also due to the reasons discussed in Section 4.1.

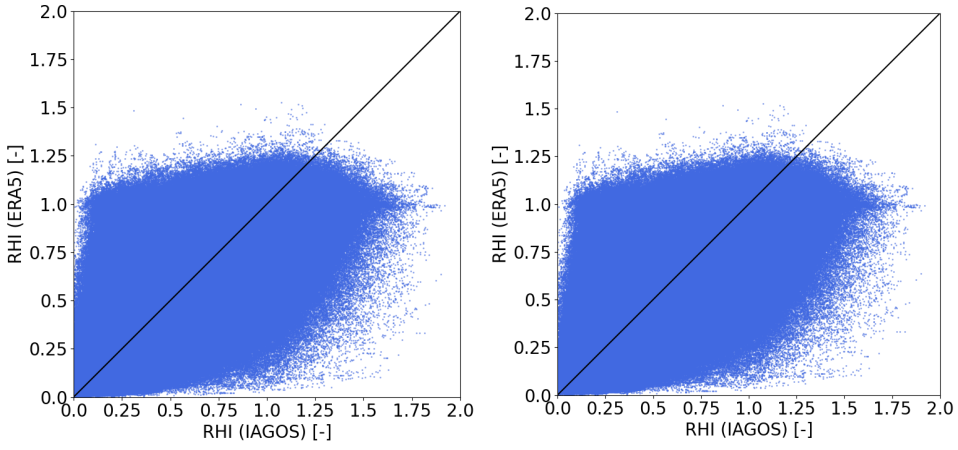

(a) No restriction on temperature

(b) Temperature $\leq$ 235.15 K

Figure 6.1: Comparison of relative humidity over ice measured with IAGOS and relative humidity over ice simulated in ERA5 reanalysis

Both figures show a disagreement between IAGOS and ERA5. There seems to be a flattening in the ERA5 dataset somewhere between an RHI value of 1.00 and 1.25, meaning that ERA5 cannot simulate values above this. Such behaviour has also previously been observed by K. Gierens et al. [20] and K. Wolf et al. [83] for ERA5 and by P. Reutter et al. [57] for ERA-interim. On the far right of the scatter plot, there are points in which IAGOS has measured a relative humidity over ice between

approximately 1.50 and 1.90, though the simulated values by ERA5 are concentrated around a value of 1. These behaviours are due to the saturation adjustment in numerical weather prediction models [83], as discussed in Section 2.3.

Another behaviour observed in Figure 6.1a is the simulation of values above ice supersaturation in ERA5; meanwhile, IAGOS measures low values of relative humidity over ice, showing a moist bias in ERA5. This occurrence is already observed at a measured RHI value of 0.25. K. Gierens et al. also observed this specific behaviour for specific seasons, primarily fall (represented by October), but also partially for summer (represented by July) [20]. Hence, perhaps there is a seasonal bias present in the estimation of relative humidity over ice within the ERA5 reanalysis. C. Dyroff et al. [14], J. Bland et al. [7] and T.G. Shepherd et al. [65] also found moist biases in the lowermost stratosphere in the ECMWF-IFS. K. Wolf et al. [83] observed a dry bias in ERA5 at pressure levels 200 to 250 hPa, which is around the tropopause. Thus, there may also be pressure level model biases in ERA5. This will be further investigated in subsequent sections.

6.2. Seasonal Comparison of Relative Humidity over Ice Between ERA5 Reanalysis and IAGOS

This section further examines the potential seasonal bias in relative humidity over ice between IAGOS and ERA5 by splitting the dataset into the four seasons defined in Chapter 4. Moreover, whether the climate is tropic or extratropic is also considered. Again, the focus is now only on cases in which the temperature is below the threshold of homogeneous freezing.

The relative humidity over ice measured by IAGOS and the corresponding relative humidity over ice (RHI) simulated by ERA5 for seasons DJF, MAM, JJA and SON are shown in Figure 6.2. Overall, the tropics show more points concentrated around the y=x line, with slightly less scattering in comparison to the extratropics below an RHI value of 1. This shows a better approximation of relative humidity over ice in the tropics below ice supersaturation. The flattening of ERA5 at an RHI value around 1.25 occurs in the extratropics, while in the tropics, this behaviour occurs closer to a value of 1.10. Moreover, when IAGOS measures a relative humidity over ice above 1.5 in the extratropics and above 1.25 in the tropics, the simulated values of RHI in ERA5 are concentrated around a value of 1. This points towards ERA5 having more trouble estimating the value of relative humidity over ice above ice supersaturation in tropical climates.

DJF seems to be the season with the least scattering above the y=x line, and JJA appears to have the most scattering for both tropics and extratropics. Below the y=x line, there is a slightly increased scattering for DJF for the extratropics, whereas more scattering below the line is observed for JJA in the tropics. The relationship seen for DJF is in line with what was observed for winter (January) by K. Gierens et al. [20]. In fall (October), K. Gierens et al. show an upward shift of the points, so more points are found above the y=x line. In this study, there is an increased number of points found above the y=x line for SON as well, though there is not a decrease in scattering below the y=x line. However, these differences may be due to K. Gierens et al. [20] only using one month of one year to represent a season.

Overall, this shows that there is a seasonal variation in the difference of relative humidity over ice between ERA5 and IAGOS, with DJF showing fewer possibilities of a moist bias in ERA5 and JJA showing more. The moist bias in JJA was also discussed by T.G. Shepherd et al. [65] in the ECMWF-IFS; a larger cold bias in the lowermost stratosphere was found in summer caused by excessive moisture (from water vapour) in the model. Hence, the model might also display a moist bias in relative humidity over ice. The fluctuations in the dry bias per season are not as clear, though ERA5 seems to have less of a dry bias in the tropics in DJF. Hence, there is a clear influence of climates and seasons on the differences to expect in relative humidity over ice between IAGOS and ERA5.

6.3. Comparison of Relative Humidity over Ice from a Regional, Pressure Level and Seasonal Perspective

Previously, a strong deviation between ERA5's simulated and IAGOS' measured relative humidity over ice (RHI) was observed. There seemed to be a seasonal deviation and also a climate dependency. This section further explores the seasonality dependency while also taking into account pressure levels and regions, where tropic and extratropic regions will be considered.

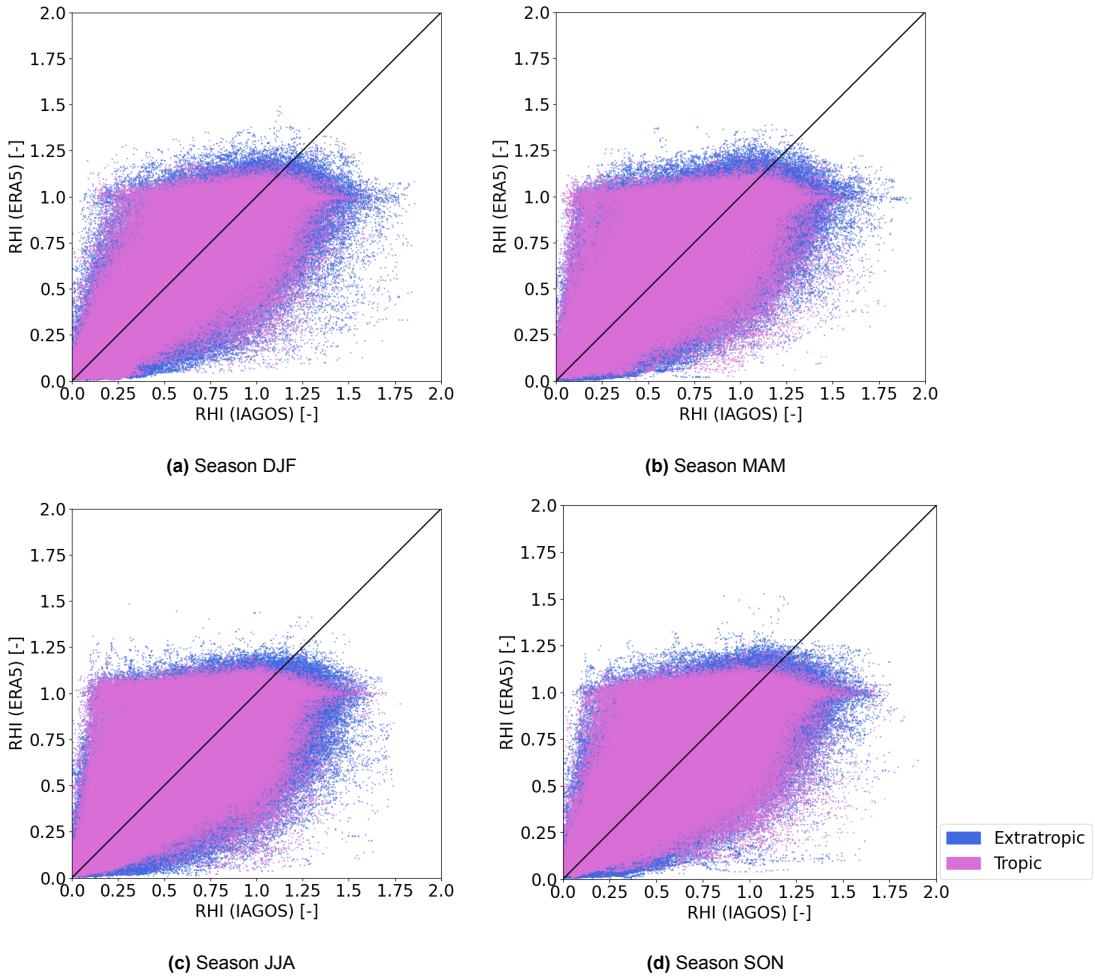

(a) Season DJF

(b) Season MAM

(c) Season JJA

(d) Season SON

Figure 6.2: Comparison of relative humidity over ice measured with IAGOS and relative humidity over ice simulated in ERA5 reanalysis per season considering threshold of homogeneous freezing

Figure 6.3 shows the vertical distribution of the mean relative humidity over ice per season and per region. ERA5 generally appears drier than IAGOS. The mean relative difference in relative humidity over ice, as seen in Section B.1 also shows this tendency. However, this tends to lie within the uncertainty range of the relative humidity sensor on board the IAGOS fleet, but just on its upper bound. Thus, most of the dry biases cannot be attributed to sensor error.

The deviation between IAGOS and ERA5 is a function of season, altitude and region. Pressure level deviations seem to be related to the location of the tropopause. In the extratropics, the relative humidity over ice increases up to a certain pressure level, in which differences between IAGOS and ERA5 also seem to increase. At a certain point, the relative humidity over ice decreases again, with better estimations by ERA5. This is most likely due to the fact that above the tropopause, relative humidity over ice decreases due to lower availability of water vapour [60, 53]. The behaviour does not exactly coincide with the calculation of the tropopause height. The cause of this was discussed in Section 5.3. Furthermore, the same observation cannot be made in the tropics as the tropopause is at a higher altitude than what is considered in this study. Hence, deviations between the datasets continue to increase.

Seasonal variations are dependent on the region and pressure level. For example, in North America, ERA5 and IAGOS show less differences in the mean RHI at pressure level 300 hPa to 200 hPa for season JJA compared to season DJF, though JJA shows higher mean values than DJF above 250 hPa. This may be influenced by the tropopause, which is located at a higher altitude in JJA compared to DJF. Below the tropopause, higher values of relative humidity over ice favour lower temperatures [60], and ERA5 is known to struggle more in the simulation of high RHI values, and lower values of RHI

are found above the tropopause. Hence, due to upper tropospheric and lower stratospheric influences, larger differences occur in DJF, even though the mean RHI is reducing, compared to in JJA. This is also why seasonal changes are not as distinct as in the study by A. Petzold et al. [53], who divided the pressure levels based on the distance to the dynamic tropopause. In Europe, more differences also appear between IAGOS and ERA5 in DJF compared to JJA, but the mean difference in DJF is higher than in North America, as is also seen in Section B.1. Europe also shows seasonal variations in line with A. Petzold et al. [53].

Differences in RHI between IAGOS and ERA5 in the tropics do not seem to be a function of seasons, which may be due a similar year round climate. In South Asia, a larger difference in the mean relative humidity over ice between ERA5 and IAGOS is noticeable for JJA. Here, ERA5 simulates much larger values than what has been measured by IAGOS, which has not been seen previously. This behaviour will be analysed further in Section 6.4. The moist bias is also outside the uncertainty range of IAGOS' relative humidity sensor, hence it is most likely a model error.

In some instances, a moist bias in the extratropics at high altitudes is also observed in ERA5. For example, starting at a pressure level of 200/225 hPa in North America for seasons JJA and SON. This is approximately in the lower stratosphere when looking at the average tropopause height. J. Bland et al. [7] and C. Dyroff et al. [14] identified a moist bias in the lowermost stratosphere in the ECMWF-IFS. T.G. Shepherd et al. [65] found a larger lower stratospheric moist bias in the ECMWF-IFS in the summer (JJA), for the extratropics. It should also be noted that some points may show a moist bias due to sensor uncertainty, but not all.

In some tropic regions, such as Central/South America, Africa, and South Asia, there are instances where IAGOS measures relative humidity over ice between pressure levels 350 hPa and 300 hPa, while no values are present for ERA5. This is due to the temperature at this pressure level. As seen in Figure 5.3, the mean temperature at pressure level 350 hPa in the tropics lies around 245 K to 250 K, which is above the threshold of homogeneous freezing and around the temperature at which ERA5 distinguishes between relative humidity over ice and relative humidity with respect to liquid. Hence, it may also be that the temperatures are too high for ERA5 to even simulate relative humidity over ice.

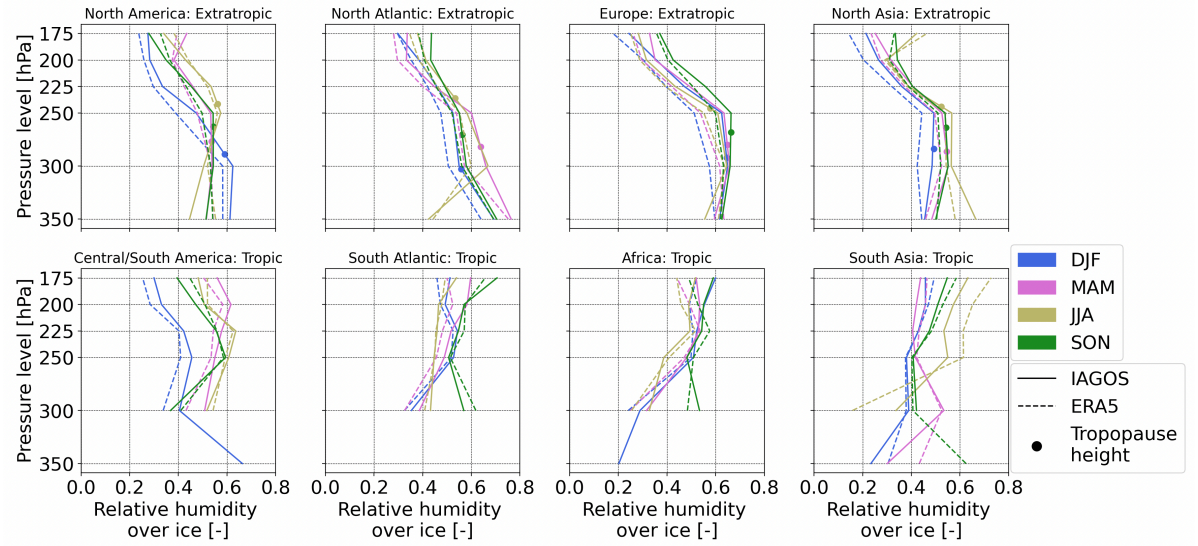

Figure 6.3: Vertical distribution IAGOS and ERA5 mean relative humidity over per season and per region, considering threshold of homogeneous freezing

The mean plus or minus one standard deviation per season and pressure level for the extratropics are presented in Figure 6.4, where the standard deviations can be found in Section B.2. The lower bound is well estimated by ERA5, meaning that lower values of relative humidity over ice are more accurately simulated. It shows that both dry and moist biases can exist at lower measured values of relative humidity over ice, which was also seen in Section 6.1.

ERA5 tends to underestimate the upper bound, showing that the model struggles to estimate higher values of relative humidity over ice and thus, ice supersaturation. This behaviour was also observed by K. Wolf et al. [83] and it was also present in ERA-interim [57]. Seasonally, ERA5 appears drier

compared to IAGOS in season DJF and MAM at higher values of relative humidity over ice. This is also the season in which overall higher values of relative humidity over ice were observed with IAGOS, as discussed in Section 6.2. Most of these dry biases lie outside the accuracy range of the humidity sensor on IAGOS aircraft, hence they can be attributed almost purely to model errors.

The underestimation of the upper bound of RHI by ERA5 is more pronounced at lower altitudes, and differences begin to decrease starting at pressure level 250/225 hPa, until 200/175 hPa. The variation of the relative difference in RHI between IAGOS and ERA5 in Section B.1 also shows a decrease in dryness of ERA5 with increasing altitude, which cannot be attributed to sensor biases. These behaviours are related to the tropopause as the probability of ice supersaturation increases until reaching the tropopause and decreases above [53]. However, the underestimation at pressure level 350 hPa, especially in the North Atlantic region, may be falsely underestimated due to a low number of data points, shown through bootstrapping of the PDFs in Section B.4. Here, the variation of the relative difference is also centred at a value of 0, with the majority of points within IAGOS' relative humidity sensor accuracy range.

At 200/175 hPa, an overestimation of the upper bound occurs in some regions and seasons, coupled by an increase in the moist bias errors, as seen in Section B.1, which are mainly found outside the accuracy range of the humidity sensor and thus a model error. This is more apparent in JJA and can be tied to the lower stratosphere moist bias in ECMWF-IFS. However, in order cases at these pressure levels, ERA5 appears drier at high values of relative humidity over ice, which may be due to upper tropospheric influences.

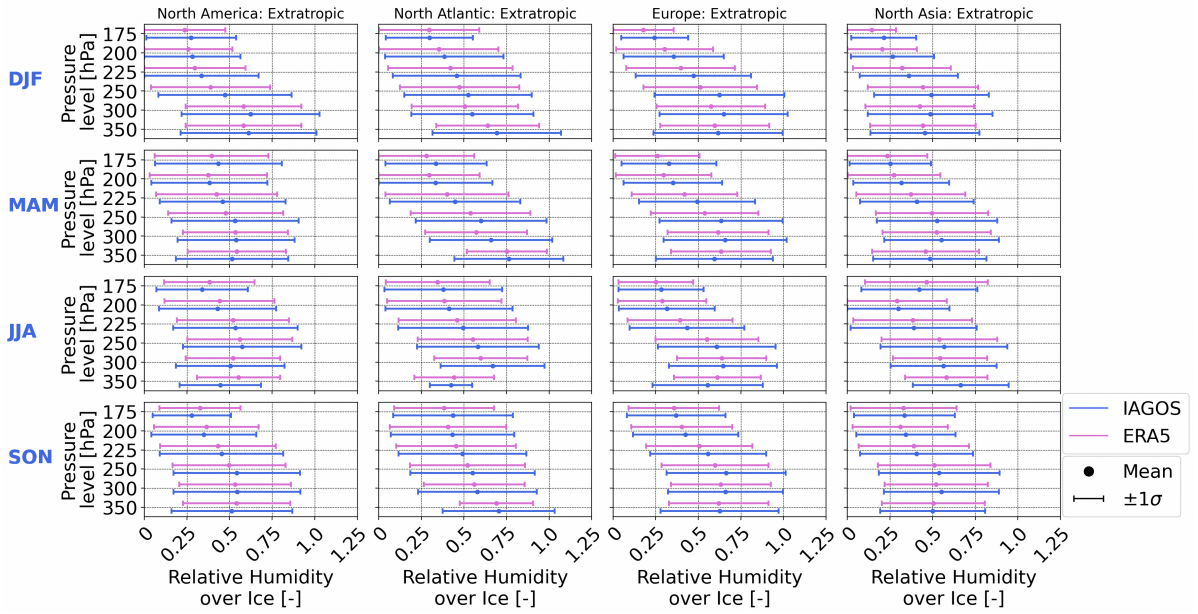

Figure 6.4: Mean $\pm 1\sigma$ of IAGOS and ERA5 relative humidity over ice per pressure level and season for extratropic regions, considering threshold of homogeneous freezing

The tropic regions in Figure 6.5, also show ERA5's tendency to underestimate the upper bound of the relative humidity over ice, but shows a better approximation of the lower bound. Moreover, the dry bias differences are more significant in DJF and MAM, as seen in Section B.1, and are mainly outside the uncertainty range of the sensor. However, in JJA, ERA5 is more susceptible to a moist bias across all tropic regions, particularly in South Asia. Some of these moist biases may be due to sensor errors but also arise due to model errors. Looking at pressure level variations, differences in the upper bound tend to increase with pressure level, with ERA5 becoming dryer than IAGOS when excluding South Asia. This is to be expected given that relative humidity over ice tends to increase with altitude in the tropics for the pressure levels considered. In DJF and MAM, the dry bias is tied to model errors. However, in JJA and SON, some of these biases may be the result of sensor uncertainties. Pressure levels 350 and 300 hPa lack enough measurements to obtain proper results. This is shown by the large variation of the mean and standard deviations, partially resulting from a different selection of points as a result of the temperature bias. In South Asia, ERA5 is consistently showing a moist bias,

which was also previously observed. Most of these moist bias errors lie outside the uncertainty range of the humidity sensor and are, thus, most likely model errors.

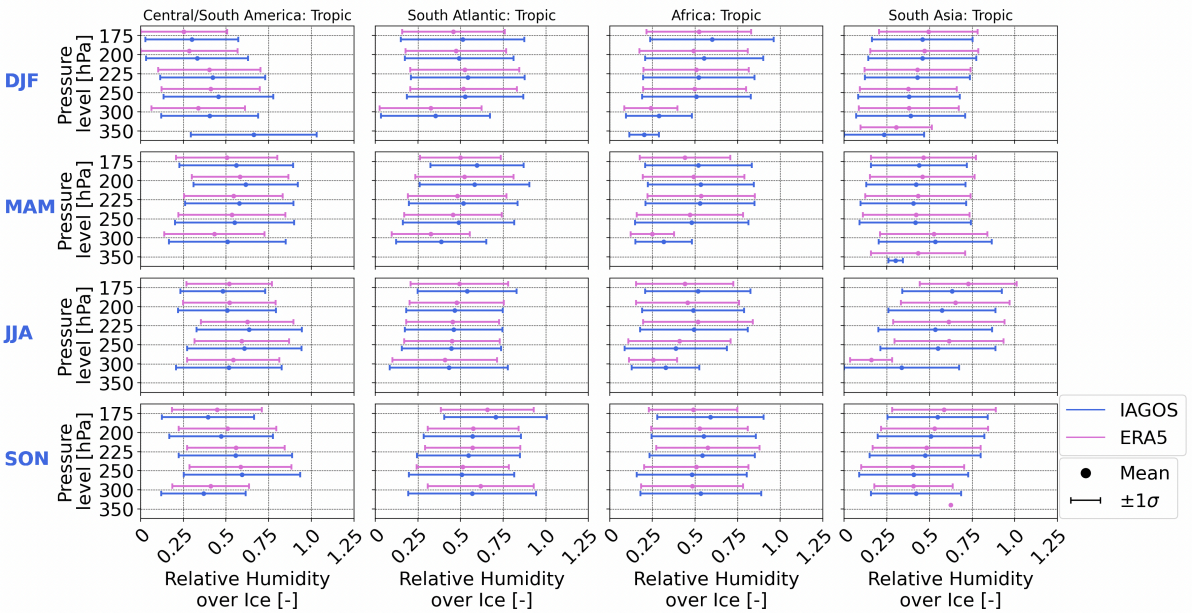

Figure 6.5: Mean $\pm 1\sigma$ of IAGOS and ERA5 relative humidity over ice per pressure level and season for tropic regions, considering threshold of homogeneous freezing

The probability density function (PDF) for relative humidity over ice measured by IAGOS and simulated by ERA5 in the extratropic regions, per pressure level and in season DJF is pictured in Figure 6.6. Bootstrapping of the PDF in Section B.4 showed pressure level 350 hPa lacked enough samples, but other pressure levels had enough measurements for analysing PDFs. Bimodal behaviour of the relative humidity over ice is mainly observed from pressure level 350 hPa to 225 hPa, in both IAGOS and ERA5. In North Asia, it can be seen from 350 to 250 hPa. Previous studies have also shown the RHI exhibiting such behaviour [60, 83, 53]. Between a relative humidity over ice of approximately 0.5 and 0.8/0.9, IAGOS and ERA5 show very similar values in the probability of occurrence. This was also present in the PDFs by K. Wolf et al. [83]. Below a relative humidity over ice of 0.5, the ERA5 PDF becomes exponential as the relative humidity over ice decreases. This mainly occurs at a pressure level of 250 hPa and lower, in all extratropic regions. Meanwhile, the IAGOS PDF shows a second peak at lower values, a dry mode. This shows that at extremely low values of relative humidity over ice, ERA5 also lacks accuracy. Above a relative humidity over ice of around 0.8 or 0.9, ERA5 forms its second peak (wet mode), centred at a value of 1. This peak is much more distinct compared to the second peak in the IAGOS dataset, which occurs after a value of 1, as also observed by K. Wolf et al. [83] and S. Sanogo et al. [60]. The large peak at RHI = 1 in ERA5 is due to the saturation adjustment and shows the difficulty of ERA5 in simulating larger values of relative humidity over ice. This can lead to issues in detecting ice supersaturation.

Similar observations can be seen for the other seasons in Section B.3. However, better approximations between IAGOS and ERA5 are seen when approaching summer in the extratropics (season JJA), particularly at lower values of the relative humidity over ice. The wet mode in ERA5 also becomes less distinct. This shows that ERA5 is better at simulating relative humidity over ice in warmer temperatures.

Figure 6.7 shows the PDF for the tropics regions per pressure level, for season DJF. Pressure levels 350 and 300 hPa due not have enough samples, as shown by bootstrapping of the PDFs. At pressure levels 250 and 225 hPa, all tropic regions show very similar PDF shapes for IAGOS and ERA5 below a value of approximately 0.9, though Central/South America shows the most deviations. At a value of 1 for the relative humidity over ice, a peak is again observed for ERA5, with IAGOS showing a smaller peak at a larger value. Contrarily to the extratropic regions, the peaks are still visible at pressure levels 200 and 175 hPa. This may be due to the higher tropopause height, meaning the relative humidity over ice is still increasing at these pressure levels. S. Sanogo et al. presented the same behaviour in the tropics using the IAGOS dataset [60]. However, this still shows the struggle of ERA5 in simulating

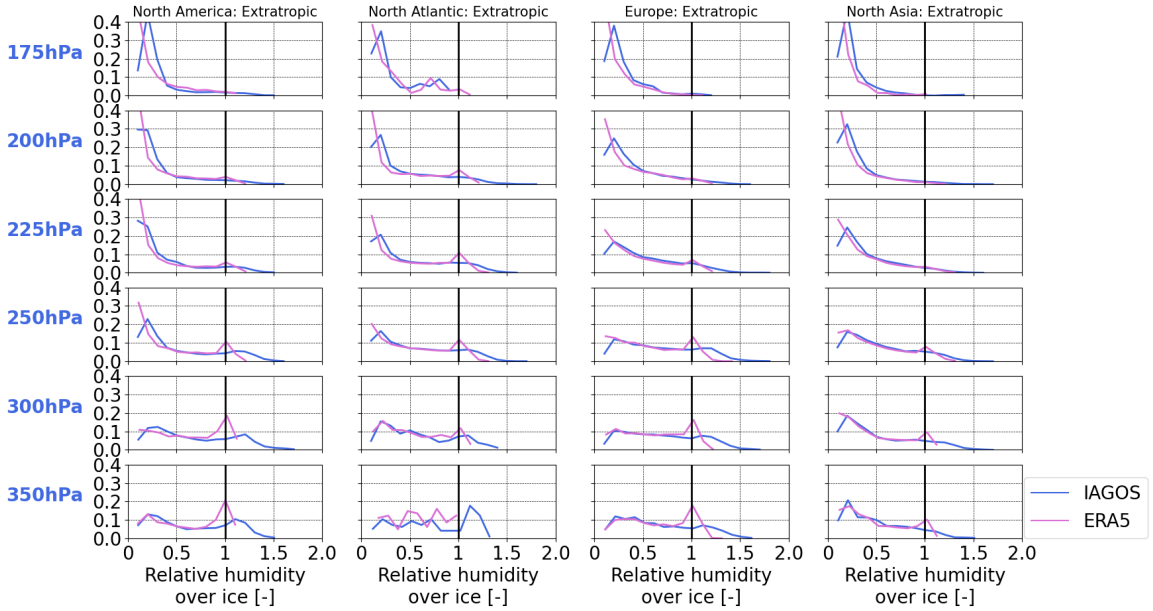

Figure 6.6: Probability density function of IAGOS and ERA5 relative humidity over ice per pressure level for the extratropic regions and season DJF, with 0.1 bin size, considering threshold of homogeneous freezing

correct values of relative humidity over ice above ice supersaturation. The IAGOS wet mode is also closer to a value of 1 in the tropics compared to the extratropics, with a faster decay of the PDF to a value of 0 above ice supersaturation. This is also in line with the results seen in Figure 6.2.

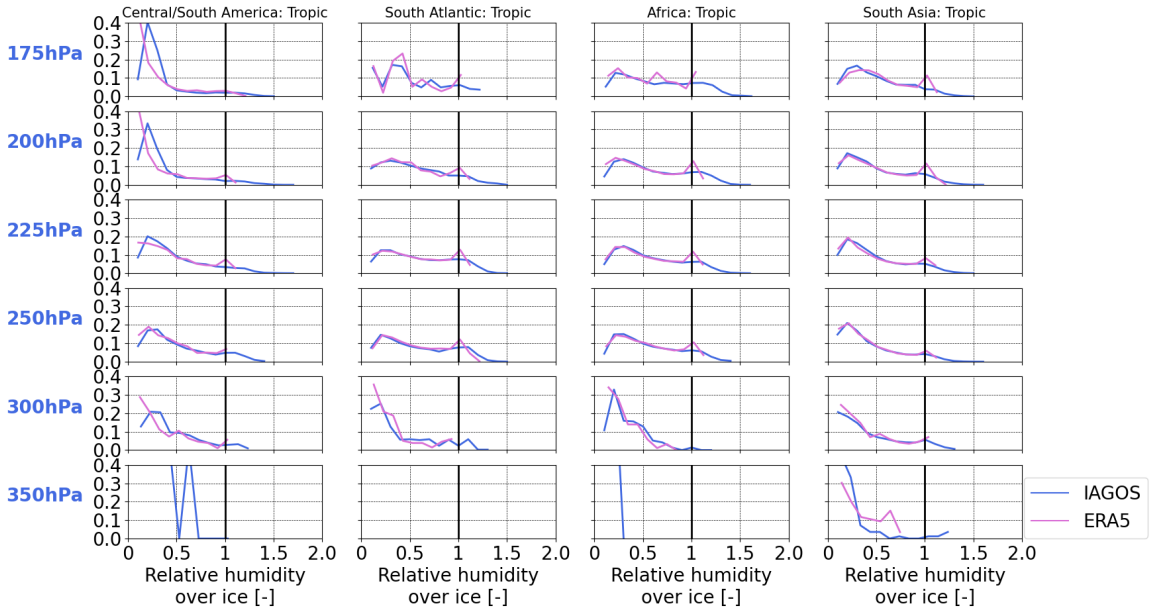

Figure 6.7: Probability density function of IAGOS and ERA5 relative humidity over ice per pressure level for the tropic regions and season DJF, with 0.1 bin size, considering threshold of homogeneous freezing

Observing the PDFS for seasons MAM, JJA and SON in the tropic regions, found in Section B.3, ERA5 and IAGOS still show good agreement below ice supersaturation. The intensity of the wet mode in ERA5 and IAGOS seems to be highly dependent on the season and region. For example, South Asia shows a much more intense peak in JJA for ERA5, with IAGOS also displaying higher probabilities of RHI above 1. However, for Africa and the South Atlantic, higher probabilities of RHI above 1 are found

in SON. Thus, in the tropic regions, the accuracy of ERA5 in predicting ice supersaturation is highly dependent on the season, region and pressure level.

The mean difference (MD) and root mean square error (RMSE) in the relative humidity over ice between IAGOS and ERA5 in the extratropic regions is shown in Figure 6.8. The mean difference error mainly remains positive and below 0.06, which is within the accuracy range of IAGOS's RHI sensor. Meanwhile, the RMSE lies, on average, between 0.125 and 0.25. This is similar to observations by K. Wolf et al. [83], who found the MD to be close to 0.04 and an RMSE around 0.15 to 0.2, for pressure levels 250 to 200 hPa. The positive MD shows that ERA5 is generally drier than IAGOS. Negative values mainly occur at pressure levels 350 and 175 hPa. The latter may be the lower stratosphere moist bias, but the error at 350 hPa is most likely due to a lack of samples.

The MD remains highest in DJF and lowest in JJA. This is most likely a result of the lower values of relative humidity over ice due to higher temperatures in JJA in the extratropics. The MD is also highest at a pressure level of 250 hPa and increases from 350 hPa to 250 hPa, for most extratropic regions and seasons. Larger overall values occur in Europe, which could be due to a lower probability of low relative humidity over ice values, as seen in Figure 6.6. Here it can also be seen that Europe has larger probabilities of values larger than 1, which is where ERA5 particularly struggles with simulating the correct relative humidity over ice. The RMSE is also slightly higher in Europe compared to the other extratropic regions. The RMSE generally decreases with the pressure level, unlike the MD, for all extratropic regions and seasons. Hence, it is difficult to say which pressure level in ERA5 experiences the largest errors in relative humidity over ice, also given that the number of data points can largely affect the RMSE as previously discussed.

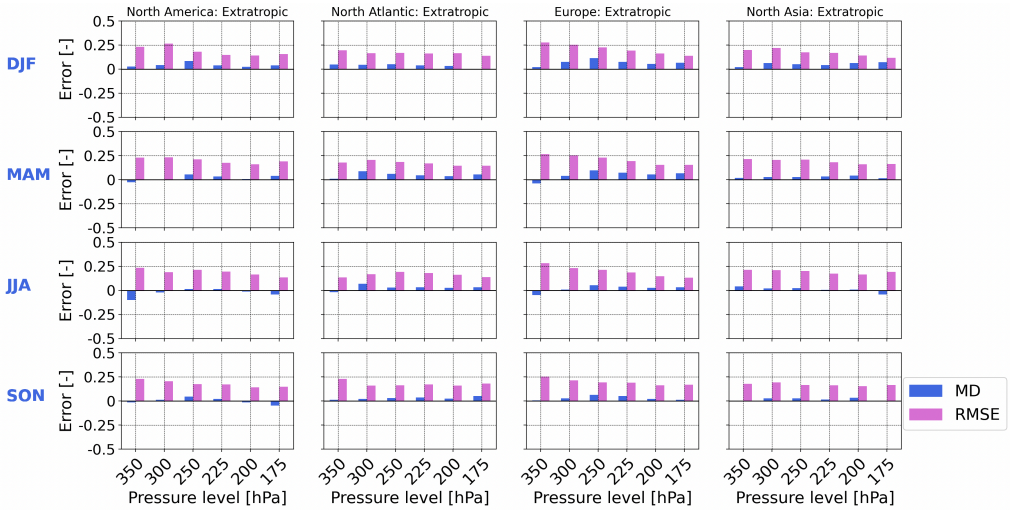

Figure 6.8: Mean difference (MD) and root mean square error (RMSE) between IAGOS and ERA5 relative humidity over ice per season and pressure level for the extratropic regions, considering threshold of homogeneous freezing

The MD and RMSE for relative humidity over ice between IAGOS and ERA5 are presented per season and pressure level for the tropic regions in Figure 6.9. Only South Asia in DJF shows error measurements at pressure level 350 hPa. The disappearance of errors at this pressure level for other tropic regions and season combinations is mainly due to temperature deviations between IAGOS and ERA5. For all tropic regions, the RMSE generally lies between 0.125 and 0.25, similar to the extratropic. The MD tends to lie between -0.1 and +0.06. The negative MD is the most prominent in South Asia, showing the moist bias in ERA5 for this particular region. The moist bias is also stronger in JJA, as seen with the larger absolute MD and larger RMSE compared to the other seasons for this region. It is most likely not due to lower temperatures in JJA because the temperatures in South Asia are slightly higher for this season, as displayed in Figure 5.5. Furthermore, according to S. Sanogo et al., warmer tropical temperatures favour lower relative humidity over ice values [60], which should lead to better error estimates as ERA5 performs better in simulating these lower values.

Observing the errors in the other tropic regions and seasons, the MD seems to be largest in DJF or MAM, which is also where temperatures can be slightly cooler, as shown in Figure 5.5. However, the RMSE does not behave in the same way. For example, in Central/South America, equal values

in the RMSE are observed in MAM, JJA and SON for pressure levels 250 and 225 hPa. Furthermore, in some regions and seasons, it decreases with pressure level, but it can also increase per pressure level. It should be kept in mind that the RMSE is also a function of the number of data points and Central/South America, South Atlantic and Africa are some of the regions with the least number of data points (see Figure 4.4b). Hence, this may be influencing the RMSE, and thus one should not only rely on this comparison.

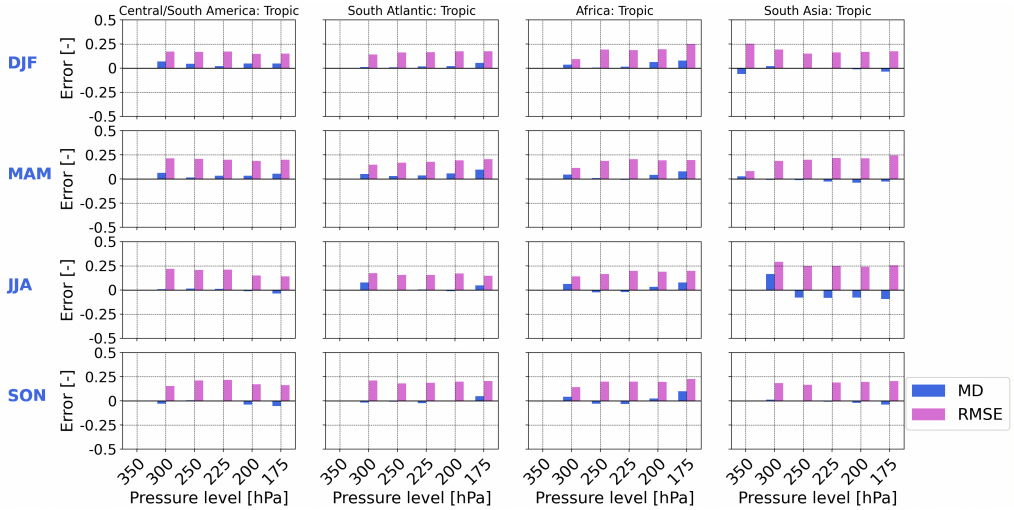

Figure 6.9: Mean difference (MD) and root mean square error (RMSE) between IAGOS and ERA5 relative humidity over ice per season and pressure level for the tropic regions, considering threshold of homogeneous freezing

This section has attempted to validate relative humidity over ice simulated by ERA5 using the IAGOS in-situ measurements from a seasonal, pressure level and regional perspective. Overall, ERA5 shows good agreement in the simulation of relative humidity over ice at values below ice supersaturation. The errors arise when trying to simulate relative humidity over ice values above 1 due to the saturation adjustment.

The extent of how accurate ERA5 is varies per region, season and pressure level. In the extratropics, ERA5 shows the largest dry bias in DJF, which is most likely due to lower temperatures, leading to higher values of relative humidity over ice measured by IAGOS. Meanwhile, errors appear to be lowest in JJA, where temperatures are higher. Moreover, at higher altitudes, ERA5 is more accurate, though a moist bias can occur. Both are related to the location of the tropopause. In the tropics, ERA5 and IAGOS tended to show more disagreements with increasing altitude due to the tropopause height, in which ERA5 became drier than IAGOS. South Asia shows a moist bias, which is more prominent in season JJA. This is also the only combination of region and season in which ERA5 shows a distinct moist bias below the tropopause. This can have the impact of falsely identifying ice supersaturated regions, leading to unnecessary avoidance and a possible increase in fuel needed for a flight, which would increase emissions such as CO_2. This behaviour in South Asia will be further investigated in Section 6.4.

6.4. Further Analysis of Relative Humidity over Ice in the Tropics

In the previous section, the South Asia region showed a moist bias in ERA5, whereas all other regions showed a dry bias. This moist bias was also much more pronounced in season JJA. However, it was difficult to tie this behaviour to temperature or other factors, such as tropopause height.

As previously discussed in Section 2.3, numerical weather prediction models, including the ERA5 reanalysis, struggle with the representation of ice supersaturation in cloudy conditions. Cloudy (cirrus clouds) and clear sky conditions can be differentiated using the number of ice particles. S. Sanogo et al. found that the tropics have a larger number of ice particles compared to those found in a band between 40°N and 60°N when considering the IAGOS dataset [60]. Furthermore, there is a correlation between high relative humidity over ice and a high number of ice particles. Thus, the high relative humidity over ice observed in South Asia could be due to a high concentration of ice particles, both in IAGOS and

ERA5.

Figure 6.10 displays the relative difference in the mean relative humidity over ice per 2°grid box between IAGOS and ERA5 in season JJA. The means in South Asia determined with ERA5 are always higher than those found with IAGOS, again showing the moist bias. There are also other similar regions, such as in Africa and the South Atlantic around the equator and in the Pacific Ocean, off the west coast of the United States.

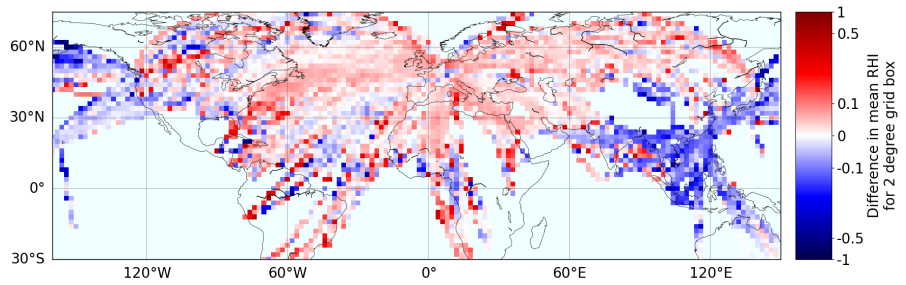

Figure 6.10: Difference in mean relative humidity over ice per 2 degree grid box between IAGOS and ERA5 for season JJA, with IAGOS as baseline, considering threshold of homogeneous freezing

The annual mean cirrus cloud occurrence determined with IAGOS by using the number of ice particles is seen in Figure 6.11. A seasonal analysis is not available. Furthermore, the number of ice particles is not a parameter which can be retrieved from ERA5. Though, the atmospheric ice content has been modelled by T. Dou et al. [13] from a seasonal perspective and is pictured in Figure 6.12. Looking at both figures, it is clear that there is a concentration of ice over the same areas where a moist bias in ERA5 occurred. For ERA5 in season JJA, the concentration of atmospheric ice seems much higher compared to the other seasons. Hence, the moist bias in ERA5 found for the South Asia region could be caused by an overestimation of ice in the atmosphere. To form a proper conclusion, a more equal measurement of ice should be considered, and the seasonal variation of the number of ice particles should be considered for the IAGOS dataset. However, it is out of the scope of this study.

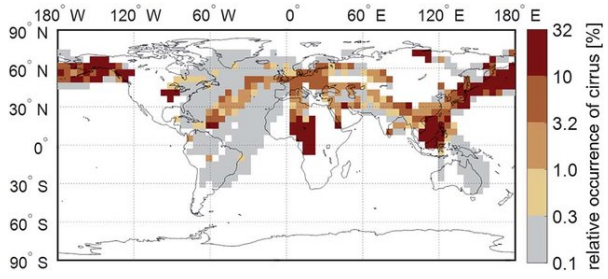

Figure 6.11: Annual mean of cirrus cloud occurrence as measured by IAGOS [54]

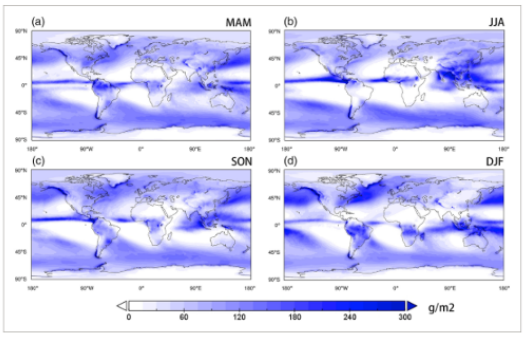

Figure 6.12: Multiyear average spatial distribution of atmospheric ice content in ERA5 [13]

6.5. Comparison of Relative Humidity over Ice from a Regional, Pressure Level and Yearly Perspective

This section analyses the relative humidity over ice simulated with ERA5 and is validated with the IAGOS in-situ measurements from a yearly, regional and pressure level perspective. Previously, seasonal, pressure level and regional influences on the deviations between IAGOS and ERA5 were identified.

Figure 6.13 displays the yearly mean variation plus or minus one standard deviation of the relative humidity over ice found with IAGOS and ERA5 for the extratropic regions. The overall yearly standard deviations can be found in Section B.5. Seasonal variations are also taken into account, just as described in Section 5.4. In general, relative humidity over ice does not show a yearly trend like tem-

perature. Nevertheless, ERA5 shows the ability to follow the trend of the large peaks, but is generally dryer than IAGOS for all years, given the higher means in IAGOS. In some instances, the ERA5 mean is higher than IAGOS, which was also occasionally observed in the seasonal analysis. This is more prominent at pressure levels 175 and 350 hPa. Behaviour at pressure level 350 hPa is most likely a result of a low number of data points, and results at 175 hPa are a combination of a low number of measurements and lower stratosphere influences as previously discussed. For further pressure level discussions, the reader is referred back to Section 6.3.

Examination of the mean plus one standard deviation, shows that the upper bound in ERA5 is generally lower than for IAGOS, as also seen in the seasonal, regional and pressure level analysis. However, in 2013 and 2014, in North America, Europe and North Asia at pressure levels 225 and 200 hPa, ERA5 has a higher upper bound. The yearly standard deviation of ERA5 is generally lower or equal to IAGOS, though, in 2013 and 2014, they were higher. However, the difference in the standard deviations is less than the uncertainty in IAGOS' sensor. Observations of yearly PDFs show ERA5 has a higher cumulative probability around the ice supersaturation compared to IAGOS, where it is also hard to detect the second mode in IAGOS. Moreover, the extratropics show a high number of samples for these two years. Hence, it can be deduced that the moist bias in ERA5 for years 2013 and 2014 is mainly due to a higher probability of values close to or above ice supersaturation in ERA5 than in IAGOS.

Fewer deviations between IAGOS and ERA5 are found for the lower bound, though ERA5 tends to be lower than IAGOS. This is due to the overall lower estimated values of relative humidity over ice in ERA5. In the cases where the upper bound is overestimated by ERA5, the lower bound is also higher in ERA5 than in IAGOS, which again is due to the higher mean in ERA5, but lower or equal standard deviation. Thus, from a yearly standpoint in the extratropic regions, ERA5 mainly shows a dry bias, but ERA5 may show a moist bias in some instances. The exact cause will be examined further after looking at the mean plus or minus one standard deviation in the tropics.

Regionally, North America shows less yearly differences between IAGOS and ERA5, with the mean difference increasing moving eastwards towards Europe, and then it slightly decreases again for North Asia. This points to a possible longitudinal influence on the relative humidity over ice. K. Wolf et al. [83] observed similar behaviour; that ERA5 generally became drier compared to IAGOS when moving eastward, considering a longitudinal range of 100°W to 20°E, and mean difference between IAGOS and ERA5 was the smallest at 100°W [83].

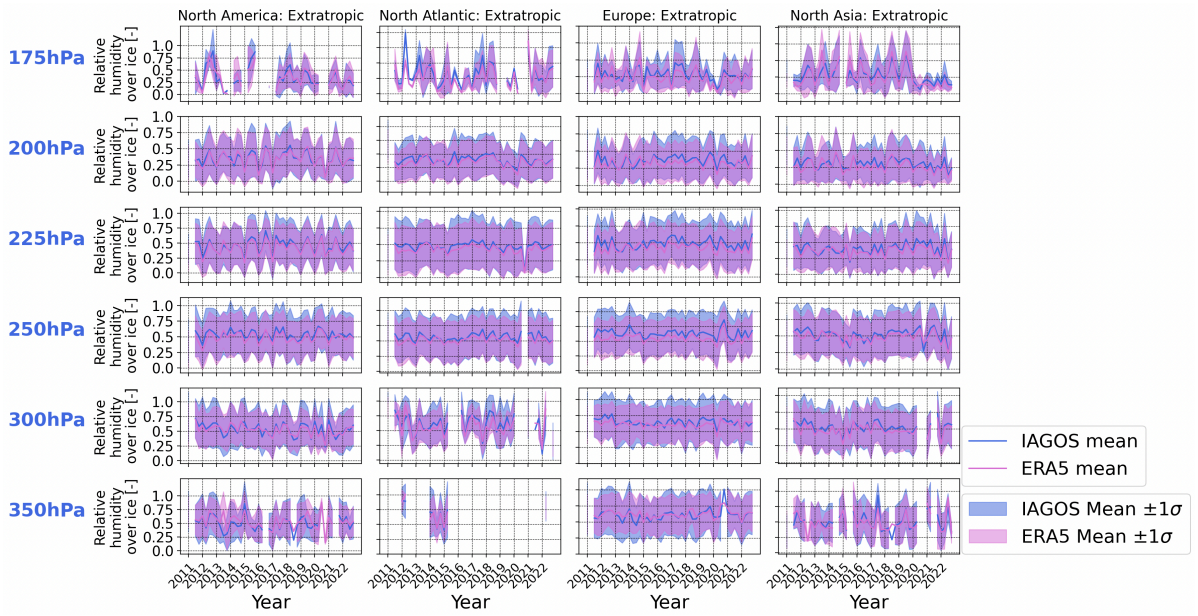

Figure 6.13: Yearly variation in IAGOS and ERA5 mean relative humidity over ice per pressure level for extratropics regions, considering threshold of homogeneous freezing

The yearly variation of the mean relative humidity over ice plus or minus one standard deviation for the tropic regions is presented in Figure 6.14. ERA5 and IAGOS show more similar values compared to

the extratropics at all pressure levels, and ERA5 still shows a good ability to follow the trend of the large peaks. Furthermore, the yearly difference between IAGOS and ERA5 is not constant. In Central/South America and South Atlantic, IAGOS can be dryer than ERA5 and vice versa. This may be the result of a low number of data points in these two regions, with 3.1% of all samples found in Central/South America and 3.8% in South Atlantic. This is also seen by the breaks in the yearly trend. The effects of the lower number of data points are not reflected in the standard deviation, which may be due to the already large sample size. However, if there are consistent changes in the regional sampling within these two regions, as in the aircraft are flying different routes every year, it would make sense that inconsistencies arise. Given the low number of flights in these regions, this is highly likely and will be examined further.

In South Asia, the ERA5 mean generally is higher than IAGOS, particularly for season JJA, but IAGOS can also show high means for this season. These peaks are present almost every year, showing that the moist bias in ERA5 in South Asia for season JJA, is consistently present every year. However, it is not present in all years. For example, the years 2011 and 2020 to 2022 show a lower variation of relative humidity over ice in ERA5 compared to IAGOS. These are also years with the lowest number of samples (Figure 5.12). In the years with more samples, ERA5 clearly has a relative humidity over ice range higher than IAGOS. It shows the importance of having a high number of samples and increasing the number of measurements should be considered for the future of the IAGOS measurement campaign.

There are also some instances of a higher upper bound and mean in ERA5 compared to IAGOS for the tropics, which is mainly observed in years 2013 and 2014 for pressure levels 200 to 250 hPa in all tropic regions. Yearly PDFs show no distinctive second mode in IAGOS and in some cases, the PDFs are also very noisy due to a low number of available data points (see Figure 5.12. However, South Atlantic, Africa and South Asia showed some of the highest sampling in these two years. Hence, it is unsure if the moist bias in ERA5 is due to a model problem in the years 2013 and 2014, or if it is due to a low number of samples.

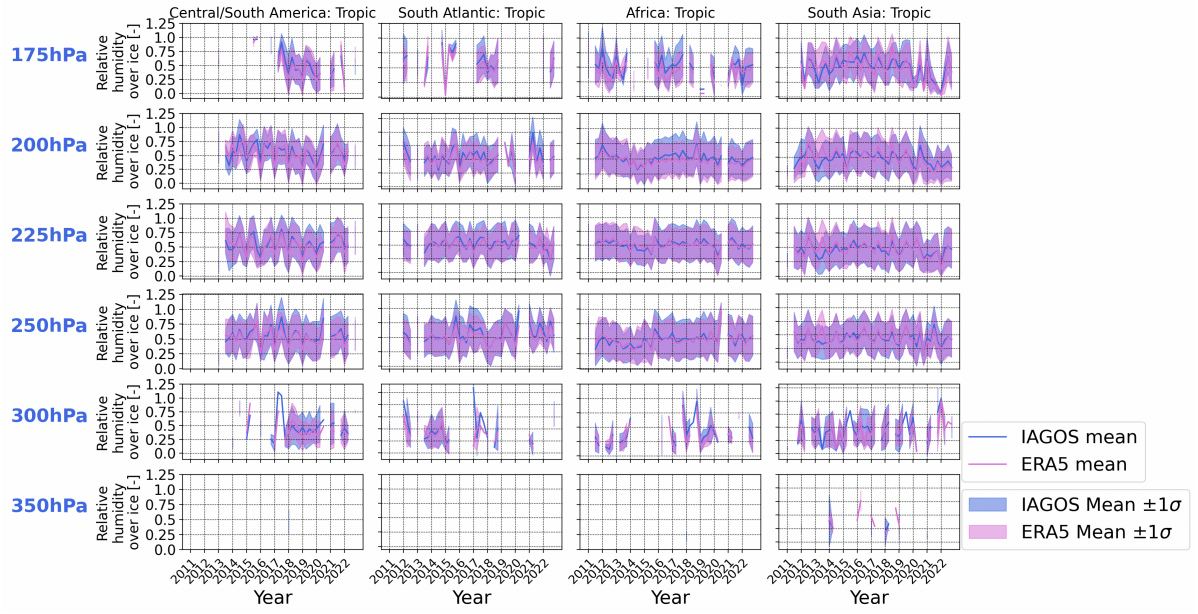

Figure 6.14: Yearly variation in IAGOS and ERA5 mean relative humidity over ice per pressure level for tropic regions, considering threshold of homogeneous freezing

To further understand the behaviour of the years 2013 and 2014, the flight density and the percentage of points in which ERA5 predicts a higher relative humidity over ice compared to IAGOS are analysed. The year 2012 will also be used for comparison purposes as it also shows a high number of samples.

The flight density in 2012, 2013 and 2014 is presented in Figure 6.15a, Figure 6.16a, and Figure 6.17a. While these three years show a similar distribution of measurements in the extratropic

regions, there are larger differences in the tropics. It can be seen that in 2013 and 2014, there were a larger amount flights to South America. The year 2012 mainly only shows flights to São Paulo, whereas the years 2013 and 2014 have flights towards São Paulo, but also to destinations in the north of South America. In addition, the year 2012 shows a far lower flight density in South Asia compared to the two other years considered. However, for Africa, fewer points were observed in 2014.

Looking at the percentage of points in which ERA5 computes a higher relative humidity over ice compared to IAGOS, certain observations can be made for the different years in Figure 6.15b, Figure 6.16b, and Figure 6.17b. First of all, as has already been mentioned several times, South Asia has a large percentage of such points. However, in 2012, due to the low number of IAGOS flights, far less of such observations were found, leading to results showing better agreements between IAGOS and ERA5. In 2013, there was an area in the South Atlantic Ocean, close to the north of South America, where ERA5 simulates a larger value of relative humidity over ice in relation to IAGOS. The relative difference lies around IAGOS's sensor accuracy, except close to the South American northern coastline, where the relative difference is higher than the uncertainty in the sensor. However, it is not due to a low number of observations. In 2014, this area still shows possibilities of a moist bias in ERA5, but it has been reduced compared to 2013.

There is also an area close to Alaska in 2012, 2013, and 2014 where a higher percentage of points shows ERA5 overestimating the relative humidity over ice compared to the rest of the North American region. The year 2013 shows the largest differences, with relative differences greater than the uncertainty of IAGOS' sensor, and 2014 the least. Number of samples seems to remain the same across all three years. Africa also does not show large changes in flight density, but 2013 and 2014 still show a larger moist bias in ERA5.

Looking at the ice content in IAGOS and ERA5 in Figure 6.11 and Figure 6.12, all four regions discussed are in areas where there is a large number of ice particles in the atmosphere or high cirrus cloud occurrence. This shows the possible influence of the atmospheric ice content in the bias of relative humidity over ice in ERA5. However, it could also be due to fewer observations in these areas that are assimilated in ERA5. Most of these areas are over the ocean, in which deployment of radiosondes is more difficult. Moreover, fewer aircraft are flying the routes in which issues arise. Hence, there may be more reliance on satellite observations. As mentioned by the Climate Data Guide, insufficient observation coverage may lead to unrealistic trends and variability in the ERA5 reanalysis because biases would not be able to be constrained in the data assimilation model [9].

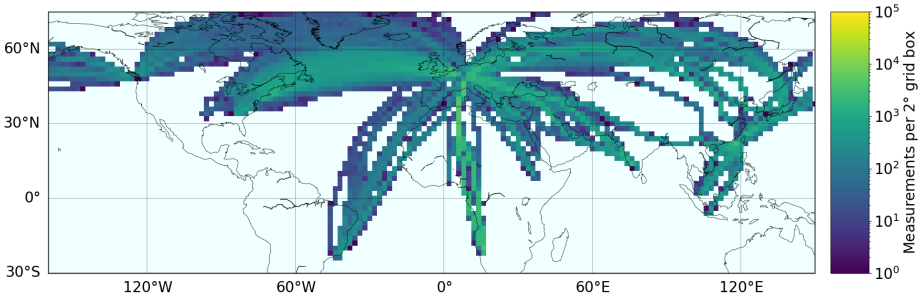

(a) Number of measurements by IAGOS per 2°grid box

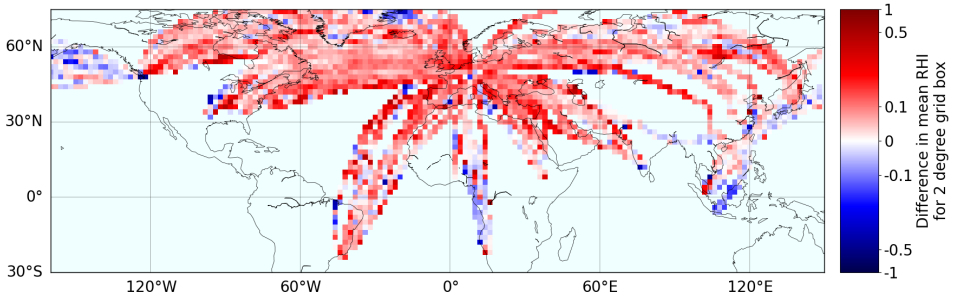

(b) Difference in mean relative humidity over ice between IAGOS and ERA5, with IAGOS as baseline

Figure 6.15: Flight density and difference in mean relative humidity over ice between IAGOS and ERA5 in 2012

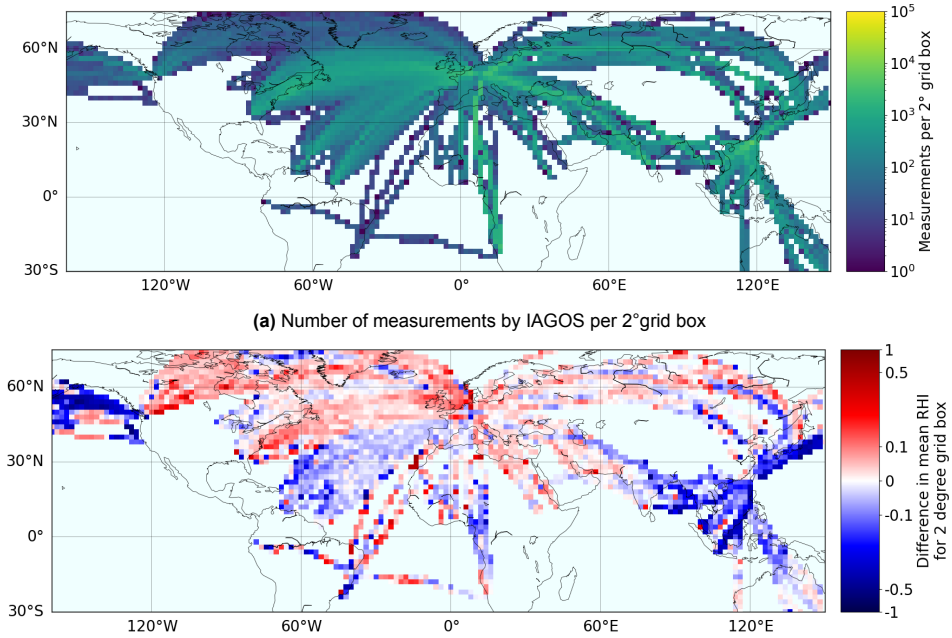

(a) Number of measurements by IAGOS per 2°grid box

(b) Difference in mean relative humidity over ice between IAGOS and ERA5, with IAGOS as baseline

Figure 6.16: Flight density and difference in mean relative humidity over ice between IAGOS and ERA5 in 2013

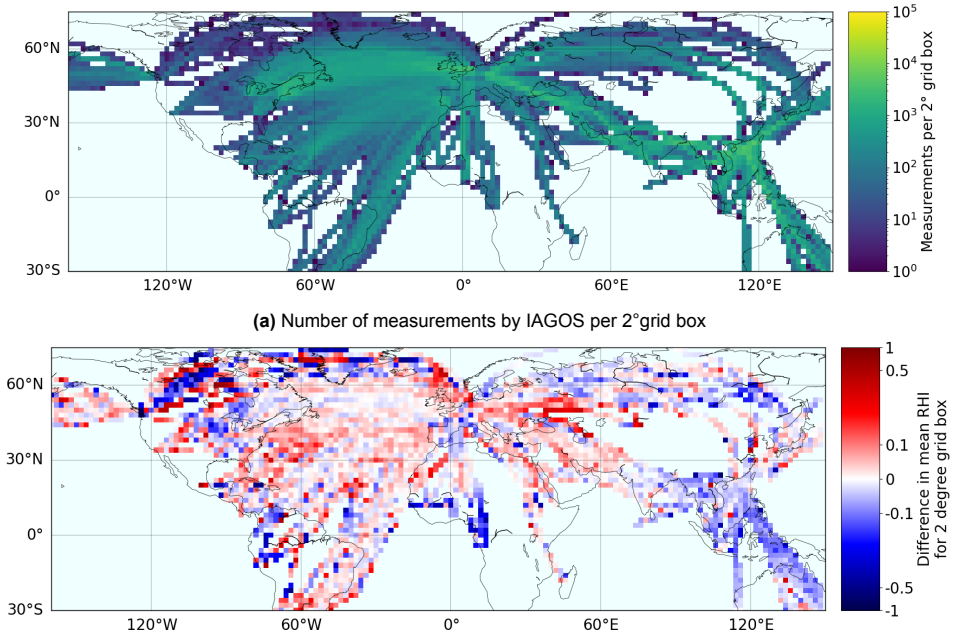

(a) Number of measurements by IAGOS per 2°grid box

(b) Difference in mean relative humidity over ice between IAGOS and ERA5, with IAGOS as baseline

Figure 6.17: Flight density and difference in mean relative humidity over ice between IAGOS and ERA5 in 2014

Thus, the behaviour seen in 2013 and 2014 may be related to changes in the regional sampling of the IAGOS fleet and an underlying issue in the behaviour of ERA5 for specific regions. This shows the importance of increasing the measurements from IAGOS while trying to sample in the same locations every year in order to better validate ERA5 from a yearly but also regional perspective.

To conclude, this section focused on validating relative humidity over ice simulated with ERA5 using the IAGOS in-situ measurements from a yearly, regional and pressure level perspective. Overall, there is a dry bias in ERA5 no matter the year, but the difference between IAGOS and ERA5 is not constant.

Moreover, the extratropics show a possible longitudinal influence in ERA5's bias, with ERA5 becoming drier than IAGOS when moving eastwards. Contrarily, 2013 and 2014 show a possible moist bias in ERA5 at some pressure levels, which is more pronounced in the tropics. This is most likely due to changes in the flight density of these years, where particular regions may show lower probabilities of values above ice supersaturation in IAGOS in comparison to ERA5. However, there may also be certain modelling issues, such as atmospheric ice content, which was seen to affect the seasonal behaviour of relative humidity over ice in the tropics. This is something that should be investigated further.

6.6. Relative Humidity over Ice Conclusion

All in all, the relative humidity over ice in ERA5 was validated using the IAGOS in-situ measurements from a regional, seasonal, pressure level and yearly perspective within this chapter. ERA5 and IAGOS generally showed good agreement in relative humidity over ice below ice supersaturation. However, large deviations were found close to or above ice supersaturation due to ERA5's saturation adjustment.

Above ice supersaturation, ERA5 mainly displayed a dry bias but sometimes experienced a moist bias above the tropopause and in particular regions. This included an area close to Alaska, over the Atlantic Ocean towards the northern part of South America, and in South Asia. This moist bias could perhaps be correlated to changes in regional sampling with IAGOS aircraft and due to inconsistencies in the modelling of atmospheric ice in ERA5 but it requires further investigation. Lastly, in the extratropics, increasing deviations between ERA5 and IAGOS were observed moving eastwards, with ERA5 showing a larger dry bias.

In terms of pressure level, fewer deviations between IAGOS and ERA5 were found at higher altitudes, when above the tropopause in extratropic regions due to lower stratospheric and upper tropospheric influences. Sometimes a moist bias in ERA5 was also identified at these high altitudes. In the tropics, the relative humidity over ice tended to increase with pressure level since the tropopause is located at a higher altitude in these regions. Sometimes a decrease at pressure level 175 hPa was observed, however, this may be due to a decrease in data points at this altitude.

From a seasonal perspective, the extratropics showed more variation, which is most likely due to larger seasonal changes observed for these regions. Season DJF typically resulted in larger differences between IAGOS and ERA5, with fewer deviations in season JJA. In the tropics, seasonal variations are not as strong. The main observation in this case was the large increase in relative humidity over ice for South Asia in JJA, which was more drastic in ERA5. Again, this could be due to a problem in the modelling of atmospheric ice in ERA5.

In terms of the yearly analysis, the relative humidity over ice itself does not show much of a yearly trend. Mainly, a dry bias was observed for ERA5, though, a potential moist bias was seen for years 2013 and 2014. This moist bias is most likely the result of changes in the flight density and location of measurements in IAGOS.

7. Validation of Ice Supersaturated Regions in ERA5 Reanalysis using IAGOS In-Situ Measurements

Given the previous validation of temperature and relative humidity over ice in ERA5, using the IAGOS in-situ measurements, the deviations in the detection of ice supersaturated regions can be examined. First, a comparison from a regional, pressure level and season perspective is given in Section 7.1. Thereafter, the occurrence of ice supersaturated regions in ERA5 and IAGOS are analysed from a regional, pressure level and yearly perspective in Section 7.2. Section 7.3 provides an overview of where exactly to expect the largest differences in ice supersaturated region occurrence between the two datasets. Lastly, Section 7.4 explores corrections of the ERA5 reanalysis dataset to achieve better detection of ice supersaturated regions with this model.

7.1. Comparison of Ice Supersaturated Regions from a Regional, Pressure Level and Seasonal Perspective

The seasonal vertical distribution of the ice supersaturated region (ISSR) fraction per region is presented in Figure 7.1. The ISSR fraction is found by counting the number of data points meeting the ice supersaturation criteria (relative humidity over ice > 1, temperature <= 235.15) and dividing by the total number of data points for the given season, pressure level, and region. This also means that the ISSR fraction is highly dependent on the available data.

Comparing the IAGOS ISSR fraction to the ERA5 ISSR fraction, it is clear that ERA5 underestimates the occurrence of ice supersaturated regions, in most conditions considered. In South Asia in JJA, ERA5 computes a higher ISSR fraction compared to IAGOS. This is due to the moist bias in the relative humidity over ice for this particular region, which was identified and examined in Chapter 6. In Central/South America, IAGOS shows an ISSR fraction between pressure levels 350 and 300 hPa, meanwhile ERA5 does not. This is most likely due to ERA5 temperatures being higher than the threshold of homogeneous freezing, as also discussed in Section 6.3.

Examining the seasonal variation of the ISSR fraction, it is mainly the extratropic regions showcasing changes per season, except for North Asia. For example, North America and Europe show higher ISSR fractions in DJF due to higher values of relative humidity over ice and larger possibilities of ice supersaturation. Here, the ISSR fraction has a maximum of almost 25%. Lower values of ISSR occurrence are found in JJA, with maximum values around 15%. This aligns with observations from A. Petzold et al. based on the MOZAIC dataset. [53], who identified a maximum ISSR fraction of almost 35% in DJF and 25% just below the tropopause. Differences may arise due to differences in the definition of the pressure levels. North Atlantic shows a higher ISSR fraction in MAM than in DJF, and not a large difference between DJF, JJA and SON. A. Petzold et al. did show similar fractions for DJF and MAM in the North Atlantic, but lower values in JJA and SON [53]. The difference in observations could be due to a number of reasons. For example, A, Petzold et al. consider the MOZAIC dataset from 1995 to 2010 [53], and it was deduced in Section 6.5 that the relative humidity over ice shows no yearly trend. Differences may also arise due to a longer latitudinal range considered for the extratropics in this study compared to the one by A. Petzold et al. [53]. Lastly, there could be an influence of the jet stream. As discussed by K. Wolf et al. [82], the location of ISSRs correlates with the location of the jet stream. Aircraft over the North Atlantic particularly make use of this. Traffic in the North Atlantic peaks in JJA and is followed closely by MAM and SON. Hence, with more traffic in seasons such as JJA and MAM [72], more ISSRs might be detected due to using the jet stream.

Above a pressure level of around 250 hPa, the extratropic regions show a decrease in the ISSR fraction due to decreases in the probability of ice supersaturation. This follows the behaviour of the

relative humidity over ice, as discussed in Section 6.3 and shows the direct influence of the relative humidity over ice on the ISSR fraction. Furthermore, the tropics show some trend of an increasing ISSR fraction with pressure level, though it is estimated to be less than a 10% increase. S. Sanogo also only showed an overall 5% increase from 325 to 175 hPa [60].

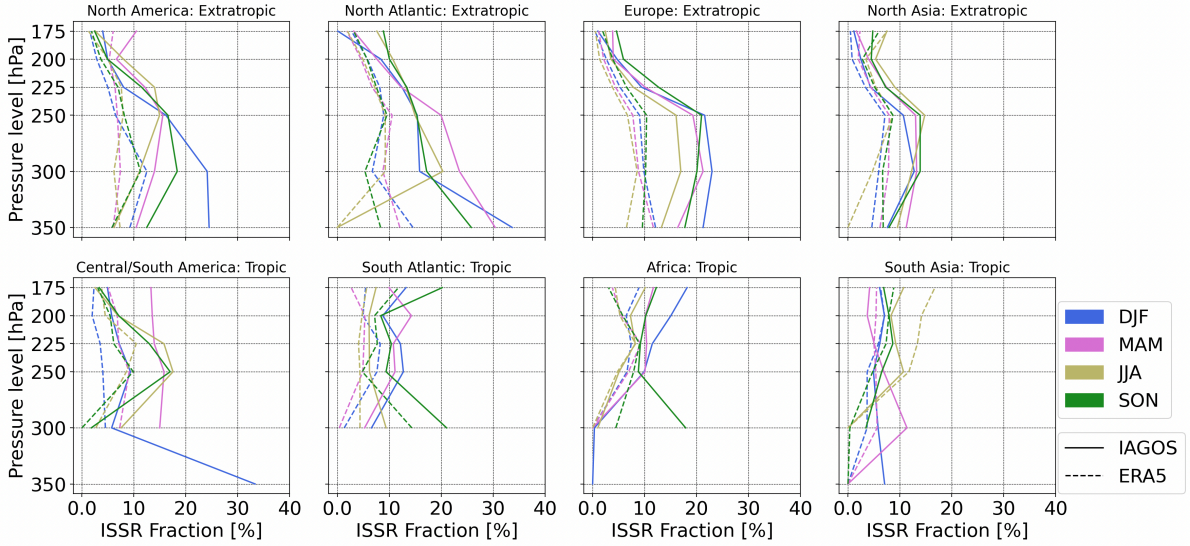

Figure 7.1: Vertical distribution of ice supersaturated region fraction for IAGOS and ERA5 per season and region

Figure 7.2 shows the hit rate and false alarm rate per pressure level and season for the extratropic regions. The hit rate tends to lie between 20 and at most, 40%. This shows that more ISSRs are undetected by ERA5 than those that are correctly estimated. In some instances, the hit rate can be 0 or around 15%. This typically occurs at pressure levels 350 hPa and 175 hPa. For example, in the North Atlantic at pressure level 350 hPa, SON shows a hit rate of around 12%, but this region and pressure level is known to not have sufficient data points for analysis. K. Gierens et al. [20] found a hit rate between 17 and 26% with ERA5 considering 4 months of data from IAGOS. For the year 2019, R. Teoh et al. [72] found a hit rate of 50% in ERA5 using IAGOS as a baseline. Hence, the findings in this study are within the ranges of hit ranges found in literature. The hit rate also tends to be slightly smaller in season JJA and MAM at higher altitudes, in line with the findings by K. Gierens et al. [20]. This is most likely related to the tropopause, and the behaviour of relative humidity over ice with altitude, as seen in Section 6.3.

Pressure level dependencies are hard to detect, which is most likely also influenced by the number of data points. However, pressure levels 250 or 225 hPa seem to be levels at which the highest hit rate occurs. This makes sense, given that these are some of the pressure levels in which the highest values of relative humidity over ice can be found. Regional differences in the hit rate are also dependent on the behaviour of this variable.

The false alarm rate is generally between 1 and 5%, which shows that ERA5 does not falsely detect a lot of ice supersaturated regions in the extratropics. K. Gierens et al. [20] also found a false alarm rate between 4 and 5%. The false alarm rate does not seem to fluctuate a lot between seasons, also in line with observations by K. Gierens et al. [20]. Some of these false alarms may be due to the cold bias as examined in Section 5.5. The false alarms at higher altitudes may be related to the lowermost stratospheric moist bias in ERA5.

The hit rate and false alarm rate per season and pressure level for the tropic regions are displayed in Figure 7.3. The hit rate in the tropics lies between 20% and 35%, which is similar to the extratropics. However, at pressure levels 350 and 300 hPa, there are often no values due to a combination of too-high temperatures and low occurrences of ice supersaturation. Pressure level deviations of the hit rate remain somewhat equal due to a small increase of ISSR occurrence with altitude in the tropics, as previously seen. Despite South Asia showing more of a moist bias in JJA, the hit rate still remains around 30 to 35%. This shows that the dry bias that still remains (see Section B.1) can cause ISSRs to not be detected.

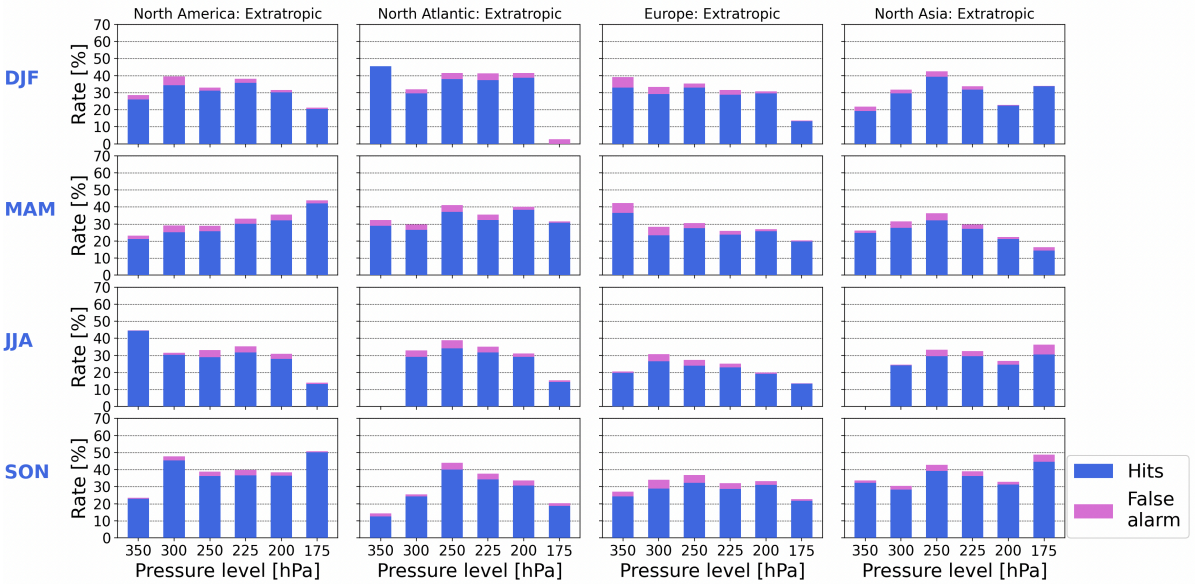

Figure 7.2: Ice supersaturated region hit and false alarm rates per season and pressure level for extratropic regions

The false alarm rates have slightly increased in the tropics, but still not higher than 10%, when not considering South Asia. This may be the result of slightly more occurrences of a moist bias in ERA5. For example, Central/South America and South Atlantic false alarm rates may be the result of the changes in IAGOS sampling or/and sampling in regions with higher occurrences of cirrus clouds/ice particles as discussed in Section 6.5. The latter is most likely also the reason for the high false alarm rates in South Asia, especially in JJA, which lie at around 15%.

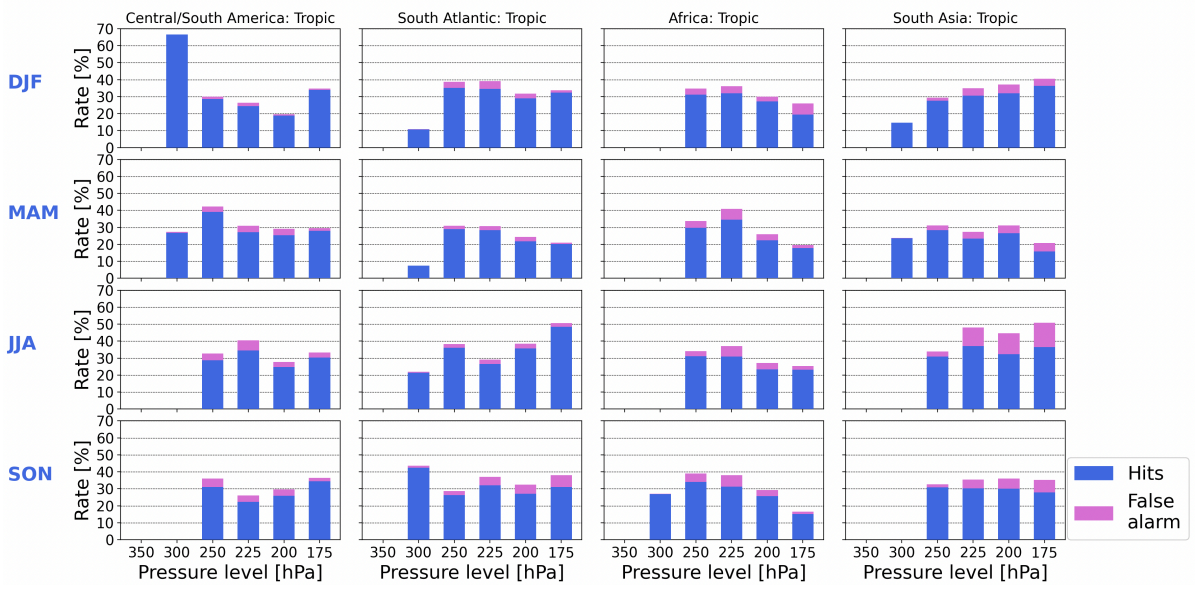

Figure 7.3: Ice supersaturated region hit and false alarm rates per season and pressure level for tropic regions

To conclude, ERA5 shows significant issues in the simulation of ice supersaturated regions, both in the extratropics and tropics. It is mainly due to the dry bias identified in the relative humidity over ice. Only up to 35%-40% of ISSRs are correctly identified by ERA5, with a low of 20%. Contrarily, ERA5 will also falsely detect 5% of points as ice supersaturated regions, while IAGOS does not. The false identification rate increases to 15% in the tropic region of South Asia for season JJA and is most likely attributed to atmospheric ice concentration irregularities in ERA5. Care should be taken of false alarms as this may cause unnecessary avoidance of a false ISSR in contrail avoidance strategies.

7.2. Comparison of Ice Supersaturated Regions from a Regional, Pressure Level and Yearly Perspective

In this section, the ice supersaturated region (ISSR) fraction found with ERA5 and IAGOS is examined from a regional, pressure level and yearly perspective. Seasonal deviations are also taken into account, as explained in Section 5.4. First, the extratropic regions are examined, followed by the tropic regions.

Figure 7.4 displays the ISSR fraction computed using the IAGOS and ERA5 datasets from a yearly, regional and pressure level perspective for the extratropic regions. It can be seen that there is no yearly trend, just as described by A. Petzold et al. [53]. This is most likely due to changes in sampling. Moreover, ERA5 generally underestimates the yearly trend, which is to be expected given the model dry bias in relative humidity over ice. Some years, such as 2013 and 2014, at pressure level 225 hPa show a better ISSR fraction approximation by ERA5. This is most likely due to the somewhat moist bias identified for ERA5 for these conditions. Furthermore, at a pressure level of 200 hPa, the overall difference between IAGOS and ERA5 has also decreased, which can be attributed to the lower overall values of relative humidity over ice at this pressure level and above, due to being above the tropopause. However, this also shows that ISSRs are possible in the lower stratosphere, but their occurrences are far less frequent. Lastly, ERA5 struggles with finding the peak, showing issues in identifying the seasonal variation of ISSRs, which was also seen in Figure 7.1.

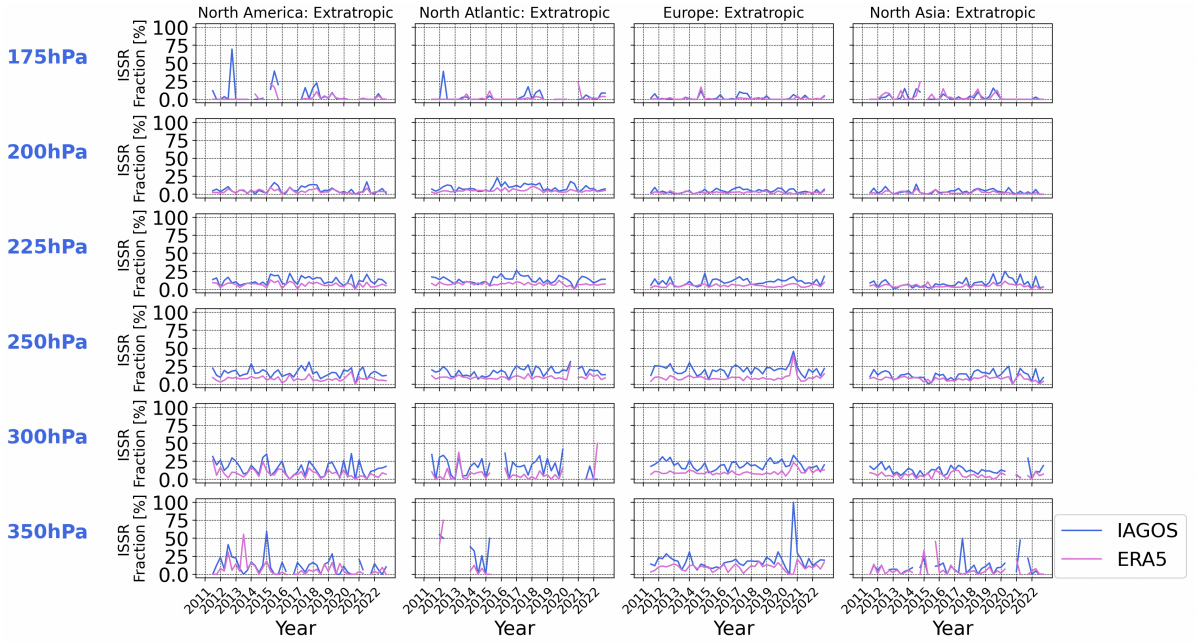

Figure 7.4: IAGOS and ERA5 yearly ice supersaturated region fractions per pressure level for extratropic regions

The yearly ISSR fraction for the tropics can be found in Figure 7.5. Again, no yearly trend can be identified. Furthermore, ERA5 is still underestimating the ISSR fraction, but the difference between IAGOS and ERA5 is smaller in the tropics. This is due to lower values of relative humidity over ice above ice supersaturation, as seen in Chapter 6. In the tropics, ERA5 is also better at the approximation of the peaks, which may be a result of lower seasonal variations of temperature and, partially, relative humidity over ice. In addition, there is a better approximation of the ISSR fraction around the years 2012-2014, which may be due to the small moist bias identified in ERA5 for these years. It is not assumed to be due to low sampling as these years showed some of the highest in the tropic regions. In South Asia, there is sometimes an overestimation of the ISSR fraction, particularly in the peaks corresponding to JJA and this is due to the moist bias in ERA5 for this region and season.

Overall, the yearly evaluation for the ice supersaturated region fraction shows no trend. Though, larger deviations between IAGOS and ERA5 are found in the extratropics compared to the tropics, due to larger probabilities of the relative humidity being larger than 1 in the extratropics. Better approximations of the ISSR fraction are found in the years 2013 and 2014 and at pressure levels where ERA5

shows possibilities of a moist bias.

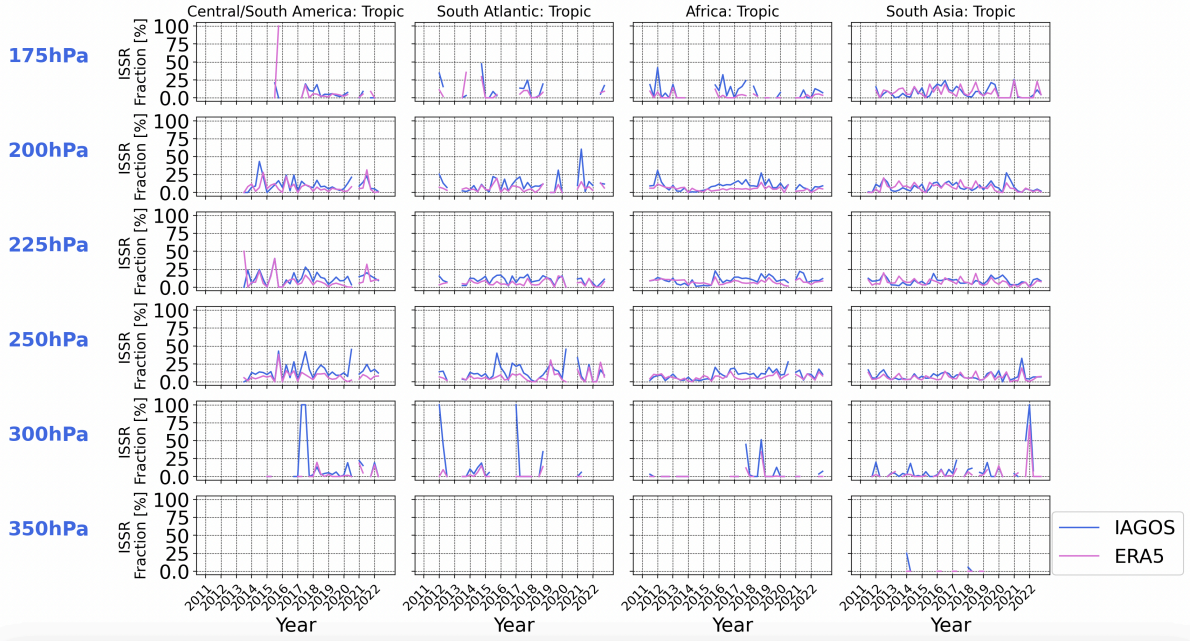

Figure 7.5: IAGOS and ERA5 yearly ice supersaturated region fractions per pressure level for tropic regions

7.3. Location and Occurrences of Ice Supersaturated Regions in ERA5 and IAGOS

In the previous sections, eight different regions were analysed. However, this does not show the exact location of the ice supersaturated regions and where exactly the major differences are located. Thus, in this section, the location and occurrences of ice supersaturated regions in ERA5 and IAGOS are examined.

The percentage difference in the ice supersaturated region (ISSR) occurrence between IAGOS and ERA5 is shown in Figure 7.6. Pressure levels, seasons and years are not taken into account. A positive percentage difference means that more ISSRs are found using the IAGOS dataset compared to ERA5, meanwhile a negative value means ERA5 finds a higher ISSR occurrence. As can be seen, the average percentage difference seems to lie around 50%, when not accounting for the behaviour in South Asia. In South Asia, mainly negative percentage differences are encountered. There are also small regions in the extratropics and the other tropic regions which show larger ISSR occurrences in ERA5 compared to IAGOS. This may be related to the behaviour observed in the years 2013 and 2014, described in Section 6.5.

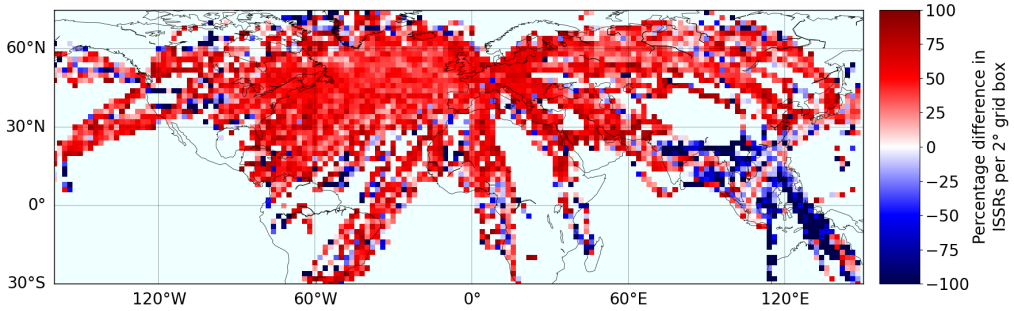

Figure 7.6: Percentage difference in ice supersaturated region occurrence between IAGOS and ERA5

ERA5 itself cannot directly be used for flight re-routing due to being a reanalysis product. It is built upon the ECFMW-IFS, which is used in operational forecasts. Hence, if using this NWP model, flights

may be unnecessarily re-routed in South Asia and other regions with ISSR false alarms. This would increase fuel and other emissions, such as CO_2, and would most likely increase the overall climate impact of that flight. It is the opposite of what is trying to be achieved with contrail avoidance. However, flights would not be successfully rerouted in case of undetected ISSRs. Furthermore, if using ERA5 to estimate the climate impact of past flights, the undetected ISSRs would lead to a lower climate impact of the flight(s) and false alarms would overestimate it. Both will give incorrect results regarding the actual impact of persistent contrails on the climate.

7.4. Effect of Changing Definition of Ice Supersaturation in ERA5

Ice supersaturation is typically defined by a relative humidity over ice above 1. However, ERA5 shows large issues in identifying ice supersaturated regions when using this definition. P. Reutter et al. examined the effect of decreasing the value of relative humidity over ice for the definition of ice supersaturation to improve ERA-interim's capability of calculating the ice supersaturated region fraction [57]. R. Teoh et al. [72] scale the ERA5 relative humidity over ice by a division coefficient and data points within ISSRs are scaled with a power-law function. K. Wolf et al. attempt to correct the relative humidity over ice in ERA5 with the bivariate quantile mapping method [83]. No attempts have been made to correct ERA5 using the same methodology as P. Reutter et al. for the ERA-interim reanalysis. Hence, in this section, the effect of changing the definition of ice supersaturation in ERA5 will be explored.

P. Reutter et al. found that to achieve the best agreement with the MOZAIC in-situ measurements, a different definition of relative humidity over ice for ice supersaturation in ERA-interim was required per layer. Below the tropopause, using a relative humidity over ice of 0.95 allowed for the best comparison, whereas for the tropopause layer, a value of 0.9 achieved better results. In the lower stratosphere, an almost perfect match was achieved between MOZAIC and ERA-interim when using a value of 0.85 for the relative humidity over ice as the definition for ice supersaturation [57]. This shows that in order to achieve the best results, it is necessary to tailor the corrections based on the atmospheric layer. However, it should be kept in mind that the study by P. Reutter et al. only considers the North Atlantic region, with no seasonal or yearly deviations taken into account. Furthermore, decreasing the relative humidity over ice definition would only work in cases where ERA5 displays a dry bias. For conditions where a moist bias is identified, such as in South Asia, the definition of relative humidity over ice for ice supersaturation in ERA5 should be increased. Hence, for this reason, using 0.85, 0.9, 0.95 and 1.05 as the definition of ice supersaturation in ERA5 will be considered.

Figure 7.7 considers the ice supersaturated region fraction in IAGOS and ERA5 with 0.85 as the definition of ice supersaturation. This generally results in overestimating the ERA5 ISSR fraction for all regions, seasons and pressure levels. This signifies that a larger value needs to be used for better approximation. Though, at a pressure level of 175 hPa in the extratropics, some improvements are noticeable. This is seen for North America in DJF, North Atlantic in SON, Europe for all seasons, and North Asia in DJF. Pressure level 175 hPa is also above the tropopause layer; hence, these findings are somewhat in line with the results found by P. Reutter et al. [57]. The reason why 0.85 might not be the best fit in this study is due to upper tropospheric and lower stratospheric influences at this pressure level, as previously discussed.

The effect of increasing the value of relative humidity over ice to 0.9 for the definition of ice supersaturation in ERA5 can be found in Figure 7.8. The ISSR fraction is still overestimated by ERA5 for most regions, seasons and pressure levels. This shows that this value is also generally too small to improve the detection of ice supersaturated regions in ERA5. However, at pressure level 250 hPa in North America for season DJF, as well as Europe for DJF and JJA, using 0.9 gives almost equal values of the ISSR fraction in IAGOS and ERA5. This is around the tropopause layer for Europe in JJA. Thus, showing that the correction may be slightly related to the tropopause layer. It is difficult to make this conclusion in this study, due to not defining the pressure levels as the distance from the tropopause and only knowing the average tropopause height.

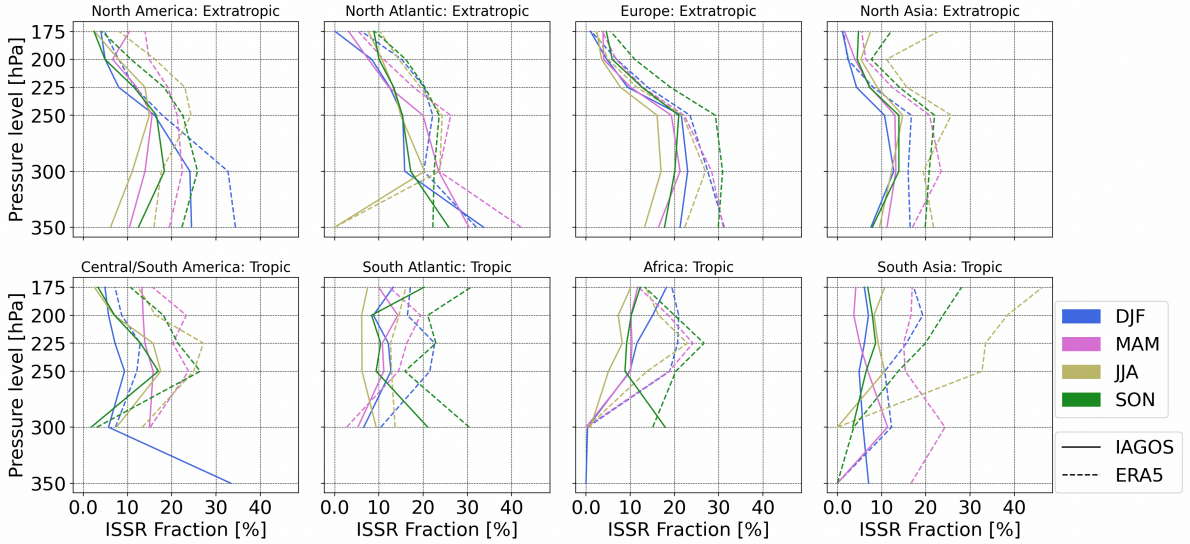

Figure 7.7: IAGOS and ERA5 ice supersaturated region fraction per season, pressure level and region, given ERA5 ice supersaturation definition of relative humidity over ice above 0.85

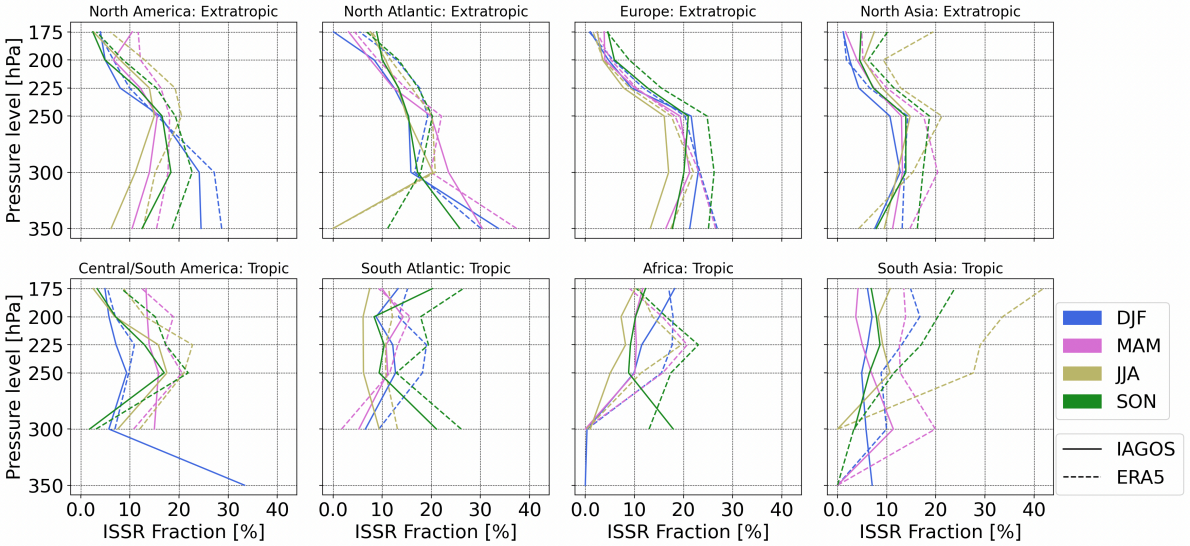

Figure 7.8: IAGOS and ERA5 ice supersaturated region fraction per season, pressure level and region, given ERA5 ice supersaturation definition of relative humidity over ice above 0.9

Moving on, Figure 7.9 shows the ISSR fraction with IAGOS and ERA5 given a definition of ice supersaturation with a relative humidity over ice above 0.95. In the extratropic regions, this definition results in better ISSR fraction calculated with ERA5, both for lower and higher altitudes. For example, in North America, using 0.95 results in a much better approximation for DJF above 225 hPa, though below this altitude, the ISSR fraction remains underestimated by ERA5. Interestingly, using 0.9 resulted in an overestimated ISSR fraction with ERA5 below 250 hPa, showing that the ISSR fraction is very sensitive to the definition provided. Furthermore, a definition of 0.95 also provides very good results for North America in MAM and SON below 250 hPa, with JJA overestimated. Not only that, ERA5 also shows a good ISSR fraction estimate with a value of 0.95 below 250 hPa in Europe for SON and below 250 hPa in North Asia for SON and DJF. However, in South Asia, this value mainly results in an overestimated ISSR fraction, as well as in the South Atlantic and Africa. In Central/South America, a good fit is achieved for season DJF for almost all pressure levels and for season SON below 250 hPa.

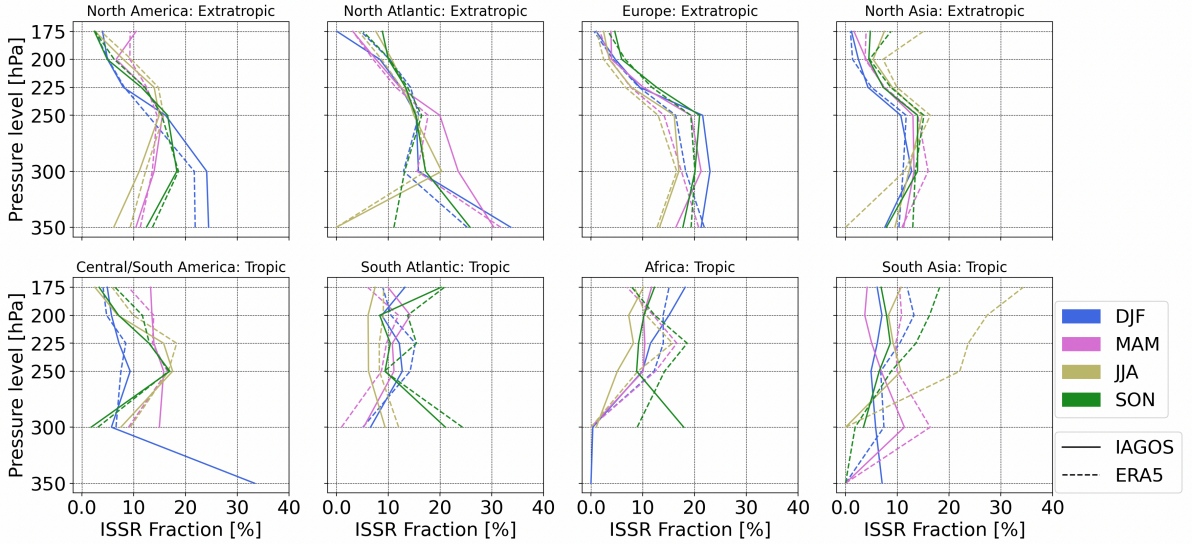

Figure 7.9: IAGOS and ERA5 ice supersaturated region fraction per season, pressure level and region, given ERA5 ice supersaturation definition of relative humidity over ice above 0.95

Lastly, using a definition of ice supersaturation for ERA5 with a value of relative humidity over ice above 1 is explored. Figure 7.10 shows the results with a value of 1.05. It is clear that using such a value almost detects no ISSRs in ERA5, showing a much larger sensitivity to a definition above 1. This is most likely due to most values being centred around 1 due to the saturation adjustment. Thus, to correct the overestimation in South Asia, care should be taken in selecting the appropriate value.

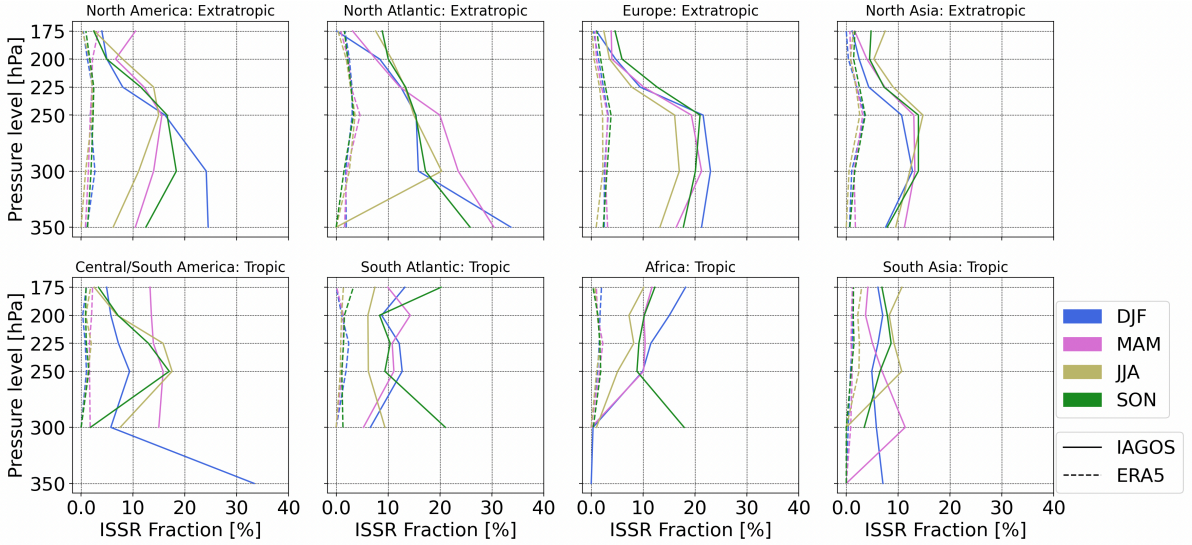

Figure 7.10: IAGOS and ERA5 ice supersaturated region fraction per season, pressure level and region, given ERA5 ice supersaturation definition of relative humidity over ice above 1.05

All in all, there is not one perfect correction to achieve better detection of ISSRs in ERA5. Values seem to lie somewhere between 0.85 and 1 and slightly above 1 for South Asia specifically. The exact value is dependent on the region, pressure level and season. Analysis of corrections from a yearly standpoint has not been taken into account due to no yearly trend in the ISSR fraction being visible and due to the uncertainty of yearly variations caused by inconsistent regional coverage, and perhaps other factors. Moreover, as seen by P. Reutter et al., one standard correction for all years will not guarantee a better estimation of the ISSR fraction in the reanalysis model per year [57]. Thus, corrections in the ice supersaturation definition for ERA5 need to be tailored for the region, season, pressure level and most likely also the year being considered.

7.5. Ice Supersaturated Region Conclusion

To conclude, this chapter focused on validating ice supersaturated regions in ERA5 using the IAGOS in-situ measurements from a regional, pressure level, seasonal and yearly perspective. The errors in the detection of ISSRs in ERA5 mainly arise due to issues in the simulation of relative humidity over ice. It was shown that the dry bias in ERA5 led to 20 to 40% hit rates, showing a large amount of undetected ISSRs in ERA5. However, there was also a small percentage of falsely detected ISSRs. At lower altitudes, such as 350 and 300 hPa in the extratropics and 300 and 250 hPa in the tropics, some of the falsely detected ISSRs arise due to the cold bias in ERA5. However, at higher altitudes, the false detection is solely due to the moist bias that is sometimes identified in ERA5.

Considering pressure level variations, pressure levels 350 to 250/225 hPa show the highest ISSR occurrence in the extratropics and are shifted to 250 to 175 hPa in the tropics. In the extratropics, the percentage of correctly identified ISSRs by ERA5 generally decreases with pressure level, above the estimated tropopause. The tropics show low pressure level variations in the ISSR fraction.

From a regional perspective, the extratropics are overall more likely for ISSR occurrence in comparison to the tropics. North Asia shows ISSRs occurring far less often than in the other three extratropic regions considered in this study. The extratropics and tropics also show similar hit rates, though the tropics show a higher percentage of false alarms in the detection of ISSRs by ERA5. This is due to ERA5 showing a moist bias more often in the tropics compared to the extratropics.

Seasonality-wise, larger hit rates occur in DJF and the lowest in JJA, for the extratropics. In the tropics, a seasonal trend is hard to detect, though the false alarm rate is the highest in JJA for South Asia.

Lastly, the yearly variation of the ISSR fraction shows not trend, but it is clear that ERA5 mainly underestimates the ISSR fraction. The peaks are better estimated in the tropics compared to the extratropics, which may be a result of less seasonal variations. In South Asia, the yearly trend can be overestimated by ERA5 due to the moist bias found for this particular region.

Thus, the ISSR fraction is highly dependent on the behaviour of relative humidity over ice. Better approximations of the ISSR fraction may be achieved by changing the value of relative humidity over ice for the definition of ice supersaturation in ERA5. The exact value needs to be tailored for the season, region, pressure level, and possibly the year. It is hard to say from a yearly perspective due to inconsistencies in measurement density and regional coverage.

8. Schmidt-Appleman Criterion

The differences in the Schmidt-Appleman criterion (SAC) between IAGOS and ERA5 are explored in this chapter. This includes investigating how the Schmidt-Appleman criterion behaves as a function of temperature, relative humidity with respect to liquid, pressure level and engine efficiency, which is presented in Section 8.1. Such an analysis helps understand why and where deviations between ERA5 and IAGOS stem from. Thereafter, the SAC using both the IAGOS and ERA5 datasets is examined from a seasonal, regional and pressure level perspective in Section 8.2 and from a yearly, regional, and pressure level perspective in Section 8.3. These two analyses will aid in understanding the differences to expect between IAGOS and ERA5. Lastly, Section 8.4 provides a global distribution of the differences in how often the SAC is met between IAGOS and ERA5, as well as the global distribution of how often the SAC is satisfied per pressure level.

8.1. Impact of Temperature, Relative Humidity with respect to Liquid, Pressure Level and Engine Efficiency on Schmidt-Appleman Criterion

The following section analyses the effect of temperature, relative humidity with respect to liquid, pressure level and engine efficiency on the Schmidt-Appleman criterion (SAC). The SAC states whether a contrail can be formed or not and is a function of these four variables. The temperature deviations between ERA5 and IAGOS are already known and have been examined in great detail. However, the relative humidity with respect to liquid has not been examined. Moreover, the complete effect of the engine efficiency and pressure level on the SAC is unknown. Hence, this section allows for a better understanding of how these variables can affect the Schmidt-Appleman criterion.

First, the effect of the pressure level on the Schmidt-Appleman criterion is shown in Figure 8.1 for a range of temperatures and relative humidity with respect to liquid. The plot shows that the higher the pressure level (lower altitude), the higher the critical temperature for contrail formation is for a given relative humidity with respect to liquid. This means a contrail can form at higher ambient temperatures. The same results were found by E. J. Roosenbrand et al. [58]. For a given temperature, the higher the pressure level (lower altitude), the lower the critical relative humidity for contrail formation. Furthermore, a change in pressure level simply causes a shift of the SAC threshold curve; decreasing the pressure level causes a leftward shift.

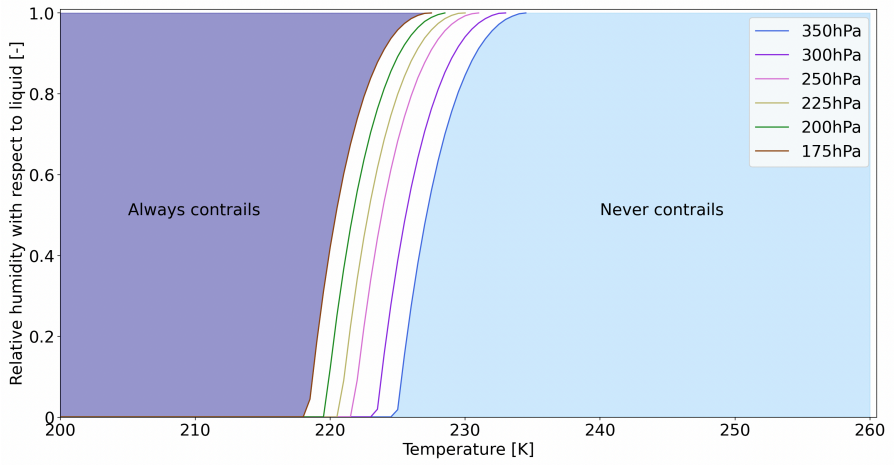

Figure 8.1: Schmidt-Appleman criterion sensitivity to temperature and relative humidity with respect to liquid at η = 30%, with the solid line indicating SAC threshold; left of solid line means SAC is met and contrails can form, right of solid line means SAC is not met and contrails cannot form. Note: only specific to the pressure levels in this study

The previous plot did not take into account the deviations in temperature and relative humidity with respect to liquid between IAGOS and ERA5. How this could affect the Schmidt-Appleman criterion will be examined next. This is done by plotting these two variables for IAGOS and ERA5 for a given pressure level, along with the SAC threshold line. The plots for pressure levels 200 and 250 hPa can be found in Figure 8.2 and Figure 8.3, respectively. ERA5 underestimates the relative humidity with respect to liquid, which is to be expected given that it is calculated using the relative humidity with respect to ice. Due to the steepness of the SAC threshold curve, the underestimation is most likely not causing a huge difference in whether the SAC is met or not. Only at high values of relative humidity with respect to liquid, above a value of approximately 0.8, it would cause a lot larger differences. This is when the SAC threshold is starting to reach its asymptotic shape. The temperature deviations between ERA5 and IAGOS seem to shift all ERA5 points leftwards compared to IAGOS, meaning more points would meet the SAC in ERA5. The shift does not seem to be large enough to cause a large difference. This will be further investigated in this chapter.

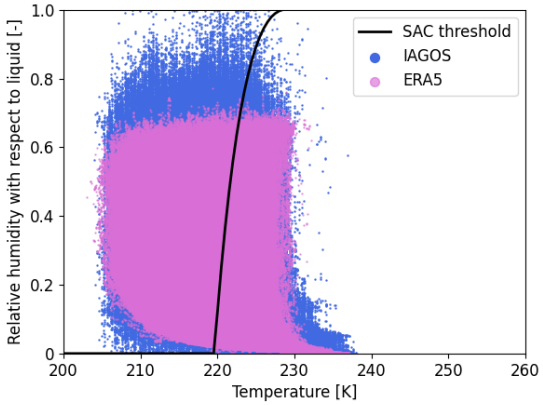

Figure 8.2: Distribution of IAGOS and ERA5 relative humidity with respect to liquid and temperature for pressure level 200 hPa and the SAC threshold for this pressure level

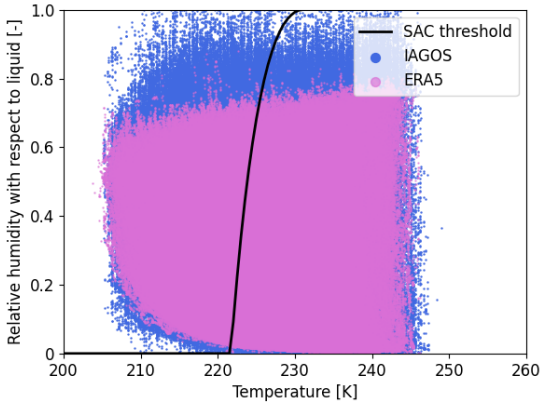

Figure 8.3: Distribution of IAGOS and ERA5 relative humidity with respect to liquid and temperature for pressure level 250 hPa and the SAC threshold for this pressure level

The influence of the aircraft engine propulsion efficiency on the Schmidt-Appleman criterion is examined. Figure 8.4 shows how the SAC threshold line varies between an efficiency of 30% and 55%, in which the higher engine efficiencies represent the future trend of this engine parameter [66]. Like with the pressure level, changing engine efficiency does not affect the slope of the SAC threshold line. As the engine efficiency increases, the curve shifts rightwards. This means that the critical temperature for contrail formation increases, allowing for contrails to form at higher ambient temperatures. However, from an engine efficiency of 30% to a value of 55%, the critical temperature increase is approximately 5 K. Given that the typical mean difference in temperature between IAGOS and ERA is 0.5 K to 1.5 K, this shift in the curve could perhaps ensure a more equal identification of points meeting the SAC between IAGOS and ERA5.

To conclude, the Schmidt-Appleman criterion is affected by several variables, such as temperature, relative humidity with respect to liquid, pressure level and engine efficiency. The pressure level and engine efficiency cause a shift in the SAC threshold curve; a larger engine efficiency and a higher pressure level increase the critical temperature for contrail formation. Furthermore, the SAC threshold curve is relatively steep and thus, the deviations in temperature are expected to have a larger impact on which samples meet or do not meet the Schmidt-Appleman criterion compared to relative humidity with respect to liquid.

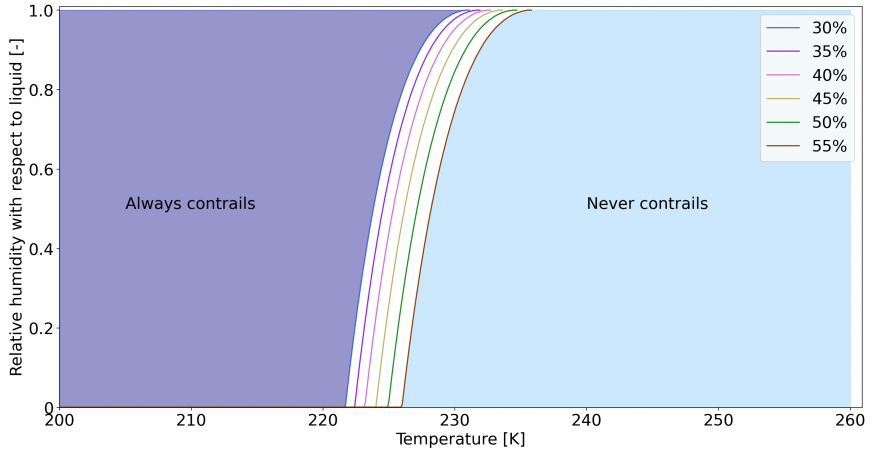

Figure 8.4: Schmidt-Appleman criterion sensitivity to aircraft engine propulsion efficiency at pressure level 250 hPa, with solid line indicating SAC threshold; left of solid line means SAC is met and contrails can form, right of solid line means SAC is not met and contrails cannot form

8.2. Schmidt-Appleman Criterion in ERA5 and IAGOS from a Regional, Seasonal and Pressure Level Perspective

The following section analyses the Schmidt-Appleman criterion (SAC) found using ERA5 and IAGOS from a regional, seasonal and pressure level perspective. It was previously seen that the SAC threshold curve was relatively steep. As a result, it was hypothesised that the deviations in relative humidity with respect to liquid between IAGOS and ERA5 should not cause large differences in which points meet the SAC, but temperature might have a larger impact. Further insights into this will be gained in this chapter.

Figure 8.5 shows the hit rate and false alarm rate for meeting the Schmidt-Appleman Criterion per pressure level and season for the extratropic regions. The percentage of overall points meeting the SAC when using the IAGOS or ERA5 dataset can be seen in Appendix C. From pressure level 250 hPa to 175 hPa, a hit rate of almost 100% is detected. This means ERA5 and IAGOS are identifying most of the same measurement points as meeting the SAC. A hit rate of 100% may not occur due to the possibility of ERA5 being warmer than IAGOS, but this may be due to sensor errors, as seen in Section A.1. K. Gierens et al. [20] also observed hit rates of 99% for the SAC.

At pressure levels 350 and 300 hPa, a reduction of the hit rate is observed for JJA. Given ERA5's cold bias at pressure levels 350 and 300 hPa, the reduced hit rates are due underestimation of the relative humidity with respect to liquid, resulting from the dry bias in the simulation of relative humidity with respect to liquid. The 0% hit rates observed in JJA are due to no measurements meeting the SAC, seen in Appendix C, as a result of high temperatures.

False alarm rates also occur and are generally between 1 and 5%, which is lower than what was seen by K. Gierens et al. [20], due to differences in the parameters of the studies. The false alarm rate is most likely attributed to the cold bias in ERA5. It remains relatively constant per season, region and pressure level and follows the behaviour of temperature deviations between IAGOS and ERA5.

The hit rate and false alarm rate for meeting the Schmidt-Appleman criterion per season and pressure level for the tropic regions are presented in Figure 8.6. A hit rate of 100% is found at high altitudes. The SAC is barely met between pressure levels 350 and 250 hPa, as seen in Appendix C. This causes zero hit and false alarm rates at these pressure levels. Moreover, pressure level 225 hPa, only shows 25% or less of the data points meet the SAC. At these pressure levels, a lower hit rate also occurs. Again, this stems from an underestimation of the relative humidity with respect to liquid due to ERA5's cold bias. At pressure level 300 to 200 hPa in South Asia, lower hit rates are also observed. This region shows a slight warm bias that cannot be entirely attributed to sensor errors, which may cause the reduced hit rate. However, it could also be the result of the overestimated relative humidity over ice seen in this region.

The tropics seem more susceptible to false alarms, especially Africa, followed by South Asia. The false alarm rate can almost reach 50% at pressure level 175 hPa for both of these tropic regions. This

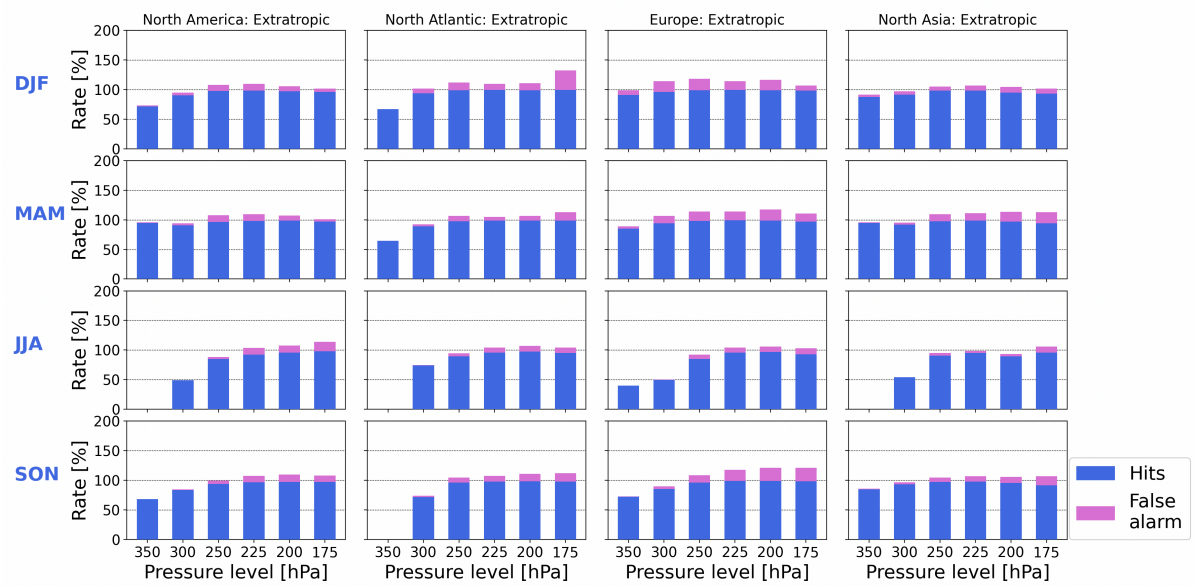

Figure 8.5: Hit rate and false alarm rate for meeting the Schmidt-Appleman criterion per season and pressure level for extratropic regions, η = 30%

is higher than what was found by K. Gierens et al. [20], but the tropics were also not considered in this study. Africa was the region with the largest temperature errors, as seen in Section 5.4, with a cold bias not explained by uncertainties in IAGOS' temperature sensor. These errors were also the lowest in JJA. Hence, this is what causes the high false alarm rates in this region, which are lower in JJA. In South Asia, a stronger warm bias was actually present at these altitudes. The false alarm rates in South Asia occur at pressure levels 200 and 175 hPa and are a result of a cold bias. However, in DJF and MAM, this cold bias may not be a model error but due to uncertainties in IAGOS' temperature sensor. The same cannot be said for MAM and JJA.

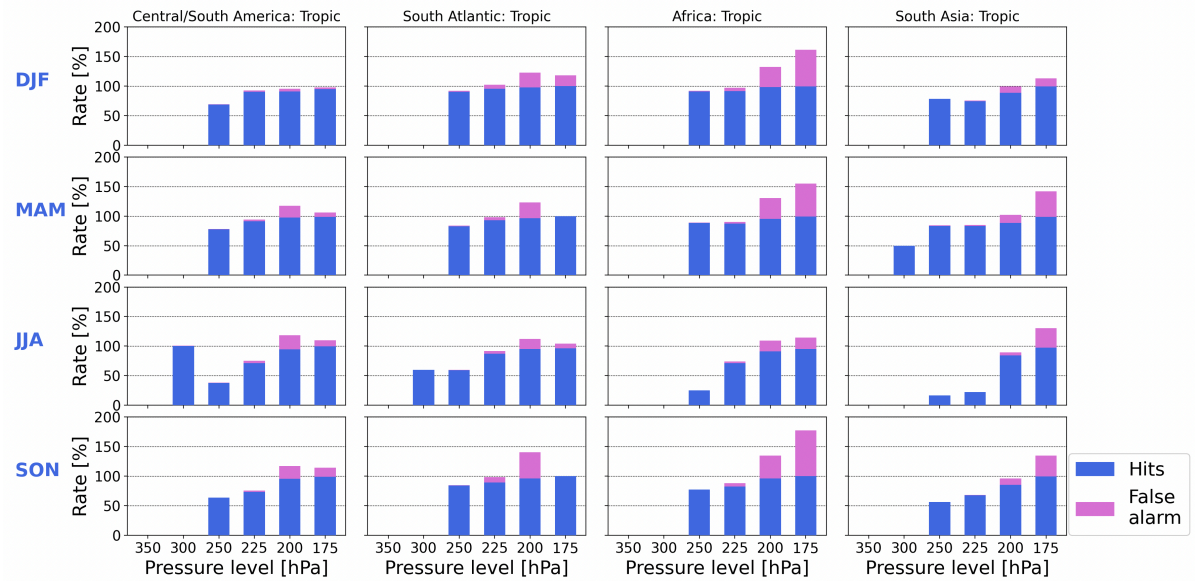

Figure 8.6: Hit rate and false alarm rate for meeting the Schmidt-Appleman criterion per season and pressure level for tropic regions, η = 30%

To conclude, from a seasonal, regional and pressure level perspective, ERA5 is relatively accurate in determining whether a measurement meets the Schmidt-Appleman criterion or not, with an average false alarm rate of approximately 5 to 10%. South Asia and Africa show false alarm rates of up to 50%.

The main reasons for the false alarms seem to stem from the cold bias in ERA5. The hit rate is almost 100% at altitudes in which contrail formation should theoretically occur. However, at lower altitudes, lower hit rates are found and may be a result of biases in the relative humidity over ice in ERA5. Hence, finding contrail formation regions with ERA5 is governed by the temperature and relative humidity over ice errors.

8.3. Schmidt-Appleman Criterion in ERA5 and IAGOS from a Regional, Yearly and Pressure Level Perspective

This section analyses the fraction of measurements meeting the Schmidt-Appleman criterion from a regional, yearly and pressure level perspective. In the previous section, ERA5 and IAGOS showed very similar results to due a relatively steep SAC threshold line, though errors still arose due to deviations in temperature and relative humidity over ice.

Figure 8.7 shows the percentage of measurements meeting the SAC per pressure level and year for the extratropics. The SAC pressure level dependency can be identified, which shows an increase in the number of points meeting the SAC from pressure level 350 hPa to 250 hPa and then stays relatively constant. At pressure level 350 hPa, both ERA5 and IAGOS show little to no points meeting the SAC; Europe shows the highest percentages. The same can also be seen in the season, region and pressure level analysis in Figure C.1. Looking at the yearly variation in mean temperature in Figure 5.10, it is clear that Europe is showing a lower mean throughout all years for pressure level 350 hPa, allowing more points to meet the SAC. Moving on, when looking at the yearly analysis, larger deviations seem to be present between IAGOS and ERA5, compared to seasonally. In some instances, such as in North Atlantic at pressure level 300 hPa in 2022 and at pressure level 175 hPa in 2018, ERA5 shows a percentage that is 20% higher than that found with IAGOS. This could be a result of more sampling in a particular season but also a low number of data points.

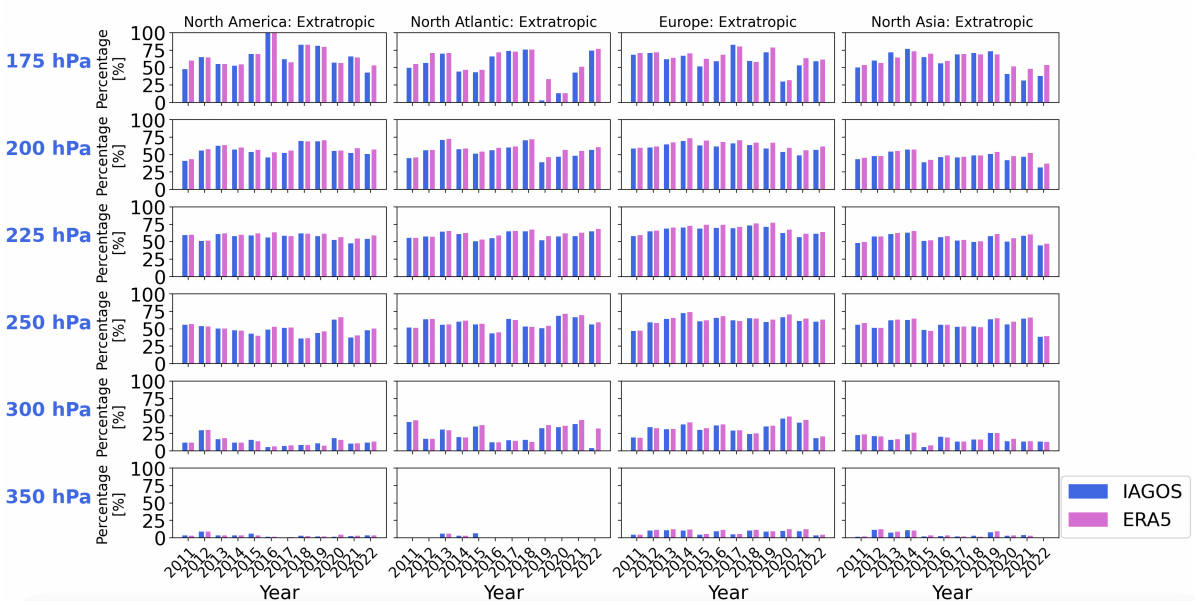

Figure 8.7: Percentage of measurements meeting Schmidt-Appleman criterion in the extratropic regions per year and pressure altitude, η = 30%

The yearly behaviour of the percentage of measurements meeting the SAC seems to be governed by the temperature. For example, at a pressure level of 250 hPa in Europe, there is an increase in temperature from 2020 to 2022 in IAGOS, while at the same time, the SAC decreases from 2020 to 2022. Furthermore, for this region and season, the temperature was higher in 2019 compared to 2020, and the fraction of measurements meeting the SAC in 2019 was less than in 2020. Thus, it is clear that the behaviour of how many points meet the Schmidt-Appleman criterion is heavily governed by the temperature. If the global temperatures continue to rise, it could lead to fewer points along a flight path meeting the Schmidt-Appleman criterion. However, the engine efficiency is also predicted to increase,

which increases the critical temperature threshold. Therefore, how the occurrence of contrail formation regions will change will be dependent on these two factors since a yearly trend in the relative humidity over ice could not be detected.

The percentage of measurements meeting the Schmidt-Appleman criterion per year and pressure level in the tropic regions is presented in Figure 8.8. At pressure levels 350 and 300 hPa, neither IAGOS nor ERA5 show any points meeting the SAC. The mean temperature at these two pressure levels lies between a mean range of 240 K and 250 K (see Figure 5.11). Meanwhile, the critical temperature for contrail formation lies between approximately 235 K and 225 K for pressure level 350 hPa, and between 232 K and 223 K for pressure level 300 hPa. This makes it clear that the temperature of the points along the flight path are not near the value for contrail formation to occur. However, high percentages of points meeting the SAC are observed at pressure levels 200 and 175 hPa. At 175 hPa, the percentages sometimes reach 100%, which may be due low available number of data points. Furthermore, the difference between IAGOS and ERA5 seems to be higher in the tropics from a yearly perspective as well, particularly in Africa for all years and South Asia starting in 2020. The issues in Africa were seen and discussed in Section 8.2, and are a recurrent pattern every year. South Asia showed a cold bias beginning in 2020, which was possibly due to a decrease in the sample size. Nevertheless, temperature biases, whether due to model error, sensor errors or insufficient sampling, directly impact the Schmidt-Appleman criteria.

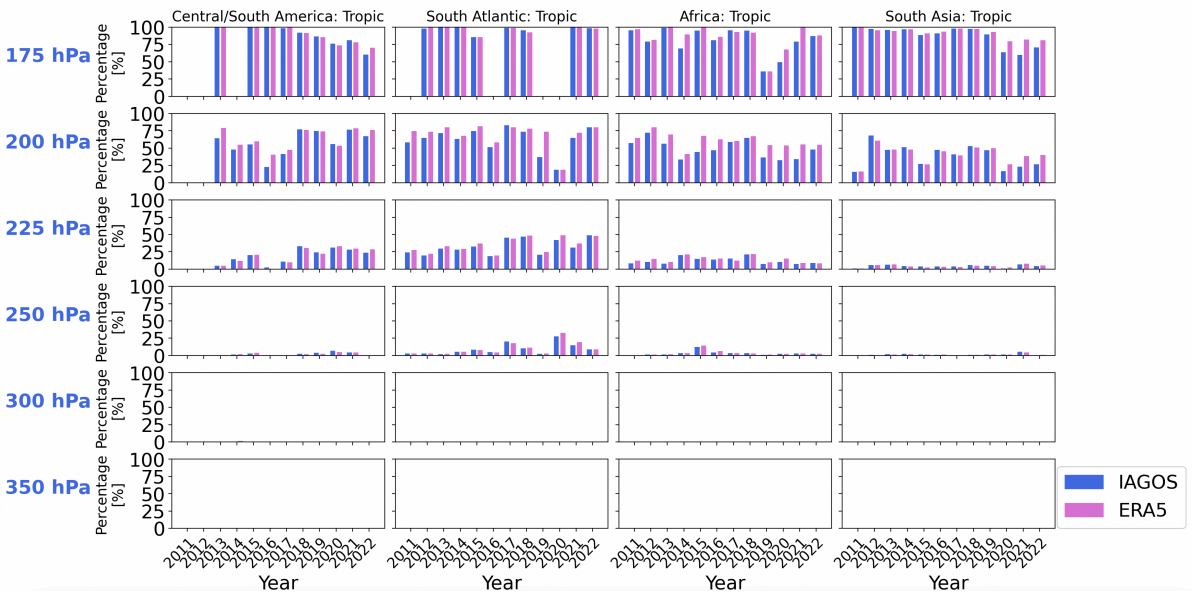

Figure 8.8: Percentage of measurements meeting Schmidt-Appleman criterion in the tropic regions per year and pressure altitude, η = 30%

8.4. Global Distribution of Schmidt-Appleman Criterion

In the previous sections, the difference in the percentage of measurements meeting the Schmidt-Appleman criterion was examined from a yearly, seasonal, regional and pressure level perspective. The regional analysis, however, provides limited insight into the location of where differences between IAGOS and ERA5 occur and also where meeting the SAC threshold might occur more often. Hence, in this section, the global distribution of the Schmidt-Appleman criterion will be investigated.

Figure 8.9 shows the percentage difference in meeting the SAC between IAGOS and ERA5, for an engine efficiency of 30% and 40%. Seasons, years and pressure levels are not taken into account. For both figures, it can be observed that the majority of the grid boxes have a percentage difference close to 0%, which was also seen in the previous analyses. It is below a latitude of 30°N, in which larger differences are observed, thus in the tropic regions. The larger differences also show that ERA5 finds more points where the SAC is met compared to IAGOS. This corresponds to the larger false alarm rates in the tropics.

When the aircraft engine propulsion engine efficiency is increased, there is a decrease in the per-

centage difference, mainly in false alarms. This is due to increased temperature for contrail formation. Hence, if using ERA5 for future engine analysis, it could allow for better prediction of where contrails could form. However, one should also take into account the expected increase in global temperatures, which can also affect the SAC.

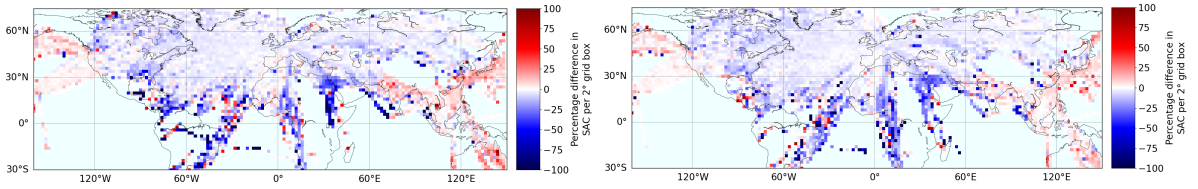

(a) η = 30% **(b)** η = 40%

Figure 8.9: Percentage difference in meeting the SAC between IAGOS and ERA5 per 2°grid box

Figure 8.10 displays the frequency of where the Schmidt-Appleman criteria is met using the IAGOS dataset. As the altitude increases, there is an increase in how often the SAC is met, as was previously discussed. This is not seen at pressure level 175 hPa due to less available data points available. At pressure level 250 hPa, the tropics only show the SAC being met close to the 30°N line, which separates the tropics and extratropics, with the majority of those points being located over the Atlantic Ocean. This also explains why the South Atlantic region in Figure C.2 and Figure 8.8 show a higher percentage of measurements meeting the SAC at this pressure level, compared to the other tropic regions. At pressure level 225 hPa, there is an increasing SAC coverage over the tropics, but the occurrence of meeting the criteria is still far less than in the extratropics. For pressure level 200 hPa, there is a strong increase in the SAC being met in the tropics, particularly over South Asia. This, in combination with the overestimation of ISSRs by ERA5 in this area, could lead to a potential overestimation of persistent contrails. This will be further investigated in the following chapter. There is also a decrease in the occurrence of meeting the SAC in the extratropics for pressure level 200 hPa. This is most prominent over North Asia and the North Atlantic regions and most likely stems from the decrease in the number of samples for this pressure level.

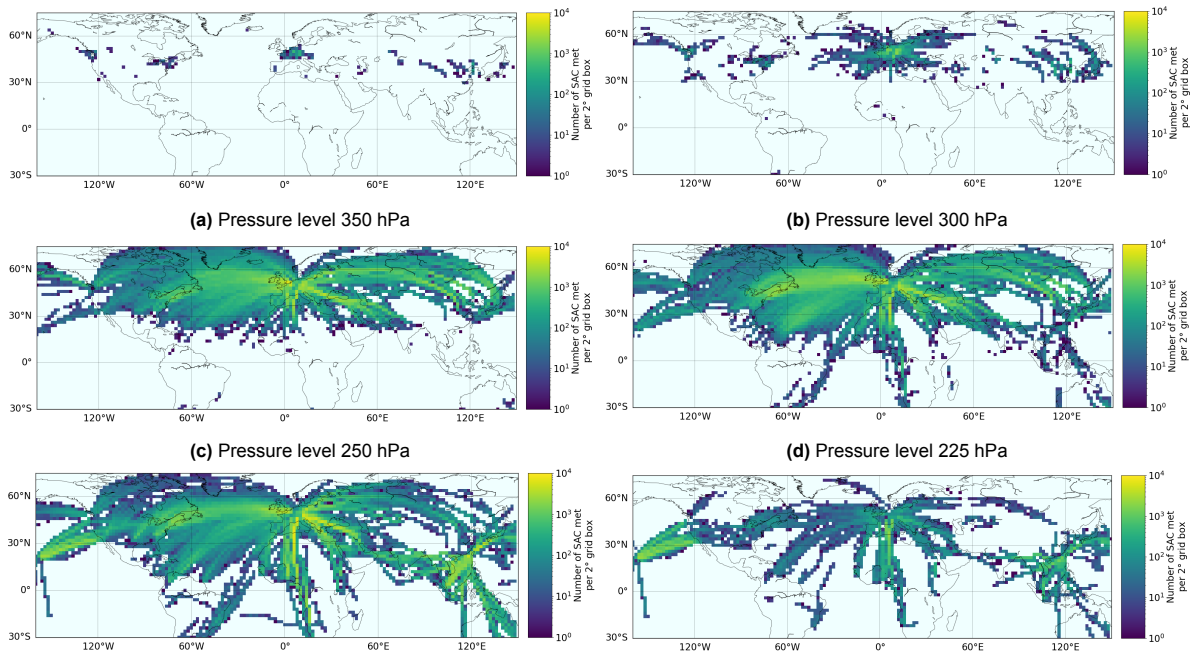

(a) Pressure level 350 hPa **(b)** Pressure level 300 hPa

(c) Pressure level 250 hPa **(d)** Pressure level 225 hPa

(e) Pressure level 200 hPa **(f)** Pressure level 175 hPa

Figure 8.10: Frequency of how often Schmidt-Appleman criterion is met per pressure level found with IAGOS measurements, with η = 30%

8.5. Schmidt-Appleman Criterion Conclusion

This chapter explored the differences to expect in the Schmidt-Appleman criterion (SAC) between IAGOS and ERA5. First, the effect of temperature, relative humidity with respect to liquid, pressure level and engine efficiency on the SAC was investigated in order to understand where and why deviations in the SAC between IAGOS and ERA5 would arise. It was concluded that due to the steepness of the SAC threshold curve, the temperature and relative humidity with respect to liquid errors in ERA5 would not have the largest impact. Moreover, increasing the engine efficiency and the pressure level causes a leftward shift of the curve, increasing the critical temperature of contrail formation, allowing contrails to form at higher temperatures.

Then, the SAC was investigated from a regional, seasonal, pressure level and yearly perspective. It was determined that ERA5 is very accurate in determining whether the SAC is met or not due to good simulation of temperatures. Reduced hit rates were observed at lower altitudes due to an underestimation of the relative humidity over ice. On average, a false alarm rate of 5 to 10% was observed, but up to 50% could occur as well. This was mainly due to the cold bias in ERA5. Moreover, yearly deviations seem to be directly influenced by temperature errors. Overall, deviations in SAC between IAGOS and ERA5 mainly depend on temperature differences, but also on relative humidity with respect to ice, particularly at lower altitudes.

9. Contrail Formation Potential

In previous chapters, it was concluded that the dry bias in the relative humidity over ice simulated by ERA5 led to several ice supersaturated regions (ISSRs) being undetected. The moist bias occurring in different regions led to false estimation of ISSRs. Moreover, ERA5 had a minor cold bias in its temperature simulation, leading to the Schmidt-Appleman criterion (SAC) sometimes being wrongly classified by ERA5. The contrail formation potential is a function of these two phenomena. This chapter will examine the influence of ice supersaturated regions, but also the Schmidt-Appleman criterion, on the contrail formation potential. First, this will be examined from a regional, seasonal and pressure level perspective in Section 9.1. Thereafter, a regional, yearly and pressure analysis is done in Section 9.2. Lastly, the specific location and difference in occurrence between IAGOS and ERA5 of the different contrail formation potential regions are shown and discussed in Section 9.3.

9.1. Contrail Formation Potential in ERA5 and IAGOS from a Regional, Seasonal and Pressure Level Perspective

The contrail formation potential uses the ice supersaturated region and Schmidt-Appleman criterion information to determine if there are no contrails, no persistent contrails, persistent contrails or reservoir conditions. This is explored from a regional, seasonal and pressure level perspective in this section. The Schmidt-Appleman criterion requires engine efficiency as an input. Hence, a value of 30% will be used as a baseline. The effect of the engine efficiency on the SAC can be found in Section 8.1. However, the effect of increasing the engine efficiency on the contrail formation potential will also be examined.

Figure D.1 shows the hit rate and false alarm rates for each of the four contrail formation potential areas per season and pressure level for the extratropic regions. For the percentage of measurements in each classification, the reader is referred to Section D.1. No contrail (NC) and no persistent contrail (NPC) regions show the highest hit rates, though not always equal to 100%. The high hit rates are due to the accurate temperature simulation in ERA5. The reason why the hit rate for NC is lower than for NPC is most likely a result of the cold bias in ERA5, leading to points being classified as meeting the SAC in ERA5 but not in IAGOS. This is why the false alarm rate for NC is low, and the false alarm rate for NPC is high. However, the false alarm rate for NPC may also be caused by ERA5's struggle in estimating ISSRs. Even if the SAC is well estimated by ERA5 but the ISSR is not accurately simulated, it will be classified as NPC and not a persistent contrail (PC) region, as it would by IAGOS. This further leads to the low hit rates of PC, which are generally between 20 and 40%. This is similar to the hit rate for ISSRs. K. Wolf et al. found a hit rate of 68% [83]. Differences may arise since this study did not consider the hit rate per season, pressure level or region. Issues in detecting ISSRs in ERA5 also lead to low reservoir (R) hit rates. Lastly, false alarms of PC and R conditions in the extratropics are rare.

Examining regional changes, reservoir conditions occur more often in the North Atlantic. Given the amount of flights crossing the North Atlantic corridor, this could have implications for contrails moving into this reservoir and could increase climate impact. It should be kept in mind that a large majority of measurements collected by IAGOS are over the North Atlantic corridor, so the observation could be slightly skewed. However, hit rates remain relatively equal between the extratropic regions. Moreover, North Atlantic and Europe show higher percentages of NPC than NC compared to North Asia and North America. Nevertheless, hit rates remain consistent between regions. However, North Atlantic and Europe do show slightly higher false alarm rates as a result. North Asia also shows lower percentages of PC regions than the other extratropic regions, though this is not reflected in the hit rate. Overall, this shows that ERA5 will feature similar detection of the four contrail formation potential in the four extratropic regions defined.

Seasonally, the extratropics in JJA show an increase in NC at lower altitudes and a general decrease in NPC due to lower occurrences of ISSRs as a result of higher temperatures and lower values of relative humidity over ice. This is reflected in an increased false alarm rate for NC and a decreased false alarm

rate for NPC. It also causes a slight reduction in the hit rate of PC conditions due to reduced hit rates of ISSRs in JJA. Moreover, DJF and MAM show a larger percentage of measurements with PC and R conditions. This does not have a large impact on hit or false alarm rates for R, but these seasons do show a slight increase in hit rates for PC conditions. This follows the seasonal behaviour of ISSR detection between IAGOS and ERA5.

From a pressure level perspective, hit rates of NC conditions decrease with increasing altitudes and match by an increase in the false alarm of NPC. This results from an increased cold bias in ERA5 at higher altitudes. Persistent contrails in extratropics are more commonly around pressure levels 250, 225 and 200 hPa, with reservoir conditions dominating at lower altitudes. This is also reflected in the hit rates for these two contrail formation potential areas. The hit rates for R conditions are zero at high altitudes as none are found with IAGOS. The hit rate for PC conditions tends to peak around pressure levels 250, 225 and 200 hPa, which was also the general trend of ISSR hit rates. The largest impact of wrongly simulating these conditions would be at the pressure levels where they are more bound to occur. This is because it would mean that overall, far more persistent contrails and reservoirs are not found, leading to more uncertainties in the climate impact or insufficient flight re-routing with an NWP model based on or similar to ERA5.

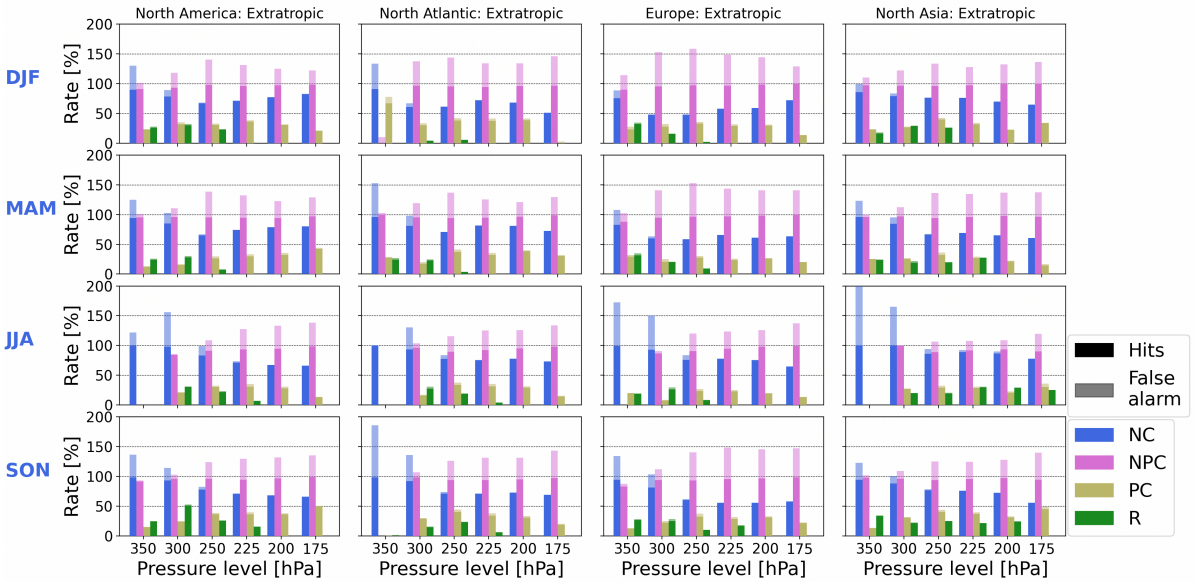

Figure 9.1: Hit rates and false alarm rates for contrail formation potential per season and pressure level in the extratropic regions, η = 30%

The hit rates and false alarm rates per season and pressure level for the tropic regions are found in Figure 9.2. The tropics are governed by no contrails at pressure levels 350 and 300 hPa due to high temperatures not allowing for contrail formation based on the Schmidt-Appleman criterion and no ISSRs due to being above the threshold of homogeneous freezing. This causes high hit rates for NC conditions and barely any hits or false alarms for the other contrail formation potential regions. If the false alarm is high for NC at these pressure levels, it is most likely the result of very few points being incorrectly misclassified as NC. Persistent contrails in the tropics generally occur at pressure levels 225 to 175 hPa and reservoir conditions from pressure levels 250 to 225 hPa. Hence, the occurrence of the hit rates at higher pressure levels. The hit rates of PC and R tend to lie between 20 and 40%, on average. As the pressure level increases, there is a tendency for the hit rate of NC conditions to decrease slightly with an increase in the false alarm of NPC. This is more noticeable in the South Atlantic and Africa, which showed a larger cold bias in ERA5. Furthermore, no large seasonal variations in the different conditions are seen in the tropics and are the result of low seasonal variations in both temperature and relative humidity over ice. However, South Asia shows a small percentage of false alarms for R and PC, which are the largest in JJA. This is to be expected, given the overestimation of RHI and thus ISSRs.

Overall, this means that when applying a model such as ERA5 for contrail mitigation in the tropics, more care should be taken at higher altitudes in comparison to the extratropic. However, in South Asia,

JJA shows higher PC and R conditions in ERA5 than IAGOS. This can lead to overestimating climate impact if recreating past flights and unnecessary avoidance of ISSRs.

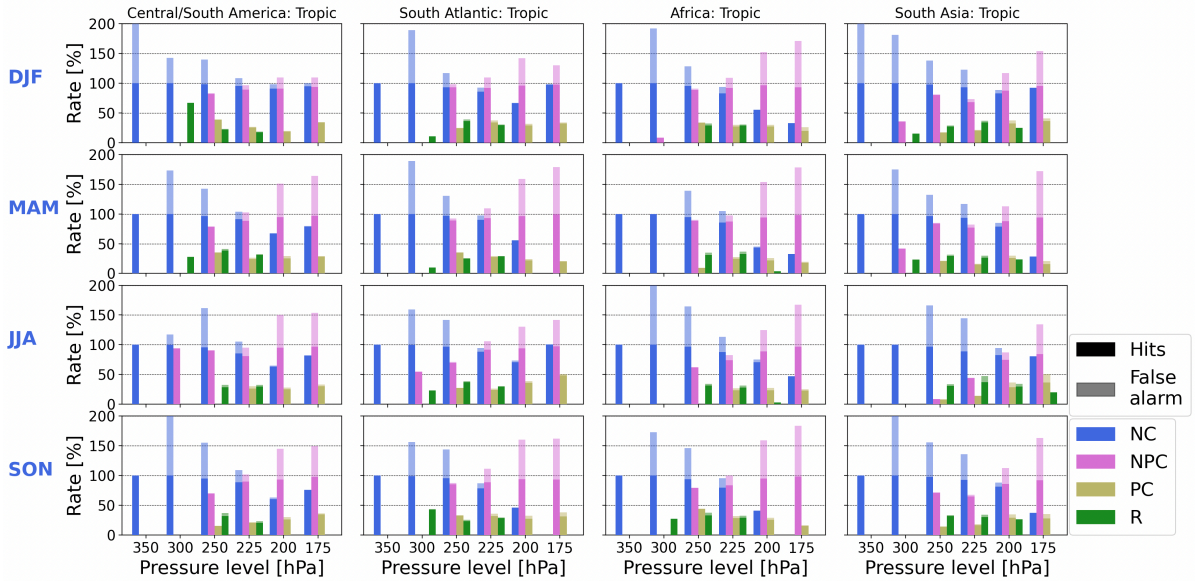

Figure 9.2: Hit rates and false alarm rates for contrail formation potential per season and pressure level in the tropic regions, η = 30%

A 4x4 contingency table, considering both the SAC and ISSR, is created to understand if errors in the ISSR or SAC are more critical on the contrail formation potential. Figure 9.3 displays the 4x4 contingency table for the extratropic regions at a pressure level of 250 hPa. The four corner boxes of each table are where ERA5 is correctly finding the NC, NPC, PC and R conditions. All other boxes are misclassifications. It can be seen that the majority of the measurements for each season are located within the correctly classified boxes, particularly the NC_i, NC_e and NPC_i, NPC_e boxes. However, when IAGOS predicts a PC region, ERA5 more often finds an NPC than a PC region. This is due to undetected ISSRs in ERA5. The same issue causes ERA5 to identify an NC more often than an R when IAGOS finds a reservoir region. There are also instances of falsely identified persistent contrail regions in ERA5 due to wrongly detected ISSRs. In these cases, IAGOS finds an NPC. Lastly, the cold bias in ERA5's temperature leads to incorrectly classifying an NPC region when IAGOS finds an NC. All in all, this shows that the misclassifications of ice supersaturated regions have the largest impact on the contrail formation potential, leading to undetected reservoir and persistent contrail conditions.

The 4x4 contingency table is shown for the tropic regions at pressure level 225 hPa in Figure 9.4. A large percentage of points are located in the NC_i, NC_e box due to the higher temperatures experienced in the tropics. This is followed by NPC_i, NPC_e due to lower occurrences of ISSRs. However, there is again a higher percentage of measurements classified in PC_i, NPC_e compared to PC_i, PC_e, as well as for R_i, NC_e compared to R_i, R_e. This is again due to undetected ISSRs in ERA5. For season JJA in South Asia, there are slightly more measurements with NC_i, R_e compared to R_i, NC_e and R_i, R_e due to the moist bias in ERA5's relative humidity over ice. Again, this shows that most misclassifications occur due to issues in the estimation of ISSRs in ERA5 that arise due to errors in the modelling of relative humidity over ice.

Effects of increasing the engine efficiency to 40% can be seen in Section D.2. As previously discussed, an increase in engine efficiency leads to an increase in the critical temperature for contrail formation and better classification of the SAC in ERA5. This is reflected in the hit rate and false alarm rate of the contrail formation potential. It causes an increase in the hit rate of NC conditions and a decrease in the false alarm rates of NPC. Moreover, the hit rates of PC and R are slightly improved. However, it makes sense that the majority of improvements are found between NC and NPC conditions, given that the engine efficiency is affecting the SAC, but not the estimation of ISSRs.

To conclude, this section analysed the contrail formation potential in ERA5 and IAGOS from a regional, seasonal and pressure level perspective. While being a function of the Schmidt-Appleman

criterion and ice supersaturated regions, differences in the contrail formation potential, particularly persistent contrail and reservoir conditions, between IAGOS and ERA5 were mainly a result of ERA5's struggle in correctly identifying ISSRs. Hence, seasonal, regional and pressure level variations in the contrail formation potential can be traced back to those seen in the relative humidity over ice between the two datasets.

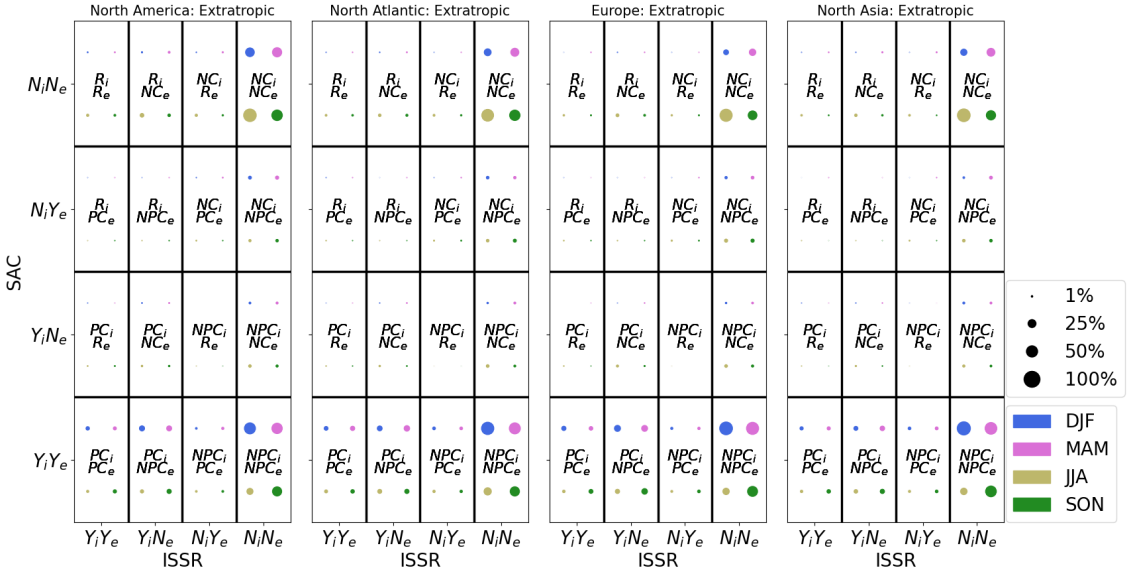

Figure 9.3: Contrail formation potential contingency table in the extratropic regions per season for a pressure level of 250 hPa, η = 30%. The percentage refers to the percentage of measurements for a specific region and season that are located within each box

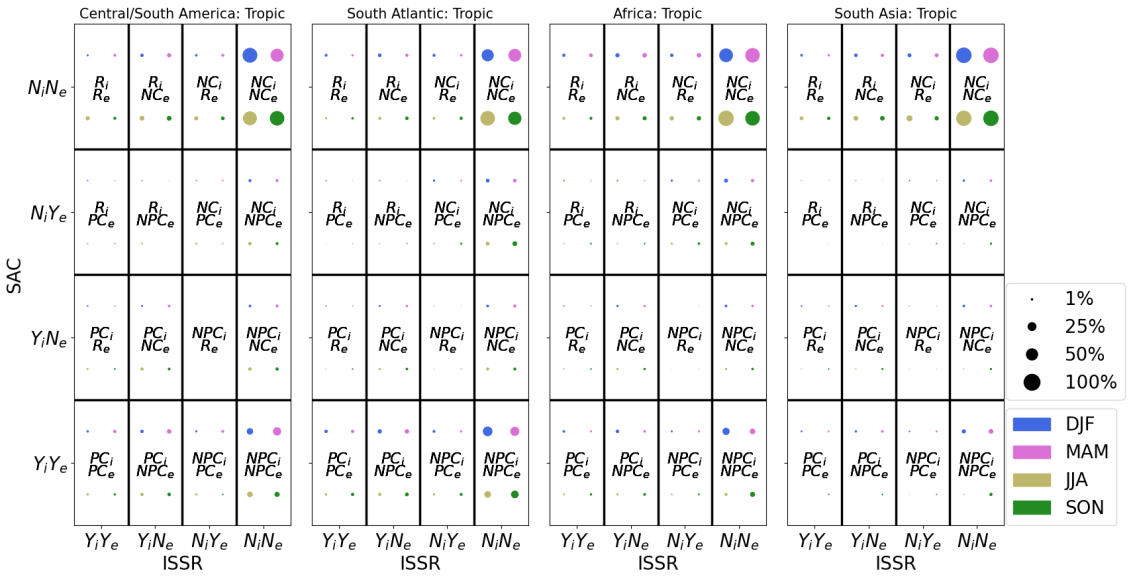

Figure 9.4: Contrail formation potential contingency table in the tropic regions per season for a pressure level of 225 hPa, η = 30%

9.2. Contrail Formation Potential in ERA5 and IAGOS from a Regional, Yearly and Pressure Level Perspective

The contrail formation potential using IAGOS and ERA5 is explored from a yearly, regional and pressure level in this section. Again, given the dependence of the contrail formation potential on the Schmidt-Appleman criterion, an engine efficiency of 30% is specified. It is already known that the occurrence of ice supersaturated regions does not display a yearly trend, and neither does the percentage of measurements meeting the Schmidt-Appleman criterion. It was seen that the Schmidt-Appleman criterion heavily follows the yearly trend of temperature.

The yearly variation of the contrail formation potential per pressure level for the extratropic regions is displayed Figure 9.5. At a pressure level of 300 hPa, reservoir conditions are a yearly occurrence, with the percentage of measurements showing this phenomenon remaining relatively consistent every year. However, ERA5 is always underestimating their occurrence. At pressure level 250 hPa, the percentage of points with reservoir conditions has reduced dramatically and as the altitude increases, only three contrail formation potential regions can be identified: no contrail, no persistent contrail and persistent contrail. It is also interesting that there is not a large variation in the yearly occurrence of PC conditions in IAGOS and ERA5. In some years, such as 2015 and 2017, there is a slightly increased number of measurements showing PC regions in IAGOS and ERA5. This corresponds to years with a high ISSR fraction in almost all seasons (see Figure 7.4). NC and NPC show more yearly variation compared to PC and R conditions, but ERA5 and IAGOS show similar yearly estimates of NC, except in the years 2020 to 2022. Here, IAGOS begins to show higher percentages of NC compared to ERA5. This is also the same years where an increasing deviation in temperature between IAGOS and ERA5 was observed in Section 5.4, with IAGOS becoming warmer. This means fewer points will meet the SAC in IAGOS, leading to no contrail conditions. At the same time, this causes a reduction in the number of points classified as NPC, but also PC, in IAGOS, meaning that if ISSRs were to be encountered, the chances of forming a persistent contrail would decrease. Hence, it seems that the temperature is the driving factor for yearly variations of contrail formation conditions, particularly no contrail and no persistent contrail.

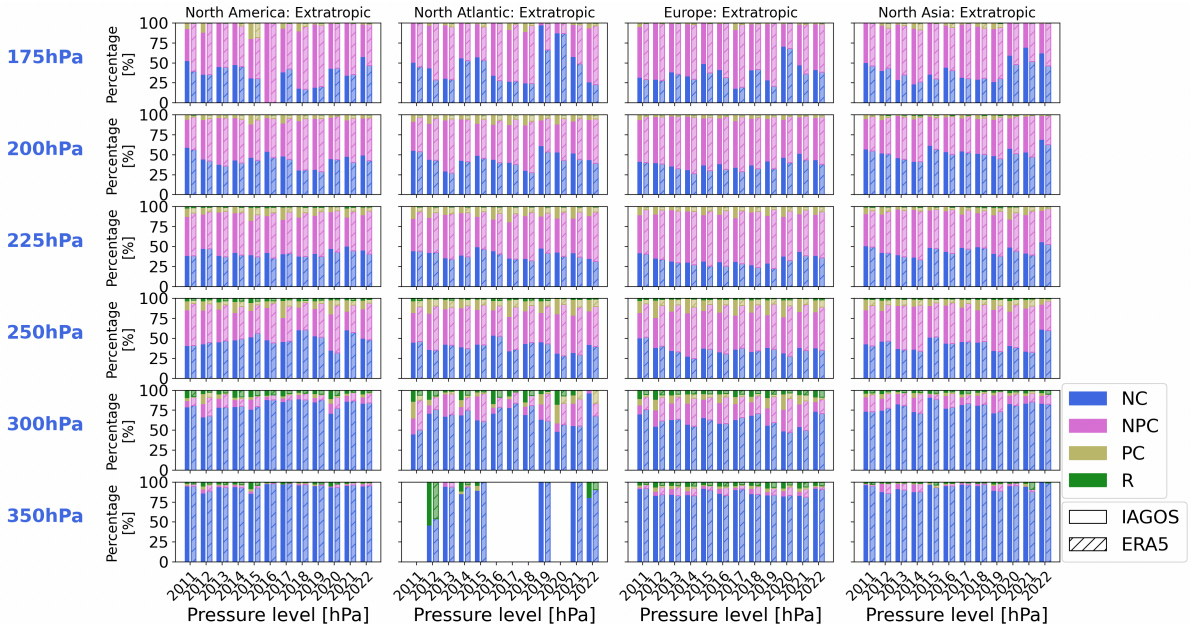

Figure 9.5: Contrail formation potential in the extratropic regions per year and pressure altitude, η = 30%

Figure 9.6 shows the yearly variation of the contrail formation potential conditions per pressure level for the tropic regions. Pressure levels 350 and 300 hPa show only no contrail conditions due to higher temperatures, which are too high for contrail formation. Interestingly, at pressure level 250, some years show no persistent contrail conditions, but all years show reservoir conditions. Yearly occurrence of reservoir conditions remains equal between IAGOS and ERA5 in Africa and South Asia, with larger

deviations noticeable in Central/South America and the South Atlantic. Looking at the yearly variation of the ISSR fraction in Figure 7.5, far greater changes are observed in Central/South America and the South Atlantic. Therefore, this is probably the cause of the larger yearly variability in the reservoir conditions. It is also interesting that some years at this pressure level show far higher NPC conditions than other years, especially in the South Atlantic and Africa. In Figure 5.11, it can be seen that the yearly mean temperature of these two years is slightly lower than the other two tropic regions, providing more suitable contrail formation regions. Lastly, the tropics also show high yearly variability of NC and NPC conditions, with a larger percentage of measurements showcasing NPC conditions in ERA5 than IAGOS. This is most likely resulting from colder temperatures in ERA5 compared to IAGOS.

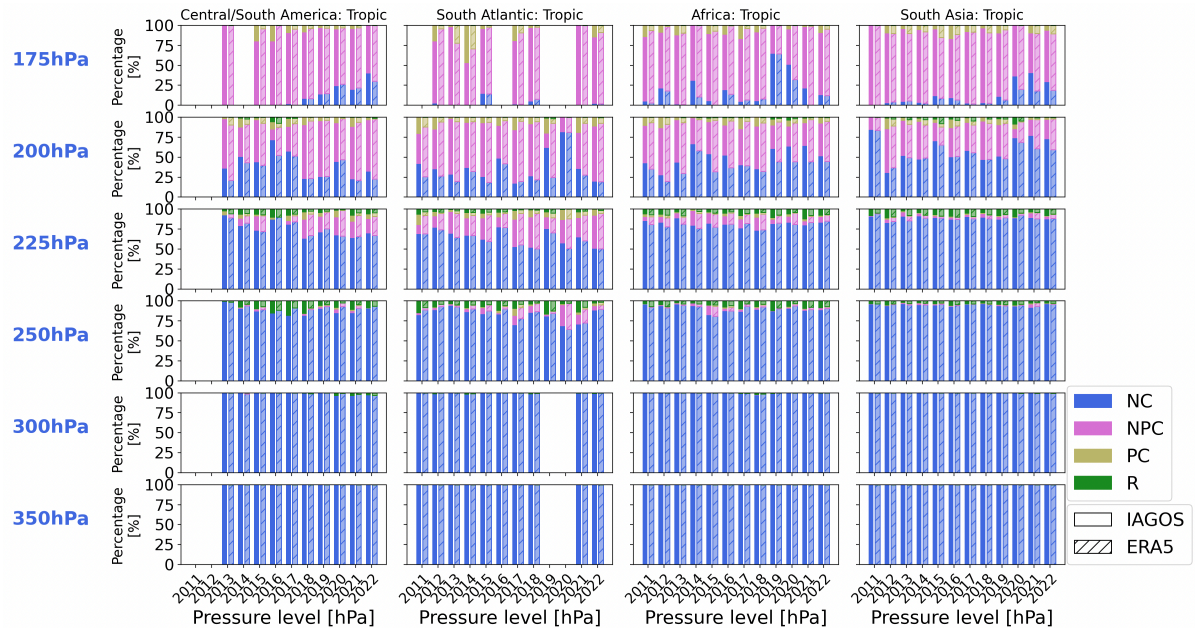

Figure 9.6: Contrail formation potential in the tropic regions per year and pressure altitude, η = 30%

In conclusion, this section analysed the yearly variability of the contrail formation potential, considering pressure levels and regions. Low yearly variability was observed in the reservoir and persistent contrail conditions. Deviations are noticeable if there are large changes in the occurrence of ice supersaturated regions. No contrail and no persistent contrail conditions show far higher yearly variability and can be attributed to temperature as this highly affects whether the Schmidt-Appleman criterion is met or not and, thus, if the ambient conditions are suitable for contrail formation.

9.3. Location and Occurrences of Contrail Formation Potential

The contrail formation potential has been analysed for the eight different regions defined. However, the exact location of the different conditions and the percentage difference between IAGOS and ERA5 have not been analysed. Thus, this will be the focus of this section.

Figure 9.7 displays the percentage difference between IAGOS and ERA5 for the four contrail formation potential conditions: no contrail, no persistent contrail, persistent contrail and reservoir. A positive percentage difference means that IAGOS measures a higher occurrence of the condition in comparison to ERA5, whereas a negative percentage difference means ERA5 measures a higher occurrence. It is interesting to notice that the no contrail and no persistent contrail figures are similar to that of the Schmidt-Appleman criterion in Figure 8.9a, and the persistent contrail and reservoir conditions resemble Figure 7.6. This shows the large influence of temperature on the no contrail and no persistent contrail conditions, and the influence of ice supersaturated regions on PC and R conditions, as has also previously been discussed.

Examining Figure 9.7a in further detail, it can be seen that most points show a percentage difference close to 0%. This is the result of the good agreement in temperature between IAGOS and ERA5, which allows for high accuracy in the flagging of the threshold for homogeneous freezing and critical

temperature for contrail formation.

Comparing Figure 8.9a and Figure 9.7b more closely, it can be seen that there is a higher percentage of ERA5 estimating NPC compared to IAGOS, than for the SAC. While the NPC is largely governed by temperature biases, if these points are found in an ISSR, they are flagged as persistent contrail regions. Thus, due to ERA5's difficulties in detecting ISSRs, more points are flagged as NPC compared to PC. However, in South Asia, IAGOS shows a higher occurrence of NPC in comparison to ERA5. This is attributed to ERA5's overestimation of ISSRs due to a moist bias in relative humidity over ice in this region, which is very prominent in season JJA.

Figure 9.7c displays a large inability to form persistent contrails south of the equator, except in South Asia. It is not due to no ice supersaturated regions, as can be observed with the reservoir condition in Figure 9.7d. Rather, it is due to the Schmidt-Appleman criterion rarely being satisfied in this region, as can be seen in Figure 8.10. Hence, persistent contrail formation is largely possible North of the equator and in South Asia, but is mainly underestimated by ERA5. Reservoir conditions also show lower occurrence in ERA5, though not in South Asia. Lastly, it is interesting to note that while China shows PC conditions, reservoir conditions are rare. This means it is common for aircraft to fly in conditions ideal for contrail formation above China.

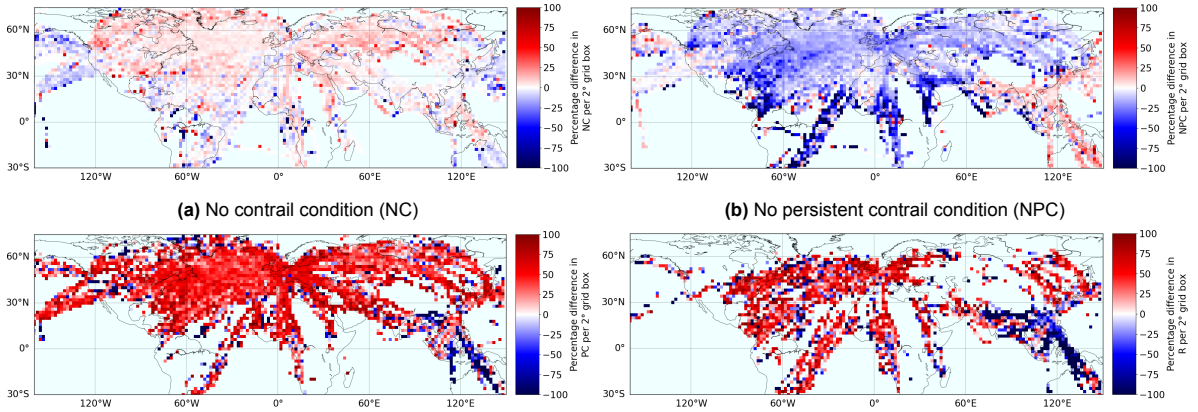

(a) No contrail condition (NC)

(b) No persistent contrail condition (NPC)

(c) Persistent contrail condition (PC)

(d) Reservoir condition (R)

Figure 9.7: Percentage difference in contrail formation potential between IAGOS and ERA5 per 2°grid box, considering η = 30%

9.4. Contrail Formation Potential Conclusion

This chapter focused on analysing the contrail formation potential using the IAGOS in-situ measurements and the ERA5 reanalysis model from a yearly, regional, seasonal and pressure level perspective. The contrail formation potential considered four conditions (NC, NPC, PC, R), which are a function of the Schmidt-Appleman criterion and the occurrence of ice supersaturated regions.

Good agreement in no contrails was found at all pressure levels, in all seasons and regions and mostly for all years. This is due to a good agreement in temperature. However, due to increasing temperature deviations from 2020 to 2022, agreement in the no contrail condition worsened. However, the good agreeement in temperature also led to relatively good accuracy in finding NPC conditions in ERA5. However, there were false alarms of NPC regions in ERA5 due to not being able to detect a large percentage of ISSRs. On the other hand, there was low accuracy in detecting persistent contrail and reservoir conditions in ERA5 due to the issues in the simulation of ISSRs, leading to points being classified as NPC or NC instead. Reservoir and persistent contrail conditions had an average hit rate between 20 and 40%. False alarms of PC and R conditions were also possible due to a moist bias in ERA5's relative humidity over ice in certain regions. Yet, this was generally below 10%.

Thus, using ERA5 to estimate the climate impact of past flights would lead to an underestimation of the impact of contrails. Meanwhile, using a numerical weather prediction similar to or based on ERA5 for flight re-routing to avoid contrails would most likely lead to unsuccessfully avoiding at least 30 to 50% of persistent contrails or reservoir regions and not fulfilling the goal of reducing the climate impact of the flight. However, in regions with a moist bias, such as South Asia, PC or R regions might unnecessarily be avoided, leading to a potential increase in fuel and other emission types.

10. Recommendations for Contrail Mitigation

This study has focused on validating ice supersaturated regions in the ERA5 reanalysis using the IAGOS in-situ measurements. It was found that ERA5 did not identify a large majority of ice supersaturated regions (ISSRs), mainly caused by errors in the simulation of relative humidity over ice. False detection of ISSRs was also possible due to inaccurate modelling in the relative humidity over ice and temperature biases in the reanalysis model. These issues further led to misclassification of contrail formation potential regions, particularly persistent contrail and reservoir regions. Based on these findings, a set of recommendations to improve contrail mitigation in the future is provided. These are as follows:

1. **Resolve ERA5 cold bias in temperature at lower altitudes:** The cold bias in ERA5 can lead to false identification of ice supersaturated regions around the threshold of homogeneous freezing when IAGOS does not measure a temperature below the threshold. However, it only accounts for 1% or less of falsely identified ISSRs. Moreover, the cold bias means that ERA5 finds more points meeting the Schmidt-Appleman criterion than IAGOS, falsely identifying areas that allow for contrail formation. When coupled with being in a location where ERA5 shows a moist bias in the relative humidity over ice, it can result in a wrongly detected persistent contrail region. This could lead to unnecessarily avoiding the region when using a numerical weather prediction (NWP) model similar to ERA5 for contrail mitigation. For example, if this behaviour stems from the ECMWF-IFS, using the operational forecasts with the IFS could result in such behaviour. This could cause an increase in the fuel used and other emissions, such as CO_2, leading to an increase in the climate impact of the flight.
2. **Resolve ERA5 dry and moist bias in relative humidity over ice:** In Chapter 6, it was seen that ERA5 mainly experienced a dry bias. However, a moist bias occurred in specific regions, such as South Asia, over the South Atlantic Ocean, and close to Alaska. The dry bias causes a large percentage of ice supersaturated regions to remain undetected. It will thus not classify a persistent contrail region if the Schmidt-Appleman criterion is also met. If using a numerical weather prediction (NWP) model similar to ERA5 for contrail mitigation, the dry bias could lead to not achieving the goal of decreasing the climate impact of the flight, as the ice supersaturated region would not be avoided. Contrarily, the moist bias can falsely identify ISSRs and, hence, also persistent contrail or reservoir regions. It is already known that some biases arise from the IFS, as discussed in Section 2.3; C. Dyroff et al. [14] showed a lower stratosphere moist bias in the ECMWF IFS and G. Rädel et al. [56] found that the ECMWF IFS 1 day forecast had a large peak at a value of 1 for relative humidity over ice, followed by a large fall-off. Thus, ERA5's moist and dry bias could stem from the IFS. This means if operational forecasts are based on the ECMWF-IFS for contrail mitigation, the moist bias would lead to unnecessarily avoiding an ISSR, which may have the opposite effect of increasing the climate impact of the flight by increasing fuel used and other emission types. Therefore, it is important to resolve why these biases occur so that they can be corrected in future cycles of the IFS and other NWP models.
3. **Remove saturation adjustment in numerical weather prediction models:** The saturation adjustment is present in several NWP models, including ERA5. In ERA5, the behaviour stems from modelling in the IFS. The saturation adjustment is responsible for the second mode of relative humidity over ice, centred at 1. In contrast, in IAGOS, it is centred at a higher value of relative humidity over ice. It is also most likely what does not allow for high relative humidity values over ice when above ice supersaturation. Overall, it causes a lack of ice supersaturation, leading to ERA5 not detecting a large percentage of ISSRs that are found with IAGOS. Hence, removing the saturation adjustment and incorporating a modelling scheme for relative humidity over ice above ice supersaturation is recommended to ensure proper detection of ice supersaturated regions.

4. **Increase measurements for number of ice particles in the extratropic regions:** As mentioned by S. Sanogo et al., the majority of data points in which the number of ice particles are measured, are collected in the tropic regions, with far fewer available samples for the extratropic regions [60]. Increasing such measurements in the extratropics will give a better idea of how this variable, and thus cirrus clouds, can affect relative humidity over ice. It may also help improve cloud representation in NWP models. This is necessary for better estimations of relative humidity over ice under cloudy conditions, where the saturation adjustment is applied.
5. **(Temporarily) Improve identification of ice supersaturated regions in ERA5 by changing the value of relative humidity over ice for the definition of ice supersaturation:** In Section 7.4, changing the definition of ice supersaturation in ERA5 was explored to attempt to improve the identification of ice supersaturated regions. Due to inconsistent deviations from a regional, seasonal, and pressure level perspective, there was not one definition that provided a great improvement for all conditions. However, it was found that a value between 0.85 and 1.05 should be used. It is recommended to optimise for the perfect value for the different conditions. This can act as a temporary measure if the biases in the relative humidity over ice are going to be resolved.
6. **Increase number of flights in IAGOS campaign:** Throughout this study, there have been discussions on the influence of the number of samples on some of the conclusions drawn, particularly from a pressure level perspective and a regional perspective. More specifically, it was seen that pressure levels 350 and 175 hPa either often lacked samples or had very few samples, leading to uncertainties in the observations made. Furthermore, some areas had far fewer measurements than others. For example, more data points were collected across the North Atlantic corridor than in Africa and Central/South America, which may skew the conclusions drawn. Therefore, it is recommended to increase the number of flights in the IAGOS campaign, particularly to increase the number of measurements on some of the pressure levels, but also regional wise. Currently, IAGOS only has a fleet of 10 aircraft [29]; in total, there are more than 24000 aircraft in service [4]. Hence, there are plenty of possibilities for IAGOS to expand its fleet. Moreover, looking at the air traffic flow in 2019 in Figure 10.1, it can be seen that there are several routes over the South Atlantic Ocean, as well as within Africa and South America. It is not as dense as within Europe or the North Atlantic corridor, but there are still possibilities for more routes to be covered by IAGOS. Moreover, this map is slightly outdated; since 2019, 7,250 new routes have opened [4]. Moreover, by 2027, the Revenue Passenger Kilometres is expected to increase by 2.5% between Europe and South America and also by 2.8% between Europe and Africa compared to 2019 [3]. Assuming the same aircraft capacities as today, this could also increase the demand for more aircraft, allowing for a more dense network of flights. Hence, IAGOS can build a larger fleet to collect more measurements.

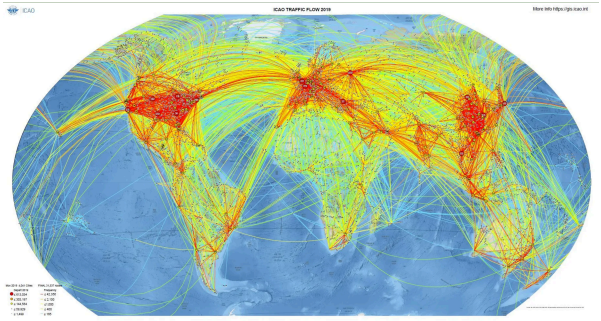

Figure 10.1: ICAO air traffic map in 2019 [32]

7. **Ensure consistency in the location of measurements in IAGOS:** In Section 6.5, changes in the statistics of relative humidity over ice from a yearly perspective were observed due to changes in the location of measurements. This caused ERA5 to have more of a moist bias in some years than others. Thus, to properly identify potential yearly biases per region, there needs to be consistency in the location of measurements in IAGOS.

11. Conclusion

In this study, the detection of ice supersaturated regions (ISSRs) in the ERA5 reanalysis was validated using the IAGOS in-situ measurements in an attempt to better understand how accurate numerical weather prediction (NWP) models are in finding the occurrence of this phenomenon. Knowledge of this is important for contrail mitigation, which can aid in reducing the climate impact of flights through re-routing strategies. Previous studies have validated ERA5 reanalysis and its predecessor, ERA-interim. However, the regional focus was on the North Atlantic corridor or the mid-latitudes, along with comparisons at different pressure levels. No in-depth validation from a seasonal or yearly perspective has been performed. Hence, this study expands on previous analysis and validates the occurrence of ISSRs in ERA5 from a pressure level, seasonal, yearly and regional perspective, including the tropics and mid-latitudes.

The study has been divided into six main parts. First, an in-depth analysis of temperature deviations between IAGOS and ERA5 was performed. This found good agreement in temperature, but a slightly cold bias in ERA5. The cold bias could slightly affect the selected points for ice supersaturation due to its influence on the threshold of homogeneous freezing. Furthermore, temperatures were better simulated by ERA5 in the tropics due to fewer seasonal variations. Increasing deviations in temperature between IAGOS and ERA5 were also found between the years 2020 and 2022 but were most likely the result of decreased sampling with IAGOS due to COVID-19.

The simulation of relative humidity over ice in ERA5 was then validated using the IAGOS in-situ measurements. Below ice supersaturation, good agreement in this variable was found. However, ERA5 struggled to simulate values above 1, mainly showing a dry bias. This behaviour is due to the saturation adjustment that is present in many numerical weather prediction models. However, certain regions showed a moist bias, including South Asia, close to Alaska and over the South Atlantic Ocean. A proposed hypothesis for this behaviour was inconsistencies in the modelling of atmospheric ice content in ERA5. Moving on, pressure level variations between IAGOS and ERA5 were present and were related to the location of the tropopause; above the tropopause, fewer variations were found due to lower availability of water vapour, leading to lower values of relative humidity over ice. In the upper troposphere, moving towards the tropopause, deviations between ERA5 and IAGOS increased as the relative humidity over ice increased, resulting from decreasing temperatures. This also affected the seasonal behaviour of relative humidity over ice. Lastly, no clear yearly variations of the relative humidity over ice were observed. However, inconsistencies in the yearly location of IAGOS measurements affected the interpretation of some regional observations.

Using the conclusions of temperature and relative humidity over ice comparisons, the occurrence of ice supersaturated regions was examined with both datasets. ERA5 lacks accuracy in simulating ice supersaturation regions and showed a general underestimation of ISSR occurrence, with 25 to 50% of ISSRs not being detected and only 20 to 40% being accurately estimated. In the regions where the reanalysis model showed a moist bias, the ISSR fraction was largely overestimated. Overall, the occurrence of ISSR showed similar behaviour to the relative humidity over ice, including seasonal, yearly, regional and pressure level variations. ERA5's cold bias had little effect on the detection of ISSRs at lower altitudes. Attempts to improve ERA5's detection of ISSRs were also done by changing the definition of the relative humidity over ice for ice supersaturation. It was concluded that the exact value needs to be tailored for the season, region and pressure level, and possibly the year; yearly uncertainties need to be examined more closely due to inconsistencies in the location of yearly measurements.

Next, the Schmidt-Appleman criterion (SAC) was examined as this determined whether the ambient conditions allow for contrail formation. The SAC depends on several variables, such as relative humidity with respect to liquid, pressure level, temperature and engine efficiency. The relative humidity with respect to liquid was calculated using the relative humidity over ice for ERA5. Still, its impact on the SAC was low due to the steep nature of the SAC threshold curve. However, it led to some inaccuracies in determining whether the SAC was met. The main influence on the SAC was temperature, with ERA5's cold temperature leading to 5 to 10% of measurements wrongly being misidentified as meeting the SAC. However, improving engine efficiencies can decrease this value.

Thereafter, the influence of ISSRs and SAC on the contrail formation potential was examined, which considers four conditions: no contrails (NC), no persistent contrails (NPC) and persistent contrails (PC). Due to good agreement in temperature between IAGOS and ERA5, no contrails were well estimated by the reanalysis model. NPC was also well estimated by ERA5, but some NPC conditions were falsely identified by ERA5 due to not accurately determining ISSRs. Larger deviations in persistent contrail and reservoir conditions were found between IAGOS and ERA5, with ERA5 underestimating their occurrence. Some PC and R conditions were misclassified as NPC or NC due to undetected ISSRs in ERA5. In the case of a moist bias in ERA5, false identification of PC and R conditions also occurred, but its occurrence was not as frequent as false NPC or NC conditions.

Hence, if wanting to deploy an NWP model similar to or based on ERA5 for flight re-routing to mitigate contrails, improvements are necessary. Otherwise, persistent contrail or reservoir regions might not successfully be avoided or unnecessarily avoided in particular regions, such as South Asia. Aspects to consider for improvement are resolving temperature and relative humidity over ice biases in ERA5 and removing the saturation adjustment. Meanwhile, temporarily improving the detection of ISSRs can be done by changing the value of the relative humidity over ice for ice supersaturation.

All in all, numerical weather prediction models, such as the ERA5 reanalysis, require large improvement in the prediction of ice supersaturated regions. Problems are mainly tied to issues in the modelling of relative humidity over ice. These issues should be resolved before the implementation of flight re-routing strategies for contrail mitigation. Otherwise, the benefit of such strategies for reducing the climate impact of flights is too uncertain or could lead to increases in the climate impact of flights, which defeats the purpose of this solution in the first place.

Recommendations for Future Work

These are recommendations for how this study can be improved or extended.

- **Differentiate between cloudy and clear sky conditions:** The largest issues with the simulation of relative humidity over ice in ERA5 were found in regions with a large number of ice particles in IAGOS, which shows the occurrence of cloudy conditions. The saturation adjustment is used when clouds form within a grid cell in ERA5 and thus lack ice supersaturation in cloudy conditions [83, 20]. Hence, this study can be extended to consider the effect of cloudy and clear sky conditions on relative humidity over ice in ERA5.
- **Further investigate the influence of atmospheric ice content on relative humidity over ice in ERA5:** It was discussed in Section 6.4 that the reason for the moist bias in ERA5 could be due to inconsistencies in the modelling of the atmospheric ice content in ERA5. However, no studies seem to have looked at the influence of the atmospheric ice on the relative humidity over ice within this reanalysis model. Hence, it is highly recommended to investigate this further as it might shed light on possible model improvements.
- **Directly compare ice content in IAGOS and ERA5:** To determine if there are inconsistencies in the modelling of atmospheric ice content in ERA5, it is necessary to make a direct comparison with in-situ measurements, such as IAGOS. However, as mentioned in Section 6.4, IAGOS and ERA5 do not provide a direct comparison with variables that can be directly retrieved from either dataset. Therefore, it is necessary to find a way to compare this type of parameter between the NWP model and the in-situ measurements.
- **Further division of regions:** Within the regions defined, some differences in behaviour were observed, such as the region in the Pacific Ocean close to Alaska or over the South Atlantic Ocean. These may have caused an impact on the overall observations within a region. This was difficult to have foreseen due to using a larger area compared to previous studies. Hence, for future work, it should be considered to further split these regions, though it should be ensured that enough measurements are available.
- **Divide pressure levels based on distance to tropopause:** The tropopause height has a large impact on the behaviour of temperature and relative humidity over ice with altitude. This study did not consider pressure levels based on the distance to the tropopause, leading to upper tropospheric and lower stratospheric influences on certain pressure levels in the extratropics. To better examine differences above and below the tropopause, it is recommended to consider pressure levels based on distance to the tropopause.

References

[1] Delft High Performance Computing Centre (DHPC). *DelftBlue Supercomputer (Phase 2)*. https://www.tudelft.nl/dhpc/ark:/44463/DelftBluePhase2. 2024.

[2] A. Agarwal et al. “Reanalysis-driven simulations may overestimate persistent contrail formation by 100%–250%”. In: *Environmental Research Letters* 17.1 (2022). DOI: 10.1088/1748-9326/ac38d9.

[3] Airbus. *Airbus Commercial Aircraft GMF 2024-2043*. 2024. URL: https://www.airbus.com/en/products-services/commercial-aircraft/market/global-market-forecast (visited on 07/30/2024).

[4] Airbus. *Global Market Forecast 2024*. 2024. URL: https://www.airbus.com/sites/g/files/jlcbta136/files/2024-07/GMF%202024-2043%20Presentation_4DTS.pdf (visited on 07/30/2024).

[5] Airbus. *The family grows (1988-1991)*. URL: https://www.airbus.com/en/who-we-are/our-history/commercial-aircraft-history/the-family-grows-1988-1991 (visited on 03/31/2024).

[6] F. Berkes et al. “In situ temperature measurements in the upper troposphere and lowermost stratosphere from 2 decades of IAGOS long-term routine observation”. In: *Atmospheric Chemistry and Physics* 17.20 (2017), pp. 12495–12508. DOI: 10.5194/acp-17-12495-2017.

[7] J. Bland et al. “Characterising Extratropical Near-Tropopause Analysis Humidity Biases and Their Radiative Effects on Temperature Forecasts”. In: *Quarterly Journal of the Royal Meteorological Society* 147.741 (2021). DOI: https://doi.org/10.1002/qj.4150.

[8] Center for Science and Technology Policy Research. *Saturation vapor pressure formulations*. 2015. URL: https://sciencepolicy.colorado.edu/~voemel/vp.html (visited on 06/30/2024).

[9] Climate Data Guide. *ERA5 atmospheric reanalysis*. 2023. URL: https://climatedataguide.ucar.edu/climate-data/era5-atmospheric-reanalysis (visited on 07/30/2024).

[10] Jennifer M. Comstock, Thomas P. Ackerman, and David D. Turner. “Evidence of high ice supersaturation in cirrus clouds using ARM Raman lidar measurements”. In: *Geophysical Research Letters* 31.11 (2004). DOI: https://doi.org/10.1029/2004GL019705.

[11] Copernicus Climate Change Service Climate Data Store. *ERA5 hourly data on pressure levels from 1940 to present*. 2018. URL: https://cds.climate.copernicus.eu/cdsapp#!/dataset/10.24381/cds.bd0915c6?tab=overview (visited on 03/08/2024).

[12] G. Dekoutsidis et al. “Characteristics of supersaturation in midlatitude cirrus clouds and their adjacent cloud-free air”. In: *Atmospheric Chemistry and Physics* 23.5 (2023), pp. 3103–3117. DOI: 10.5194/acp-23-3103-2023.

[13] T. Dou et al. “Estimation of the Atmospheric Ice Content Mass, Spatial Distribution, and Long-Term Changes Based on the ERA5 Reanalysis”. In: *Geophysical Research Letters* 47.15 (2020). DOI: https://doi.org/10.1029/2020GL088186.

[14] C. Dyroff et al. “Comparison of ECMWF analysis and forecast humidity data with CARIBIC upper troposphere and lower stratosphere observations”. In: *Quarterly Journal of the Royal Meteorological Society* 141.688 (2014). DOI: https://doi.org/10.1002/qj.2400.

[15] ECMWF. *ERA5 CDS: Data corruption*. 2023. URL: https://confluence.ecmwf.int/display/CKB/ERA5+CDS%3A+Data+corruption (visited on 06/30/2024).

[16] ECMWF. *Modelling and Prediction*. URL: https://www.ecmwf.int/en/research/modelling-and-prediction (visited on 03/31/2024).

[17] D. G. Feist et al. “Middle atmosphere water vapour and dynamical features in aircraft measurements and ECMWF analyses”. In: *Atmospheric Chemistry and Physics* 7.20 (2007), pp. 5291–5307. DOI: 10.5194/acp-7-5291-2007.

[18] R. Ferrare et al. “Lidar Measurements of Relative Humidity and Ice Supersaturation in the Upper Troposphere”. In: *Advances in Laser Remote Sensing*. Ecole Polytechnique, Sept. 2001, pp. 317–320.

[19] J. Fontes. “Chapter 12 - Humidity Sensors”. In: *Sensor Technology Handbook*. Elsevier, 2005.

[20] K. Gierens, S. Matthes, and S. Rohs. “How Well Can Persistent Contrails Be Predicted?” In: *Aerosapce* 7.12 (2020). DOI: https://doi.org/10.3390/aerospace7120169.

[21] K. Gierens, P. Spichtinger, and U. Schumann. “Ice Supersaturation”. In: *Atmospheric Physics: Background - Methods - Trends*. Springer, 2012.

[22] K. Gierens et al. “A distribution law for relative humidity in the upper troposphere and lower stratosphere derived from three years of MOZAIC measurements”. In: *Annales Geophysicae* 17.9 (1999), pp. 1218–1226. DOI: 10.1007/s00585-999-1218-7.

[23] K. Gierens et al. “Ice-Supersaturated Regions and Subvisible Cirrus in the Northern Midlatitude Upper Troposphere”. In: *Journal of Geophysical Research-Atmospheres* 105.18 (2000). DOI: 10.1029/2000JD900341.

[24] K. Gierens et al. “On ice supersaturation over the Arctic”. In: *Meteorologische Zeitschrift* 29.2 (2020). DOI: 10.1127/metz/2020/1012.

[25] K. Gierens et al. “The Effect of Ice Supersaturation and Thin Cirrus on Lapse Rates in the Upper Troposphere”. In: *Atmospheric Chemistry and Physics* 22.11 (2022). DOI: https://doi.org/10.5194/acp-22-7699-2022.

[26] H. Hersbach et al. “The ERA5 global reanalysis”. In: *Quarterly Journal of the Royal Meteorological Society* 146.730 (2020). DOI: https://doi.org/10.1002/qj.3803.

[27] L. Hoffmann and R. Spang. “An assessment of tropopause characteristics of the ERA5 and ERA-Interim meteorological reanalyses”. In: *Atmospheric Chemistry and Physics* 22.6 (2022), pp. 4019–4046. DOI: 10.5194/acp-22-4019-2022.

[28] IAGOS. *HUMIDITY SENSOR (ICH, PART OF PACKAGE1)*. URL: https://www.iagos.org/iagos-core-instruments/h2o/ (visited on 08/30/2024).

[29] IAGOS. *IAGOS FLEET*. URL: https://www.iagos.org/iagos-fleet/ (visited on 03/31/2024).

[30] IAGOS. *IAGOS-CORE*. URL: https://www.iagos.org/iagos-core-instruments/ (visited on 08/30/2024).

[31] IAGOS Data Portal. *Observed and Modelled Variables*. 2024. URL: https://iagos.aeris-data.fr/parameters/ (visited on 03/27/2024).

[32] ICAO. *Traffic Flow Global Data (Shape File)*. URL: https://store.icao.int/en/traffic-flow-global-data-shape-file (visited on 07/30/2024).

[33] B. Ingleby, B. Candy, et al. “The Impact of COVID-19 on Weather Forecasts: A Balanced View”. In: *Geophysical Research Letters* 48.4 (2020). DOI: https://doi.org/10.1029/2020GL090699.

[34] IPCC. “7.4.1.2. Propulsive and Overall Efficiency”. In: *Aviation and the Global Atmosphere* (1999).

[35] SevenStorm JUHASZIMRUS. URL: https://www.pexels.com/photo/airplane-contrails-2091318/.

[36] A. Kunz et al. “Comparison of Fast In situ Stratospheric Hygrometer (FISH) measurements of water vapor in the upper troposphere and lower stratosphere (UTLS) with ECMWF (re)analysis data”. In: *Atmospheric Chemistry and Physics* 14.19 (2014), pp. 10803–10822. DOI: 10.5194/acp-14-10803-2014.

[37] N. Lamquin, C.J. Stubenrauch, and J. Pelon. “Upper Tropospheric Humidity and Cirrus Geometrical and Optical Thickness: Relationships Inferred from 1 Year of Collocated AIRS and CALIPSO Data”. In: *Journal of Geophysical Research* 113.D8 (2008). DOI: https://doi.org/10.1029/2008JD010012.

[38] N. Lamquin et al. “A global climatology of upper-tropospheric ice supersaturation occurrence inferred from the Atmospheric Infrared Sounder calibrated by MOZAIC”. In: *Atmospheric Chemistry and Physics* 12.1 (2012). DOI: https://doi.org/10.5194/acp-12-381-2012.

[39] N. Lamquin et al. “Evaluation of upper tropospheric humidity forecasts from ECMWF using AIRS and CALIPSO data”. In: *Atmospheric Chemistry and Physics* 9.5 (2009), pp. 1779–1793. DOI: 10.5194/acp-9-1779-2009.

[40] J. Low et al. “Ground-based contrail observations: comparisons with flight telemetry and contrail model estimates”. In: *EGUsphere [preprint]* (2024). DOI: 10.5194/egusphere-2024-1458.

[41] H. Mannstein, A. Brömser, and L. Bugliaro. “Ground-based observations for the validation of contrails and cirrus detection in satellite imagery”. In: *Atmospheric Measurement Techniques* 3.3 (2010), pp. 655–669. DOI: 10.5194/amt-3-655-2010.

[42] V.R. Meijer. “Satellite-based Analysis and Forecast Evaluation of Aviation Contrails”. PhD thesis. Massachusetts Institue of Technology, 2024.

[43] C.P. Nadeau, M. C. Urban, and J. R. Bridle. “Climates Past, Present, and Yet-to-Come Shape Climate Change Vulnerabilities”. In: *Trends in Ecology Evolution* 32.10 (2017), pp. 786–800. DOI: https://doi.org/10.1016/j.tree.2017.07.012.

[44] National Geographic. *Encyclopedic Entry - Tropics*. 2023. URL: https://education.nationalgeographic.org/resource/tropics/ (visited on 03/31/2024).

[45] P. Neis et al. “Quality assessment of MOZAIC and IAGOS capacitive hygrometers: insights from airborne field studies”. In: *Tellus B: Chemical and Physical Meteorology* 67.1 (2015). DOI: 10.3402/tellusb.v67.28320.

[46] NOAA. *Atmospheric Remote Sensing: Instruments*. URL: https://csl.noaa.gov/groups/csl3/instruments/dial/lidar.html#:~:text=A%20lidar%20system%20uses%20laser,climate%20modeling%2C%20and%20environmental%20monitoring. (visited on 05/15/2024).

[47] NOAA. *Numerical Weather Prediction*. URL: https://www.ncei.noaa.gov/products/weather-climate-models/numerical-weather-prediction (visited on 03/31/2024).

[48] NOAA. *The High-Resolution Rapid Refresh (HRRR)*. 2020. URL: https://rapidrefresh.noaa.gov/hrrr/ (visited on 08/30/2024).

[49] NOAA. *What is Lidar?* URL: https://oceanservice.noaa.gov/facts/lidar.html (visited on 05/15/2024).

[50] E. K. Oikonomou and A. O’Neill. “Evaluation of ozone and water vapor fields from the ECMWF reanalysis ERA-40 during 1991–1999 in comparison with UARS satellite and MOZAIC aircraft observations”. In: *Journal of Geophysical Research: Atmospheres* 111.D14 (2006). DOI: https://doi.org/10.1029/2004JD005341.

[51] H. Petetin et al. “Characterising tropospheric O_3 and CO around Frankfurt over the period 1994–2012 based on MOZAIC–IAGOS aircraft measurements”. In: *Atmospheric Chemistry and Physics* 16.23 (2016), pp. 15147–15163. DOI: 10.5194/acp-16-15147-2016.

[52] A. Petzold et al. “Global-scale atmosphere monitoring by in-service aircraft – current achievements and future prospects of the European Research Infrastructure IAGOS”. In: *Tellus B: Chemical and Physical Meteorology* 67.1 (2015), p. 28452. DOI: 10.3402/tellusb.v67.28452.

[53] A. Petzold et al. “Ice-Supersaturated Air Masses in the Northern Mid-Latitudes from Regular In-Situ Observations by Passenger Aircraft: Vertical Distribution, Seasonality and Tropospheric Fingerprint”. In: *Atmospheric Chemistry and Physics* 20.13 (2020). DOI: https://doi.org/10.5194/acp-20-8157-2020.

[54] A. Petzold et al. “Upper tropospheric water vapour and its interaction with cirrus clouds as seen from IAGOS long-term routine in situ observations”. In: *Faraday Discussios* 200 (2017). DOI: https://doi.org/10.1039/C7FD00006E.

[55] PST. *Humidity Academy Theory 6 – The Capacitive Sensor*. URL: https://www.processsensing.com/en-us/blog/capacitive-sensor-technology.htm (visited on 08/30/2024).

[56] G. Rädel and K.P. Shine. “Validating ECMWF forecasts for the occurrence of ice supersaturation using visual observations of persistent contrails and radiosonde measurements over England”. In: *Quarterly Journal of the Royal Meteorological Society* 136.652 (2010). DOI: https://doi.org/10.1002/qj.670.

[57] P. Reutter et al. “Ice supersaturated regions: properties and validation of ERA-Interim reanalysis with IAGOS in situ water vapour measurements”. In: *Atmospheric Chemistry and Physics* 20.2 (2020). DOI: https://doi.org/10.5194/acp-20-787-2020.

[58] E.J. Roosenbrand, J. Sun, and J.M. Hoekstra. “Examining Contrail Formation Models with Open Flight and Remote Sensing Data”. In: *SESAR Innovation Days 2022* (2022).

[59] A. Ruzmaikin, H. H. Aumann, and E. M. Manning. “Relative Humidity in the Troposphere with AIRS”. In: *Journal of the Atmospheric Sciences* 71.7 (2014), pp. 2516–2533. DOI: 10.1175/JAS-D-13-0363.1.

[60] S. Sanogo et al. “Variability in the properties of the distribution of the relative humidity with respect to ice: implications for contrail formation”. In: *Atmospheric Chemistry and Physics* 24.9 (2024), pp. 5495–5511. DOI: 10.5194/acp-24-5495-2024.

[61] U. Schumann. “Formation, Properties and Climatic Effects of Contrails”. In: *Comptes Rendus Physique* 6.4-5 (2005). DOI: doi:10.1016/j.crhy.2005.05.002.

[62] U. Schumann. “On conditions for contrail formation from aircraft exhausts”. In: *Meteorologische Zeitschrift* 5.1 (Mar. 1996), pp. 4–23. DOI: 10.1127/metz/5/1996/4.

[63] U. Schumann et al. “Air traffic and contrail changes over Europe during COVID-19: a model study”. In: *Atmospheric Chemistry and Physics* 21.10 (2021), pp. 7429–7450. DOI: 10.5194/acp-21-7429-2021.

[64] U. Schumann et al. “Contrail Study with Ground-Based Cameras”. In: *Geoscientific Model Development* 5.3 (2012). DOI: https://doi.org/10.5194/amt-6-3597-2013.

[65] T.G. Shepherd et al. *Report on Stratosphere Task Force*. eng. June 2018. DOI: 10.21957/0vkp0t1xx. URL: https://www.ecmwf.int/node/18259.

[66] Z. S. Spakovszky. *11.5 Trends in thermal and propulsive efficiency*. URL: https://web.mit.edu/16.unified/www/FALL/thermodynamics/notes/node84.html.

[67] D. Sperber and K. Gierens. “Towards a more reliable forecast of ice supersaturation: Concept of a one-moment ice cloud scheme that avoids saturation adjustment”. In: *EGUsphere* 2023 (2023), pp. 1–23. DOI: 10.5194/egusphere-2023-914.

[68] P. Spichtinger and M. Leschner. “Horizontal scales of ice-supersaturated regions”. In: *Tellus Series B-Chemical and Physical Meteorology* 68 (2016).

[69] P. Spichtinger et al. “Ice supersaturation in the tropopause region over Lindenberg, Germany”. In: *Meteorologische Zeitschrift* 12.3 (June 2003), pp. 143–156. DOI: 10.1127/0941?2948/2003/0012?0143.

[70] Jerry M. Straka. “Saturation adjustment”. In: *Cloud and Precipitation Microphysics: Principles and Parameterizations*. Cambridge University Press, 2009, pp. 78–100.

[71] SURFERTODAY. *The differences between the GFS and ECMWF weather models*. 2024. URL: https://www.surfertoday.com/surfing/the-differences-between-the-gfs-and-ecmwf-weather-models#:~:text=Numerical%20weather%20prediction%20models%20use,buoys%2C%20balloons%2C%20and%20aircraft. (visited on 03/31/2024).

[72] R. Teoh et al. “Aviation Contrail Climate Effects in the North Atlantic from 2016 to 2021”. In: *Atmospheric Chemistry and Physics* 22.16 (2022). DOI: https://doi.org/10.5194/acp-22-10919-2022.

[73] “The contribution of global aviation to anthropogenic climate forcing for 2000 to 2018”. In: *Atmospheric Environment* 244 (2021), p. 117834. DOI: https://doi.org/10.1016/j.atmosenv.2020.117834.

[74] Le Van Thien et al. “Comparison of Aura MLS Water Vapor Measurements with GFS and NAM Analyses in the Upper Troposphere–Lower Stratosphere”. In: *Journal of Atmospheric and Oceanic Technology* 27.2 (2010), pp. 274–289. DOI: 10.1175/2009JTECHA1317.1.

[75] Gregory Thompson et al. “On the fidelity of high-resolution numerical weather forecasts of contrail-favorable conditions”. In: *Atmospheric Research* 311 (2024), p. 107663. DOI: https://doi.org/10.1016/j.atmosres.2024.107663.

[76] A.M. Tompkins, K. Gierens, and G. Rädel. “Ice Supersaturation in the ECMWF integrated forecast system”. In: *Quarterly Journal of the Royal Meteorological Society* 133.622 (2007). DOI: https://doi.org/10.1002/qj.14.

[77] B. Trewin. *The climates of the Tropics, and how they are changing*. James Cook University, 2014.

[78] L. Wilhelm. “Meteorological Conditions for Strongly Warming Contrails and the Statistics of Contrail’s Instantaneous Radiative Forcing”. MA thesis. University of Hohenheim, 2022.

[79] L. Wilhelm, K. Gierens, and S. Rohs. “Meteorological Conditions That Promote Persistent Contrails”. In: *Applied Sciences* 12.9 (2022). DOI: https://doi.org/10.3390/app12094450.

[80] L. Wilhelm, K. Gierens, and S. Rohs. “Weather Variability Induced Uncertainty of Contrail Radiative Forcing”. In: *Aerospace* 8.11 (2018). DOI: https://doi.org/10.3390/aerospace8110332.

[81] W. Woiwode et al. “Technical note: Lowermost-stratosphere moist bias in ECMWF IFS model diagnosed from airborne GLORIA observations during winter–spring 2016”. In: *Atmospheric Chemistry and Physics* 20.23 (2020), pp. 15379–15387. DOI: 10.5194/acp-20-15379-2020.

[82] K. Wolf, N. Bellouin, and O. Boucher. “Long-term upper-troposphere climatology of potential contrail occurrence over the Paris area derived from radiosonde observations”. In: *Atmospheric Chemistry and Physics* 23.1 (2023). DOI: https://doi.org/10.5194/acp-23-287-2023.

[83] K. Wolf et al. “Correction of temperature and relative humidity biases in ERA5 by bivariate quantile mapping: Implications for contrail classification”. In: *EGUsphere [preprint]* (2023). DOI: 10.5194/egusphere-2023-2356.

[84] World Bank Group. *What is Climate Change?* URL: https://climateknowledgeportal.worldbank.org/overview#:~:text=Climate%5C%20change%5C%20is%5C%20the%20significant,change%5C%20from%5C%20natural%5C%20weather%5C%20variability (visited on 03/31/2024).

[85] xarray. *Interpolating data*. 2024. URL: https://docs.xarray.dev/en/stable/user-guide/interpolation.html (visited on 05/22/2024).

A. IAGOS and ERA5 Temperature

A.1. Difference Between IAGOS and ERA5 Temperature as a Function of Pressure Level, Region and Season

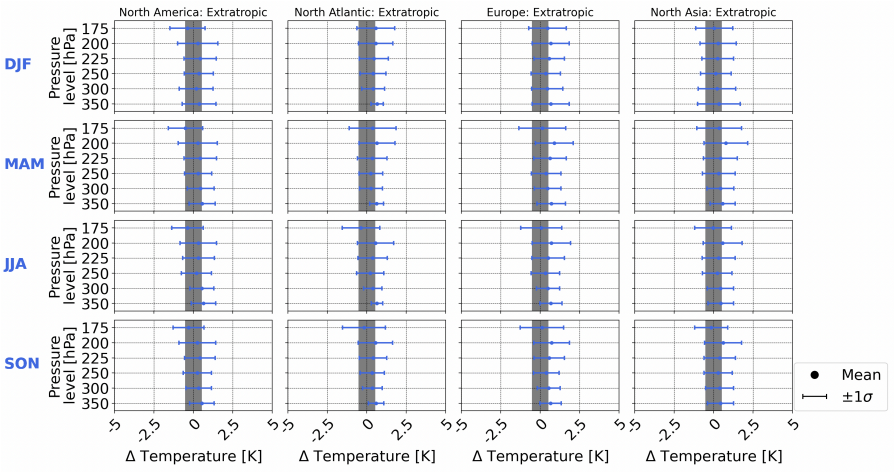

Figure A.1: Variation of difference in temperature between IAGOS and ERA5, with IAGOS as baseline, per region, pressure level and extratropic regions. Grey shaded area corresponds to uncertainty of IAGOS's temperature sensor.

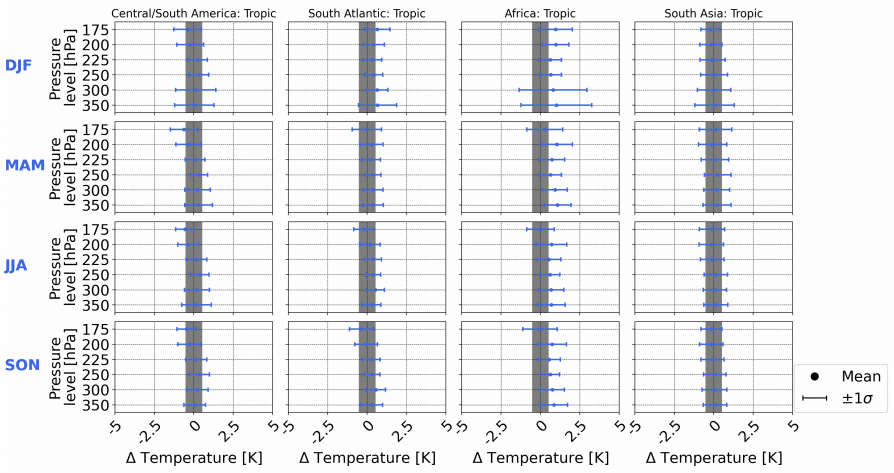

Figure A.2: Variation of difference in temperature between IAGOS and ERA5, with IAGOS as baseline, per region, pressure level and tropic regions. Grey shaded area corresponds to uncertainty of IAGOS's temperature sensor.

A.2. IAGOS and ERA5 Temperature as a Function of Pressure Level, Region and Season - Standard Deviation

Table A.1: Standard deviation of IAGOS and ERA5 temperature per season and pressure level for extratropic regions

	North America								North Atlantic							
	IAGOS				ERA5				IAGOS				ERA5			
Pressure Level	**DJF**	**MAM**	**JJA**	**SON**	**DJF**	**MAM**	**JJA**	**SON**	**DJF**	**MAM**	**JJA**	**SON**	**DJF**	**MAM**	**JJA**	**SON**
175 hPa	5.84	5.46	4.13	4.00	5.46	5.07	3.75	3.59	5.83	7.12	5.43	5.04	5.51	6.39	4.99	4.34
200 hPa	6.02	6.13	4.56	4.87	5.61	5.66	4.17	4.50	6.15	6.77	5.46	5.32	5.88	6.43	5.06	4.99
225 hPa	5.47	5.27	3.91	4.84	5.28	5.02	3.61	4.61	5.63	6.05	4.75	4.85	5.45	5.81	4.47	4.65
250 hPa	4.91	4.60	4.32	5.28	4.74	4.37	4.00	5.12	5.00	4.83	4.12	4.76	4.86	4.72	3.86	4.58
300 hPa	5.47	5.32	4.76	5.63	5.17	5.08	4.50	5.38	3.77	4.06	3.58	4.14	3.48	3.74	3.41	4.04
350 hPa	5.20	5.48	4.57	5.75	4.92	5.29	4.30	5.56	3.22	3.76	3.11	3.34	3.24	3.62	2.94	3.32

	Europe								North Asia							
	IAGOS				ERA5				IAGOS				ERA5			
Pressure Level	**DJF**	**MAM**	**JJA**	**SON**	**DJF**	**MAM**	**JJA**	**SON**	**DJF**	**MAM**	**JJA**	**SON**	**DJF**	**MAM**	**JJA**	**SON**
175 hPa	5.42	5.36	4.31	4.59	5.29	4.82	3.84	4.08	4.15	4.84	4.62	3.56	4.14	4.40	3.92	3.32
200 hPa	5.43	5.48	4.88	4.58	5.22	5.19	4.52	4.30	5.42	5.18	4.80	4.90	5.53	4.98	4.37	4.80
225 hPa	4.90	4.93	4.64	4.17	4.74	4.70	4.36	3.95	5.93	5.48	5.90	5.75	5.99	5.32	5.71	5.59
250 hPa	4.00	4.10	3.88	3.99	3.85	3.98	3.69	3.84	5.92	5.52	6.70	6.15	5.98	5.45	6.63	6.13
300 hPa	3.99	4.06	3.61	4.34	3.70	3.83	3.45	4.16	6.14	6.13	5.89	7.74	6.17	6.06	5.79	7.67
350 hPa	4.68	4.14	3.55	4.63	4.41	4.00	3.44	4.52	5.64	6.25	4.73	7.40	5.61	6.16	4.70	7.48

Table A.2: Standard deviation of IAGOS and ERA5 temperature per season and pressure level for tropic regions

	Central/South America								South Atlantic							
	IAGOS				ERA5				IAGOS				ERA5			
Pressure Level	**DJF**	**MAM**	**JJA**	**SON**	**DJF**	**MAM**	**JJA**	**SON**	**DJF**	**MAM**	**JJA**	**SON**	**DJF**	**MAM**	**JJA**	**SON**
175 hPa	4.87	3.27	2.16	2.37	4.55	2.91	1.96	2.20	4.01	1.95	2.10	1.82	3.68	1.53	2.17	1.50
200 hPa	4.51	3.94	2.95	3.02	4.26	3.48	2.60	2.68	3.52	2.82	2.21	2.36	3.32	2.53	2.10	2.12
225 hPa	3.59	3.81	2.58	2.73	3.51	3.58	2.33	2.43	3.65	3.47	2.35	2.45	3.51	3.33	2.25	2.33
250 hPa	3.91	3.60	3.11	3.24	3.78	3.47	2.92	3.05	4.36	3.96	2.88	3.24	4.22	3.83	2.81	3.15
300 hPa	4.20	4.27	3.49	3.41	3.90	4.01	3.47	3.22	3.52	4.19	3.68	3.32	3.38	4.14	3.75	3.34
350 hPa	4.13	3.88	2.45	2.68	3.73	3.60	2.08	2.43	2.54	2.84	2.62	2.74	2.31	2.67	2.63	2.59

	Africa								South Asia							
	IAGOS				ERA5				IAGOS				ERA5			
Pressure Level	**DJF**	**MAM**	**JJA**	**SON**	**DJF**	**MAM**	**JJA**	**SON**	**DJF**	**MAM**	**JJA**	**SON**	**DJF**	**MAM**	**JJA**	**SON**
175 hPa	2.34	2.27	2.17	1.63	1.89	1.99	2.07	1.39	1.84	2.19	2.26	1.80	1.79	1.91	2.04	1.73
200 hPa	2.93	2.79	2.44	2.39	2.70	2.57	2.28	2.31	2.47	2.62	2.86	2.42	2.38	2.57	2.74	2.38
225 hPa	3.22	2.91	2.42	2.56	3.03	2.72	2.33	2.47	2.49	2.82	2.60	2.39	2.44	2.76	2.46	2.37
250 hPa	4.25	3.74	2.58	3.30	4.08	3.58	2.47	3.15	3.96	4.32	3.84	3.97	3.86	4.18	3.58	3.83
300 hPa	5.07	4.29	3.52	4.19	4.44	4.08	3.39	3.98	3.64	3.92	2.91	3.44	3.55	3.92	2.85	3.38
350 hPa	3.40	2.40	2.47	2.59	2.31	2.09	2.32	2.31	3.81	3.68	2.31	3.08	3.67	3.67	2.19	3.05

A.3. IAGOS and ERA5 Temperature as a Function of Pressure Level, Region and Season - Probability Density Functions

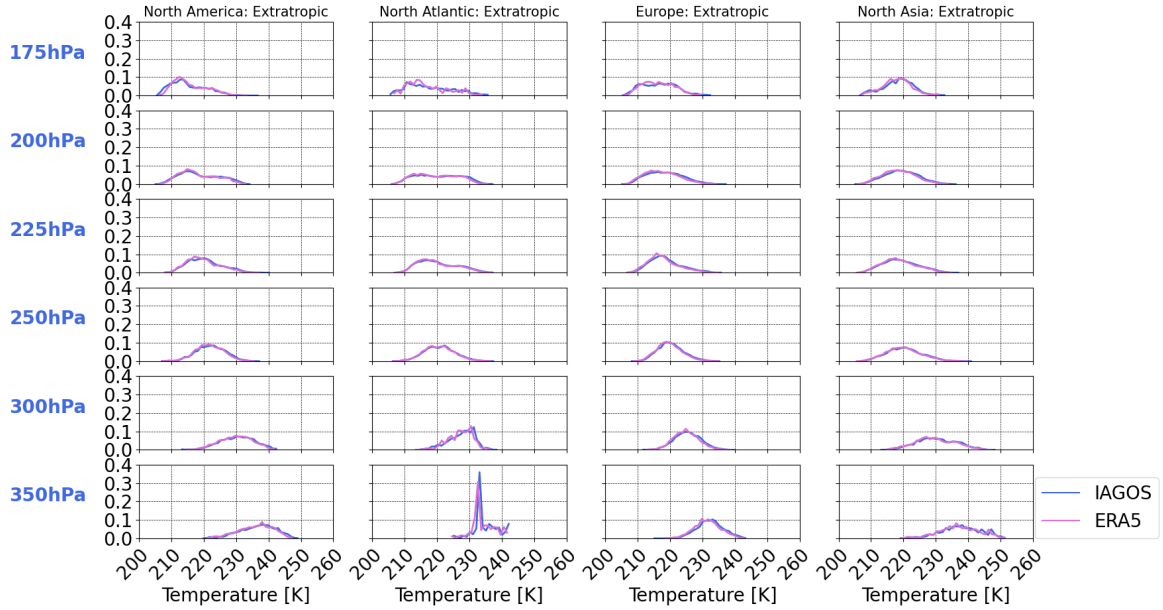

Figure A.3: Probability density function of IAGOS and ERA5 temperature per pressure level for the extratropic regions and season MAM

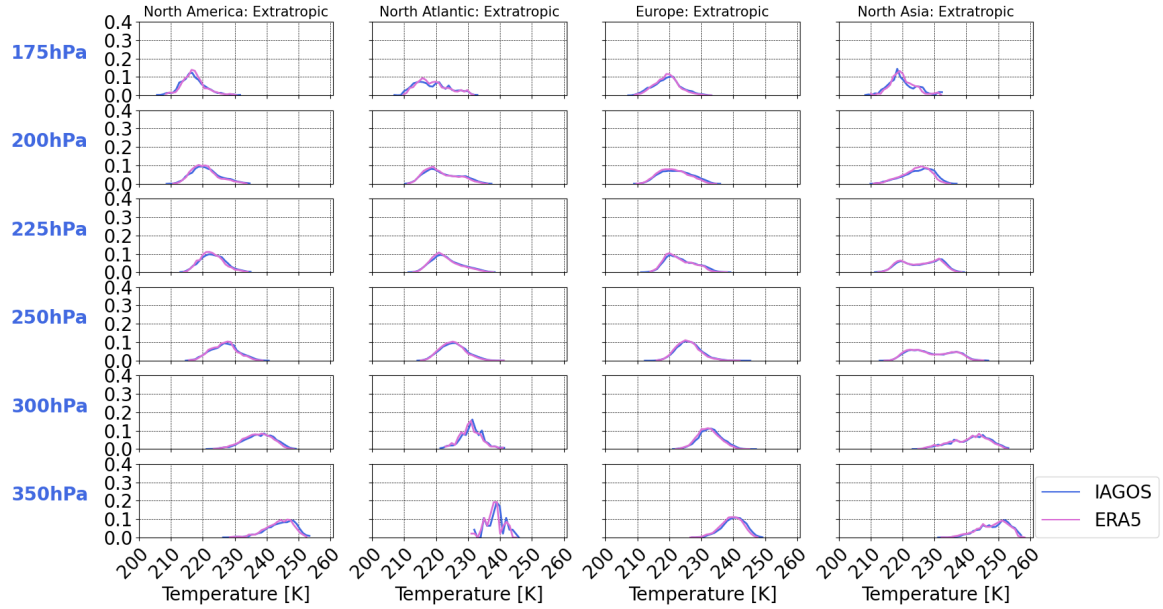

Figure A.4: Probability density function of IAGOS and ERA5 temperature per pressure level for the extratropic regions and season JJA

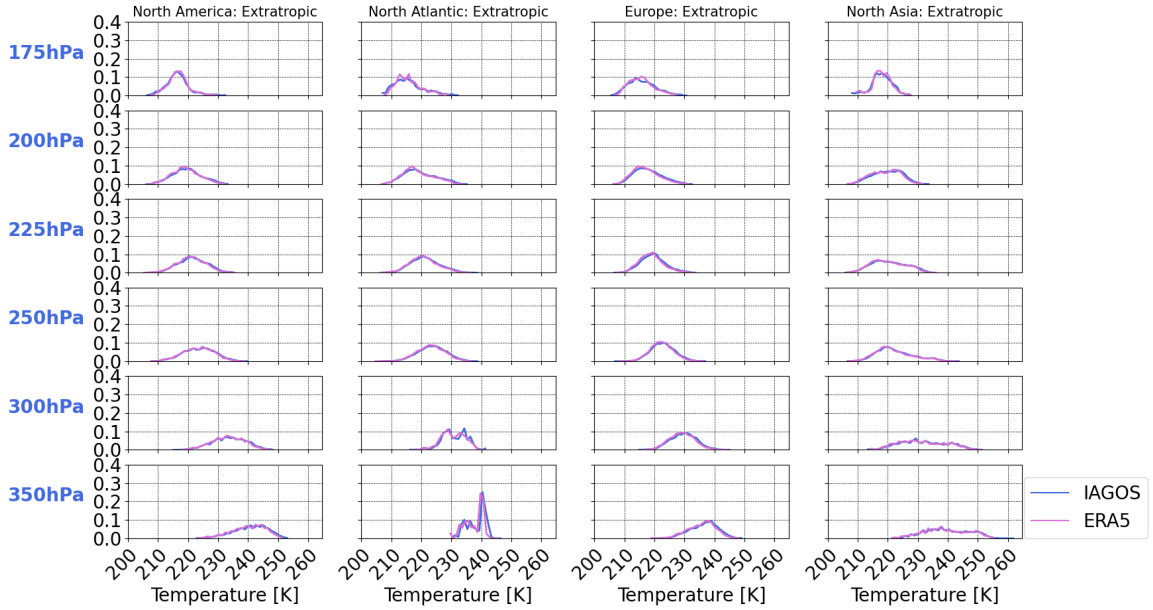

Figure A.5: Probability density function of IAGOS and ERA5 temperature per pressure level for the extratropic regions and season SON

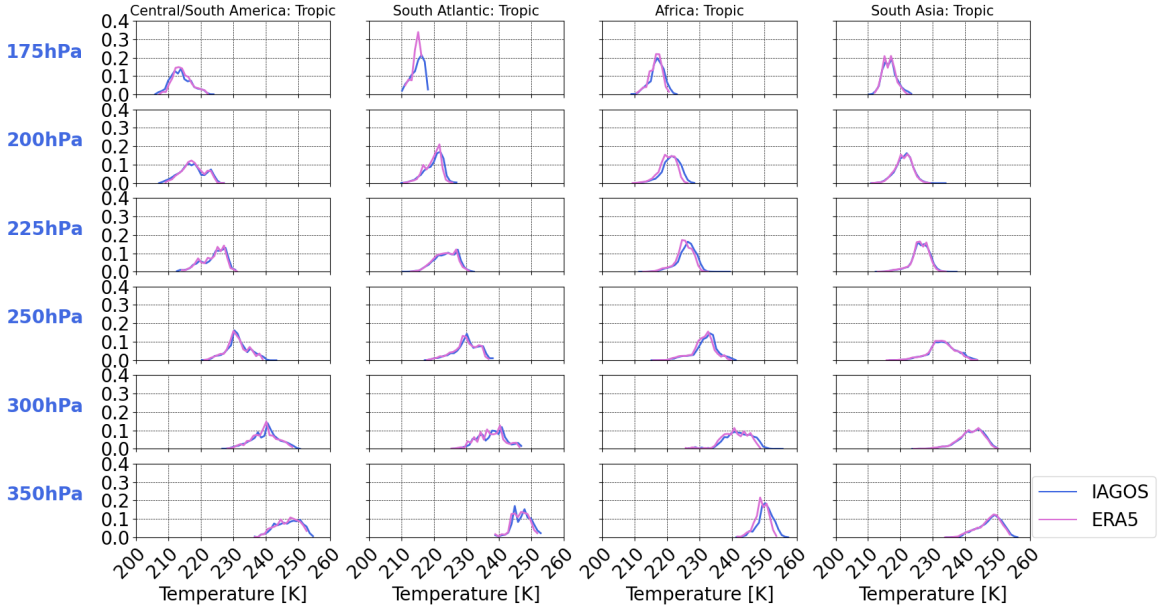

Figure A.6: Probability density function of IAGOS and ERA5 temperature per pressure level for the tropic regions and season MAM

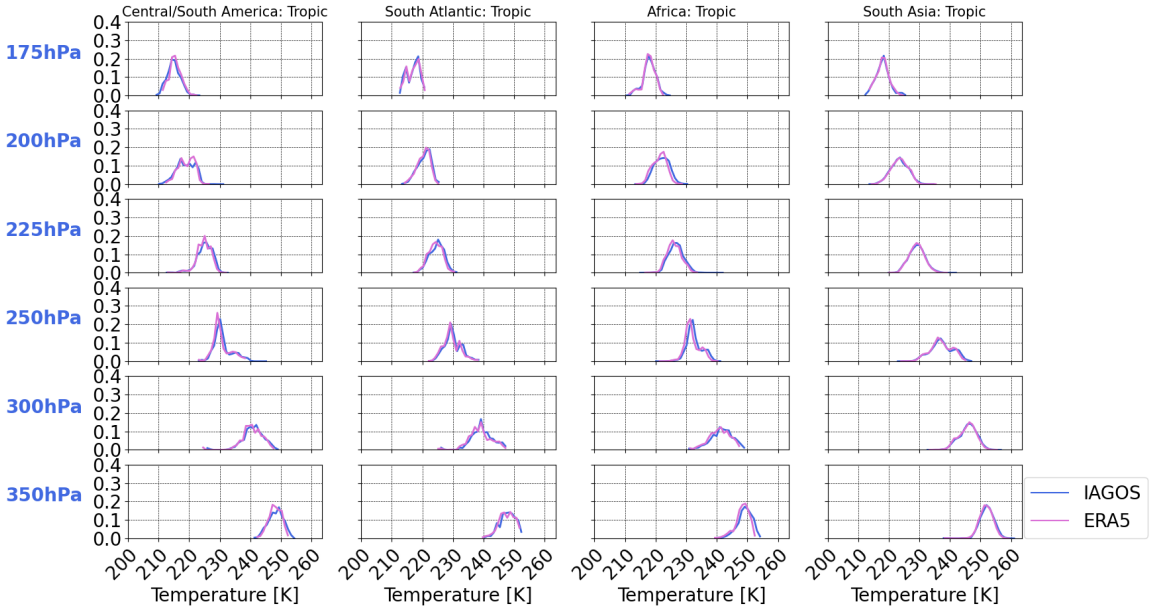

Figure A.7: Probability density function of IAGOS and ERA5 temperature per pressure level for the tropic regions and season JJA

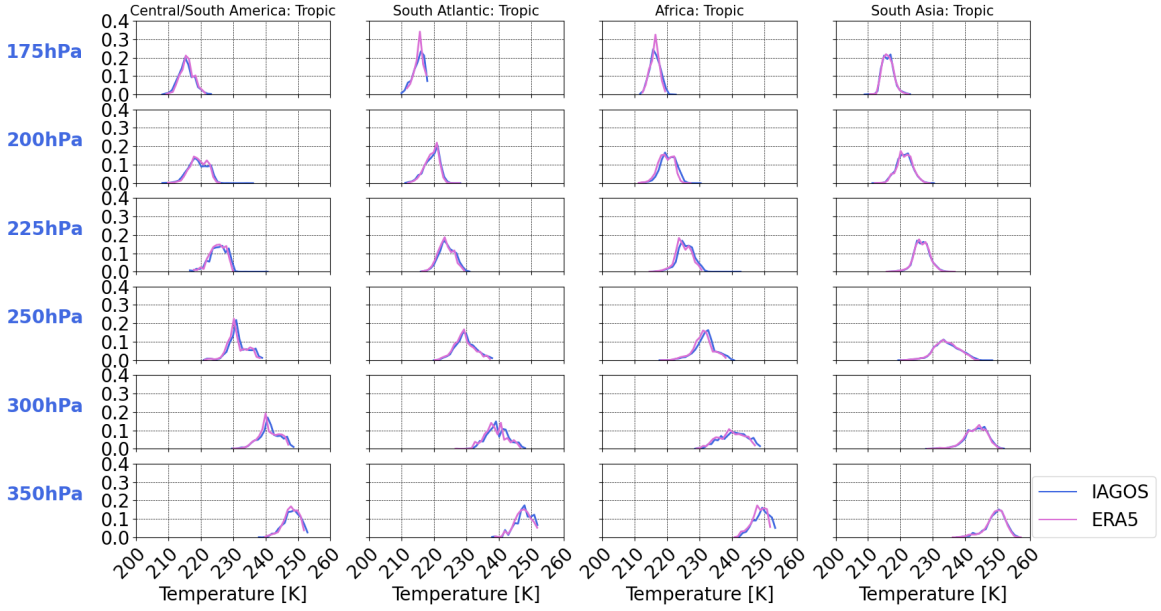

Figure A.8: Probability density function of IAGOS and ERA5 temperature per pressure level for the tropic regions and season SON

A.4. IAGOS Temperature as a Function of Pressure Level, Region and Season - Bootstrapping of Probability Density Functions

Bootstrap test to ensure there are enough points to generate probability density functions for temperature. 100 subsamples were taken from IAGOS measurements and plotted against the PDF for the entire sample. It is found that there are generally enough samples per region, season and pressure level. However, North Atlantic sometimes lacks samples at pressure level 350 hPa. The tropic regions generally lack some samples at 175 and 350 hPa.

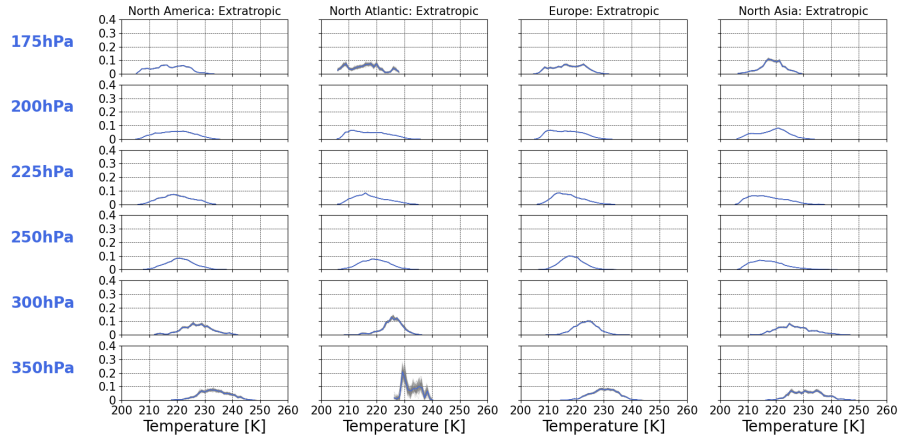

Figure A.9: Bootstrapping of probability density function for IAGOS temperature per pressure level for the extratropic regions and season DJF

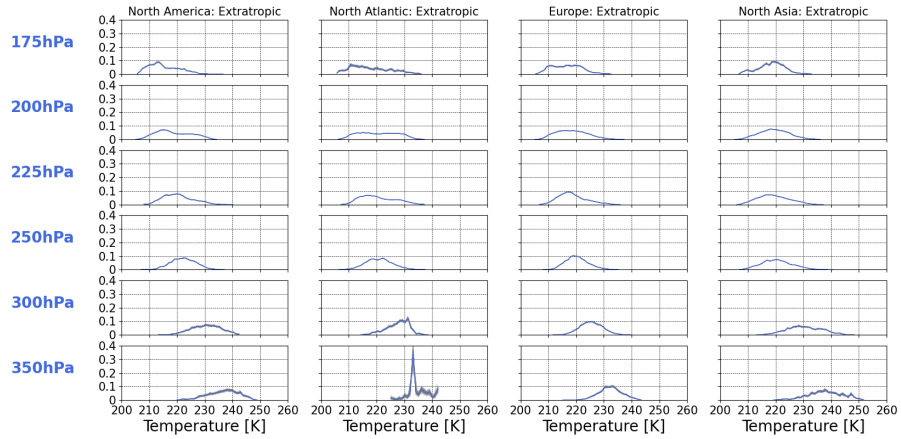

Figure A.10: Bootstrapping of probability density function for IAGOS temperature per pressure level for the extratropic regions and season MAM

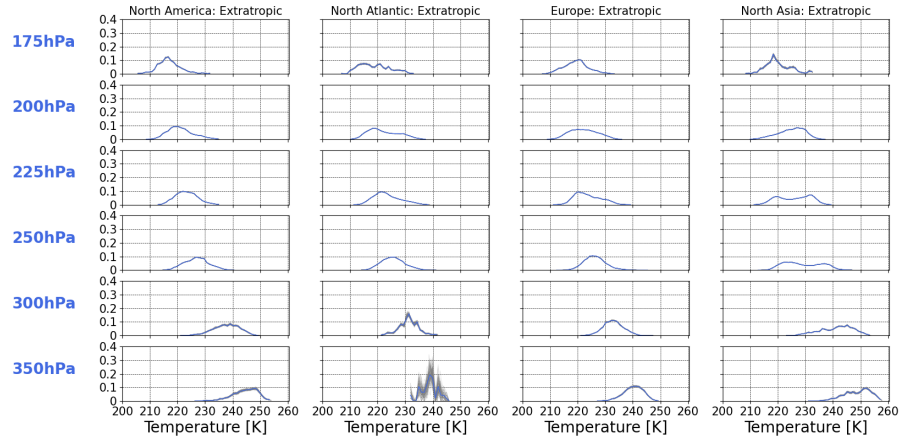

Figure A.11: Bootstrapping of probability density function for IAGOS temperature per pressure level for the extratropic regions and season JJA

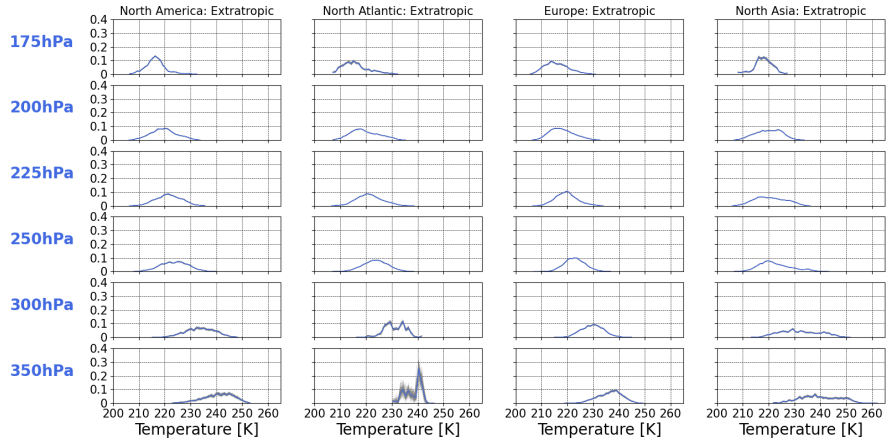

Figure A.12: Bootstrapping of probability density function for IAGOS temperature per pressure level for the extratropic regions and season SON

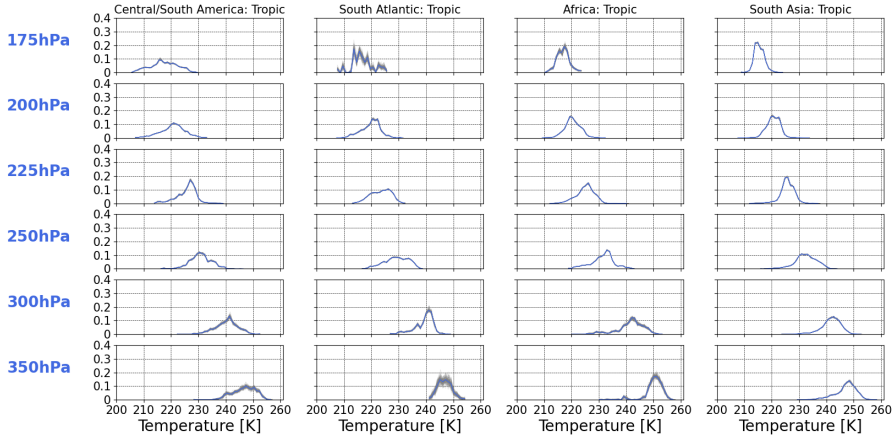

Figure A.13: Bootstrapping of probability density function for IAGOS temperature per pressure level for the tropic regions and season DJF

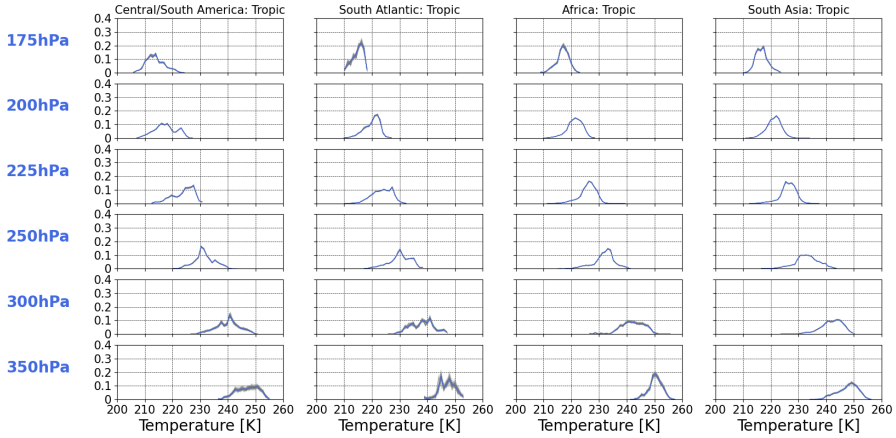

Figure A.14: Bootstrapping of probability density function for IAGOS temperature per pressure level for the tropic regions and season MAM

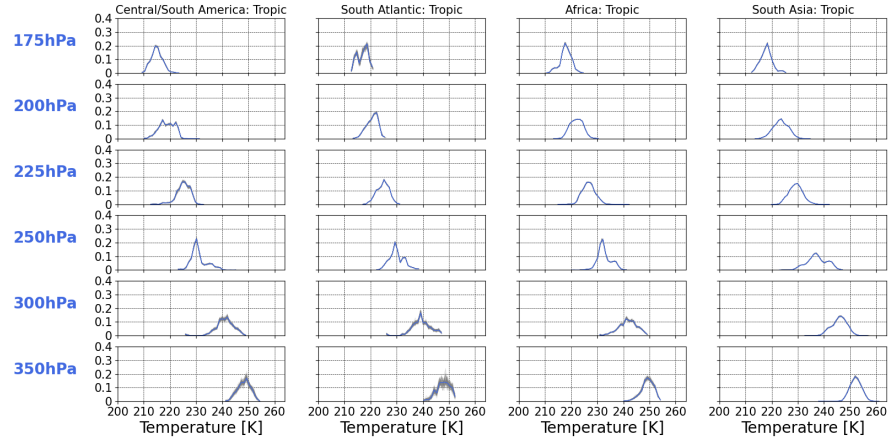

Figure A.15: Bootstrapping of probability density function for IAGOS temperature per pressure level for the tropic regions and season JJA

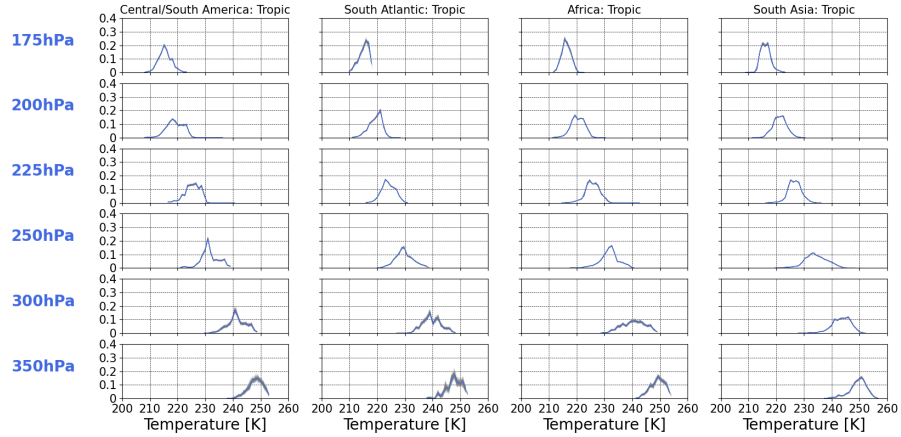

Figure A.16: Bootstrapping of probability density function for IAGOS temperature per pressure level for the tropic regions and season SON

A.5. IAGOS and ERA5 Temperature as a Function of Pressure Level, Region and Year - Standard Deviation

Table A.3: Standard deviation of IAGOS and ERA5 temperature per year and pressure level for North America

	North America																							
	IAGOS												ERA5											
Pressure Level	**2011**	**2012**	**2013**	**2014**	**2015**	**2016**	**2017**	**2018**	**2019**	**2020**	**2021**	**2022**	**2011**	**2012**	**2013**	**2014**	**2015**	**2016**	**2017**	**2018**	**2019**	**2020**	**2021**	**2022**
175 hPa	3.28	4.87	8.81	5.95	7.56	0.98	4.41	4.56	4.37	5.95	5.40	5.52	2.91	4.39	7.93	5.51	7.51	0.43	4.17	4.20	4.11	5.67	5.03	5.13
200 hPa	4.78	5.75	5.14	5.61	5.28	5.20	5.19	4.83	5.06	6.32	5.68	5.46	4.60	5.44	4.96	5.31	5.18	5.01	4.96	4.51	4.60	5.77	5.14	5.19
225 hPa	5.28	5.65	4.84	4.83	4.75	4.79	4.74	4.70	4.70	5.56	4.90	5.20	5.28	5.53	4.68	4.64	4.49	4.63	4.50	4.49	4.43	5.28	4.60	4.98
250 hPa	6.02	5.49	5.62	4.74	4.76	5.11	5.10	4.94	5.01	5.22	4.90	5.04	5.96	5.34	5.41	4.50	4.54	4.77	4.94	4.90	4.86	5.04	4.66	4.89
300 hPa	6.88	7.57	6.97	5.58	6.17	6.57	5.90	5.86	6.14	5.43	6.60	6.30	6.76	7.23	6.79	5.32	5.76	6.16	5.64	5.70	5.83	5.20	6.24	6.13
350 hPa	7.27	7.17	7.06	6.03	6.99	6.69	6.08	5.98	6.30	5.09	6.91	6.76	7.11	7.00	6.91	5.78	6.52	6.36	5.92	5.76	6.06	4.80	6.63	6.63

Table A.4: Standard deviation of IAGOS and ERA5 temperature per year and pressure level for North Atlantic

	North Atlantic																							
	IAGOS												ERA5											
Pressure level	**2011**	**2012**	**2013**	**2014**	**2015**	**2016**	**2017**	**2018**	**2019**	**2020**	**2021**	**2022**	**2011**	**2012**	**2013**	**2014**	**2015**	**2016**	**2017**	**2018**	**2019**	**2020**	**2021**	**2022**
175 hPa	3.71	3.49	5.50	7.43	8.58	4.52	5.52	5.06	2.10	6.78	6.18	5.09	3.32	3.33	5.28	7.23	8.33	4.18	5.25	4.70	1.86	6.89	5.64	4.48
200 hPa	5.68	5.91	5.08	5.96	6.46	6.05	6.03	5.67	6.15	5.64	6.04	6.35	5.44	5.79	4.87	5.71	6.26	5.73	5.69	5.36	5.84	5.39	5.76	5.99
225 hPa	5.23	6.00	5.10	5.46	5.80	5.59	5.76	5.45	5.89	6.21	5.24	5.71	5.10	5.92	4.97	5.24	5.56	5.27	5.52	5.27	5.60	6.03	4.97	5.53
250 hPa	5.28	5.29	5.57	4.99	4.92	5.21	4.77	5.21	4.97	5.13	5.23	5.38	5.24	5.19	5.45	4.77	4.72	5.04	4.65	5.13	4.88	5.11	5.05	5.34
300 hPa	3.87	4.13	6.55	4.10	3.15	4.69	4.74	3.72	5.29	4.18	4.02	5.42	3.68	4.02	6.24	3.85	2.92	4.42	4.67	3.46	5.09	4.05	3.85	4.94
350 hPa	NA	1.42	3.86	3.92	3.97	NA	NA	NA	NA	NA	NA	3.20	NA	1.45	3.78	3.85	3.72	NA	NA	NA	NA	NA	NA	3.04

Table A.5: Standard deviation of IAGOS and ERA5 temperature per year and pressure level for Europe

	Europe																							
	IAGOS												ERA5											
Pressure level	2011	2012	2013	2014	2015	2016	2017	2018	2019	2020	2021	2022	2011	2012	2013	2014	2015	2016	2017	2018	2019	2020	2021	2022
175 hPa	5.14	5.07	5.48	5.37	4.93	5.17	4.39	4.34	4.62	5.67	5.29	4.49	4.74	4.80	5.05	5.25	4.42	4.86	4.01	3.97	4.18	5.43	5.11	4.15
200 hPa	5.44	5.75	5.40	5.33	5.37	5.37	5.24	4.96	5.34	6.63	5.88	5.49	5.27	5.58	5.10	4.99	5.20	5.08	4.94	4.72	5.12	6.39	5.60	5.26
225 hPa	5.46	5.63	5.39	5.07	4.75	5.48	5.09	4.39	4.96	5.93	5.51	5.35	5.37	5.51	5.19	4.82	4.60	5.21	4.87	4.25	4.77	5.73	5.26	5.23
250 hPa	4.80	5.25	5.12	4.57	4.56	4.91	4.71	4.58	4.95	4.78	5.18	4.91	4.79	5.17	4.88	4.45	4.43	4.85	4.64	4.45	4.80	4.76	5.00	4.92
300 hPa	4.94	5.56	5.44	5.24	5.04	6.01	5.19	5.31	5.41	5.81	5.49	4.75	4.81	5.47	5.20	5.04	4.76	5.82	5.05	5.13	5.25	5.53	5.18	4.74
350 hPa	5.31	5.80	6.06	5.21	5.26	5.99	5.44	6.20	5.65	5.76	5.90	5.34	5.24	5.72	5.89	5.10	5.03	5.89	5.32	6.04	5.54	5.65	5.74	5.36

Table A.6: Standard deviation of IAGOS and ERA5 temperature per year and pressure level for North Asia

	North Asia																							
	IAGOS												IAGOS											
Pressure level	2011	2012	2013	2014	2015	2016	2017	2018	2019	2020	2021	2022	2011	2012	2013	2014	2015	2016	2017	2018	2019	2020	2021	2022
175 hPa	5.11	4.41	3.71	3.85	2.93	5.39	4.09	4.24	3.63	5.08	3.84	4.18	5.10	4.06	3.82	3.62	2.72	4.91	3.69	3.96	3.38	4.98	3.81	4.00
200 hPa	5.70	5.73	5.65	5.54	5.57	5.77	5.45	5.06	5.49	6.16	6.07	5.60	5.48	5.57	5.53	5.65	5.44	5.62	5.25	4.89	5.41	6.02	5.77	5.46
225 hPa	6.21	6.33	6.69	6.90	6.66	6.72	7.02	6.33	6.62	6.05	7.68	6.88	6.11	6.20	6.50	6.79	6.59	6.78	6.90	6.26	6.58	5.86	7.40	6.67
250 hPa	6.40	7.24	7.05	7.72	8.31	8.36	7.49	7.72	7.94	8.84	7.00	8.08	6.37	7.21	6.94	7.72	8.38	8.41	7.41	7.63	7.90	8.73	6.88	7.96
300 hPa	8.56	8.54	8.91	8.22	7.43	9.00	7.90	8.14	9.58	7.75	7.57	7.30	8.32	8.52	8.69	8.04	7.37	9.06	7.79	8.12	9.60	7.66	7.43	7.23
350 hPa	7.89	9.62	9.42	9.16	7.89	7.94	8.24	8.17	9.09	7.78	8.13	8.46	7.90	9.61	9.36	9.03	7.97	8.16	8.26	7.99	9.15	7.67	8.01	8.41

Table A.7: Standard deviation of IAGOS and ERA5 temperature per year and pressure level for Central/South America

	Central/South America																							
	IAGOS												ERA5											
Pressure Level	2011	2012	2013	2014	2015	2016	2017	2018	2019	2020	2021	2022	2011	2012	2013	2014	2015	2016	2017	2018	2019	2020	2021	2022
175 hPa	NA	NA	0.28	NA	0.47	0.30	1.57	3.25	3.57	4.49	5.07	5.26	NA	NA	0.14	NA	0.50	0.13	1.33	2.97	3.32	4.16	4.64	3.09
200 hPa	NA	NA	2.20	1.72	2.20	1.21	1.72	3.55	3.62	4.92	4.95	3.30	NA	NA	2.27	1.66	2.13	1.17	1.63	3.27	3.36	4.68	4.31	3.12
225 hPa	NA	NA	1.75	2.79	2.83	1.59	2.19	3.22	3.40	4.70	3.98	2.47	NA	NA	1.61	2.68	2.78	1.48	2.15	3.07	3.08	4.50	3.60	2.44
250 hPa	NA	NA	2.60	3.82	3.86	2.57	2.21	2.83	4.24	4.60	3.24	3.97	NA	NA	2.50	3.69	3.68	2.47	2.14	2.68	3.97	4.41	3.14	3.95
300 hPa	NA	NA	2.79	3.13	3.22	3.07	3.55	3.68	3.49	4.56	4.48	3.68	NA	NA	2.67	3.19	3.18	2.84	3.21	3.48	3.35	4.40	4.19	3.69
350 hPa	NA	NA	1.87	1.89	2.06	2.48	3.11	3.13	2.94	4.35	4.18	3.21	NA	NA	1.64	1.70	2.01	2.03	2.58	2.85	2.71	4.01	3.87	3.27

Table A.8: Standard deviation of IAGOS and ERA5 temperature per year and pressure level for South Atlantic

	South Atlantic																							
	IAGOS												ERA5											
Pressure Level	2011	2012	2013	2014	2015	2016	2017	2018	2019	2020	2021	2022	2011	2012	2013	2014	2015	2016	2017	2018	2019	2020	2021	2022
175 hPa	NA	1.51	0.98	0.84	3.24	NA	1.81	2.72	NA	NA	0.06	2.32	NA	1.11	0.77	0.70	3.34	NA	1.66	2.58	NA	NA	0.11	2.05
200 hPa	1.38	2.24	1.91	2.75	3.00	3.03	2.46	2.90	0.99	2.23	3.13	3.25	1.16	2.09	1.80	2.57	2.74	2.86	2.29	2.73	1.14	1.85	3.05	3.14
225 hPa	2.44	2.85	2.49	3.28	3.61	2.56	2.99	2.99	2.74	3.19	2.93	3.01	2.40	2.76	2.40	3.19	3.42	2.41	2.91	2.84	2.66	3.11	2.83	2.99
250 hPa	3.91	3.17	2.48	3.86	3.91	2.76	4.30	3.45	2.31	2.54	3.88	3.15	3.82	3.05	2.39	3.74	3.78	2.55	4.28	3.36	2.26	2.46	3.83	3.49
300 hPa	2.24	2.62	3.06	3.64	4.47	2.75	3.04	3.11	NA	NA	1.79	3.38	2.15	2.72	2.97	3.52	4.20	2.67	2.97	3.11	NA	NA	1.56	3.29
350 hPa	2.28	2.96	2.56	2.91	2.56	2.20	2.55	2.49	NA	NA	2.19	2.93	2.17	2.93	2.37	2.73	2.10	1.76	2.32	2.51	NA	NA	2.07	2.90

Table A.9: Standard deviation of IAGOS and ERA5 temperature per year and pressure level for Africa

	Africa																							
	IAGOS												ERA5											
Pressure Level	2011	2012	2013	2014	2015	2016	2017	2018	2019	2020	2021	2022	2011	2012	2013	2014	2015	2016	2017	2018	2019	2020	2021	2022
175 hPa	1.97	2.78	1.99	2.68	2.13	3.19	2.16	1.73	2.96	1.61	1.83	2.16	1.91	2.41	1.87	1.89	1.99	2.66	2.01	1.59	3.31	1.56	1.43	1.97
200 hPa	2.25	2.21	2.35	2.38	3.00	3.01	2.76	2.50	3.01	2.75	2.85	2.51	2.18	2.11	2.23	2.29	2.87	2.90	2.62	2.53	2.88	2.66	2.69	2.29
225 hPa	2.64	2.82	2.50	3.09	3.31	3.04	2.71	2.88	2.57	3.03	2.39	2.54	2.63	2.76	2.33	2.94	2.95	2.89	2.56	2.75	2.48	2.87	2.31	2.42
250 hPa	2.89	2.94	2.83	3.18	4.77	4.37	3.78	3.60	3.34	3.81	3.36	3.88	2.82	2.83	2.73	3.14	4.45	4.16	3.59	3.44	3.22	3.75	3.28	3.71
300 hPa	3.38	3.11	3.11	2.52	3.01	3.35	4.21	4.14	5.24	3.39	4.03	4.37	3.21	3.00	3.09	2.47	2.78	3.14	3.93	3.57	4.92	3.16	3.81	4.14
350 hPa	2.66	2.58	2.78	1.58	1.82	1.81	2.28	3.23	1.76	1.97	2.97	1.88	2.59	2.43	2.77	1.63	1.54	1.64	1.59	2.27	1.59	1.88	2.57	1.57

Table A.10: Standard deviation of IAGOS and ERA5 temperature per year and pressure level for South Asia

	South Asia																							
	IAGOS												ERA5											
Pressure Level	2011	2012	2013	2014	2015	2016	2017	2018	2019	2020	2021	2022	2011	2012	2013	2014	2015	2016	2017	2018	2019	2020	2021	2022
175 hPa	0.88	1.73	1.93	2.04	1.64	2.02	1.49	2.12	2.46	2.50	2.80	3.25	0.62	1.73	1.90	2.01	1.76	1.97	1.44	2.00	2.22	1.77	2.24	2.76
200 hPa	2.95	2.27	2.36	2.74	2.94	2.76	2.64	2.81	2.84	3.00	3.30	3.37	2.93	2.23	2.37	2.72	3.00	2.79	2.60	2.75	2.70	2.82	3.07	3.16
225 hPa	2.64	3.01	2.79	2.64	3.12	2.59	2.69	2.76	2.90	3.67	3.39	3.03	2.65	3.07	2.80	2.62	3.17	2.59	2.64	2.69	2.83	3.63	3.13	2.90
250 hPa	3.99	4.68	4.44	4.54	4.45	4.46	3.77	4.20	4.68	5.44	5.09	4.51	3.89	4.47	4.29	4.37	4.46	4.36	3.61	3.99	4.52	5.43	4.94	4.42
300 hPa	3.86	3.49	3.64	4.00	3.43	3.96	3.58	3.83	4.03	3.96	5.30	3.52	3.89	3.42	3.63	3.96	3.54	4.10	3.52	3.64	3.96	3.95	5.12	3.58
350 hPa	4.44	3.46	3.31	3.93	3.53	3.94	3.58	3.76	3.77	5.32	5.61	3.88	4.36	3.40	3.25	3.81	3.59	4.12	3.41	3.55	3.69	5.50	5.55	3.69

B. IAGOS and ERA5 Relative Humidity over Ice

B.1. Difference Between IAGOS and ERA5 Relative Humidity over Ice as a Function of Pressure Level, Region and Season

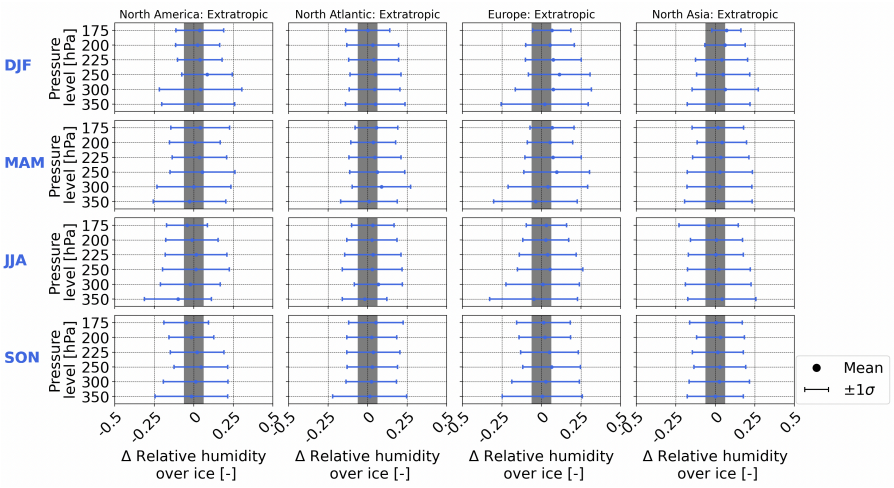

Figure B.1: Variation of difference in relative humidity over ice between IAGOS and ERA5, with IAGOS as baseline, per region, pressure level and extratropic regions. Grey shaded area corresponds to uncertainty of IAGOS's relative humidity sensor.

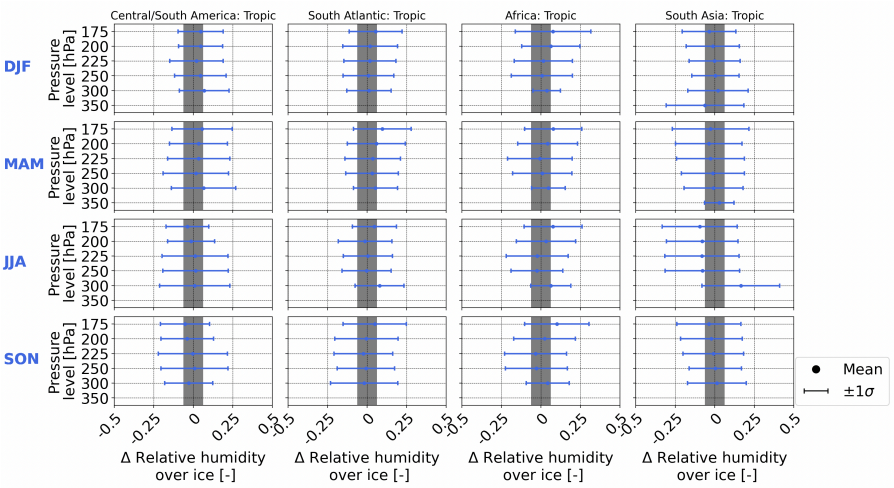

Figure B.2: Variation of difference in relative humidity over ice between IAGOS and ERA5, with IAGOS as baseline, per region, pressure level and tropic regions. Grey shaded area corresponds to uncertainty of IAGOS's relative humidity sensor.

B.2. IAGOS and ERA5 Relative Humidity over Ice as a Function of Pressure Level, Region and Season - Standard Deviation

Table B.1: Standard deviation of IAGOS and ERA5 relative humidity over ice per season and pressure level for extratropic regions

	North America								North Atlantic							
	IAGOS				ERA5				IAGOS				ERA			
Pressure level	**DJF**	**MAM**	**JJA**	**SON**	**DJF**	**MAM**	**JJA**	**SON**	**DJF**	**MAM**	**JJA**	**SON**	**DJF**	**MAM**	**JJA**	**SON**
175 hPa	0.26	0.37	0.27	0.23	0.26	0.33	0.27	0.24	0.26	0.30	0.34	0.35	0.29	0.29	0.31	0.29
200 hPa	0.30	0.34	0.34	0.31	0.30	0.34	0.32	0.31	0.35	0.34	0.37	0.36	0.35	0.33	0.34	0.34
225 hPa	0.34	0.37	0.36	0.36	0.33	0.36	0.33	0.34	0.37	0.38	0.38	0.38	0.36	0.36	0.35	0.35
250 hPa	0.39	0.37	0.35	0.37	0.35	0.34	0.31	0.33	0.37	0.38	0.36	0.37	0.35	0.35	0.32	0.34
300 hPa	0.40	0.34	0.32	0.37	0.34	0.31	0.28	0.33	0.36	0.36	0.31	0.35	0.31	0.30	0.27	0.30
350 hPa	0.40	0.33	0.24	0.35	0.34	0.29	0.24	0.31	0.38	0.32	0.12	0.33	0.30	0.24	0.23	0.22

	Europe								North Asia							
	IAGOS				ERA5				IAGOS				ERA5			
Pressure level	**DJF**	**MAM**	**JJA**	**SON**	**DJF**	**MAM**	**JJA**	**SON**	**DJF**	**MAM**	**JJA**	**SON**	**DJF**	**MAM**	**JJA**	**SON**
175 hPa	0.20	0.28	0.25	0.29	0.19	0.25	0.22	0.27	0.19	0.24	0.34	0.30	0.16	0.26	0.36	0.31
200 hPa	0.29	0.29	0.28	0.31	0.28	0.28	0.26	0.30	0.24	0.28	0.31	0.29	0.21	0.27	0.32	0.28
225 hPa	0.34	0.34	0.34	0.34	0.32	0.31	0.31	0.31	0.29	0.33	0.37	0.33	0.29	0.32	0.35	0.32
250 hPa	0.38	0.36	0.35	0.35	0.33	0.32	0.30	0.31	0.34	0.35	0.37	0.35	0.32	0.33	0.34	0.33
300 hPa	0.38	0.36	0.32	0.34	0.32	0.30	0.26	0.29	0.37	0.34	0.31	0.34	0.32	0.32	0.28	0.30
350 hPa	0.38	0.34	0.32	0.35	0.32	0.29	0.25	0.29	0.32	0.33	0.28	0.31	0.31	0.31	0.24	0.30

Table B.2: Standard deviation of IAGOS and ERA5 relative humidity over ice per season and pressure level for tropic regions

	Central/South America								South Atlantic							
	IAGOS				ERA5				IAGOS				ERA5			
Pressure level	**DJF**	**MAM**	**JJA**	**SON**	**DJF**	**MAM**	**JJA**	**SON**	**DJF**	**MAM**	**JJA**	**SON**	**DJF**	**MAM**	**JJA**	**SON**
175 hPa	0.27	0.33	0.25	0.27	0.28	0.30	0.25	0.26	0.36	0.27	0.29	0.30	0.30	0.24	0.29	0.27
200 hPa	0.30	0.31	0.29	0.30	0.29	0.28	0.27	0.29	0.32	0.32	0.28	0.28	0.30	0.29	0.28	0.27
225 hPa	0.31	0.32	0.31	0.33	0.30	0.29	0.27	0.29	0.33	0.32	0.29	0.30	0.32	0.29	0.27	0.28
250 hPa	0.32	0.35	0.33	0.34	0.29	0.31	0.28	0.30	0.34	0.33	0.29	0.31	0.31	0.29	0.28	0.27
300 hPa	0.28	0.34	0.31	0.25	0.27	0.29	0.27	0.22	0.32	0.26	0.35	0.37	0.30	0.23	0.31	0.31
350 hPa	0.37	NA	NA	NA	NA	NA	NA	NA	NA	NA	NA	NA	NA	NA	NA	NA

	Africa								South Asia							
	IAGOS				ERA5				IAGOS				ERA5			
Pressure level	**DJF**	**MAM**	**JJA**	**SON**	**DJF**	**MAM**	**JJA**	**SON**	**DJF**	**MAM**	**JJA**	**SON**	**DJF**	**MAM**	**JJA**	**SON**
175 hPa	0.36	0.31	0.31	0.31	0.31	0.27	0.29	0.26	0.30	0.28	0.29	0.29	0.29	0.31	0.28	0.30
200 hPa	0.35	0.31	0.30	0.31	0.32	0.30	0.30	0.28	0.32	0.29	0.31	0.31	0.32	0.31	0.32	0.31
225 hPa	0.33	0.32	0.32	0.31	0.31	0.31	0.32	0.30	0.31	0.31	0.33	0.33	0.31	0.31	0.33	0.32
250 hPa	0.32	0.33	0.30	0.32	0.30	0.31	0.30	0.31	0.30	0.33	0.34	0.32	0.28	0.31	0.32	0.30
300 hPa	0.19	0.17	0.20	0.35	0.16	0.13	0.14	0.30	0.32	0.33	0.35	0.27	0.29	0.32	0.12	0.23
350 hPa	0.09	NA	NA	NA	NA	NA	NA	NA	0.28	0.04	NA	NA	0.21	0.28	NA	NA

B.3. IAGOS and ERA5 Relative Humidity over Ice as a Function of Pressure Level, Region and Season - Probability Density Functions

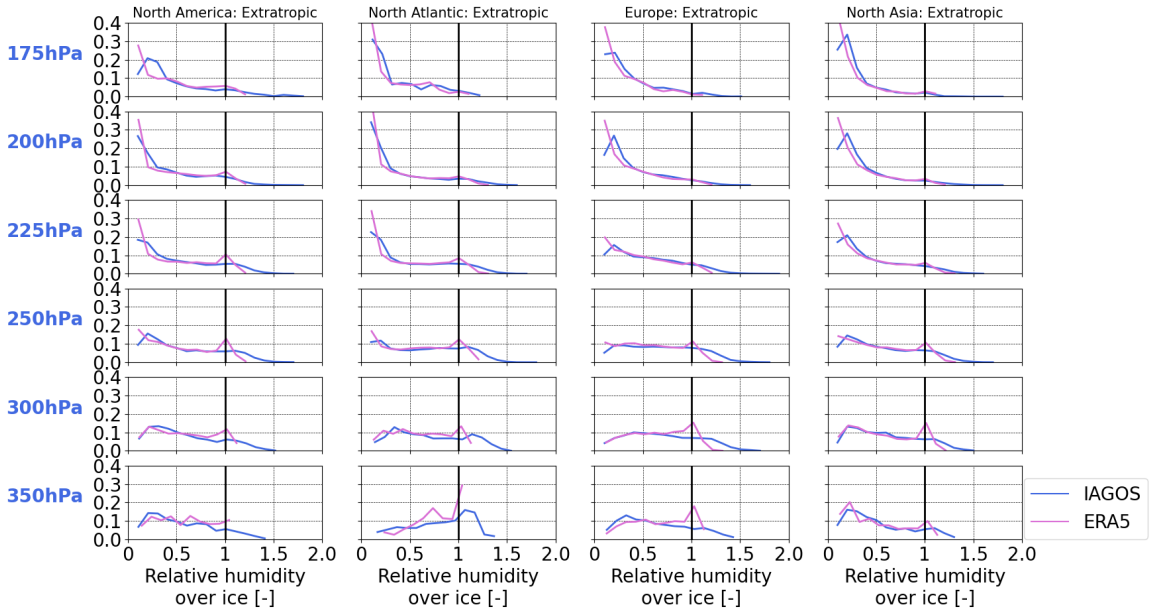

Figure B.3: Probability density function of IAGOS and ERA5 relative humidity over ice per pressure level for the extratropic regions and season MAM

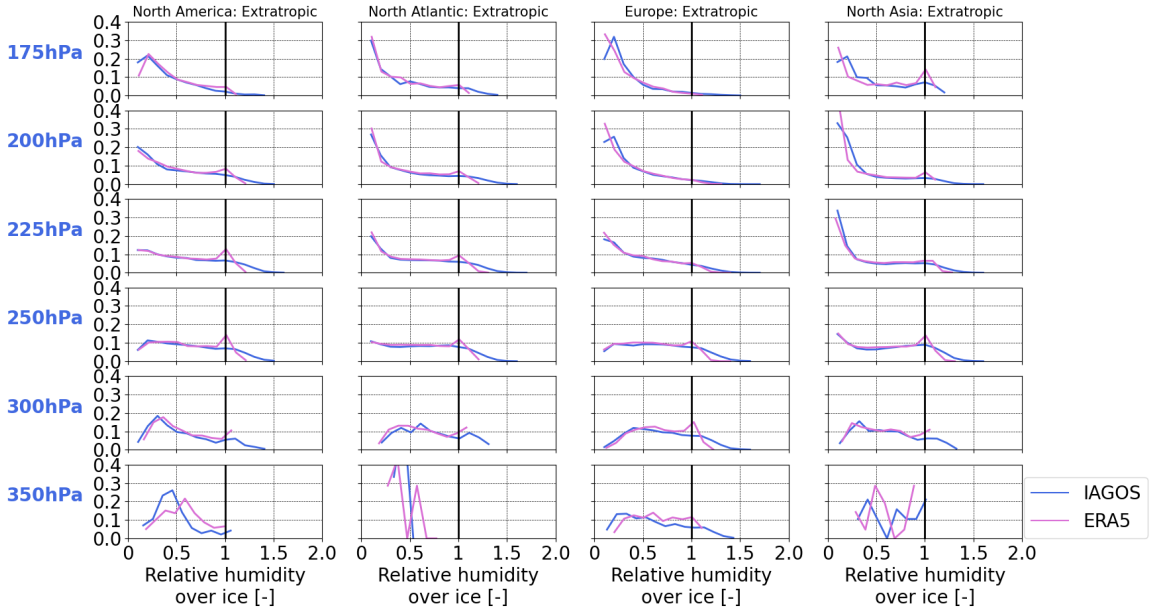

Figure B.4: Probability density function of IAGOS and ERA5 relative humidity over ice per pressure level for the extratropic regions and season JJA

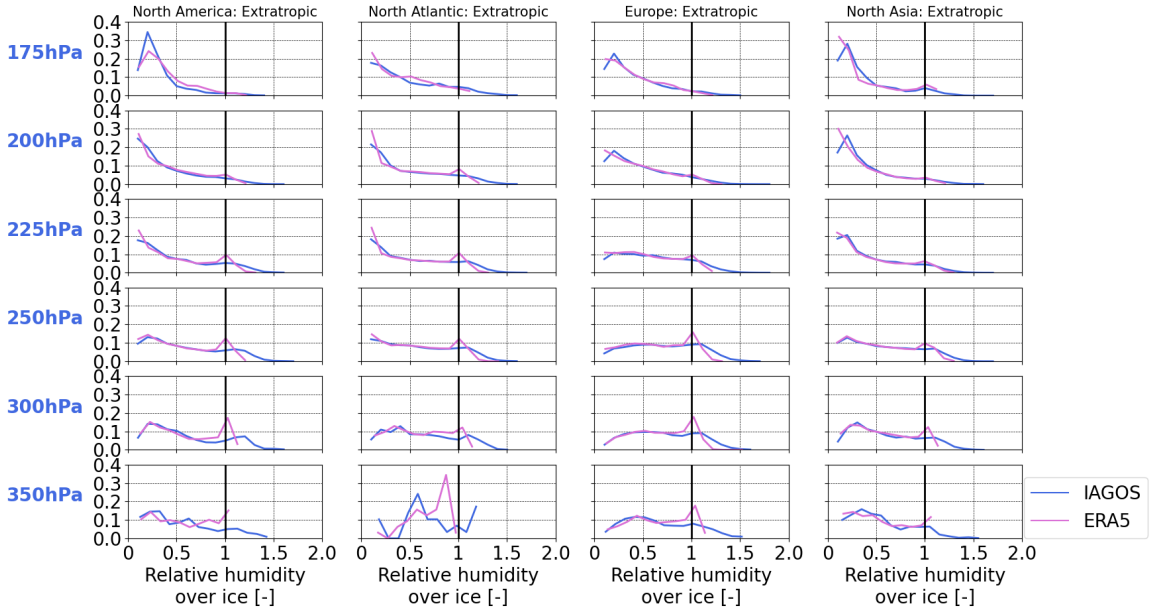

Figure B.5: Probability density function of IAGOS and ERA5 relative humidity over ice per pressure level for the extratropic regions and season SON

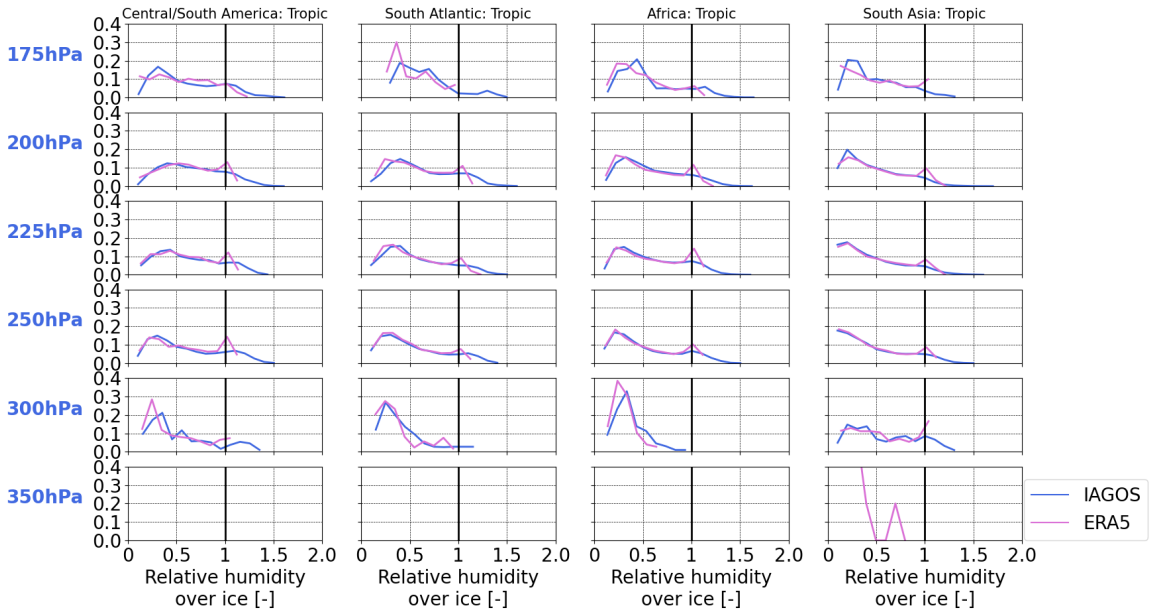

Figure B.6: Probability density function of IAGOS and ERA5 relative humidity over ice per pressure level for the tropic regions and season MAM

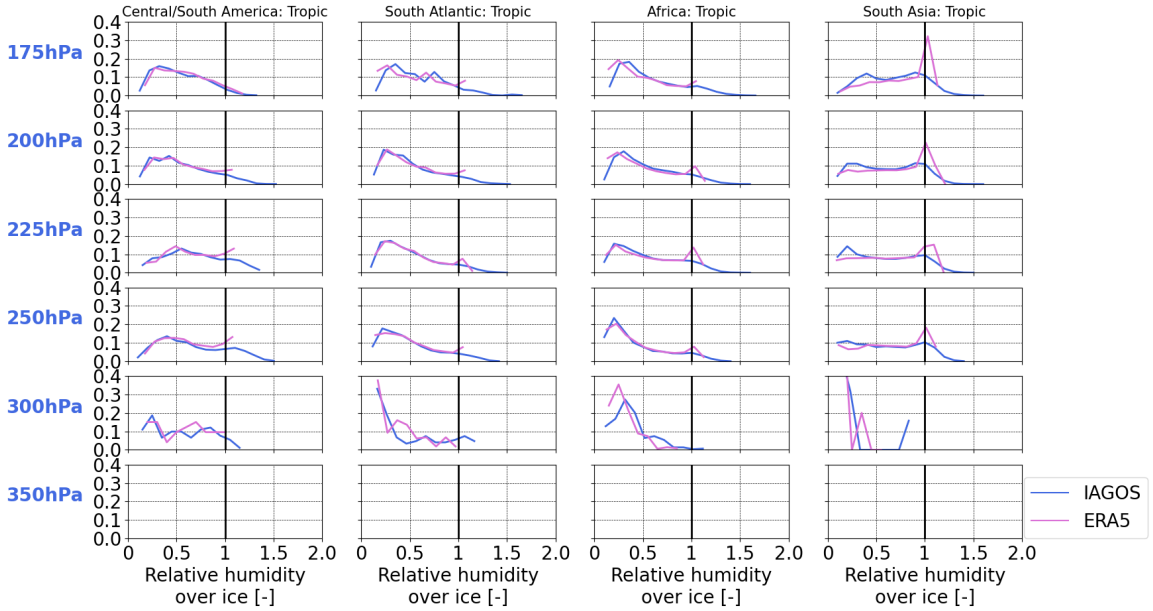

Figure B.7: Probability density function of IAGOS and ERA5 relative humidity over ice per pressure level for the tropic regions and season JJA

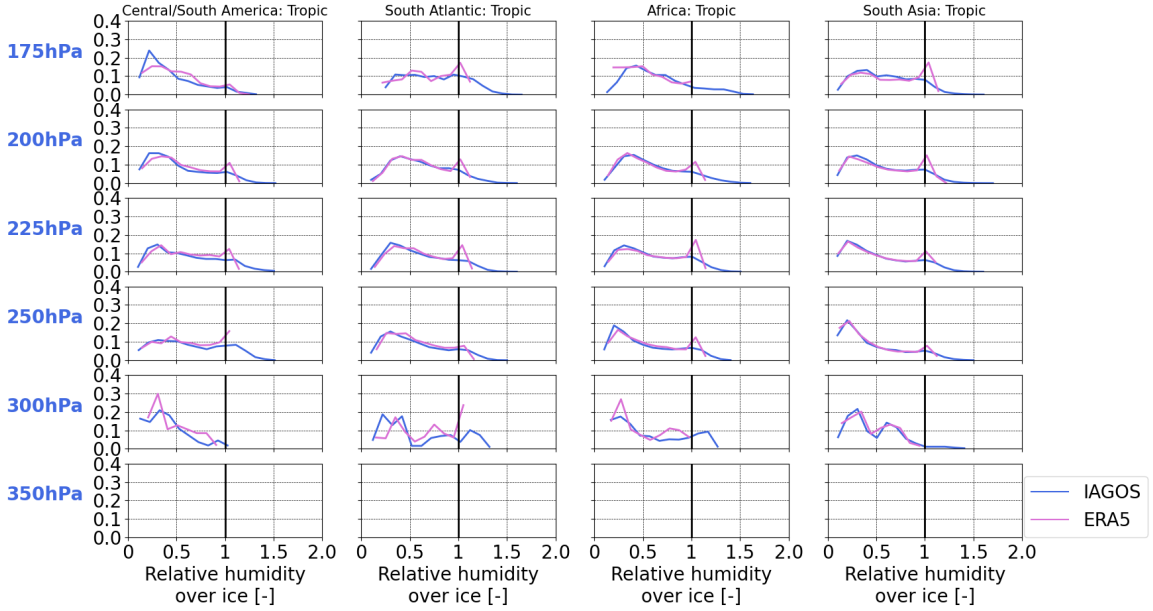

Figure B.8: Probability density function of IAGOS and ERA5 relative humidity over ice per pressure level for the tropic regions and season SON

B.4. IAGOS Relative Humidity over Ice as a Function of Pressure Level, Region and Season - Bootstrapping of Probability Density Functions

Bootstrap test to ensure there are enough points to generate probability density functions for relative humidity over ice. 100 subsamples were taken from IAGOS measurements and plotted against the PDF for the entire sample. In the extratropics, pressure level 350 hPa lacks measurements for displaying a PDF. In the tropics, these issues arise at pressure level 350 and 300 hPa, and sometimes 175 hPa.

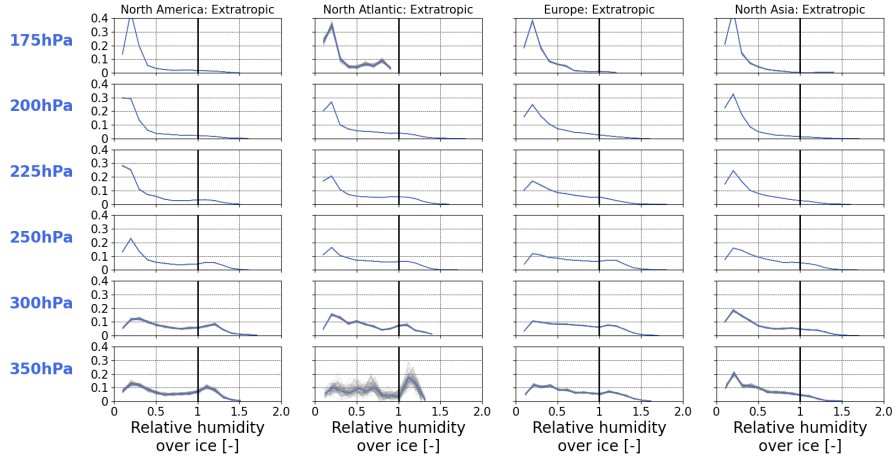

Figure B.9: Bootstrapping of probability density function for IAGOS relative humidity over ice per pressure level for the extratropic regions and season DJF

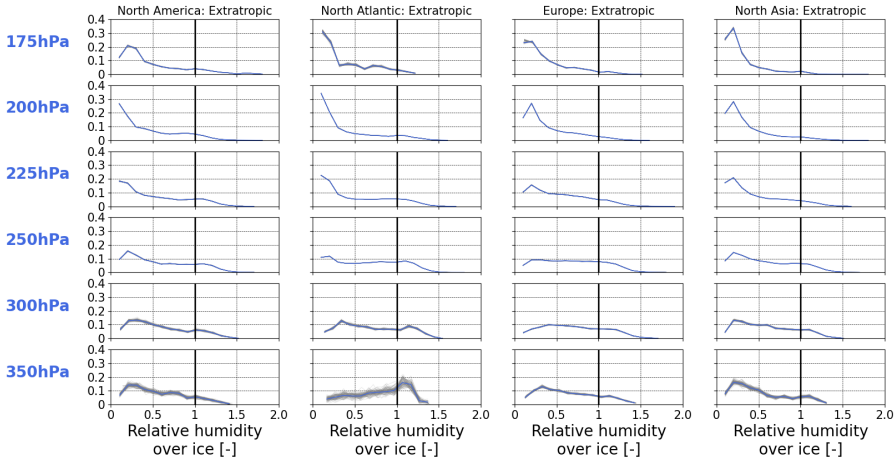

Figure B.10: Bootstrapping of probability density function for IAGOS relative humidity over ice per pressure level for the extratropic regions and season MAM

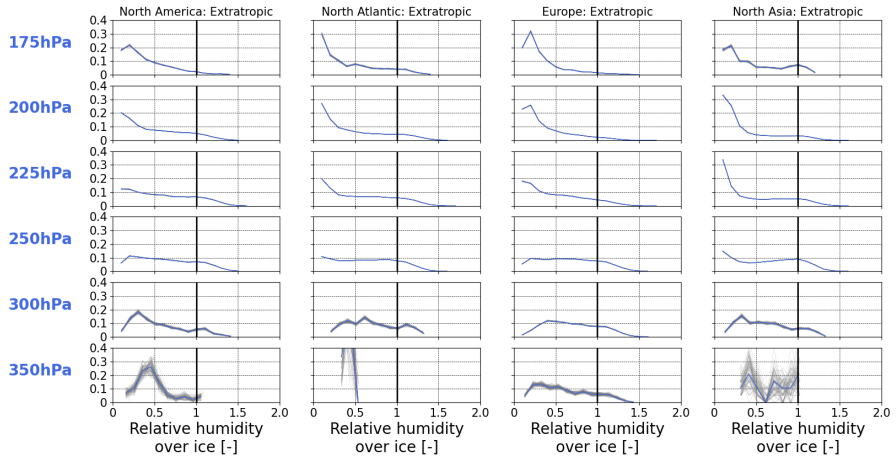

Figure B.11: Bootstrapping of probability density function for IAGOS relative humidity over ice per pressure level for the extratropic regions and season JJA

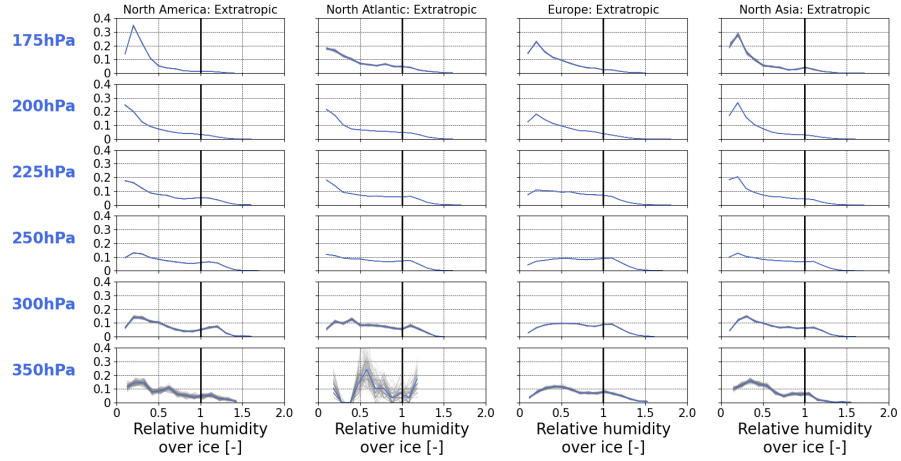

Figure B.12: Bootstrapping of probability density function for IAGOS relative humidity over ice per pressure level for the extratropic regions and season SON

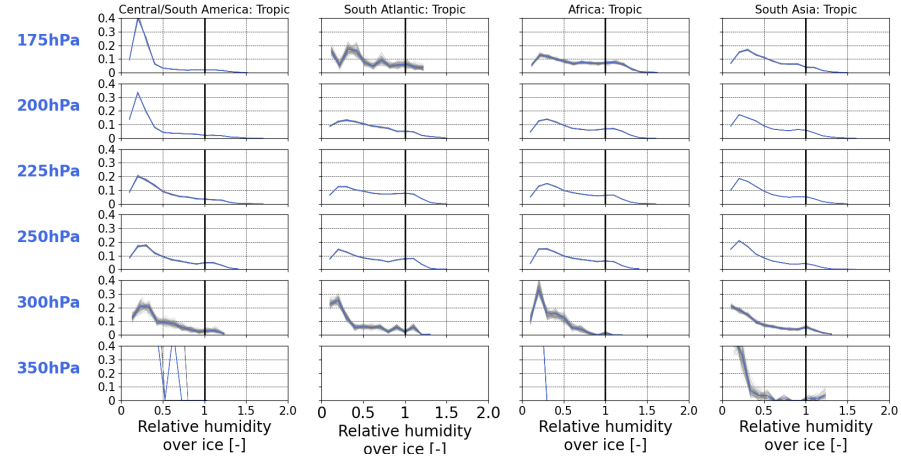

Figure B.13: Bootstrapping of probability density function for IAGOS relative humidity over ice per pressure level for the tropic regions and season DJF

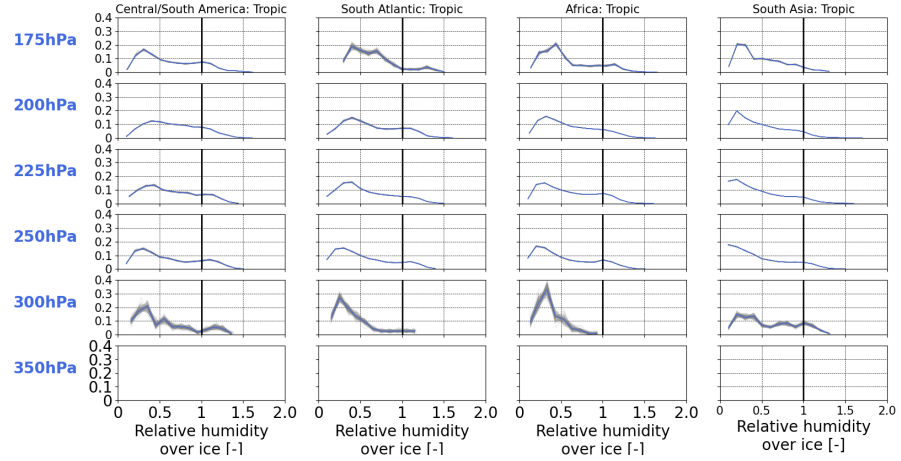

Figure B.14: Bootstrapping of probability density function for IAGOS relative humidity over ice per pressure level for the tropic regions and season MAM

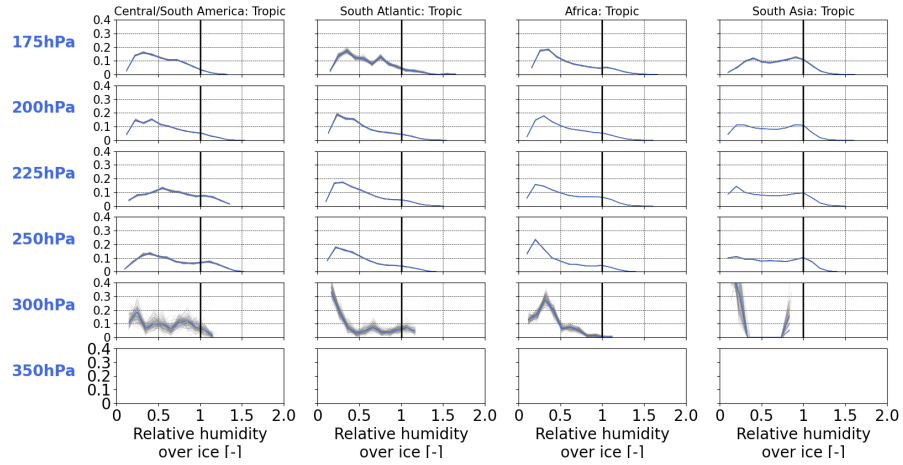

Figure B.15: Bootstrapping of probability density function for IAGOS relative humidity over ice per pressure level for the tropic regions and season JJA

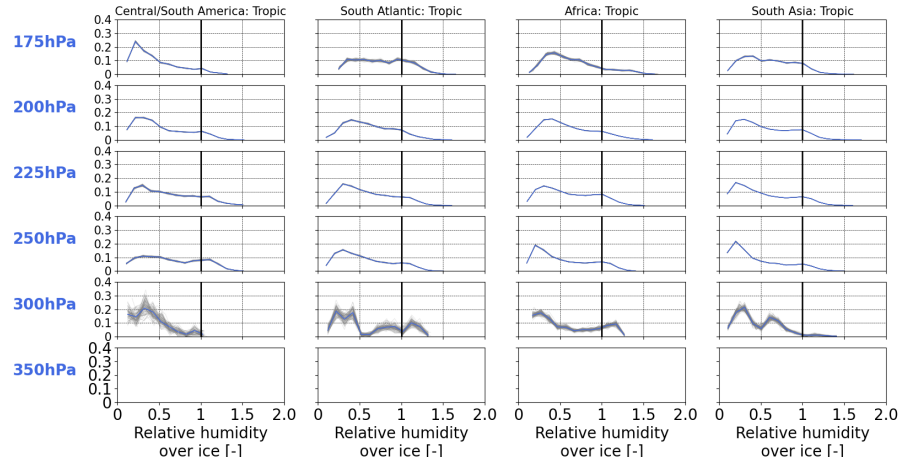

Figure B.16: Bootstrapping of probability density function for IAGOS relative humidity over ice per pressure level for the tropic regions and season SON

B.5. IAGOS and ERA5 Relative Humidity over Ice as a Function of Pressure Level, Region and Year - Standard Deviation

Table B.3: Standard deviation of IAGOS and ERA5 relative humidity over ice per year and pressure level for North America

	North America																							
	IAGOS												ERA5											
Pressure level	2011	2012	2013	2014	2015	2016	2017	2018	2019	2020	2021	2022	2011	2012	2013	2014	2015	2016	2017	2018	2019	2020	2021	2022
175 hPa	0.28	0.40	0.17	0.20	0.40	0.02	0.33	0.36	0.25	0.18	0.18	0.27	0.26	0.31	0.33	0.32	0.43	0.03	0.26	0.29	0.28	0.22	0.24	0.29
200 hPa	0.31	0.34	0.30	0.31	0.39	0.33	0.37	0.34	0.31	0.27	0.33	0.31	0.28	0.33	0.33	0.36	0.35	0.34	0.34	0.31	0.32	0.28	0.33	0.31
225 hPa	0.36	0.36	0.34	0.34	0.39	0.37	0.39	0.37	0.36	0.33	0.37	0.36	0.34	0.35	0.35	0.35	0.36	0.35	0.34	0.34	0.34	0.33	0.34	0.34
250 hPa	0.36	0.38	0.36	0.37	0.36	0.34	0.40	0.36	0.36	0.41	0.37	0.36	0.32	0.34	0.34	0.34	0.33	0.32	0.34	0.31	0.32	0.35	0.34	0.33
300 hPa	0.37	0.40	0.37	0.36	0.36	0.36	0.35	0.34	0.37	0.37	0.33	0.36	0.33	0.33	0.32	0.32	0.32	0.31	0.31	0.31	0.31	0.32	0.30	0.30
350 hPa	0.40	0.40	0.36	0.34	0.40	0.31	0.32	0.38	0.37	0.32	0.33	0.32	0.32	0.33	0.31	0.31	0.34	0.30	0.31	0.34	0.31	0.27	0.30	0.28

Table B.4: Standard deviation of IAGOS and ERA5 relative humidity over ice per year and pressure level for North Atlantic

	North Atlantic																							
	IAGOS												ERA5											
Pressure level	2011	2012	2013	2014	2015	2016	2017	2018	2019	2020	2021	2022	2011	2012	2013	2014	2015	2016	2017	2018	2019	2020	2021	2022
175 hPa	0.17	0.23	0.32	0.22	0.31	0.14	0.36	0.35	0.06	0.11	0.27	0.33	0.28	0.13	0.31	0.28	0.32	0.17	0.26	0.32	0.08	0.12	0.30	0.31
200 hPa	0.35	0.37	0.34	0.32	0.37	0.39	0.39	0.37	0.34	0.38	0.35	0.34	0.32	0.33	0.33	0.34	0.35	0.36	0.34	0.35	0.33	0.33	0.33	0.34
225 hPa	0.39	0.39	0.36	0.34	0.39	0.40	0.41	0.37	0.39	0.40	0.39	0.37	0.35	0.36	0.35	0.35	0.35	0.36	0.36	0.34	0.36	0.35	0.35	0.35
250 hPa	0.38	0.39	0.35	0.35	0.37	0.37	0.39	0.36	0.38	0.40	0.38	0.39	0.34	0.36	0.34	0.34	0.34	0.33	0.33	0.33	0.33	0.37	0.33	0.35
300 hPa	0.26	0.34	0.25	0.36	0.30	0.33	0.34	0.35	0.38	0.36	0.31	0.35	0.25	0.30	0.27	0.31	0.27	0.24	0.28	0.28	0.29	0.29	0.30	0.38
350 hPa	NA	0.22	0.00	0.38	0.38	NA	NA	NA	NA	NA	NA	0.25	NA	0.18	0.00	0.28	0.28	NA	NA	NA	NA	NA	NA	0.19

Table B.5: Standard deviation of IAGOS and ERA5 relative humidity over ice per year and pressure level for Europe

	Europe																							
	IAGOS												ERA5											
Pressure level	2011	2012	2013	2014	2015	2016	2017	2018	2019	2020	2021	2022	2011	2012	2013	2014	2015	2016	2017	2018	2019	2020	2021	2022
175 hPa	0.29	0.20	0.22	0.22	0.19	0.24	0.34	0.24	0.19	0.18	0.23	0.23	0.23	0.25	0.25	0.23	0.20	0.20	0.25	0.23	0.16	0.13	0.24	0.25
200 hPa	0.32	0.28	0.26	0.27	0.30	0.28	0.32	0.32	0.30	0.32	0.28	0.29	0.27	0.27	0.28	0.29	0.30	0.27	0.28	0.29	0.28	0.28	0.27	0.29
225 hPa	0.34	0.36	0.30	0.31	0.34	0.34	0.36	0.33	0.34	0.37	0.35	0.35	0.30	0.31	0.32	0.32	0.31	0.32	0.30	0.31	0.29	0.33	0.31	0.33
250 hPa	0.34	0.38	0.34	0.35	0.35	0.35	0.36	0.35	0.38	0.39	0.37	0.36	0.31	0.32	0.31	0.31	0.32	0.31	0.31	0.31	0.32	0.34	0.32	0.34
300 hPa	0.31	0.35	0.35	0.36	0.31	0.34	0.34	0.35	0.35	0.39	0.33	0.33	0.27	0.28	0.29	0.29	0.29	0.29	0.29	0.29	0.29	0.34	0.31	0.30
350 hPa	0.36	0.36	0.36	0.38	0.30	0.34	0.34	0.36	0.36	0.36	0.35	0.34	0.29	0.29	0.29	0.30	0.30	0.30	0.29	0.31	0.30	0.33	0.30	0.31

Table B.6: Standard deviation of IAGOS and ERA5 relative humidity over ice per year and pressure level for North Asia

	North Asia																							
	IAGOS												ERA5											
Pressure level	2011	2012	2013	2014	2015	2016	2017	2018	2019	2020	2021	2022	2011	2012	2013	2014	2015	2016	2017	2018	2019	2020	2021	2022
175 hPa	0.14	0.28	0.21	0.32	0.09	0.30	0.24	0.32	0.33	0.11	0.11	0.15	0.10	0.31	0.31	0.35	0.16	0.35	0.18	0.34	0.35	0.13	0.09	0.10
200 hPa	0.32	0.32	0.23	0.31	0.27	0.27	0.29	0.32	0.32	0.28	0.23	0.22	0.28	0.31	0.29	0.30	0.29	0.26	0.26	0.31	0.30	0.28	0.22	0.19
225 hPa	0.35	0.36	0.30	0.30	0.31	0.32	0.37	0.35	0.36	0.41	0.37	0.32	0.34	0.34	0.32	0.32	0.30	0.30	0.32	0.33	0.33	0.36	0.34	0.29
250 hPa	0.36	0.36	0.34	0.34	0.34	0.35	0.35	0.37	0.37	0.36	0.35	0.34	0.33	0.33	0.34	0.33	0.32	0.32	0.32	0.33	0.34	0.33	0.33	0.31
300 hPa	0.32	0.36	0.33	0.37	0.31	0.34	0.35	0.35	0.33	0.34	0.33	0.31	0.30	0.32	0.30	0.32	0.30	0.31	0.33	0.32	0.29	0.31	0.30	0.31
350 hPa	0.29	0.30	0.30	0.30	0.30	0.35	0.31	0.32	0.35	0.35	0.27	0.26	0.29	0.29	0.29	0.28	0.36	0.32	0.31	0.30	0.32	0.31	0.28	0.28

Table B.7: Standard deviation of IAGOS and ERA5 relative humidity over ice per year and pressure level for Central/South America

	Central/South America																							
	IAGOS												ERA5											
Pressure level	2011	2012	2013	2014	2015	2016	2017	2018	2019	2020	2021	2022	2011	2012	2013	2014	2015	2016	2017	2018	2019	2020	2021	2022
175 hPa	NA	NA	0.05	NA	0.07	0.160	0.27	0.32	0.28	0.26	0.26	0.21	NA	NA	0.18	NA	0.08	0.01	0.22	0.28	0.30	0.26	0.31	0.34
200 hPa	NA	NA	0.28	0.30	0.27	0.28	0.30	0.33	0.29	0.31	0.32	0.23	NA	NA	0.28	0.28	0.29	0.27	0.30	0.30	0.30	0.28	0.31	0.22
225 hPa	NA	NA	0.29	0.32	0.31	0.32	0.33	0.34	0.31	0.33	0.32	0.31	NA	NA	0.31	0.29	0.29	0.30	0.28	0.31	0.28	0.28	0.29	0.31
250 hPa	NA	NA	0.29	0.32	0.32	0.35	0.36	0.36	0.32	0.32	0.33	0.31	NA	NA	0.28	0.28	0.33	0.29	0.31	0.31	0.29	0.28	0.30	0.30
300 hPa	NA	NA	NA	0.35	0.30	0.15	0.30	0.31	0.26	0.31	0.36	0.31	NA	NA	NA	0.35	0.31	0.10	0.27	0.30	0.22	0.24	0.30	0.32
350 hPa	NA	NA	NA	NA	NA	NA	NA	0.19	NA	NA	NA	NA	NA	NA	NA	NA	NA	NA	NA	NA	NA	NA	NA	NA

Table B.8: Standard deviation of IAGOS and ERA5 relative humidity over ice per year and pressure level for South Atlantic

	South Atlantic																							
	IAGOS												ERA5											
Pressure level	2011	2012	2013	2014	2015	2016	2017	2018	2019	2020	2021	2022	2011	2012	2013	2014	2015	2016	2017	2018	2019	2020	2021	2022
175 hPa	NA	0.31	0.23	0.22	0.30	NA	0.32	0.25	NA	NA	0.01	0.30	NA	0.24	0.29	0.18	0.27	NA	0.28	0.27	NA	NA	0.01	0.28
200 hPa	0.28	0.31	0.26	0.30	0.30	0.32	0.31	0.31	0.29	0.23	0.36	0.31	0.29	0.27	0.27	0.29	0.29	0.29	0.27	0.29	0.20	0.14	0.30	0.28
225 hPa	0.35	0.29	0.27	0.32	0.31	0.31	0.33	0.33	0.32	0.36	0.32	0.30	0.32	0.28	0.28	0.31	0.29	0.27	0.29	0.30	0.30	0.32	0.30	0.29
250 hPa	0.37	0.32	0.28	0.32	0.32	0.35	0.35	0.30	0.32	0.2	0.32	0.27	0.34	0.29	0.28	0.29	0.29	0.30	0.30	0.28	0.30	0.26	0.29	0.25
300 hPa	0.05	0.38	0.21	0.32	0.13	NA	0.48	0.45	NA	NA	0.22	0.34	0.05	0.26	0.17	0.30	0.12	NA	0.26	0.36	NA	NA	0.11	0.32
350 hPa	NA	NA	NA	NA	NA	NA	NA	NA	NA	NA	NA	NA	NA	NA	NA	NA	NA	NA	NA	NA	NA	NA	NA	NA

Table B.9: Standard deviation of IAGOS and ERA5 relative humidity over ice per year and pressure level for Africa

	Africa																							
	IAGOS												ERA5											
Pressure level	2011	2012	2013	2014	2015	2016	2017	2018	2019	2020	2021	2022	2011	2012	2013	2014	2015	2016	2017	2018	2019	2020	2021	2022
175 hPa	0.32	0.32	0.31	0.03	0.30	0.33	0.35	0.28	0.23	0.27	0.24	0.30	0.30	0.26	0.26	0.18	0.28	0.25	0.28	0.27	0.26	0.18	0.17	0.29
200 hPa	0.31	0.32	0.28	0.24	0.29	0.31	0.33	0.32	0.33	0.34	0.29	0.30	0.31	0.31	0.30	0.27	0.29	0.28	0.29	0.30	0.31	0.31	0.28	0.30
225 hPa	0.32	0.31	0.29	0.27	0.30	0.31	0.33	0.32	0.34	0.33	0.35	0.33	0.31	0.31	0.32	0.32	0.31	0.29	0.30	0.29	0.32	0.30	0.31	0.32
250 hPa	0.31	0.32	0.26	0.28	0.31	0.34	0.33	0.32	0.35	0.32	0.34	0.33	0.31	0.31	0.28	0.30	0.33	0.31	0.29	0.29	0.32	0.29	0.32	0.33
300 hPa	0.22	0.19	0.14	NA	0.03	0.35	0.37	0.35	0.26	0.09	0.16	0.26	0.16	0.16	0.15	NA	NA	0.31	0.35	0.33	0.23	0.10	0.20	0.20
350 hPa	NA	NA	NA	NA	NA	NA	NA	0.08	NA	NA	NA	NA	NA	NA	NA	NA	NA	NA	NA	NA	NA	NA	NA	NA

Table B.10: Standard deviation of IAGOS and ERA5 relative humidity over ice per year and pressure level for South Asia

	South Asia																							
	IAGOS												ERA5											
Pressure level	2011	2012	2013	2014	2015	2016	2017	2018	2019	2020	2021	2022	2011	2012	2013	2014	2015	2016	2017	2018	2019	2020	2021	2022
175 hPa	0.04	0.30	0.29	0.30	0.27	0.32	0.28	0.28	0.31	0.16	0.33	0.28	0.02	0.28	0.32	0.30	0.29	0.32	0.30	0.31	0.30	0.22	0.33	0.35
200 hPa	0.20	0.31	0.30	0.31	0.31	0.34	0.31	0.31	0.32	0.36	0.25	0.26	0.14	0.31	0.32	0.32	0.31	0.33	0.32	0.32	0.31	0.33	0.25	0.27
225 hPa	0.31	0.33	0.30	0.32	0.33	0.33	0.33	0.32	0.33	0.34	0.29	0.33	0.29	0.33	0.33	0.33	0.32	0.33	0.33	0.33	0.31	0.32	0.29	0.33
250 hPa	0.33	0.35	0.29	0.31	0.31	0.34	0.32	0.31	0.34	0.37	0.30	0.32	0.30	0.34	0.31	0.30	0.30	0.33	0.31	0.31	0.32	0.33	0.26	0.31
300 hPa	0.06	0.33	0.29	0.29	0.30	0.29	0.34	0.36	0.34	0.30	0.28	0.24	0.09	0.35	0.29	0.28	0.32	0.29	0.33	0.31	0.29	0.29	0.25	0.28
350 hPa	NA	NA	NA	0.44	NA	NA	0.15	0.26	0.24	NA	0.04	NA	NA	0.10	NA	0.16	NA	0.25	0.22	0.20	0.16	NA	0.05	NA

C. Schmidt-Appleman Criterion

The percentage of measurements in IAGOS and ERA5 meeting the Schmidt-Appleman Criterion per pressure level and season, for the extratropic and tropic regions.

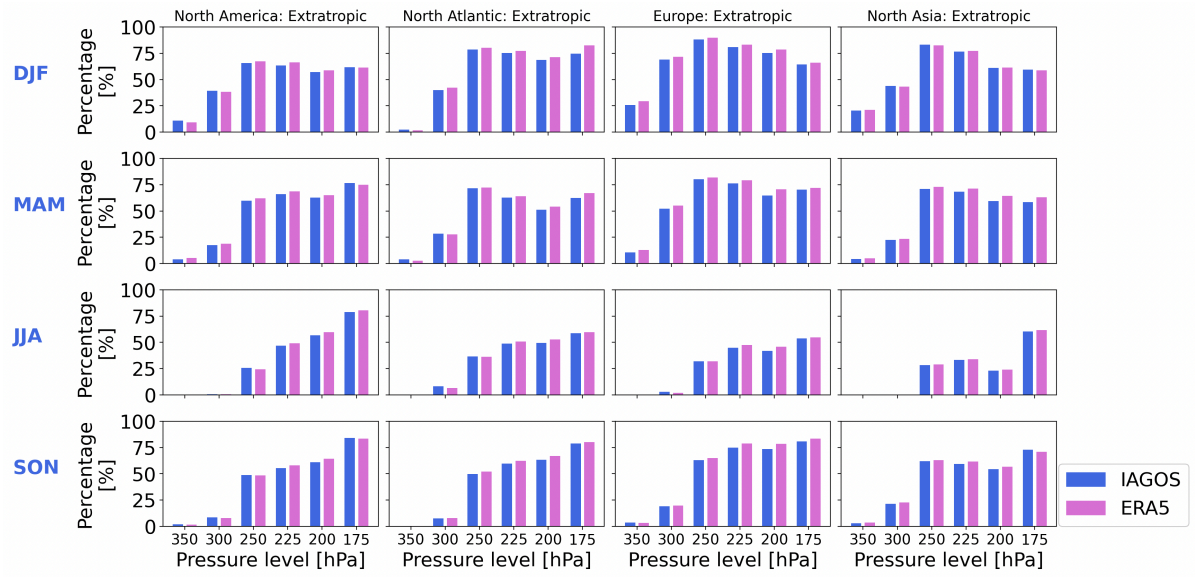

Figure C.1: Percentage of measurements meeting Schmidt-Appleman criterion in the extratropic regions per season and pressure altitude, η = 30%

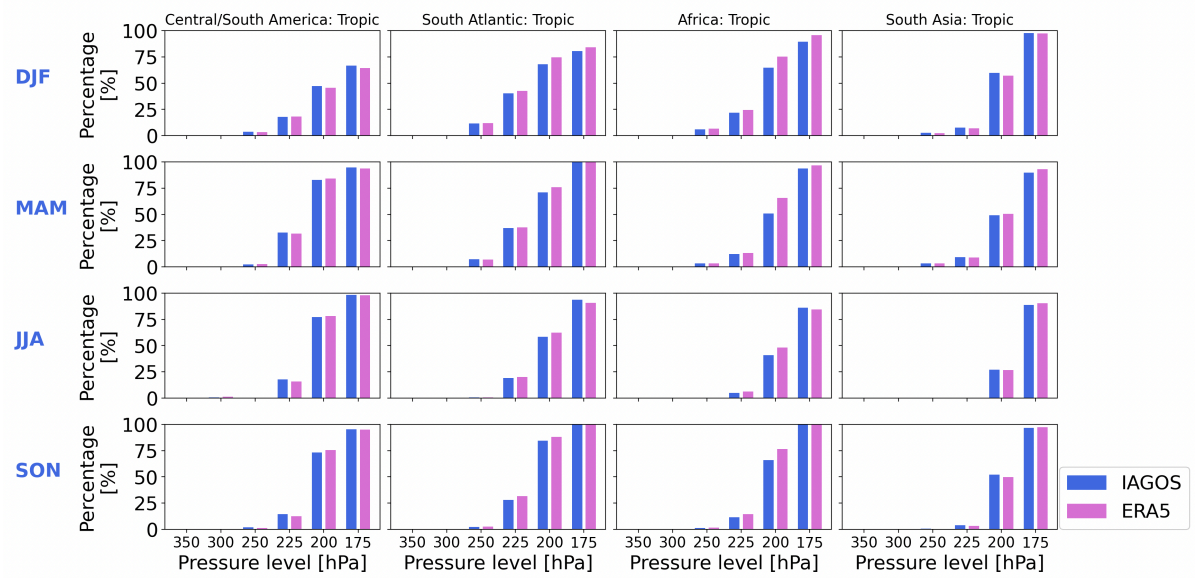

Figure C.2: Percentage of measurements meeting Schmidt-Appleman criterion in the tropic regions per season and pressure altitude, η = 30%

D. Contrail Formation Potential

D.1. Seasonal Occurrences of Contrail Formation Potential

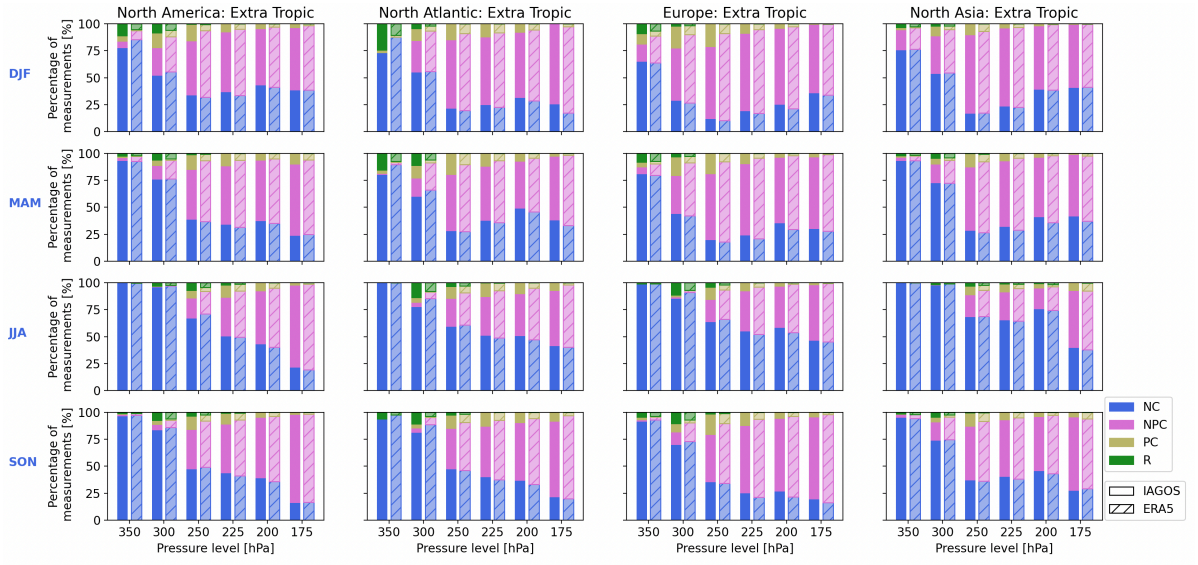

Figure D.1: Contrail formation potential in the extratropic regions per season and pressure altitude, η = 30%

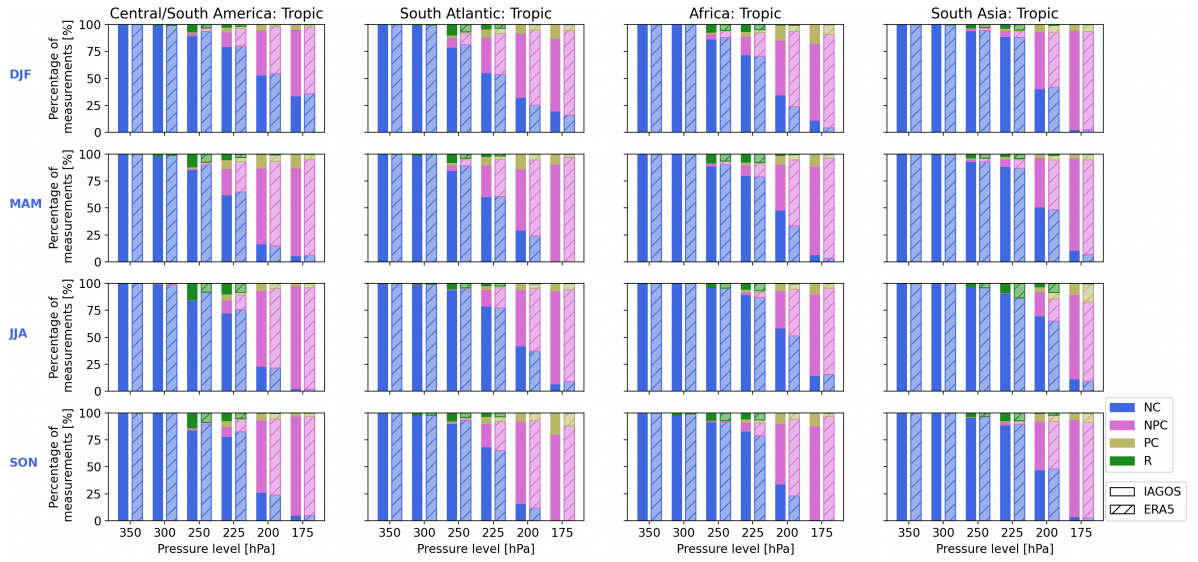

Figure D.2: Contrail formation potential in the tropic regions per season and pressure altitude, η = 30%

D.2. Effect of Engine Efficiency on Seasonal Occurrence of Contrail Formation Potential

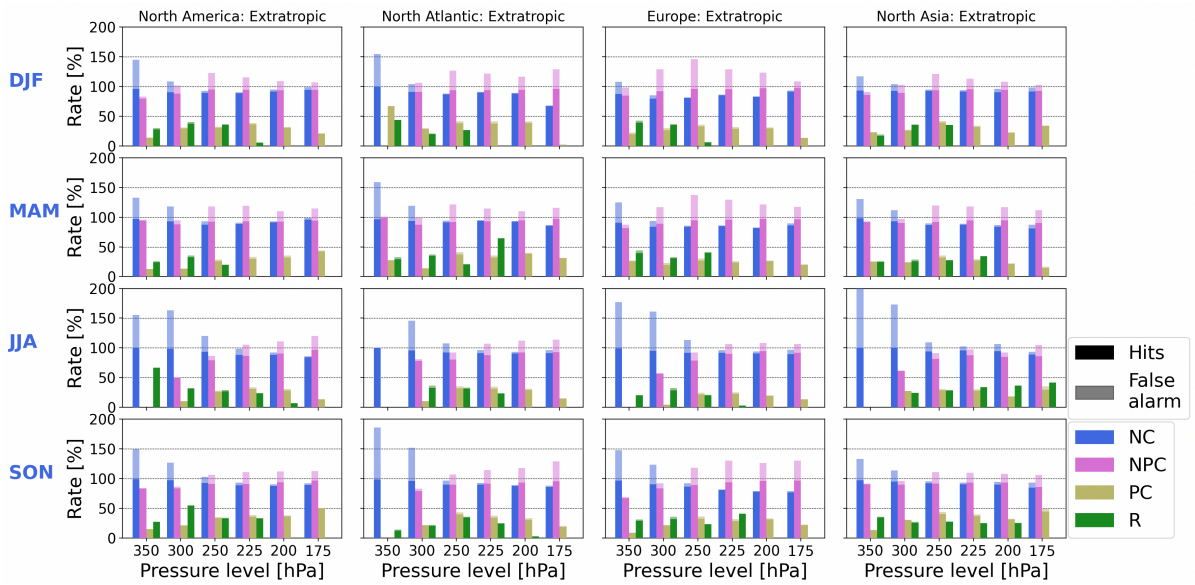

Figure D.3: Hit rates and false alarm rates for contrail formation potential per season and pressure level in the extratropic regions, η = 40%

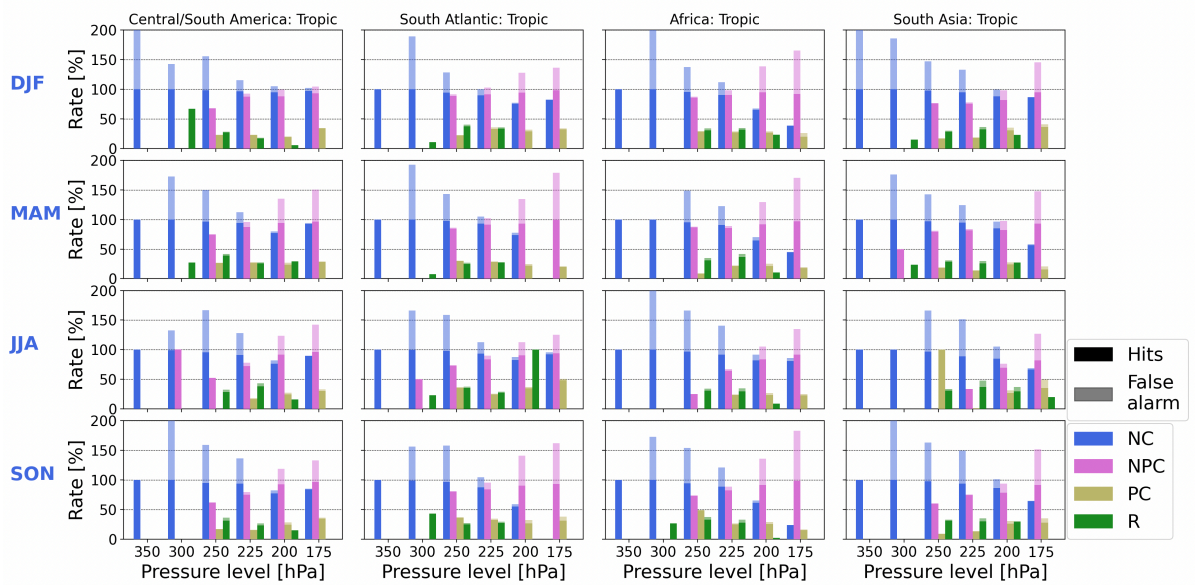

Figure D.4: Hit rates and false alarm rates for contrail formation potential per season and pressure level in the tropic regions, η = 30%